Evaluation of Thoracic Response in Side Impact Crash

By

Brock Watson

A thesis
presented to the University of Waterloo
in fulfillment of the
thesis requirement for the degree of
Master of Applied Science
in
Mechanical Engineering

Waterloo, Ontario, Canada, 2010

I hereby declare that I am the sole author of this thesis. This is a true copy of the thesis, including any required final revisions, as accepted by my examiners.

I understand that my thesis may be made electronically available to the public.

Abstract

Mitigating injury in side impact has been an important topic of research for decades. In the mid 1980's the American government began a program intended to improve the crashworthiness of vehicles in side impact. This program ultimately led to the introduction of a dynamic side impact test (Federal Motor Vehicle Safety Standard (FMVSS) 214), which new vehicles must pass, along with a very similar test aimed at consumer awareness (New Car Assessment Program (NCAP) side impact test). The work presented in this thesis involved the study and simulation of these tests to evaluate occupant response in side impact, with a focus on the thoracic response.

In the first portion of the work presented here, an in-depth study of the National Highway Traffic Safety Administration (NHTSA) crash test database was performed. In this study the results of the side impact crash tests of 72 vehicles were examined to understand the general trends seen in this type of testing with regards to vehicle velocity, side intrusion, and occupant injury prediction. A series of average velocity profile curves was created from accelerometer data at 18 measurement points on each vehicle crash tested. Additionally the injury criterion measured by the front seat occupant was plotted against several vehicle variables (such as mass and occupant arm to door distance) to study the effect these variable had on the injury predicted by the occupant. No single variable was shown to have a strong correlation to injury, although increasing door intrusion distance, peak lateral velocity, the Head Injury Criterion (HIC), and pelvic acceleration were found to positively correlate to thoracic injury. In addition, increasing vehicle model year, vehicle mass, and arm to door (AD) distance showed negative correlations with thoracic injury.

Following the survey of the NHTSA database, a finite element model of the NHTSA side impact test was developed. This model included a full scale Ford Taurus model, a NHTSA barrier model and three side impact anthropometric test device (ATD) occupant models, each representing a different 50^{th} percentile male dummy. Validation of this model was carried out by comparing the simulated vehicle component velocity results to the corridors developed in the NHSTA crash test database study as well as comparing these velocities, the vehicle deformation profile, and the occupant velocity, acceleration and rib deflection to several Ford Taurus crash tests from a similar vintage to the finite element model. As this model was intended as a 'baseline' case to study side impact and occupant kinematics in side impact, side airbags were

not included in this model. A lack of experimental data and a lack of consensuses within the automotive crash community on the proper method of modeling these devices and their effectiveness in real world impacts also led to their exclusion.

Following model validation, a parametric study was carried out to assess the importance of the initial position of the occupant on the vehicle door velocity profile and the predicted occupant injury response. Additionally the effect of the door trim material properties, arm rest properties and the effect of seat belt use were studied. It was found that the lateral position of the occupant had an effect on the door velocity profile, while the vertical and longitudinal position did not. The use of seatbelts was shown to have no significant effect in these simulations, due to minimal interaction between the restraint system and occupant during side impact. Furthermore, there was a general decreasing trend in the injury predicted as the initial position of the occupant was moved further inboard, down and forward in the vehicle. Stiffer interior trim was found to improve the injury prediction of the occupant, while changing the material of the foam door inserts had no effect. It was found that in general the occupant remained in position, due to the inertia of the occupant, while the seat began moving towards the centerline of the vehicle. Future considerations could include more advanced restraint systems to couple the occupant more effectively to the seat, or to develop side interior trim that engages the occupant earlier to reduce the relative velocity between the occupant and intruding door. Overall, the model correlated well with experimental data and provided insight into several areas which could lead to improved occupant protection in side impact. Future work should include integrating side airbags into the model, widening the focus of the areas of injury to include other body regions and integrating more detailed human body models.

Acknowledgements

This is the part of most theses were students lie about how wonderful their supervisors have been. Luckily, I can tell the truth. Duane, you have been, far and away, the best supervisor I could have asked for. Without your constant encouragement and seemingly endless patience, this thesis would read more like a 4th grade report on how I spent my summer vacation or a rambling, incoherent (more so) mess rather than a proper piece of scholarly work. You've forced me to learn what to do when I don't know what to do and have given me some amazing opportunities and advice along the way. For this and everything else, I will be forever grateful.

I greatly appreciated the financial support provided to me during my thesis by General Motors of Canada, The Premier's Research Excellence Award, Auto21 and the Department of Mechanical and Mechatronics Engineering. Additionally the talents of First Technolgy Safety Systems (FTSS), Dynamore GbmH, Livermore Softeware Technology Corporation, and the National Crash Analysis Center in developing the original models used in the creation of the models for this thesis must be recognized.

I would like to thank the members of my extended research group for providing an 'interesting' environment in which to spend these past few years. In particular, thanks must go out to Chris (both of you), Jose, and Jeff for taking me under their wings and showing me the ropes, and to Ken and Brett for providing a great foundation during the early part of this work. Also John, Jason, Jen and Ryan; thanks for being a great set of officemates and for generally tolerating me during my course of study. To the Friday Gradhouse lunch crew; thank you for making my time here tolerable (and in some cases actually fun) by giving me something to look forward to at the end of every long and difficult (?) week. To the countless other friends, colleagues, and acquaintances who have helped me along, shared in wasting some time, and taught me a great multitude of lessons in my time in Waterloo, I thank you. Jason, it's been great sharing the same "Master's story arc" with you. Brian you've been a worthy adversary.

Last but certainly not least, a huge thank you must be extended to my family; both genetic and otherwise. No words can express what your constant love and support has meant to me throughout not only my time working on this thesis, but in all things that I do. Finally, to my parents; I have been fortunate in my life to receive a number of irreplaceable gifts, but the two of you have been undoubtedly the best.

"Computers are useless. They can only give you answers."

- Pablo Picasso

Table of Contents

List of Figures

List of Tables

List of Acronyms

AD	Arm to Door Distance
AIS	Abbreviated Injury Scale
ATD	Anthropometric Test Device (Crash Test Dummy)
BIW	Body in White
CG	Center of Gravity
CV	Coefficient of Variability
ECE	Economic Commission for Europe
ES	European Side Impact Dummy (EuroSID)
ES-2	EuroSID 2
ES-2re	EuroSID 2 with rib extensions
FMVSS	Federal Motor Vehicle Safety Standard
HIC	Head Injury Criterion
IIHS	Insurance Institute for Highway Safety
ISS	Injury Severity Score
LSTC	Livermore Software Technology Company
MAIS	Maximum AIS
MDB	Moving Deformable Barrier
NCAP	New Car Assessment Program
NHTSA	National Highway Traffic Safety Administration
OOP	Occupant Out-of-position
PMHS	Post Mortem Human Subject
R95	Regulation 95
TRA	Traumatic Rupture of the Aorta
TTI	Thoracic Trauma Index
USSID	United States Side Impact Dummy
VC	Viscous Criterion
WSID	World Side Impact Dummy

Chapter 1 Introduction

1.1 Background

Because of the high mortality rates involved with automobile collisions, occupant safety is a major consideration for automotive engineers. This is especially true with the ever increasing number of vehicles on the road, particularly in developing nations. The study of automotive injury can trace its roots back to the work of John Stapp who pioneered the field by studying the effects of rapid deceleration on the human body [Stapp, 1957]. Following this work, safety began to come to the forefront of automotive design due to the implementation of vehicle safety legislation and an increase in consumer awareness of the importance of vehicle safety [Nader, 1972].

The sophistication of occupant protection has grown from two point lap belts to include pretensioning three point restraints, numerous airbags, collapsible steering wheels, energy absorbing crumple zones and a plethora of other technology designed to keep vehicle occupants safe in the event of a collision. With the improvements in safety feature present in modern vehicles the complexity of the regulatory tests used to evaluate vehicle performance has also increased. In particular the anthropometric test dummies (ATDs), better known as crash test dummies, have grown from simple human like shapes with an approximate weight distribution of a human body, to highly advanced, highly instrumented devices that can measure acceleration, deflection, force and moment in a number of body regions to provide a thorough understanding of the dynamic and kinematic loads being applied to the device.

While the response of these ATDs is designed mimic to that of post mortem human subjects (PMHS), ATDs are not perfect analogs of human beings and thus their ability to measure and predict injury that could occur to a living person is limited and are only able to provide information from those instruments that were installed prior to testing. Due to the relatively limited amount of data that can be extracted from a given crash test, computer modeling has become increasing prevalent in the design of new vehicles and the research of occupant protection. An added benefit of using computer modeling is a reduction in the cost associated

with physical crash testing, which can become exorbitantly expensive, particularly during the design phase when multi-million dollar prototype vehicles must be destroyed to understand their characteristics in a collision.

1.2 Motivation for Research

Automotive collisions kill 1.2 million people every year and injure 20 to 50 million more, making road traffic accidents the 11th most common cause of death worldwide [World Health Organization, 2004]. 2889 Canadians were killed in automotive collisions in 2000, while 15,281 were seriously injured [Statistics Canada, 2007]. The American National Highway Traffic Administration (NHTSA) keeps extensive records of all fatalities and serious injuries that occur in the US and have consistently found that the most common direction of fatal crashes is in the direction of travel, followed by side impact. Of the 20,376 vehicles involved in fatal crashes in the United Sates in 2008 the initial points of impact were 61.5% frontal, 23.8% side, 6.9% rear, and 6.9% other (including non-collision fatalities and unknown). Of the 1,624,000 injurious crashes that same year the initial points of impact were 51.1% frontal, 26.1% side, 21.3% rear, and 1.5% other [NHTSA, 2009]. While side impact is not the most commonly injurious or fatal type of impact, it does cause a significant portion of the occupant harm incurred on the road today.

Prior to new side impact testing being implemented, NHTSA performed a survey of front seat, near side impacts. They found that thoracic injuries accounted for 38% of fatalities and 59% of serious injuries, face and head injuries accounted for 40% of fatalities and 13% of injuries, and abdominal impact led to 8% of fatalities and 7% of injuries [NHTSA, 2004]. The relative importance of the head and the thorax in side impact are roughly the same in terms of percentage of fatalities though the thoracic region is injured nearly three times as often. These statistics show the importance of furthering the measures taken to protect the thorax in side impact.

By tracking the number of fatal vehicle collisions in the US using the Fatality Analysis Reporting System (FARS) database [NHTSA, 2010a], it becomes apparent that over the past several years, the number of fatalities has been in a steady decline (see Figure 1.1). This downward trend is also shown in the Canadian fatality statistics shown in Figure 1.2 [Statistics Canada, 2007].

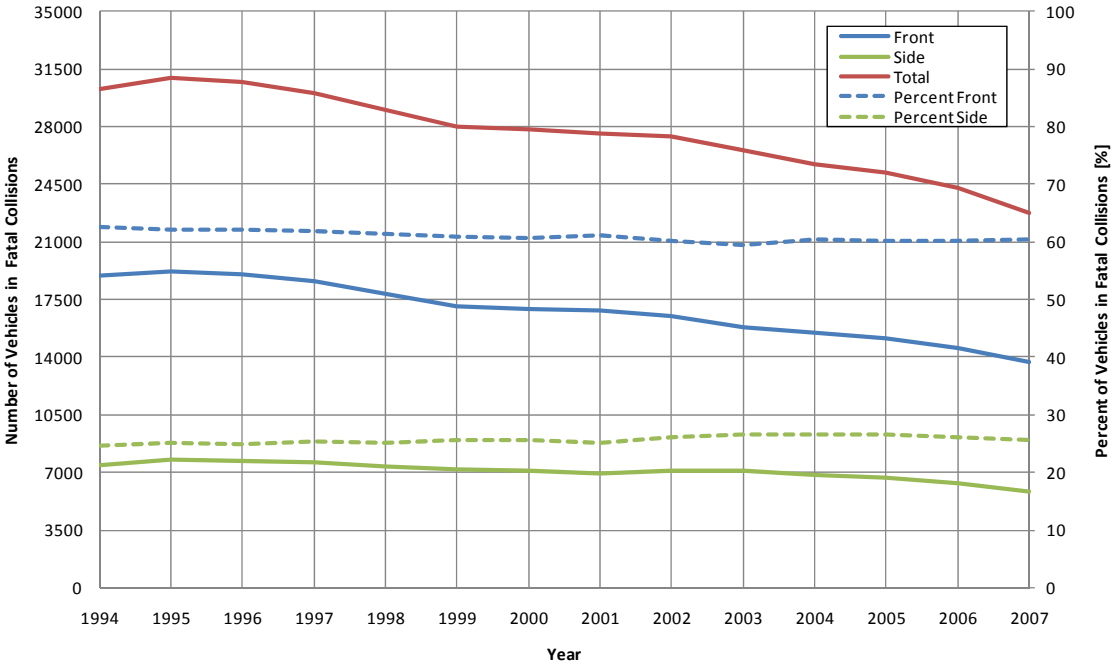

Figure 1.1 Vehicle numbers and percentage of vehicles involved in fatal collisions by direction of impact [NHTSA, 2010a]

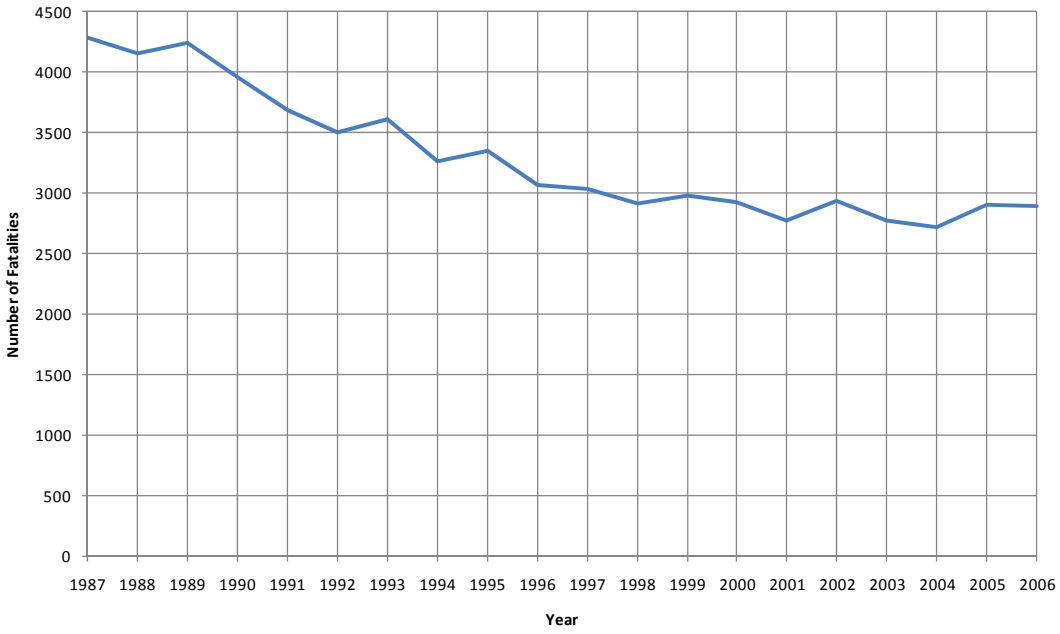

Figure 1.2: Number of roadway fatalities in Canada between 1987 and 2006 [Statistics Canada, 2007]

Figure 1.1 shows that while the proportion of fatalities in the frontal direction is dropping slightly, the proportion of fatal collisions with the side as the principle direction of impact is increasing. This is occurring despite the inclusion in 1993 of a dynamic side impact regulatory test that nearly all vehicles must pass before being sold in the United States [NHTSA, 2004].

Even prior to the implementation of the regulatory side impact test, automakers began to redesign their vehicles to improve their fleet's side impact protection. This is evidenced by the decrease in the Thoracic Trauma Index (TTI), a measure used to evaluate thoracic injury in side impact, from tests performed on four door cars between 1981 and 2002, shown in Figure 1.3 [reproduced from Kahane, 2007]. Kanane suggested this drop in TTI score was related to improvements in design of vehicle side crash structures, increased use of door padding, and the introduction of side airbags. This research also found that two door cars had generally higher TTI scores compared to their four door counterparts, and that the reduction in two door cars sold during the reporting period had a large effect on the overall decrease in the TTI score. This point highlights the importance one must place on consumer choice when looking at these statistics and the impact that people's choice has on the overall public safety statistics.

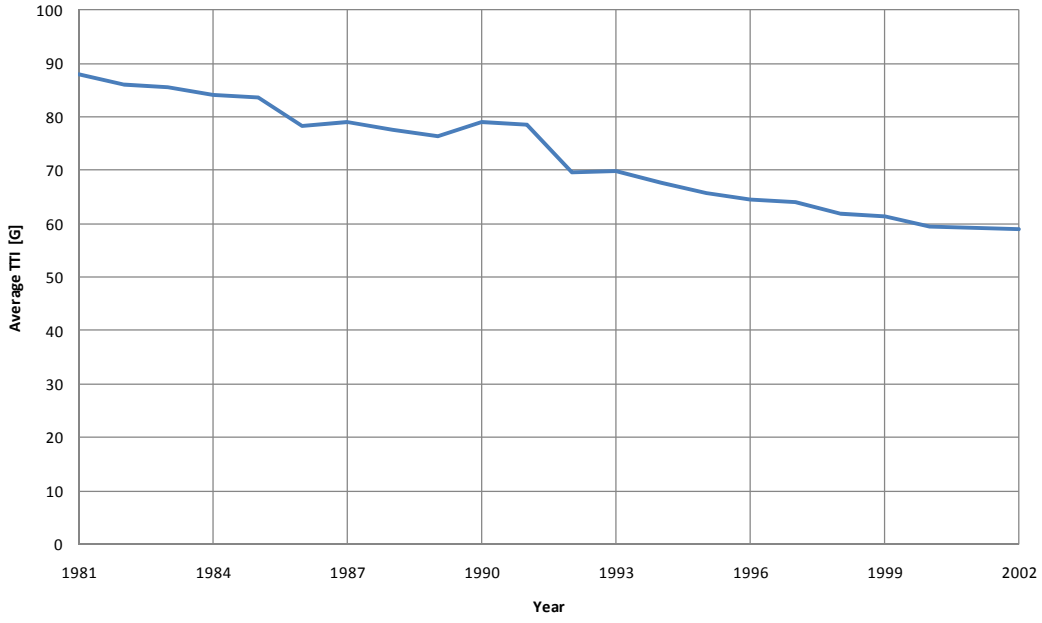

Figure 1.3: Average TTI in compliance tests between 1981 and 2002 [Kahne, 2007]

1.3 Objectives and Scope of Research

The overarching goal of the research presented here was to better understand the side impact crash, and the response of the occupant to this type of collision, specifically, injury to the thoracic region. Due to the nature of side impact it would be impossible to obtain meaningful information by attempting to study all possible combinations of impact point, impact angle, impacting vehicle speed, impacting (bullet) vehicle type, and impacted (target) vehicle type. The work presented here focused primarily on regulatory testing carried out by NHTSA as part of its New Car Assessment Program (NCAP) to provide consumer information to allow the public to choose the safest car. In these tests, the bullet vehicle is replaced by a moving deformable barrier (MDB) with a prescribed speed, impact point and impact angle. The goal of this work was to study these types of impacts in two ways. First an extensive review of the NHTSA crash test database was performed to provide context to the loading imparted to the occupant and to understand the dynamics of the vehicle during impact. Following this, several models (including a full vehicle model, occupant models and an MDB model) which were independently developed were integrated to create a realistic, full scale side impact test model. The response of the test model was compared to the experimental results studied from the NHTSA database and the response of the simulation was found to realistically mimic the experimental response. Further validation was carried out comparing the model with the response of crash tests of specific vehicles in the NHTSA database that closely resembled the full car model. With validation of the model completed, a study was carried out to discover the effect of the placement of the crash test dummy in the driver's seat prior to impact as well as the effect of changing several materials in the vehicle interior to the injury predicted by the occupant models.

Chapter 2 of this thesis outlines several key background areas to allow an understanding of the work performed in this research. This includes a brief discussion of thoracic anatomy and injuries to the thorax in automotive crash. This chapter also discusses testing that has been carried out to assess human tolerance to impact, and devices and metrics used to measure trauma in side impact, along with current trends in occupant and automotive collision modeling. Chapter 3 presents a study based on data taken from the NHTSA vehicle crash test database for side impact tests recently carried out. Chapter 4 describes the finite element models used in this research, along with their integration to develop the full scale car side impact models. The

results of the simulations are presented in Chapter 5 along with experimental results of full scale crash testing performed by NHTSA on similar vehicles to provide context for the verification and validation of the model. Following the presentation of the validation and verification of the full scale side impact crash model, Chapter 6 presents results from a parametric study which studied the effect of the occupant initial position on the vehicle response. Additionally differences in response between three side impact ATD's are presented and discussed, along with the effect of changes to the materials used for several interior door trim pieces. Finally, Chapter 7 presents the conclusions and recommended future work that could be carried out to further the work presented in this thesis.

Chapter 2 Background

2.1 Introduction

This chapter lays out the general background needed to understand and study thoracic injury resulting from side impact. Thoracic anatomy and common thoracic injuries are outlined, followed by methods used to measure injury during impact. A brief discussion of the postmortem human testing that was used to develop thoracic injury criteria is presented as well, followed by the development of ATDs used in side impact crash testing. A brief outline of side impact crash testing, side sled testing and the numerical modeling of the side impact is also presented.

2.2 Thoracic Anatomy

In the most basic sense, the thorax is the body region of an animal between its head and abdomen. In humans this is essentially the region surrounded by the rib cage. Within the thoracic cavity are the heart, the lungs, the great vessels, the esophagus and trachea, and several other important components of the lymphatic system, the endocrine system, and the nervous system. Due to the importance of the organs in this region in sustaining life (particularly the heart, lungs and great blood vessels), the protection of the thorax is of paramount importance in sustaining life.

2.2.1 Rib Cage

The rib cage, shown in Figure 2.1, consists of the structural components which, along with the skin, muscle and fascia comprise the body cavity. The major components of the rib cage are the ribs, the sternum, the costal cartilage and the thoracic vertebrae.

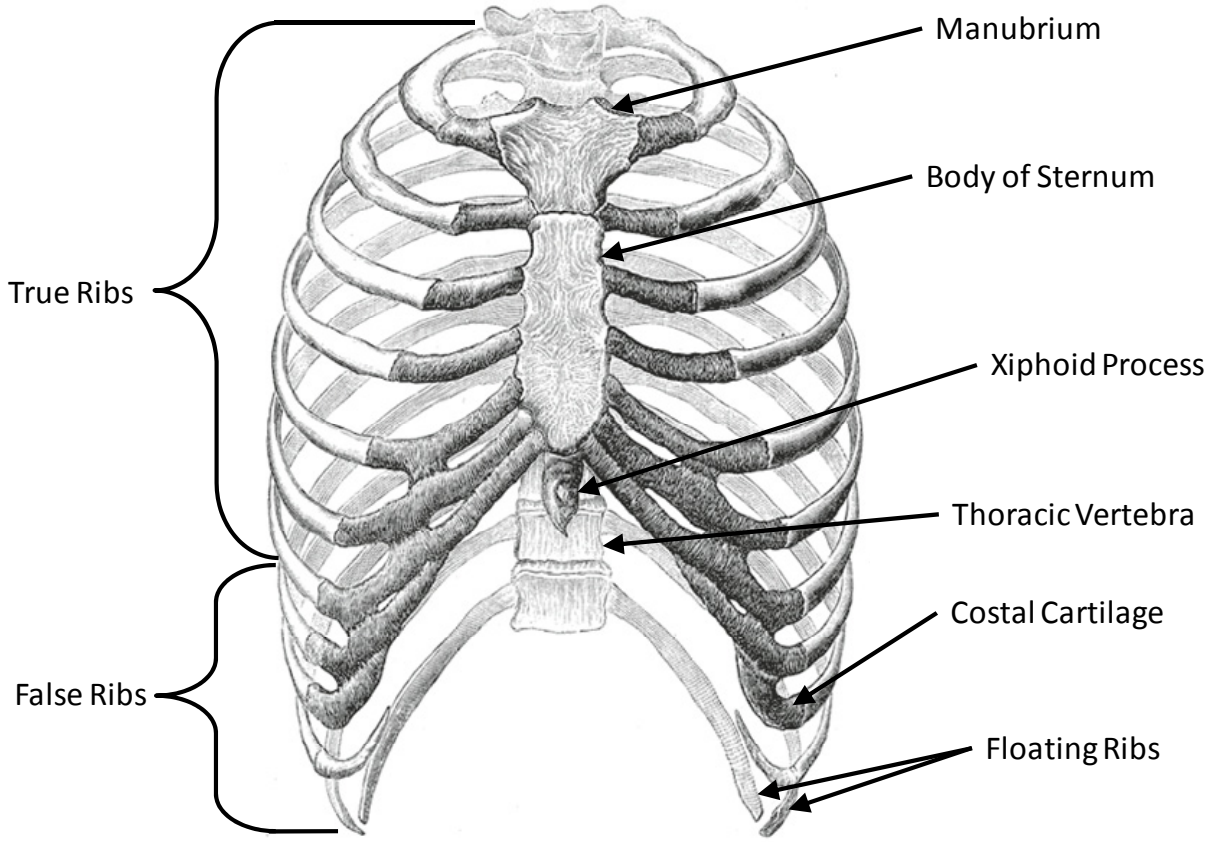

Figure 2.1: The human rib cage [Gray, 1918]

Ribs are generally labeled as either true ribs or false ribs. There are 24 ribs in the human thorax; 12 on each side. The first though seventh rib (first being the most superior rib, and counting down inferiorly) are termed true ribs. These ribs are connected directly to the sternum by strips of hyaline cartilage called costal cartilage. This cartilage allows a certain amount of articulation providing some compliance of the thorax [Gray, 1918]. Ribs 8 to 12 are termed the false ribs, since they do not connect directly to the sternum. Instead, the cartilage from the eighth, ninth and tenth rib connect to the each other and then to the cartilage of the seventh rib. The eleventh and twelfth rib are often termed floating ribs as they are only attached to at the posterior to the thoracic vertebrae [Tortora, 1999].

The ribs themselves are simply curved long flat bones, with a slightly larger head at the posterior end to allow articulation with the vertebrae. As mentioned earlier the anterior ends of the first 10 ribs are covered with costal cartilage which connects these ribs to the sternum. Ribs are similar to long bones in that they are essentially tubes of cortical (dense) bone filled with cancellous

(spongy) bone [Romanes, 1981]. The space between the ribs is termed the intercostal space which is filled with muscle and other soft tissue.

The sternum is a large flat bone that forms the anterior boundary of the thoracic cage. It is formed by three sections that fuse together by the age of 21 [Romanes, 1981]. These three sections are the body of the sternum, which is inferior to the maunbrium, and superior to the xiphoid process. The body is a long flat plate which consists of four plates fused together. The costal cartilage of the second through seventh ribs connects to the body, while the first ribs costal cartilage connects to the manubrium. The xiphoid process' primary function is to provide attachment points for abdominal muscles [Trotora, 1999].

The thoracic spine consists of 12 vertebrae which sit inferior to the seventh cervical vertebra and superior to the first lumbar vertebra. Each vertebra has facets on the posterior portion that articulate with the corresponding numbered rib. In the first though ninth vertebra, there is also a portion that articulates with the rib inferior to it [Gray, 1918]. The vertebra consists of a body which is roughly heart shaped and disk like which is designed to support the body's weight. Posterior to the body the vertebral foramen provides space for the spinal cord to pass through to send neurological signals between the brain and the rest of the body. Surrounding this space is the vertebral arch which protects the spinal column transversely and posterior. Between each body there is a vertebral disc which provides a medium to support articulation between vertebrae [Romanes, 1981].

2.2.2 Heart

The heart is the muscular organ responsible for pumping blood throughout the human body to ensure the supply of oxygen. The heart is separated into four chambers, the left and right atrium and the left and right ventricle. The right atrium receives deoxygenated blood from the circulatory system which is then passed to the right ventricle to be sent to the lungs to receive oxygen. The oxygenated blood then returns to the heart in the left atrium before being passed to the left ventricle to send the oxygenated blood to the rest of the body [Tortora, 1999]. Figure 2.2 shows the heart, along with the lungs, great vessels and trachea.

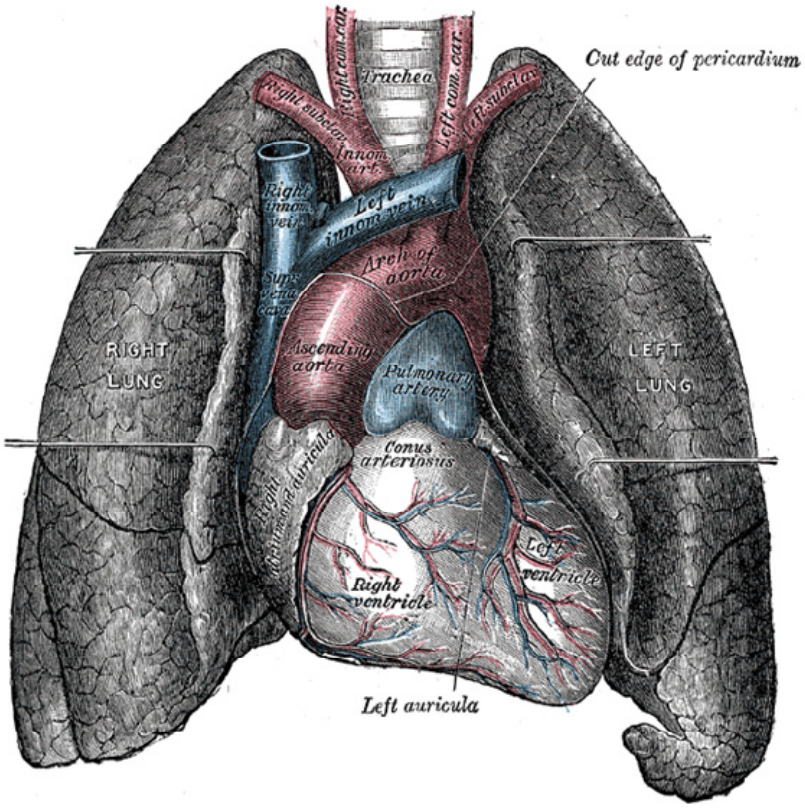

Figure 2.2: The heart, lungs, great vessels and trachea [Gray, 1918]

2.2.3 Lungs

The lungs function to exchange oxygen inhaled from the atmosphere with carbon dioxide generated by the body. Air is transported into the lungs via the trachea (also known as the windpipe) which runs from the throat to the bronchi. The bronchi split the trachea into left and right branches, to each lung. The bronchi then branch out into the bronchioles, which in turn branch into the alveolar sacs. The alveoli, where the gas exchange takes place are housed within these sacs. The lungs themselves are divided into lobes, the right having three lobes (superior, middle, and inferior) and the left having two (superior and inferior). While the lungs nearly fill the entire thoracic cavity, they have an average mass of approximately 1.2 kg in an adult male [Romanes, 1981]. The lungs are surrounded by the plural membrane, which is composed of the parietal pleura which is attached to the chest wall, and the visceral pleura which it attached to the lungs. Between these two membranes, lie the pleural cavity which is fluid filled to allow lubrication assisting the movement between the layers of membrane during normal breathing.

Because the left and right pleura are separated, it is possible for one side to be compromised and not affect the other lung.

2.2.4 Great Vessels

The great vessels are the primary blood vessels in the human body, the most important of which include the aorta, the vena cavae, the pulmonary artery and the pulmonary veins. These vessels carry nearly all the blood that passes through the heart and are therefore are paramount to sustaining life. Figure 2.3 shows a schematic diagram of the heart's chambers and the great vessels used to transport blood to and from the heart.

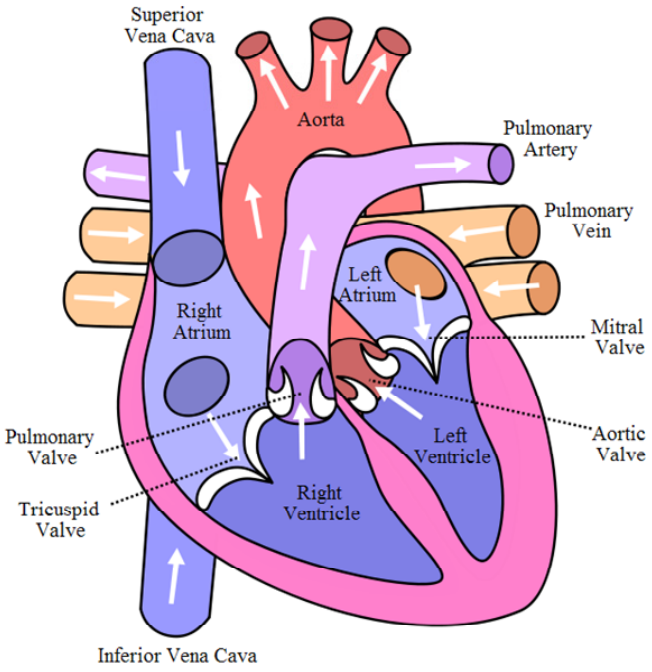

Figure 2.3: Great vessels and heart chambers

The pulmonary artery and veins are the vessels used to transport blood to and from the lungs. The pulmonary artery leaves the right ventricle and carries deoxygenated blood from the heart to the lungs. The artery branches after leaving the right ventricle to send blood to both lungs. Once the blood becomes oxygenated in the lungs, it is sent back to the heart's right ventricle via the pulmonary veins [Tortora, 1999].

The major vessels in the systemic circulatory system are the vena cavae and the aorta. The vena cavae is composed of two veins; the inferior vena cava and the superior vena cava. These two

veins are responsible for returning deoxygenated blood from the upper (superior) and lower (inferior) body regions. Both veins bring their contents to the right atrium of the heart. The Superior vena cava is fairly short, and branches into the left and right brachiocephalic veins near the lower boarder of the first costal cartilage. The inferior vena cava by contrast is significantly longer, starting at the fifth lumbar vertebra and running along the spine until passing through the diaphragm and ending at the heart [Romanes, 1981].

The oxygenated blood is carried from the left ventricle to the rest of the body by the aorta. The aorta is generally subdivided into three regions, the ascending aorta, the aortic arch and the descending aorta, which is split into the descending thoracic aorta and the descending abdominal aorta. The base of the ascending aorta begins at the left ventricle of the heart. The ascending aorta extends roughly 5 cm superiorly to the arch. The aortic arch curves interiorly and develops into the descending aorta which begins at roughly the same level as the T4 vertebra. On the superior surface of the aortic arch, three vessels which supply blood to the head, neck and upper extremities have their root. In order of origin, these arteries are; the brachiocephalic trunk, the left common carotid artery, and left subclavian artery. The ligamentum arteriosum tethers the inferior surface of the aortic arch to the superior surface to the pulmonary artery. This structure is developed from the fetal circulatory system when the ductus arteriosus, which allows blood flow between the aortic arch and the pulmonary trunk, closes. Branching from the descending aorta are a number of small arteries which send blood to the intercostals tissue. These arteries, along with the thoracic pleura provide a relatively rigid mount for the thoracic aorta to the walls of the chest cavity starting at the bottom of the T3 vertebra [Tortora, 1999].

2.3 Automotive Thoracic Injury

Trauma can be widely divided into two categories; blunt (non-penetrating) trauma and penetrating trauma. In penetrating trauma, a foreign object enters the body and leaves some form of entrance wound. Typical penetrating trauma includes gunshot and stab wounds. This type of wound is not generally incurred in an automobile collision [Pike, 1990] due to modern developments in vehicle interiors, such as the use of softer plastics rather than steel for trim components.

The following section outlines several common thoracic injuries in automotive medicine, including rib cage fracture, heart contusion and cardiac tamponade, pulmonary injury, pneumothorax, hemothorax and traumatic rupture of the aorta. Addition the abbreviated injury scale, a method used to measure injury severity, is outlined.

2.3.1 Abbreviated Injury Scale

The Abbreviated Injury Scale (AIS) was developed by the American Association for Automotive Medicine as a system to classify injury (originally injuries from automobile crashes) into one of seven categories, based on factors such as threat to life, treatment cost, permanent impairment and quality of life post injury. While it is explicitly stated that a particular AIS score is not strictly driven by the survivability of such an injury, there is a strong correlation between the AIS score and mortality of an injury [Gennarelli and Wodzin, 2005]. The scale has been updated several times since its inception in 1971, with the most recent update being released in 2005 [Gennarelli and Wodzin, 2006]. This scale identifies all injuries by a six digit identifier, followed by a single digit to describe the severity. The first digit refers to the body region which was injured as outlined in

Table 2.1. The next five digits are used to classify the specific injury. For example, a superficial laceration to the face has an AIS code of 210602.1, while a rupture of the left ventricle has and AIS code of 441014.6.

Table 2.1: AIS coding of body regions

Body Region	First AIS Digit
Head	1
Face	2
Neck	3
Thorax	4
Abdomen and Pelvic Contents	5
Spine	6
Upper Extremities	7
Lower Extremities, Pelvis and Buttocks	8
External and Thermal Injuries	9
Other Trauma	0

Table 2.2 shows the AIS score with the severity of each level and an estimate of the fatality rate for at each score. The 'Fatality Range' column shown in this table is reported from several studies reviewed by Pike [1990], who credits the discrepancies in fatality rates to these studies using different medical databases and statistical methods.

Table 2.2 : AIS scores and approximate fatality range [Pike, 1990]

AIS	Severity	Fatality Range [%]
1	Minor	0.0
2	Moderate	0.1 - 0.4
3	Serious	0.8 - 2.1
4	Severe	7.9 - 10.6
5	Critical	53.1 - 58.4
6	Virtually Unsurvivable	

Table 2.3 shows an example of a small number of thoracic injuries and their corresponding AIS scores.

Table 2.3 : Thoracic injuries and corresponding AIS values [Cavanaugh, 2000]

AIS	Rib Cage Injury	Soft Tissue Injury
1	Single Rib Fracture	Skin abrasion, contusion, laceration
2	2 - 3 Rib Fractures, Sternum Fracture	major skin laceration, partial thickness tear of bronchus
3	>4 Rib Fractures, 2 - 3 Rib Fractures with hemothorax or pneumothorax	minor heart contusion, unilateral lung contusion
4	>4 Rib Fractures with hemothorax or pneumothorax, Flail chest	severe heart contusion, intimal tear of aorta
5	Bilateral Flail Chest	major aortic laceration, heart perforation, ventricular heart rupture

Because AIS provides a single metric to assess the injury incurred by an occupant, it has traditionally be used in developing ATDs and injury criteria as a guideline to what is an acceptable risk to an occupant. An AIS of 4 is seen as life threatening [King, 2000] and as such, AIS 3 (and occasionally AIS 4) is often the level of injury that is the cut-off deemed to be acceptable risk for an occupant in a collision.

One of the drawbacks in assessing injury with AIS is that multiple injuries are not taken into account. Two common methods of addressing this are the Maximum AIS (MAIS) and Injury Severity Score (ISS) systems. The MAIS system simply reports the maximum AIS score of any injury that the patient receives. This system has the advantage of being simple to report and simple to work with when doing epidemiological studies, unfortunately this system does not differentiate how multiple injuries affect the overall harm observed by the patient. The ISS is calculated by squaring the AIS of the three most injured body regions. This provides a score between 0 and 75. Any AIS 6 injury automatically sets this score to 75 [Gennarelli and Wodzin, 2005]. The advantage of this system is that multiple severe injuries have a greater effect on the score and therefore ISS provides some sense of the overall injury sustained by the patient.

2.3.2 Rib Fracture

Rib fracture occurs when a direct impact to the rib results in bending stress. Essentially the ribs act similar to curved beams and often fail due to this significant bending load. Because bone generally has lower failure strength in tension than compression, ribs tend to fail on the side of the rib in tension. The most common site for rib fracture is the point of impact and the posterior curvature (angle) of the rib, which is the location of greatest curvature [Pike, 1990]. In general the fourth rib and below are fractured more frequently than the higher ribs, and a fracture of the first rib is a sign of severe trauma [Trinkle and Richardson, 1981]. While a rib fracture is not, in and of itself, a very severe injury (it is similar to any other bone fracture) the proximity of the rib to so many life sustaining organs increases the risk associated with this type of injury. Puncture of the heart, lungs, or great vessels is possible and therefore makes this type of injury quite dangerous [Pike, 1990].

Flail chest is a condition that results when several adjacent ribs are fractured in multiple locations. Essentially the structural integrity of the chest wall is compromised and a section of the wall is free to move separate from the rest of the ribs. When a patient has incurred flail chest, the section that has broken away from the chest wall moves inwards during inspiration and outward during exhalation. This motion is counter to the motion of the rest of the chest and reduces the efficacy of respiration, causing pain during breathing [Peters, 1985].

2.3.3 Heart Injury

The two most common injuries to the heart are cardiac temponade and myocardial contusion [Trinkle and Richardson, 1981]. Cardiac temponade occurs when a laceration of the heart causes the pericardium to fill with blood. This blood increases the pressure surrounding the heart thereby reducing the ability of the heart to effectively pump blood to the rest of the body. This laceration from the heart can occur if the sternum is pressed inwards and the heart is "pinched" between the sternum and spine. It has also been shown that there is a greater risk for rupture of the heart if the heart is filled with blood (ie. at the end of the diastole phase of the cardiac cycle) [Roberts and Beckman, 1970].

Myocardial contusion is a bruising of the middle layer of muscle tissue in the heart (the myodcardium). Contusion to this muscle can lead to changes in the cardiac cycle which, if severe enough can cause cardiac arrest. This is quite different from a condition known a commotio cordis, which is another form of blunt trauma which leads to cardiac arrest. This condition arises due to a blunt impact to the chest which occurs during the rise of the t-wave of the cardiac cycle. This type of injury often occurs to athletes in sports such a baseball, hockey and cricket, when the athlete is hit by the ball or puck [Geddes and Roeder, 2005]. There is no physical change to the heart tissue in commotion cordis, unlike myocardial contusion.

2.3.4 Traumatic Rupture of the Aorta

Traumatic Rupture of the Aorta (TRA) is a disruption of the blood flow from the heart to the rest of the body due to a tear, either partial or complete, of the aorta. This injury frequently occurs due to a transverse tear near the region known as the aortic isthmus. In this region the aorta is well attached to the sub clavian artery and this attachment is thought to increase the stress on the aorta in this region. Despite a significant amount of work, the mechanism of this injury is still not clearly understood, however a series of impact tests have shown that axial stretching of the aorta during impact is present in cadaveric tests that reproduce this type of rupture [Hardy et al., 2008]. This injury is quite uncommon in the absolute sense, however tearing of the aorta is present in between 10% and 20% of all automotive fatalities [Viano, 1983] and the survival rate is quite low, with a 9% scene survival rate and 1.5% overall survival rate of diagnosed cases [Richens et al., 2003].

2.3.5 Lung injury

A common injury resulting from blunt impact is contusion (bruising) and laceration of the lung tissue. A contusion of the lung is caused by rupture of the alveoli, causing fluid to accumulate in the lungs which can lead to reduced lung function. This reduced lung function causes a lack of oxygen throughout the body and thus can be an extremely dangerous injury. This injury is also common in survivors of explosions. In addition to the microscopic contusion, macroscopic tears of the lungs (laceration) may also cause interruption of basic lung functions. These injuries can occur during penetrating thoracic trauma, but may also occur when a portion of a fractured rib enters and tears the lung tissue.

Pneumothorax and hemothorax are the terms used to describe an injury where either air or blood, respectively, enters the pleural sac. Hemothorax is often the result of physical trauma, whereby the pleural sac is punctured and a blood vessel of the lung is lacerated allowing blood to pool in the lung cavity [Cavanaugh, 1993]. Similarly, pneumothorax occurs when ambient air is allowed to enter the pleural cavity via a tear in the pleural sac. A very dangerous type of pneumothorax is referred to as tension pneumothorax. In this injury air enters the pleural space from the lung, however during exhalation the tear closes, essentially acting as a one way valve allowing the pressure in the pleural space to increase. This increasing pressure causes the lung to lose the partial vacuum in the pleural cavity necessary for respiration [Pike, 1990].

A combination of these two conditions is often termed hemopneumothorax. Additionally these condition as can be either unilateral, effecting only a single lung, or bilateral effecting both lungs. With the accumulation of air and/or blood within the pleural cavity, force is exerted onto the lung reducing the ability of the lung to expand during regular respiration, and can lead to a collapse [Pike, 1990].

2.4 Human Surrogate Impact Tolerance Testing

There is a need to use a representative surrogate when attempting to identify the loads which can be imparted onto the human body before serious injury occurs. While initial testing the field of impact biomechanics was performed on live test subjects (often the researchers themselves), these loads were often considered to be “safe” and would only capture the kinematics of the human body for a given loading case. To truly understand the loading conditions that would be

required to cause serious harm to the human body, cadaveric or Post Mortem Human Subjects (PMHS) are often used. In addition to cadaveric specimens, animal testing has been carried out on primate, bovine, dog [Patrick and Sato, 1970], rabbit [Lau and Viano 1981], and porcine [Kroell et al., 1986; 1981] surrogates. This form of testing allowed the study of physiological response that would not be possible with cadaveric testing, such as bruising and muscle response [Patrick and Sato, 1970].

In order to account for basic anthropometric variation of the human population there is the need for the scaling of results obtained from cadaveric testing. In general, this process involves creating a non-dimensionalized ratio based on a physical characteristic of the cadaver (such as the mass of the specimen) and some reference characteristic, often of the 50^{th} percentile male. Two specific methods for this type of scaling were described by Eppinger el al. [1984] and Mertz [1984].

Generally there are two types of testing that are performed to test the response of human surrogates: pendulum impact and sled testing. Pendulum testing is often performed when specific body regions are of interest, while sled testing is primarily used to develop understanding of the response of the body to what is described as "full engagement" with the impacting device. The following sections will outline some of the testing that has been performed to assess the response of the human chest when subjected to pendulum and side sled impact.

2.4.1 Pendulum Testing

The earliest pendulum testing was performed by researchers investigating impacts to the sternum resulting from unrestrained occupants in frontal collisions impacting non-collapsible steering wheels. In one of the earliest studies [Kroell et al., 1971], a 6" diameter wooden impactor of varying mass mass was sent at speeds between 22.5 kph and 51.5 kph into the sternum of unembalmed cadavers. The force-deflection characteristics of each specimen, along with any skeletal or soft tissue damage (lacerations) were recorded. The main outcome of this study was that age, gender and physical stature of the subject resulted in large variation in the response, and that the use of PMHS filled gaps in the knowledge from sub-injurious human testing and animal testing. Following this work, more testing was carried out [Kroell et al., 1974], in which the

authors confirmed the velocity dependant (viscoelastic) property of chest compression, and developed linear correlations between maximum impactor force and AIS and maximum chest compression (deflection of chest divided by the original chest depth) and AIS. The compression correlation was considered to be a better indicator of injury than the peak force, with r^2 values of 0.772 and 0.524 respectively.

In the late 1980s, researchers at Wayne State University performed a series of side impact pendulum tests on cadaveric specimens [Viano et al., 1989a] and swine [Viano et al., 1989b]. In these tests the specimens were impacted with a 15 cm diameter circular pendulum with a mass of 23.4 kg. These tests were performed at 4.3 m/s, 6.7 m/s and 9.4 m/s. For the cadaveric specimens, the injury of primary interest was rib fracture, while for the porcine specimens, soft tissue damage was the primary injury of interest. In both series of tests, the compression, VC (instantaneous velocity of compression times the compression), thoracic spine acceleration, rear-side rib acceleration and pendulum force (acceleration times mass) were measured. Additionally logistic regression was performed on the results for both the AIS 3+ (4 or more rib fractures) and the AIS 4+ case (9 or more rib fractures) and a series of risk curves were created. For the human subjects, it was found that VC had the best ability to predict injury, although compression was found to be a good indicator for low speed impacts while acceleration was found to be a better indicator of injury at higher velocities. It is important to note that in these tests, the pendulum did not impact in a purely lateral orientation, instead the cadaver was rotated approximately 30^o to ensure that the pendulum impacted the cadaver through the center of gravity of the specimen.

Following this work, impact testing involving a limited stroke pendulum was presented [Chung et al., 1999]. Until this point the pendulums used in this type of testing had been free flight, which Chung argued, was not representative of a typical side impact. In these limited stroke tests, a 6 inch diameter, 50 kg impactor with a maximum stroke of 305mm was used to impact the cadavers at 5.6 m/s. In two of these tests, a piece of foam was inserted between the face on the impactor and the cadaver's thorax to assess the effect of this type of padding. The pendulum was allowed to accelerate to its peak velocity in the first 152 mm of travel, followed by 102 mm of free flight or contact with the foam padding. The remaining distance allowed for engagement with the specimen. In these tests the subject was impacted with purely lateral force. The researchers found that rib deflection and T12 acceleration showed good correlation to injury,

while TTI (the average peak acceleration of the lower spine and struck-side ribs) and VC showed no correlation to injury. It is important to note that the authors attributed the weak correlation to VC and TTI due to the small sample size (6 tests) and to the use of rib fracture rather than soft tissue damage to define injury. The author also noted that, in general, there was less evidence of lung and liver damage in cadaveric tests than one would expect in living subjects due to lack of blood flow and tissue function. In the 2 specimens which had padding placed between their ribcage and the face of the impactor, the compression was higher, while the TTI was lower, with the VC values unchanged. Additionally it was found that the presence of padding increased the number of rib fractures.

2.4.2 Sled Testing

The first use of side-sled testing was performed by researchers at the University of Heidelberg [Kallieris et al., 1981]. In these tests, a frontal impact sled was reworked for use in the lateral direction. This sled used a drop weight tied to a gear reduction to allow the sled to reach the desired test speed, followed by a rapid deceleration. The cadaver was placed on a bench like seating surface 90^{o} to the direction of travel which was coated with a low friction coating. When the sled came to rest, the cadaver slid down the bench and into a series of end plates. Four test conditions were used in this testing; a 15 mph rigid wall test, a 20 mph rigid wall test, a 20 mph test into a urethane foam pad, and a 20 mph test into a wall with a fiberglass pad. Accelerations of the ribs, head, spine and pelvis were measured and time history plots were created. This study found that the responses were consistent for a given loading case despite a wide range in injury (rib fracture) outcomes. This work was later extended with the addition of force plates to the wall to measure the force response during the impact [Marcus et al., 1983]. It was found that with no scaling to account for occupant stature, there was a dramatic variation in force response. An image of the end plate configuration is shown in Figure 2.4, along with subsequent designs used by other researchers.

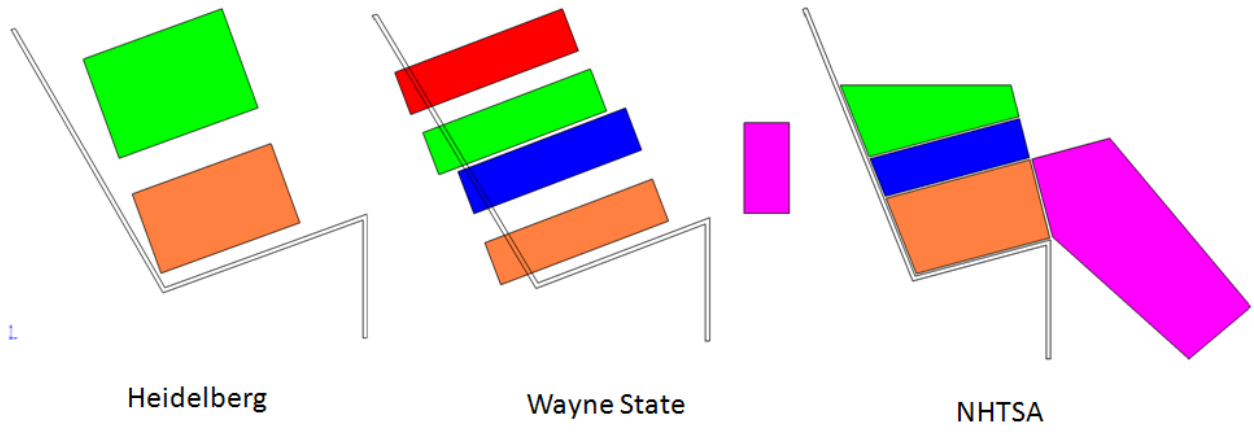

Figure 2.4: End plate configuration of side test sleds

This work was followed by a series of tests performed at Wayne State University. Modifications were made to the design of the end plates to better isolate the force imparted to specific regions of the body. Figure 2.4 shows this configuration, with the shoulder plate in red, the thoracic plate in green, the abdominal plate in blue, the pelvic plate in orange and the knee plate in purple. In the first series of tests [Cavanaugh et al., 1990] twelve cadavers were tested in one of three different configurations; a flat rigid wall, a rigid wall with a 6 inch pelvic offset, or a flat padded wall. The velocities used in this series of testing were between 6.7 m/s and 10.5 m/s. In addition to the instrumentation used by Marcus et al., high-speed video was taken during testing to measure chest deflection. In these tests, it was found that rib cage compression at T5 and VC_{max} at this level were the best predictors of injury and that most acceleration based criteria did not perform as well at predicting injury. The introduction of a pelvic offset did not reduce thoracic injury and while soft foam seemed to aid in the prevention of injury, there was a point (roughly 20 psi) where some older subjects were injured while younger subjects were not, introducing the idea of a necessity for a trade off in designing the interior of a vehicle. It is important to note that in this series of testing AIS levels were normalized with respect to subject age using the following equation:

$$AIS_{Normalized} = AIS_{Actual} - 0.025\,(Age - 45)$$

(Equation 2.1)

A series of testing was also performed by researchers at the Medical College of Wisconsin as part of a major research program sponsored by NHTSA during the development of new side

impact legislation. One of the major differences between this work and previous experiments was the use of a chest band designed to measure the deflection contours of the test subject's chest, originally developed by Eppinger [1989]. Work was presented that showed that the chest band was a viable method to measure the desired chest contours in a non-invasive fashion [Pintar et al., 1996]. Following this validation, work was presented on testing carried out on the NHTSA sled at 2 different speeds; 24 kph and 32 kph [Pintar et al., 1997]. The cadaveric specimens were instrumented with accelerometers on the 4^{th} and 8^{th} rib and the 12^{th} thoracic vertebra, along with the chest bands to measure thoracic deflection. In this series of tests the impacted wall was configured to be either flat and rigid; rigid with a 12 cm pelvic plate offset or flat with 10 cm of foam with a compressive stiffness of 103 kPa covering the end plates. The results of this testing indicated that pelvic fracture was likely to occur with the offset wall configuration due to excessive pelvic force as measured by the pelvic load plate, though loads to the abdominal and thoracic load plates were reduced. For the padded wall cases the measured accelerations were lower than for the rigid wall case. A number of injury criteria were evaluated using logist regression and found that TTI was a good measure of injury while VC was not though the authors commented that VC was generally meant to capture soft tissue damage, while in this testing only skeletal injuries were considered. This work was further extended later to investigate oblique angle impacts due to their prevalence in real-world side impacts. This was done by rotating the abdominal and thoracic force plates on the NHTSA sled inward by between 20^{o} to 30^{o} [Yoganandan et al., 2008]. The results of these tests indicate that chest deflection was greater for the oblique impacts than purely lateral loading.

2.5 Thoracic Injury Criteria

Ideally, one would like to be able to perform local measurements on tissue as it is damaged to identify the mechanical loading that causes injury. For example work has been performed in an attempt to measure the strain which an aorta can be subjected to prior to failure [Shah, 2007], and simulate the strain, strain rate, and local pressure which correlates to lung damage [Yuen et al., 2008]. Unfortunately, it is impractical to work at this level of detail due to insufficient experimental work to characterize the resistance of all organ and cell level tissue to injury and the impracticality of measuring this level of detail during a crash test. Due to the impracticalities

of assessing tissue level injuries in side impact testing some form of global response is necessary to infer injury.

To assess the safety of a vehicle, a human surrogate which provides uniform, repeatable results and is reusable necessitates the use of anthropometric test devices, also known as crash test dummies. While these dummies, respond in a similar fashion to actual human occupants in their global response, their internal structure (steel ribs, dampers to mimic internal organ response, etc.) preclude the ability to use more sophisticated local measurements to assess injury. Global responses have traditionally been measured by standard engineering testing instrumentation, such as load cells, accelerometers, and potentiometers. Values based on these measurements have been correlated to injury from post mortem human subject testing. This is generally done by performing a test on a PMHS, measuring the response of interest, then performing an autopsy to see what injuries have been incurred by the test specimen, such as broken ribs, lacerations and punctures of soft tissue. These injuries are then related to an AIS score which is back-correlated to the response measured during the test. These injury threshold values are then transferred to their respective ATDs.

The major thoracic injury criterion that have been used to assess thoracic injury include acceleration criteria, chest deflection and compression, the thoracic trauma index (TTI), and the viscous criterion (VC). These criteria are outlined in the sections below.

2.5.1 Acceleration

The first step in attempting to utilize a global criteria to test the limits of the human body to impact injury were developed by Col. John Stapp of the United States Airforce. In his now famous experiments, volunteers were placed on a sled propelled by rocket power and decelerated, in the most severe cases, from 174 mph to a standstill in 27.5 feet [Stapp, 1957] (approximately 37 G average deceleration). During these tests, higher levels of acceleration were tested on swine and primate test subjects. It was quickly discovered that the survivability of extreme deceleration was dependant not only on the peak acceleration, but also the amount of time that the subject was subjected to this loading. Another important outcome from this research was that a highly restrained occupant could survive a much more aggressive impact due to transmission of force through relatively ‘hard points’ of the body such as the pelvis and

shoulder [Eiband, 1959]. As work continued in the impact biomechanics field, the level of instrumentation increased to the point that multiple accelerometers were placed on various boney structure throughout the subject. In nearly every case of the cadaveric testing discussed in Section 2.4, accelerometers were installed at various locations on the specimen, most often the head, impacting side ribs, and spine. In most crash test dummies, there are also accelerometers at these locations to allow for some level of comparison between cadaveric studies and testing involving crash test dummies.

Due the extensive amount of research that has been carried out to test the human tolerance to acceleration, chest acceleration continues to be used in a number of regulatory tests throughout the world. This includes the American frontal impact test, where dummies representing the average (50^{th} percentile) male must not sustain an acceleration of over 60 G for more than 3 ms. Additionally, a new side impact test has been introduced recently in which a small female (5^{th} percentile) dummy is place in a vehicle that is impacted into a rigid pole. In this test the lower spine acceleration of the dummy must not exceed 82 G [Carhs, 2009].

2.5.2 Thoracic Force

The use of force to quantify injury in impact was first driven by chest impacts into non-collapsible steering wheels. Early experimentation in this area involved using a frontal sled to mimic a frontal car crash where an unrestrained cadaver was placed on a sled that was decelerated from speeds between 10 mph and 20 mph [Partick et al., 1967]. This study found that rib fractures were present at loads above 1340 lb (5.9 kN). During side impact pendulum testing performed in the 1980s, [Viano et al., 1989a] risk curves were developed to assess the potential for injury based on the force calculated by multiplying the mass of the pendulum with its accelerometer trace. These curves are shown in Figure 2.5. It is important to note however, that in this testing, VC and chest compression were found to be better indicators of injury. Figure 2.5 also shows the logist analysis of the thoracic plate force in the side sled study by Cavanaugh et al. [1990].

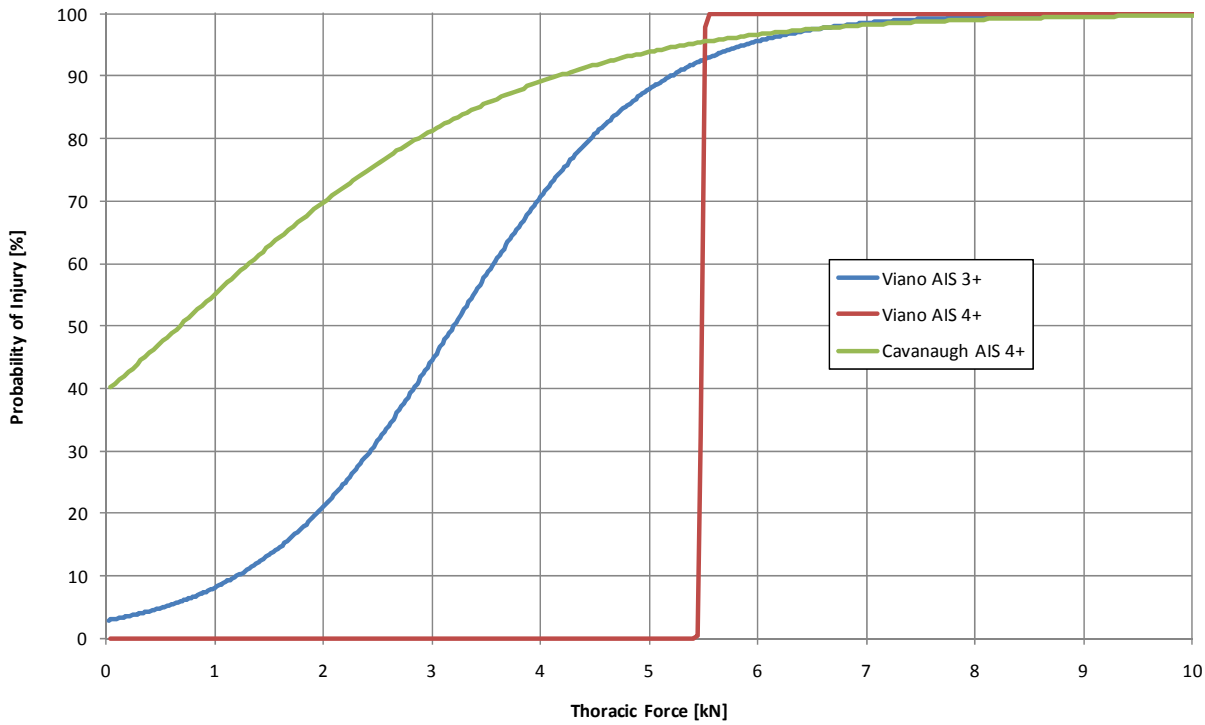

Figure 2.5: Cadaver thoracic force risk curves

Of the sled tests discussed in section 2.4.2 which included force measurement on the end plates, none found that thoracic force was the best indicator of injury. Despite this, one of the primary documents used to assess the biofidelity of ATDs relies heavily on pendulum force-deflection response to compare the response of cadaveric specimens and ATDs [ISO, 1999]. Additionally, the federal regulation regarding the calibration testing of crash test dummies prior to regulatory crash tests involves using a force-time history.

2.5.3 Chest Deflection and Compression

It was discovered that force and acceleration alone could not adequately be used to define a subject's likelihood of injury [Neatherly et al., 1975]. One reason that was proposed for this was that measuring acceleration does not differentiate between whole body acceleration and local acceleration due to differential motion between body parts. Chest compression was often measured by analyzing high speed video of an impact event [Kroell et al., 1971; 1974; Cavanaugh et al., 1990, 1993] and, more recently by a chest band using a series of steel bands and strain gauges to measure the curvature of the band at any given location on the chest

[Eppinger, 1989]. This system was found to give results with a mean difference of 2% when compared to video analysis techniques [Pintar el al., 1996]. For measuring deflection on ATDs string potentiometers are often used [FTSS, 2005] though more modern ATDs are beginning to use an optical infrared LED system [FTSS, 2007].

Often chest deflection, defined as the distance the chest deflects from its undeformed state (a length measurement), is normalized and reported as a compression value (a percentage). Generally with cadavers, this measurement is based on the exterior dimension from the skin above the sternum to the skin above the spine for frontal cases, and the skin on either side of the ribs for the side case. Occasionally, the half-thorax compression is used in which a plane between the sternum and spine is defined and compression is based on the change in length between the outer surface of the rib and this plane. With side impact ATDs the number that is generally used for compression is the distance between the steel surfaces of the 'ribs' of the dummy (or half this value for half thorax compression). This means that the compression of the foam which general sits on outside of the thoracic cavity of the dummy is not considered. In some cases, this is accounted for with a scaling factor [Cichos et al., 2006].

A number of studies have looked at maximum cadaver chest compression to create correlations with injury. Risk curves were created by Viano [1989] in their side pendulum studies, Cavanaugh [1990] with the Wayne State side impact sled, and Pintar et al. [1997] with the NHTSA side impact sled. The risk curves generated from these tests are shown in Figure 2.6.

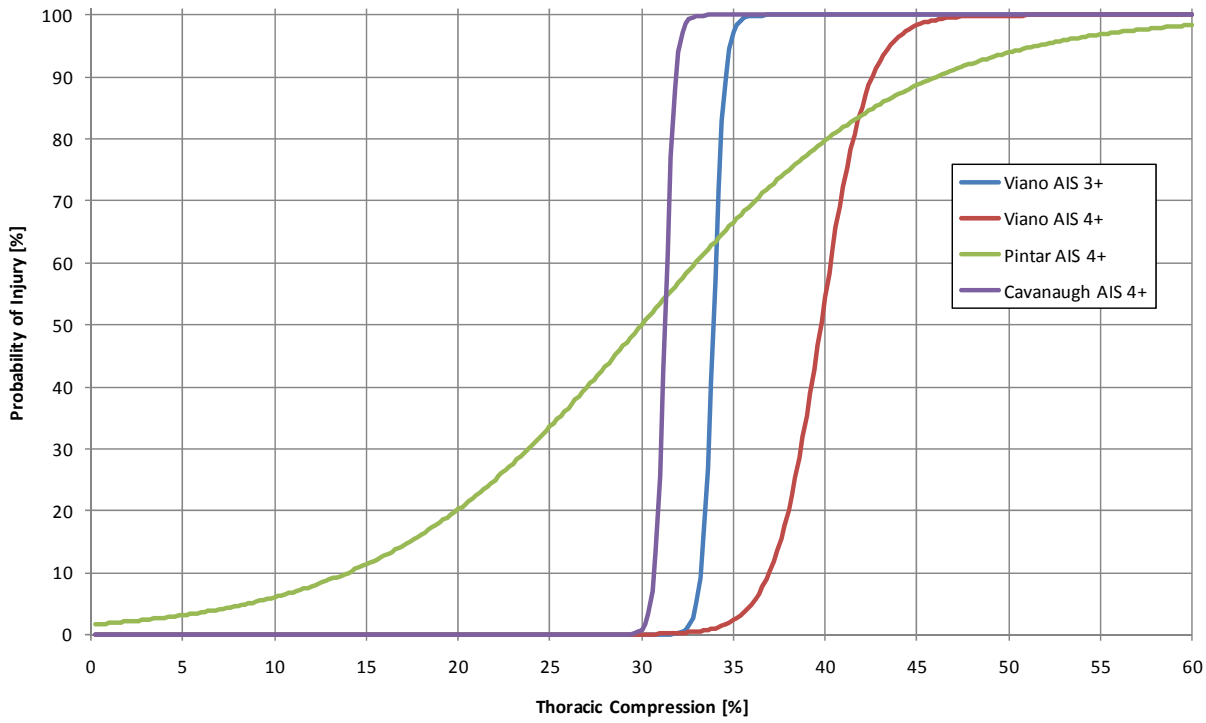

Figure 2.6: Cadaver thoracic compression risk curves

In Viano's work, it was found that compression was a very good indicator of thoracic injury, though in a series of tests performed on anesthetized swine focusing more on soft tissue injury [Viano et al., 1989 b], compression was found to only be a good indicator for low to mid speed impacts. Injuries resulting from higher speed impacts (pendulum speeds of 8.2 m/s) were better predicted with force and acceleration criteria in those tests indicating that chest compression may be a better indicator for 'crushing injuries'. The authors further explained that while a number of tests in frontal impact had shown a very strong correlation between compression and thoracic injury, the lung may act as a 'cushion' to the heart and prevent pulmonary damage. This is unlike the frontal case where the heart may become trapped between the sternum and the spine and may therefore be severely damaged. In the work by Cavanaugh et al. [1990], compression performed very well as an indicator of injury. It is important to note that in this study, compression was measured based on the half thorax method, unlike in Viano's work which used the full thorax measurement. Additionally, this work measured deflection using a chest band at the T5 vertebra, while Viano used film analysis. Cavanaugh noted these differences, and pointed out that compression performed well in both types of tests despite their differences in method. In

the side sled testing of Pintar et al. [1997], compression (based on full thorax measurement at two chest band locations) was found to not be a particularity good predictor of injury. The wider shape of the sigmoid function from this test may be due to the use of multiple chest bands which were better able to capture the maximum thoracic deformations and thus create more scatter between tests where there was an AIS 4+ level injury and tests where there was not an AIS 4+ injury.

Prior to implementation of a new federally mandated side impact crash test, NHTSA performed a statistical analysis based on the series of cadaver side impact tests performed on the NHTSA sled [Kuppa et al., 2003]. This analysis found that when age was taken into account, chest compression was the best indicator of injury. Using this information, they further developed a series of risk curves based on the EuroSID2 with rib extensions (ES-2re), which was the dummy proposed to be used in the regulatory test. This was done by performing the same sled tests on the dummy as were performed on the cadaveric specimens and attempting to correlate the response of the ES-2re with the cadavers. It was discovered that the deflection response of the ES-2re was significantly different than that of the cadavers. Despite this, the authors were able to develop risk curves based on the response of the ES-2re dummy, which are shown in Figure 2.7. A re-analysis of this data was performed prior to the implementation of the latest New Car Assessment Program (NCAP) for side impact, which uses a slightly different curve to predict injury (also shown in Figure 2.7). Very little information was given in the final rule as to the reason behind this change [NHTSA, 2008a]. It is important to note that the deflection presented in Figure 2.7 is based on an ATD half thoracic distance of 140 mm.

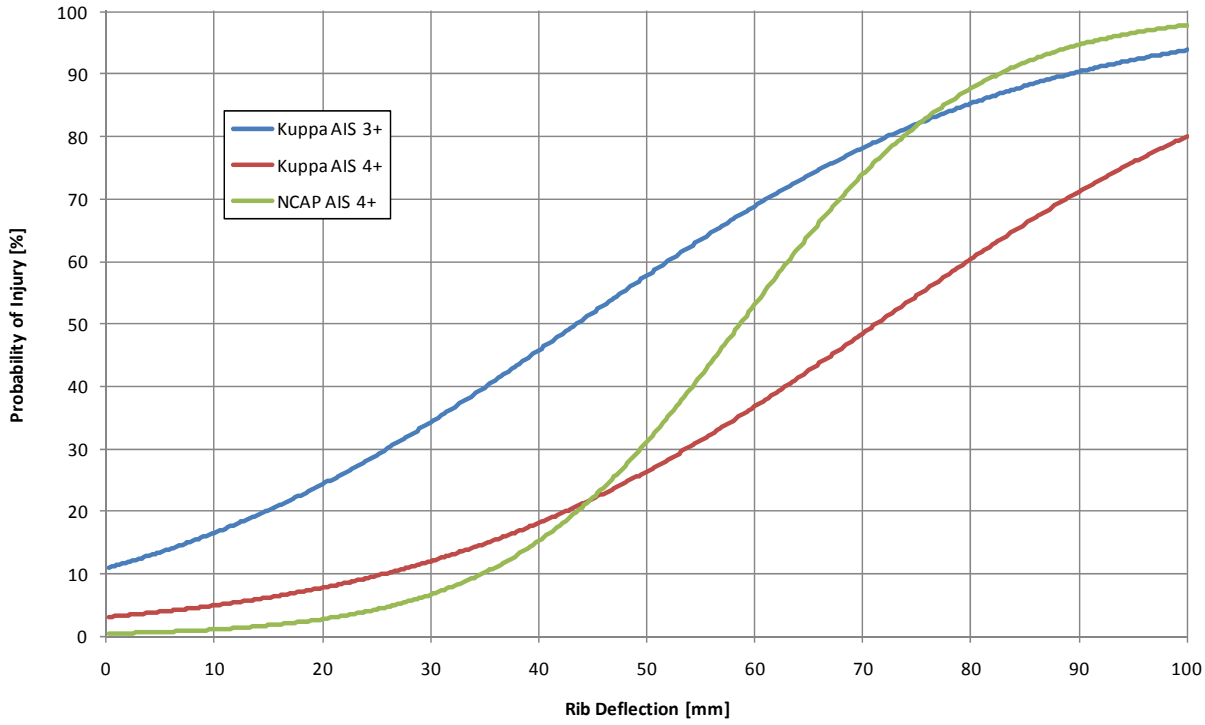

Figure 2.7: Injury risk curves for ES-2re rib deflection

The limit of chest deflection allowed during the regulatory side impact test performed in Eurpoe is 42 mm for the 50th percentile male occupant while in the American standard (starting with 2011 model year vehicles) the maximum allowable deflection is 44 mm [Carhs, 2009].

2.5.4 Thoracic Trauma Index

The Thoracic Trauma Index (TTI) is an acceleration based injury criteria developed alongside the initial American side impact regulatory test to measure injury. Using a dataset of sled, pendulum and full car impact tests on cadaveric specimens, researchers looked at accelerations of the upper struck side rib, T12 vertebra and pelvis to attempt to determine the best predictor of injury [Eppinger et al., 1984]. The authors were aware that age and cadaver mass could affect the probability of injury, so these effects were factored into the injury metrics studied. It was found that maximum upper (fourth) rib and T12 accelerations were the best predictors of injury, so these maximum accelerations along with age and mass were used in the final development of the injury criterion. Following this work, additional cadaver tests were performed in a vehicle undergoing a full scale crash test, along with a series of tests using an ATD (USSID) under

similar conditions [Morgan et al., 1986]. In this testing, the upper (fourth) and lower (eighth) rib of the cadavers were instrumented with accelerometers to better capture the kinematics of the occupant. It was decided that with the new rib acceleration available, the maximum of both ribs would replace the maximum upper rib acceleration in the criteria proposed by Eppinger et al. This form of TTI is described by the equation:

$$TTI = 1.4 \times Age + 0.5 \times (Rib_y + T12_y) \times \frac{Mass}{Mass_{Std}}$$

(Equation 2.2)

Where 'Age' is the age of the cadaveric specimen in years, Rib_y is the maximum lateral acceleration of either the upper or lower rib, $T12_y$ is the maximum acceleration of the T12 vertebra, Mass is the mass of the cadaveric specimen, and $Mass_{Std}$ is 75 kg. A change to this formulation was suggested by Morgan et al. [1986] due to 'an inherent and natural attenuation of the peak upper rib'. This formulation uses the maximum of either the lower acceleration or a normalized function of the upper rib of the form;

$$Rib_{UpperNorm} = 1.3 \times Rib_{Upper} - 2.02$$

(Equation 2.3)

It was found that using this TTI formulation, the probability of injury distribution was better able to explain rib injury, and was therefore recommended for future use. It should be noted that unlike the other injury criteria described here, TTI has only ever been used to assess injury due to side impact. This is due to the lack of physical meaning between rib and spine accelerations in frontal impact (though an analogy could be drawn between sternum and spine acceleration).

In the side sled testing performed by Cavanaugh et al [1990], the TTI was measured and reported. It was found that TTI had a worse correlation to injury than thoracic force, left rib lateral acceleration, left rib compression, and viscous response. Pintar el at. [1997] also studied TTI in their sled testing and found that TTI was a better indicator of injury than compression and viscous response. They suggest a robustness of this criterion due to their rigid wall testing and the 'real world' vehicle testing used in the development of this criterion both finding it to be the best predictor of injury. In a critique of the criterion by Viano [1987], it was noted that the

predicted response given from TTI occurs very early in the response trace from the occupant, while actual injury to the thorax occurs after this response is predicted, indicating some disconnect between injury and the response of the occupant. Viano suggested that the use of some form of deformation based criterion would be a much better indicator of injury.

Figure 2.8 shows several risk curves developed by researchers mentioned previously. This plot clearly shows that the AIS 4+ risk predicted by Pintar and Morgan are nearly identical.

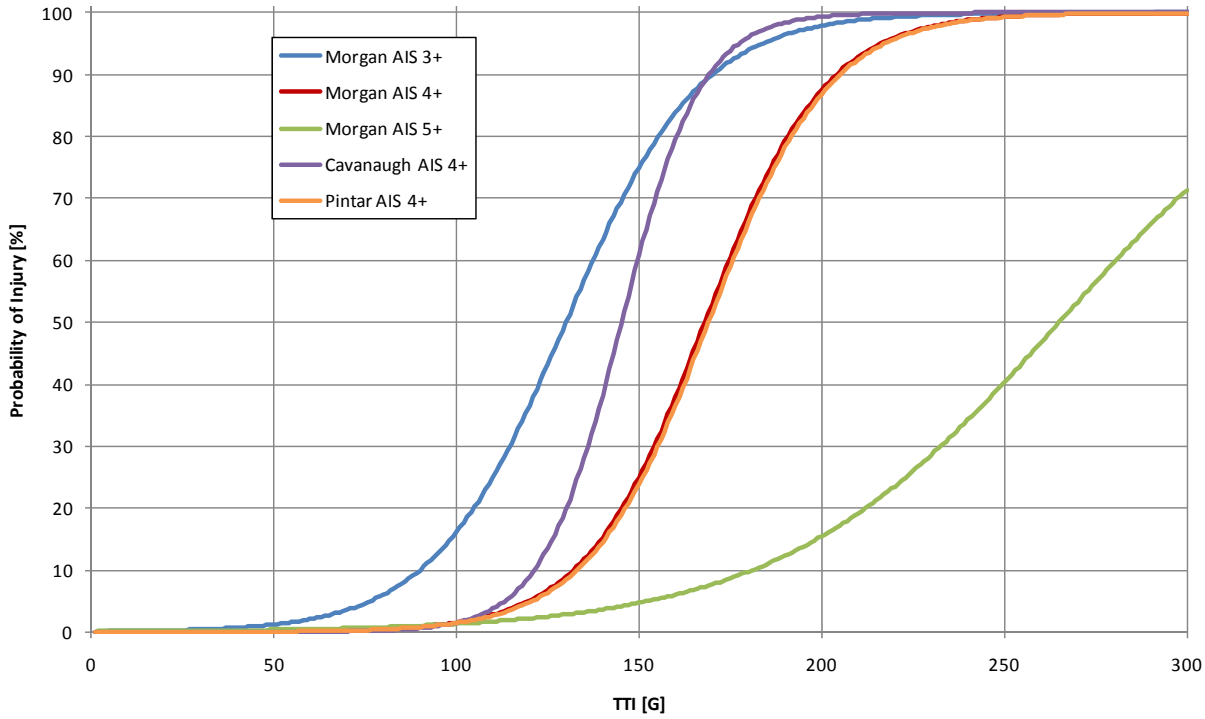

Figure 2.8: Cadaver TTI risk curves

TTI has been used to assess injury in American federal side impact testing since this testing was initiated. The pass/fail threshold for both front and rear occupants was set at 85 G for four door vehicles and 95 G for two door vehicles [Carhs, 2009]. Starting with model year 2011, this criterion was no longer be used in these tests, being superseded by the deflection criterion described previously.

2.5.5 Viscous Criterion

In a series of experiments on anesthetized swine, it was found that there was a higher level of injury for impacts from higher velocity pendulums, despite these pendulum impacts producing lower levels of chest compression [Kroell et al., 1981; 1986]. In these tests, the swine were impacted in a ventrodorsal direction (analogous to a frontal impact on the sternum of a human subject), with a rigid pendulum at speeds between 8 m/s and 30 m/s. To control the compression of the chest, the pendulum masses were changed according to the input velocity (21 kg for the 8 m/s impact, 10.4 kg for the 14 m/s impact and 4.9 kg for the 30 m/s impact). The researchers discovered that there was roughly an equal influence between the velocity of the impactor and the compression of the chest in predicting injury outcome. Due to the use of living subjects, soft tissue damage was investigated in this study. These soft tissue damages were seen at fairly low levels of compression provided that the velocity of the impactor was high. It was also found that the mortality rate was higher for increased velocity impacts of constant chest compression.

Following this work, further development was carried out utilizing these concepts. In Viano and Lau [1985], a mechanical analog of the human chest involving springs, masses and dampers, was analyzed in terms of energy absorbed during impact. This analysis pointed out that the energy absorbed by the viscous response material of the human body (the damper in the simplified analog) was dependent on the velocity history of the applied load, signifying the importance of the velocity of the chest wall during impact. A more formal definition of the Viscous Criterion (VC) was given in Lau and Viano [1986]. In the most common definition of VC, the normalized compression time history is multiplied by the differentiated deflection time history (velocity history). This produces what is termed the 'viscous response'. The number that is quoted as the VC or VC_{max}, is the peak value of this time history. A graphical representation of this process is shown in Figure 2.9. In addition to the definition of VC, this work also proposed an appropriate rage of velocity over which this criterion should be used. Essentially the argument was that for low velocity impacts (below roughly 3 m/s) and quasi-static loading, compression is more appropriate than VC in predicting injury because the response of the thorax is dominated by the crushing of tissue, and the viscous response is low. They also suggested that above 30 m/s VC is not necessarily valid due to the very low compression which is needed to cause injury in this

velocity regime. Above this speed, for ballistic and blast trauma, different injury criteria are required to accurately predict injury.

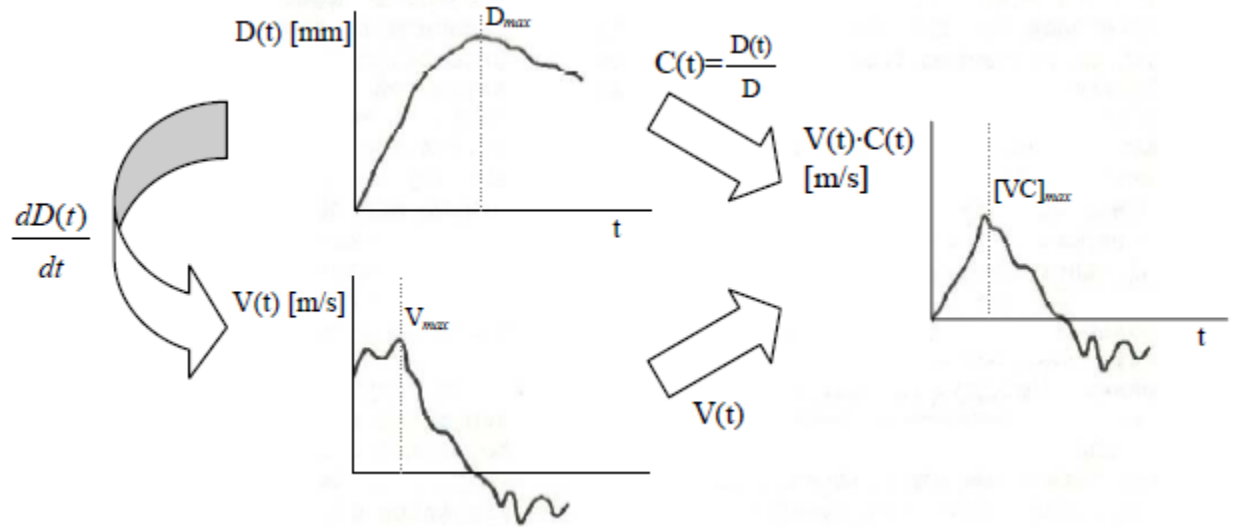

Figure 2.9: Graphical representation of VC [Lau and Viano, 1986]

Viano et al. followed this work with a series of side pendulum impact experiments on human cadavers to compare the predictive ability of VC to other side impact thoracic injury criteria [Viano et al., 1989a; Viano 1989]. In this study, VC_{max} was found to be a good predictor of injury. The authors suggest that VC is a better predictor of soft tissue injury than acceleration based and compression based criteria, in part, due to the timing of the maximum response VC occurring close to the time of soft tissue damage. Additionally the lack of rib intrusion does not necessarily mean that serious soft tissue damage has not occurred. They did however, note the importance of limiting the compression of the thorax to reduce crushing injuries. For this series of experiments, risk curves associated with VC were created for skeletal injury. These curves are shown in Figure 2.10. In the sled testing performed by Cavanaugh et al. [1990] and Pintar et al. [1997], the VC_{max} was studied along with several other injury criteria. Cavanaugh found that VC correlated well with injury and pointed out that both sled and pendulum testing performed by Viano et al. independently showed this to be the case. In the Pintar et al. findings VC_{max} was found to be a worse predictor of injury than TTI. This may have been partly explained due to VC being considered a better predictor of soft tissue injury than skeletal injury. The use of cadaveric specimens meant that many soft tissue injuries may not have appeared and the majority

of the high level AIS injuries in this study were from skeletal fracture. Both of these series of sled tests produced injury risk curves which are also shown in Figure 2.10.

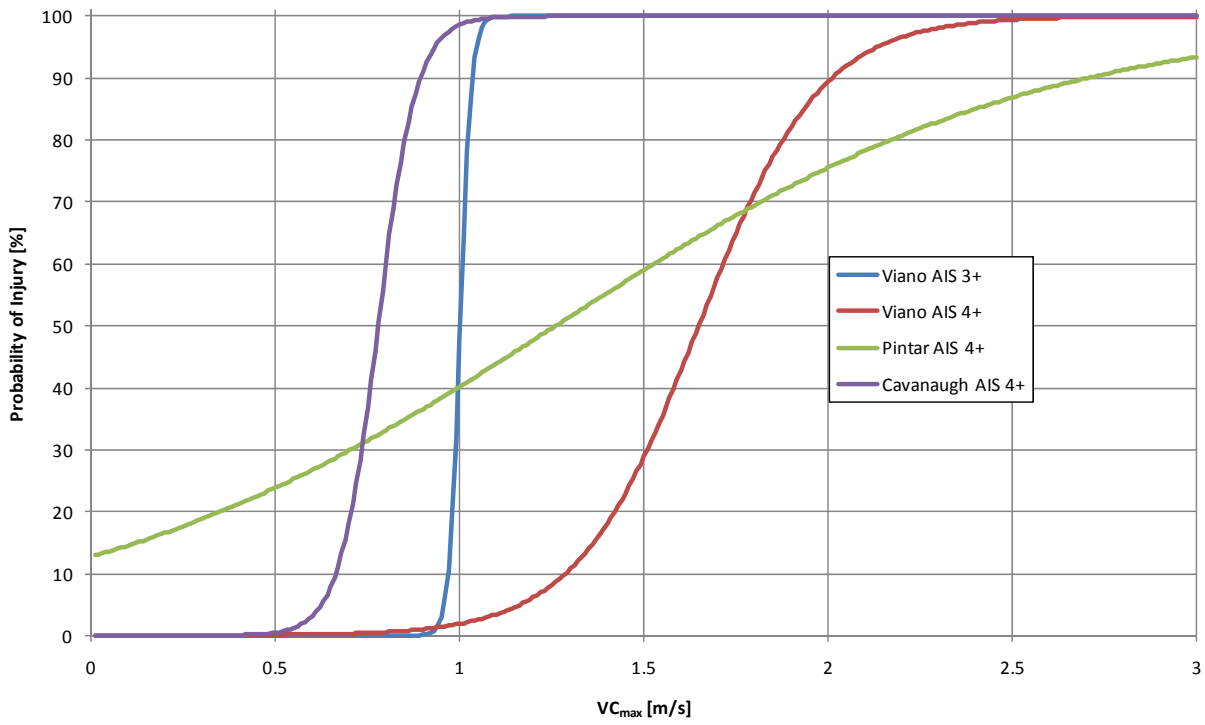

Figure 2.10: Cadaver VC_{max} side impact risk curves

VC_{max} is currently used as the thoracic injury criterion in side impact regulatory testing performed in Europe. For the 50th percentile male occupant the maximum allowable VC_{max} is 1 m/s [Carhs, 2009].

2.6 Anthropometric Test Devices for Side Impact

Beginning with the initial research into impact biomechanics, there was recognition of the need for analogs of the human body for various impact scenarios that would be too dangerous for volunteer subjects. This need led to the development of anthropometric test devices (ATDs) more commonly known as crash test dummies. The earliest ATD's were crude devices that mimicked the size and mass of various parts of the human body, but did not necessarily mimic the actual response of the human body subjected to impact loading. As these devices became more advanced, the interior structures changed to metallic ribs using spring and damper systems to allow the ATD chest compression to closely mimic the human body. Additionally, more

accelerometers and force transducers were added as dummies advanced to increase the amount of data collected from a given test. In general these devices are direction specific meaning that they are developed for a single direction of loading (front, side or rear). The initial development for side impact ATDs started with the development of the United States Side Impact Dummy (USSID), when early testing with the Hybrid III frontal crash dummy (the standard ATD used in frontal impact testing throughout the world) proved to be unsuccessful. A short time later, the EuroSID development began for use in European regulation. Both of these dummies were eventually used in regulatory testing in their region of origin, and starting with model year 2011, a modified version of the EuroSID (ES-2re) was used in the American regulatory tests. After the introduction of these two ATDs the BioSID was developed with the aim to improve biofideltiy (the ability to replicate human response) over the USSID and the ES. While BioSID was shown to have the best biofidelity for a side impact dummy available at that time, it was never adopted in any large scale regulatory testing. Most recently, the WorldSID was developed to further improve biofidelity and also to provide a single ATD for use throughout the world in side impact testing.

In assessing ATD biofidelity, the ISO standard 9790 [ISO, 1999] outlines tests ATD are to be subjected to based on a number of the cadaveric tests described previously. The individual test result is given a score of 10 if the dummy response falls within the corridor of the cadaveric specimens, a score of 5 if the response is outside these corridors by less than on corridor width and 0 if the response is outside of either of these corridors. A weighted sum of the individual test results is then compiled and a score between 0 and 10 is calculated, with a higher score being considered more biofidelic. It is important to note that even if the response of the ATD falls within these corridors, the lack of frangibility (ability to break) of ATDs, which is required to reuse the device, still leads to a certain amount of non-human like response.

This section outlines the development and testing of three side impact specific 50^{th} percentile male ATDs. While there are other side impact dummies, the three outlined below have been used in side impact modeling of thesis these and are thus more pertinent to the discussion of this work than other ATDs such as the BioSID or the SID-II.

2.6.1 United States Side Impact Dummy

Development of the United States Side Impact Dummy (USSID) was begun in the late 1970's when interest began in implementing a dynamic side impact protection test, which would eventually become the dynamic portion of Federal Motor Vehicle Safety Standard (FMVSS) 214 [Morgan et al., 1981]. The ATD was initially based off of a 50th percentile Hybrid II frontal impact dummy and developed by researchers at the University of Michigan. The arms from that dummy were replaced with foam blocks to reduce the complications that could arise with the interactions between the arms and interior trim in side impact [FTSS, 2010]. The thoracic region of this dummy is composed of 5 steel ribs covered in a foam material, shrink wrapped in urethane. A single adjustable damper is used to control the deflection characteristics of the thorax. Figure 2.11 shows a fully assembled USSID, while Figure 2.12 shows the geometry of the interior rib section with the foam padding removed.

Figure 2.11: Fully assembled USSID [FTSS, 2010]

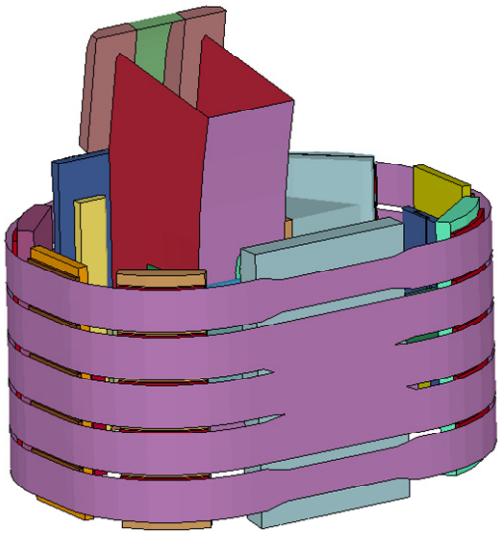

Figure 2.12: CAD of interior thoracic region of USSID

In its standard configuration, the USSID is instrumented with lateral accelerometers on the left side upper and lower ribs, the lower and upper thoracic spine and the pelvis. A triaxial accelerometer is located at the head CG, and a linear displacement transducer can be placed in the thorax to measure the middle rib deflection. Additionally, 6 axis load cells can be fit in the lumbar spine, the neck and the femur. The overall mass of the USSID is designed to be 76.5 kg and the erect sitting height is designed to be 899 mm [FTSS, 2010].

2.6.2 EuroSID

At roughly the same time that the USSID was being developed, the European Commission began development of the EuroSID, which was designed to be used in their regulatory test, ECE R95. There were several technical reasons why American regulators were unwilling to change to use the EuroSID, primarily due to binding of the ribs on the back plate of the dummy. This binding led to a 'flat top' in the rib deflection of the dummy, where the deflection would reach a maximum and stay at that level until the rib module rebounded. To prevent this binding a needle bearing rib guide module was designed, along with several other changes to various parts of the dummy. These changes led the developers to rename the dummy the EuroSID-2 (ES-2) [van Ratingen, 2001]. With the implementation of these changes, the American regulators investigated the use of the ES-2 in their standard tests, but noted an issue of the gap between the ribs and back plate of the dummy catching on the seat in some crash tests [Samaha et al., 2001].

This issue was dealt with by including a set of bent steel plates between the ribs and the back plate to reduce the likelihood of this phenomenon occurring. Again this version of the EuroSID was renamed, this time to ES-2re (rib extension). A report by the European Enhanced Vehicle-safety Committee found that there were slight, but measurable differences between the response of the ES-2 and the ES-2re. They suggested that ECE R95 not change to adopt the use of the ES-2re, but to implement a penalty for any side impact where excessively high force was measured on the back plate of the dummy [EEVC, 2006]. This effectively led to the use of two different dummies by the American and European regulators. For the simulation work carried out in this thesis, the ES-2re model was used, as this represents the most up-to-date version of this ATD. The thoracic region of the ES-2re is composed of three rib modules consisting of steel ribs with a spring / damper system to control the deflection characteristics of the thorax. One large difference between the USSID and the ES is the use of a movable upper arm on the ES rather than the fixed interior foam arm of the USSID. Figure 2.13 shows a fully assembled ES-2re, while the interior rib modules are shown in Figure 2.14.

Figure 2.13: Fully assembled ES-2re [FTSS, 2005]

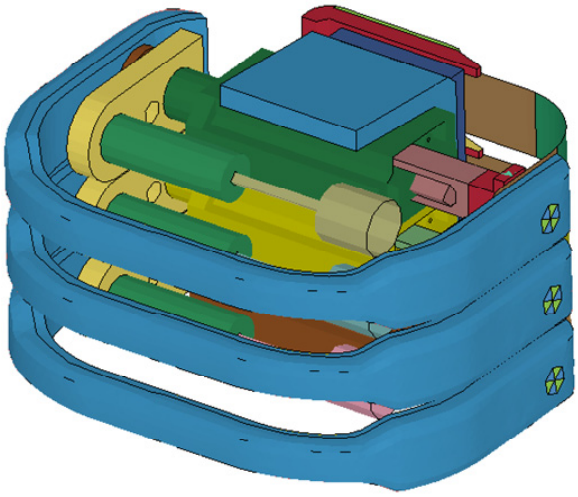

Figure 2.14: CAD of interior thoracic region of ES-2re

The ES-2re can be instrumented with triaxial accelerometers at the head CG, the upper and lower thoracic spine and the pelvis. Single axis (lateral) accelerometers are mounted on the struck side of the three ribs and the lateral displacement of the ribs is measured with linear potentiometers between the interior surfaces of the steel ribs. Additionally, forces at various points in the dummies body can be measured by load cells installed at the upper and lower neck, shoulder, back plate, abdomen, pelvis and femur. The overall mass of the ES-2re is designed to be 72.0 ($\pm$ 1.2) kg and the erect sitting height is designed to be 909 ($\pm$ 7) mm [FTSS, 2005].

2.6.3 WorldSID

Prior to the adoption of the ES-2re for American regulatory testing, ISO formed a workgroup to develop a new SID. The reasoning behind this was twofold. First, the use of separate ATDs in regional regulatory testing was seen as a major barrier to harmonization and second, both the USSID and ES had low biofidelity scores based on the ISO 9790 evaluation criterion. The USSID was rated as "unacceptable" while the ES was rated as "marginal" [Scherer et al., 2001]. The thoracic region of the WorldSID is composed of three sets of Nitinol ribs mounted onto a rigid spine running through the middle of the thorax. In addition to the three thoracic ribs, a shoulder rib and two abdominal ribs are used to control the deflection of the dummy's torso [FTSS, 2007]. Each rib consists of two bands, one circular inner band and one outer band that conforms to the exterior shape of the dummy. The outer ribs on each side of the dummy are connected with a sternum plate on the anterior surface of the dummy, while the interior bands are

connected to the spine. Like the ES, an upper arm is attached at the clavicle, however there is an optional full arm that can be attached to study arm interaction with airbags during impact [Scherer et al., 2001]. The fully assembled WorldSID is shown in Figure 2.13, while Figure 2.16 depicts the interior thoracic region.

Figure 2.15: Fully assembled WorldSID [FTSS, 2007]

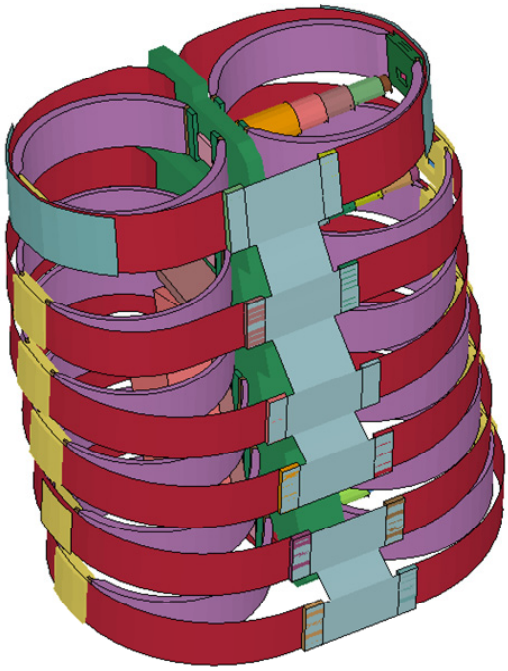

Figure 2.16: CAD of interior thoracic region of WorldSID

In the standard configuration, the WorldSID can be instrumented with triaxial linear accelerometers at the head CG, the struck side ribs and the pelvis, a triaxial rotational accelerometer at the head CG, six axis load cells at the upper and lower neck, the pelvis, and the lower leg. To measure chest deflection each rib is fitted with a telescoping infrared measurement system rather than a standarad potentiometer [Shcerer et al., 2001]. The WorldSID has a mass of 77.3 kg and the erect sitting height is designed to be 870 mm [Moss et al., 2000].

Despite claims that the WorldSID is the most biofidelic side ATD available today the WorldSID has not been adopted by any major regulatory body in compliance or consumer awareness testing at present.

2.6.4 Biofidelity of Side Impact Dummies

One of the first publications to assess the biofidelity of a side impact ATD was presented by Morgan et al. [1986]. In this analysis, the acceleration traces from the USSID were compared to acceleration traces from cadaver tests from a series of full scale automotive side impacts. The authors found that the response of the USSID was within the bounds of the scatter seen from cadaver testing, and thus the response of the USSID was considered to be biofidelic. This claim was challenged when it was shown that the USSID did not exhibit human like compression characteristics [Viano, 1987]. It was suggested that using global acceleration as a measure of biofidelity was a poor choice due to the inability of accelerometers to differentiate between global motion of the body and local differential accelerations (deformation) which cause injury. An early comparison of the biofidelity of the USSID and the EuroSID found that most responses tested were considered ‘very remote for the specification and is regarded as unacceptable’, though the EuroSID responded slightly closer to the cadaver tests [Benjellai et al., 1988]. With each subsequent redesign of the EuroSID, and the introduction of the WorldSID, each dummy has been tested against the ISO 9790 standard. The scores from these tests, both overall and for each body region, with 10 being the most biofidelic, are shown in Table 2.4 [adapted from Scherer et al., 2009]

Table 2.4: Side ATD biofideltiy scores

		USSID	EuroSID	ES-2	ES-2re	WorldSID
BioFidelity Rating	Head	0	5	5	5	10
	Neck	2.5	7.8	4.4	4.2	5.3
	Shoulder	0	7.3	5.3	4.5	10
	Thorax	3.1	5.4	5.2	4	8.2
	Abdomen	4.4	0.9	2.6	4.1	9.3
	Pelvis	2.5	1.5	5.3	3.2	5.1
	Overall	2.3	4.4	4.6	4.2	8

According to the standard, a score of 10 to 8.7 is considered 'Excellent', a score of 8.6 to 6.6 is considered 'Good', a score of 6.5 to 4.5 is considered 'Fair', a score of 4.4 to 2.7 is considered 'Marginal', and a score below 2.6 is considered 'Unacceptable'. Using this definition, the thoracic response of the USSID and ES-2re are marginal, the EuroSID and ES-2 are fair, and the WorldSID good. The overall biofidelity of the USSID is unacceptable, the EuroSID and ES-2re are marginal, the ES-2 fair, and the WolrdSID is good. It should be noted that this data was presented by the developers of the WorldSID, an ISO workgroup. In looking at these biofidelity scores, it is interesting to note that the ES-2re fairs worse in this testing then the ES-2, despite being revised to address practical short comings of the ES-2. It is also important to note that in the testing presented in Table 2.4 not all tests were performed for all ATDs.

The biofidelity of the USSID, the ES-2 and a prototype version of the WorldSID were also evaluated using slightly different type of biofidelity ranking by Rhule et al. [2002]. In this biofidelity ranking, the response of the dummy is compared to a series of cadaver tests to get a score for a given response in a given test, which is then combined with other scores to give a overall biofidelity score, similar to the ISO 9790 approach. The score that is calculated is slightly different, however, as it is a ratio of the squared sum of the difference between dummy response and the mean cadaver response and the squared sum of the difference between the mean cadaver response plus one standard deviation and the mean cadaver response. This method tends to favor responses that are close to the mean cadaver response of a given test, rather than those that simply fall within the scatter of the tests. Using this method, Rhule et al. found that the WolrdSID had the best biofidelity, followed by the ES-2 and then the USSID.

2.7 Side Impact Crash Testing

A number of agencies throughout the world carry out crash testing to assess the safety of vehicles. The European Union and American versions of these tests are the most well known and widely used. The side impact portion of the crash testing used in these two regions is outlined in the following section, along with a discussion of the Canadian legislation currently in force with regards to side impact protection.

In addition to the tests outlined below, there are independent new car assessment programs carried out in Japan, Australia, South Korea, and China [Carhs, 2009]. Additionally the Insurance Institute for Highway Safety (IIHS) of the United States carries out their own independent safety test program aimed at increasing consumer awareness [IIHS, 2010].

2.7.1 Side Impact Testing in the United States

Due to the growing concern over side impact fatalities and injuries, NHTSA proposed a dynamic side impact regulatory test (Federal Motor Vehicle Safety Standard 214 (FMVSS214)) that all vehicles sold in the United States are required to pass. This was first proposed on March 17, 1988, with the final rule implemented on October 30, 1990, with a phase period in such that by model year 1997 all vehicles would be required to pass [Hultman et al., 1991]. In 1997 the New Car Assessment Program (NCAP) was widened to include a side impact test in addition to the frontal impact test used to assess new vehicles at that time. The same tests procedure used in FMVSS214 was adopted for NCAP, where a Moving Deformable Barrier (MDB) is sent towards a stationary target vehicle. For the NCAP test, the velocity of the barrier was increased from 54 kph in the FMVSS test to 61 kph. This increase in speed was justified as increasing the ability to differentiate between vehicles with good side impact occupant protection, and those without. In 2004 changes to FMVSS214 were proposed which would change the ATD from a pair of USSIDs front and rear to a ES-2re in the front and a 5^{th} percentile female dummy (SID-IIs) in the rear. In addition to the MDB test, the new rule proposed the implementation of an additional rigid pole test. In this test, the vehicle being tested would be sent into a 254 mm (10”) diameter rigid pole at a speed of 32 kph (20 mph). This test was included to improve the safety of impacts into narrow objects such as utility poles and trees. The implementation of these rule changes was phased in beginning with the 2010 model year, with all vehicles being sold by the 2013

model year being required to pass this series of tests [NHTSA, 2004]. Following this, the NCAP testing system was updated and the changes which were implemented in the FMVSS214 test procedure were included in the side impact portion of the NCAP test. Essentially the new side NCAP MDB test is the same as the older test, with the USSIDs replaced with an ES-2re in the front seat and a 5th percentile female SID-IIs in the rear. This implementation of the new NCAP procedure was originally to have begun with model year 2010 [NHTSA, 2008b], but was later delayed by one year [NHTSA, 2008a]. The discussion that follows is intended to describe only the MDB tests, since these are the tests which are pertinent to the main body of this thesis. Additionally the term 'old' refers to the original version of the FMVSS and NCAP tests, while 'new' refers to the latest version of these tests.

In the MDB tests, the front of the MDB is fitted with a honeycomb structure to simulate the front bumper and crumple zone of an impacting vehicle. The dimensions of this structure are shown in Figure 2.17, along with the crush resistance of the honeycomb materials.

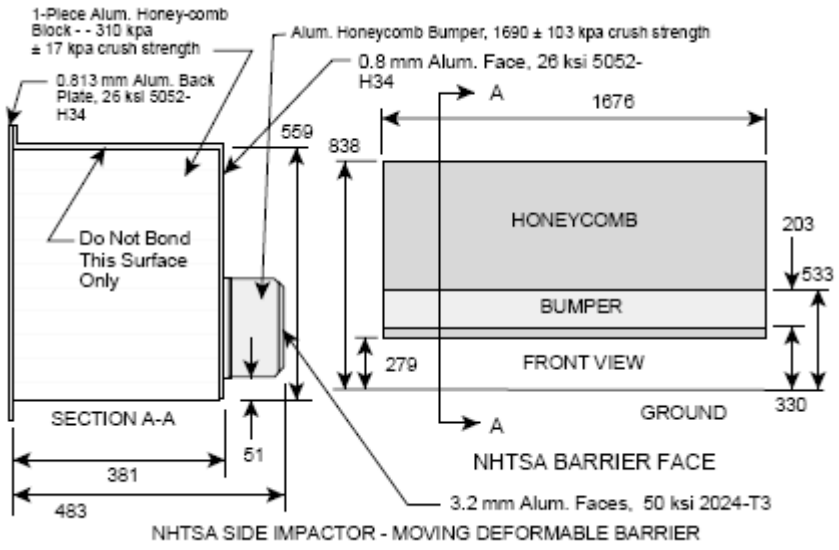

Figure 2.17: Dimensions and material properties of MDB front structure [NHTSA, 2006]

The wheels of the 1368 kg barrier are crabbed (turned) 27° to simulate relative motion between the target vehicle and the MDB. The nominal forward velocity of the barrier is 61 km/h in the NCAP test and 54 kph in the FMVSS214 test. The intent in choosing this mass and these velocities was to capture a large percentage of the vehicles involved in these types of collisions and the types of speeds often seen in these collisions. While these parameters were never

intended to cover all possible side impact situations, there have still been questions raised as to the applicability of these values [Thomas and Frampton, 1999], particularly since collisions at these speeds are less severe than the majority of fatal collisions. The longitudinal position at which the barrier strikes the target vehicle is defined by the front left side of the barrier which must impact the car at a point 940 mm forward of the midpoint of the target vehicles wheelbase. Figure 2.18 shows a finite element model of the barrier immediately prior to impact along with the component velocities used in each test.

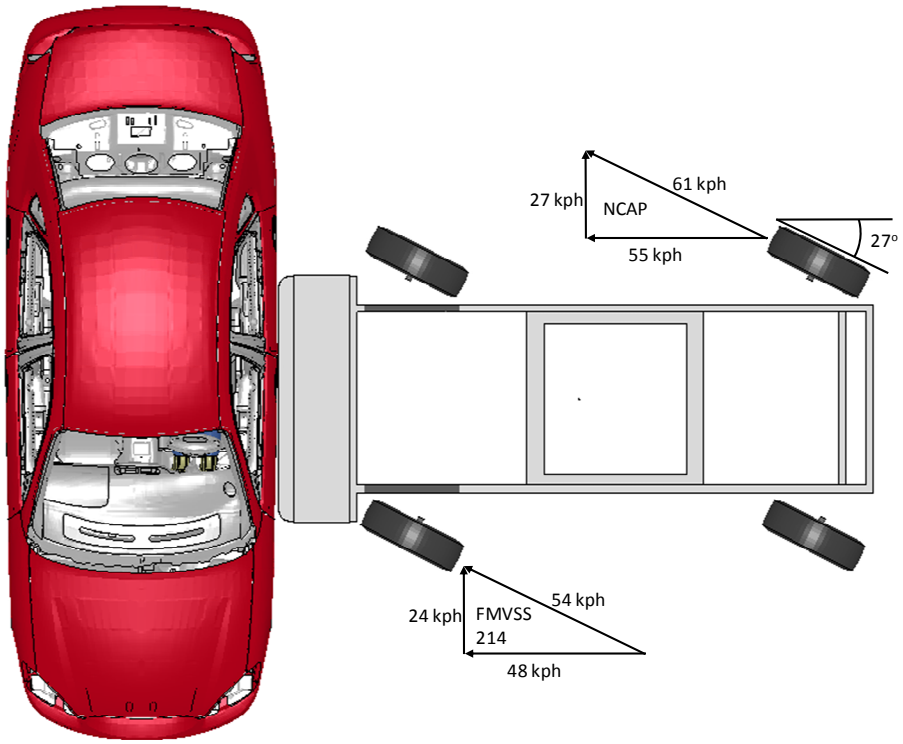

Figure 2.18: Side impact MDB test velocities

In the old version of this test, two USSIDs were placed in the vehicle on the struck side to measure the impact loads on driver and rear driver's-side passenger. In the FMVSS214 test, the maximum allowable TTI was 85 G for four door vehicles and 95 G for two door vehicles, while the maximum allowable pelvis acceleration was limited to 130 G. TTI was the only injury criteria used in the old NCAP test to determine the side star rating, as shown in Table 2.5 [adapted from Chan et al., 1998], however if the Head Injury Criteria (HIC) [Versace, 1971] value was excessively high, the vehicle was flagged with a safety concern warning [Safercar.gov,

2009]. Prior to testing the position of the dummy relative to a number of interior trim pieces (door interior trim, steering wheel, side window, etc.) were recorded.

Table 2.5: NCAP star rating

Rating	TTI Range [G]
★★★★★	≤ 57
★★★★	58 - 72
★★★	73 - 91
★★	91 - 98
★	> 98

The new versions of these tests replace the USSIDs with an ES-2re (50^{th} percentile male ATD) and a SID-IIs (5^{th} percentile female ATD) in the front and rear seat, respectively. The injury limits for the FMVSS214 test were changed to a HIC_{36} score of 1000, chest deflection of 44, abdominal force of 2.5 kN, and a pelvic force of 6 kN for the ES-2re and a HIC_{36} of 1000, a chest acceleration of 82 and a pelvic force of 5.525 kN for the SID-IIs [Carhs, 2009]. Rather than providing a star rating for each position in the vehicle for each test in the new NCAP, a new all-encompassing procedure was developed which incorporates injury metrics from a frontal impact test, a side MDB test, a side pole test and a rollover test. Each occupant's injury criteria are then compared to scores from other vehicles to provide a score for each occupant in each test. The star ratings of each occupant are then combined to present an overall rating for each direction of loading, which are then combined to provide an overall vehicle safety score [NHTSA, 2008c]. The MDB portion of these tests measures the HIC_{36} and pelvic force of both the ES-2re and the SID-IIs and the rib deflection and abdominal force of the ES-2re. These values are then compared to risk curves developed by Kuppa [2006] to assess the probability of injury.

In addition to the instrumentation on ATDs used in these tests, accelerometers at 18 vehicle locations record the response of the vehicle during impact. Of these 18 locations, five locations on the vehicle doors and the rear seat structure accelerometer are considered optional [NHTSA 1997] and are often excluded. Figure 2.19 shows the position of these accelerometers, which are listed in Table 2.6, along with the number of axes for each accelerometer and the abbreviation used throughout the rest of this thesis.

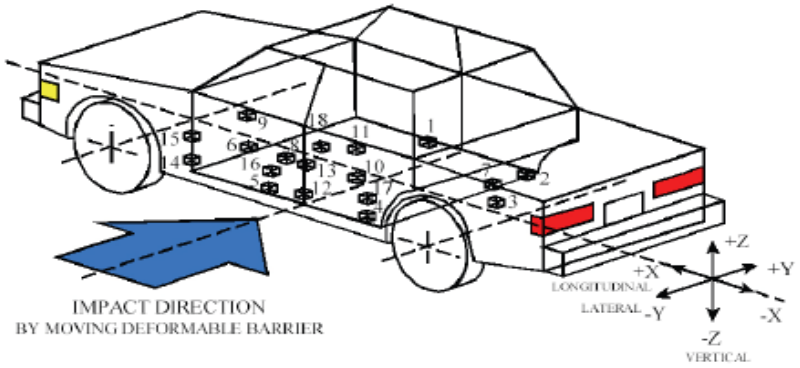

Figure 2.19: Vehicle accelerometer locations [Advanced Information Engineering Services, 2005]

Table 2.6: Locations of vehicle accelerometers during side impact testing

Accelerometer #	Location	# of Axes	Abbreviation	Optional
1	Right Sill at Front Seat	3 (X,Y,Z)	RF Sill	No
2	Right Sill at Rear Seat	3 (X,Y,Z)	RR Sill	No
3	Rear Floorpan Above Axel	3 (X,Y,Z)	FLrPn	No
4	Left Sill at Rear Door	1 (Y)	LR Sill	No
5	Left Sill at Front Door	1 (Y)	LF Sill	No
6	Left Front Door Centerline	1 (Y)	LF Dr CL	Yes
7	Right Rear Occupant Compartment	1 (Y)	RR Occ	No
8	Left Front Door Mid-Rear	1 (Y)	LF Dr MR	Yes
9	Left Front Door Upper Centerline	1 (Y)	LF Dr UCL	Yes
10	Left Rear Door Mid-Rear	1 (Y)	LR Dr MR	Yes
11	Left Rear Door Upper Centerline	1 (Y)	LR Dr UCL	Yes
12	Left Lower B Post	1 (Y)	L B Pst	No
13	Left Middle B Post	1 (Y)	M B Pst	No
14	Left Lower A Post	1 (Y)	L A Pst	No
15	Left Middle A Post	1 (Y)	M A Pst	No
16	Front Seat Track	1 (Y)	Ft St Trk	No
17	Rear Seat Structure	1 (Y)	Rr St	Yes
18	Vehicle Center of Gravity	3 (X,Y,Z)	CG	No

Due to the importance of the vehicles ability to resist intrusion in side impact, the crash profile of the vehicle side structure is also reported in these tests. Essentially the distance between a plane parallel to, and offset 1000 mm laterally from the center plane of the vehicle and a series of points on the vehicle before and after impact are measured. The measurements are taken at five height levels off the ground; the top of the side sill, the H-point, mid-door, the window sill, and the top of the window. A measurement is taken at every 150 mm along each of these heights

along the length of the car. These measurements prior to and after impact are compared to provide information on the vehicle's resistance to intrusion.

Prior to these tests being implemented, a series of closely controlled experiments were carried out by Ford to ascertain the variability present in these tests [Hultman et al., 1991] . In these experiments, 6 1991 Ford Taurus' were impacted using the test procedure that was proposed in FMVSS214. The responses of the USSIDs placed in the front seats in these tests were compared using the coefficient of variability (CV) measure (the standard deviation of the peak response divided by the average of the peak response). It was found that the CV for the ATD TTI was 5.0% while the pelvis acceleration CV was 8.3%. It was also found that the upper rib and spine acceleration had higher CV than the lower spine and rib acceleration. The researchers also found that there was a significant amount of variation in the amount of measured door intrusion, suggesting a possible difference in door intrusion velocity, which plays an important role in thoracic injury.

2.7.2 Side Impact Testing in the European Union

At roughly the same time that FMVSS214 was being developed, the European Union began to develop its own dynamic side impact regulation leading to Regulation 95 (R95) developed by the Economic Commission for Europe (ECE) which described the testing procedures that passenger vehicles sold within the Europe Union would be required to pass. This MDB test was eventually incorporated into the EuropNCAP program, with the injury criteria changed from a pass / fail criteria to a scale which was used to assess the comparative occupant protection of the vehicle being tested. Additionally two child ATDs were added to the rear seat of the EuroNCAP MDB test [Hobbs and McDonough, 1998].

Like the American NCAP program the intent of EuroNCAP was to gather information taken from several dynamic tests and represent this information as a single star rating to inform the public of the relative safety of a given vehicle. In its current form this involves a frontal impact test, a side MDB test, a side pole test, a set of pedestrian tests and a series of equipment and interior geometry checks. In each test a score is assigned based on the response of the dummy in the dynamic tests, or the presence or absences of a given safety feature (for example the presence of electronic stability control gives the vehicles 3 points). These scores are then sorted into 4

categories, adult protection, child protection, pedestrian protection and 'Safety Assist'. A weighted average of these components is computed and an overall vehicle star rating is assigned based on the score and the model year of the vehicle [EuroNCAP, 2009a].

In the current MDB EuroNCAP test, an ES-2 dummy is place in the front drivers side seat (at least 20% of vehicles tested by EuroNCAP are right-hand drive versions), and an ATD of a 3 year old and 18 month old are placed in the rear. Unlike the American MDB test, there is very little instrumentation on the actual vehicles, with only one single-axis (lateral) accelerometer placed on the unstruck B pillar to measure the vehicle response. During the testing, the 900 kg barrier is sent into the side of the vehicle such that the centerline of the barrier is coincident with the H-point of the driver ATD. The front potion of the barrier is composed of 6 zones, each with different material crush characteristics. These zones, along with the dimensions of the barrier front are shown in Figure 2.20. The lower zones (Zones 1 through 3) in Figure 2.20 are considerably more stiff than the upper zones (Zones 4 through 6), and the center zones are slightly stiffer than the side zones [EuroNCAP, 2009b].

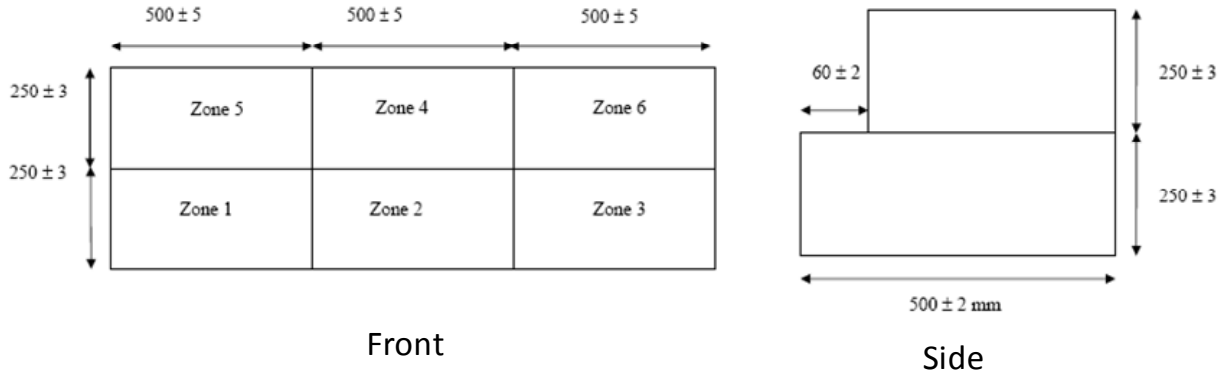

Figure 2.20: EuroNCAP barrier front

During the test, the HIC_{36}, the chest deflection, VC, abdominal force and pelvic force are recorded and used in the NCAP score for the ES-2. The limits for these scores set in R95 are 1000, 42 mm, 1 m/s, 2.5 kN and 6 kN respectively [ECE, 1995].

At one time, NHTSA studied the possibility of creating a functional equivalent between their FMVSS214 test and the R95 test. In a study carried out to assess the differing results of these two tests from vehicles that had been tested under both metrics, NHTSA found that the vehicles that met FMVSS 214 did not necessarily meet R95. Additionally the responses of the vehicles

(particularity the crush pattern) were not the same due to the different barrier front end structures. Also, the applicability of the lower mass MDB of the European test was questioned due to the prevalence of light trucks and SUVs in the United States. The researchers concluded that there were significant differences between both the vehicle and occupant response and that due to the differences in injury metrics, harmonizing the two standards or creating a functional equivalent would not be possible. They did however note that with the introduction of the WorldSID it may be possible to harmonize the ATD and injury criteria that were used [Samaha et al., 1998].

2.7.3 Side Impact Testing in Canada

Under current Canadian law, there is no dynamic test procedure required for a vehicle to be sold within Canada. Instead CMVSS 214 requires a quasi-static door crush tests, where a rigid, 305 mm diameter cylinder is forced (using displacement control) 457 mm into the center of the driver's side door with the force being measured. The crush resistance is calculated from the force displacement profiles generated during the test [Transport Canada, 1996]. The initial (first 152 mm) crush resistance must be at least 10.01 kN, while the intermediate (first 305 mm) crush resistance must be at least 15157 kN for vehicles tested with no seats and 19.46 kN for vehicles tested with the seats in place. The peak crush resistance (measured over the entire crush distance) must be equal to the lesser of either twice the vehicle's curbweight or 31.14 kN for vehicles tested without the seat installed or the lesser of either three and a half times the vehicle's curbweight or 53.38 kN for vehicles tested with their seat installed [Canadian Department of Justice, 2009]. Despite the lack of a dynamic side impact test being required by the Canadian government, a group of automakers signed a memorandum of understanding with Transport Canada stating that only vehicles which have passed the American FMVSS 214 or the European ECE R95 tests will be sold by their dealers within Canada [Canada Gazette, 2002].

2.8 Side Component Sled Testing

In a comparison of frontal and side impacts performed by Lau et al. [1991], the general description of an automotive side impact described the intruding door as "punching" the occupant. This was contrasted to the frontal impact where the occupant (particularity if unbelted) is essentially in free flight. This meant that the velocity profile of the door, the

occupants distance to the door prior to impact and the compliance of the door are all important factors in the outcome of the collision for the occupant. It has been generally accepted that the best way to provide a favorable outcome for an occupant in side impact is to control the velocity of the intruding door (and thus crush distance) by creating a very strong vehicle side structure [Hobbs, 1995].

Due to the high cost and amount of time required to perform a full scale vehicle test, there have been several attempts to develop a simplified representation of a side impact by using sled systems to impact an occupant with interior door trim pieces. In general this has been done experimentally by using a pneumatic or servomotor controlled side sled apparatus. The intent with these devices is to mimic the motion of the side door relative to the occupant. There are a number of different was to achieve this motion [Miller and Gu, 1997; Miller et al., 2002, Sundararajanet al, 1995; Aekbote et al, 2007 Aekbote et al, 1999; Payne et al., 1997; Stein, 1997; Chung, et al., 1997; Saari et al., 2004] but in all cases the velocity traces used for both the door and the motion of the seat are from an actual crash tests. Studies have found that door trim and occupant restraint systems can be evaluated using these methods, but they are not suitable for analysis of the response of the vehicle [Chou et al., 2007]. Because the vehicles door response is used as an input in these tests, any modifications that would change this response could render the results invalid.

Most of this type of research in side impact has assumed that there is little to no coupling of the interaction between the occupant and the car door in an automotive impact. The prevailing notion is that the mass of the vehicle impacting the occupant's door is large enough that the impacting vehicle completely dominates the dynamics of the impacted vehicle's responses and that the effects caused by the occupant are negligible.

2.9 Numerical Modeling of Side Impact

Due to the complexity and time consuming nature of performing physical crash testing, the use of computer modeling has become widespread in assessing the crash characteristics of a vehicle or component prior to physical testing. Simulations of side impact testing general fall into one of two categories; component sled modeling or full scale side impact modeling. Component sled modeling is concerned with modeling the tests (or a similar scenario) discussed in Section 2.8,

while full scale modeling is concerned with the crashworthiness and occupant response in a full vehicle model. The modeling of side sled impacts is often attractive due to the decrease in computational cost associated with not modeling the full vehicle.

There have been a number of researchers who have investigated side sled testing using both multibody dynamics models [Huang et al., 1994; Morris et al., 1999] and finite element models [Teng et al., 2007; Kent et al., 2001; Campbell et al., 2009; Watson et al., 2009] in which door velocity profiles were prescribed to an intruding door. In all cases the input velocities were taken from actual crash tests. In an extension of these types of simulations, MIRA researchers performed a series of multibody simulations where the initial offset of the dummy from the car door and the shape and magnitude of the crash impulse were altered to gain insight into the effects of these parameters on occupant response [Allan-Stubbs, 1998]. They found that injury was predominantly affected by the first peak of the door velocity profile, while the trough and second peak often seen in the door velocity profile (discussed later in Section 3.3) generally had smaller effects on the injury criteria measurements made by the dummy models.

One early model of a full scale side impact was developed by Deng [1988, 1993] using the CAL3D software package. Essentially the vehicle was represented by a series of rigid links which were linked together using hinge joints of varying stiffness. An occupant was modeled using a series of spring, masses and dampers which were tuned to provide a response similar to an actual human occupant. Using this model, a parametric study was performed where the stiffness of the hinge joints were varied to study the outcome of the model. Deng found that stiffening the joint between the lower B pillar and the car floor and the lower A pillar and the car floor provided a significant benefit to the occupant, while the connections at the roof were significantly less important.

A slightly more complex full scale model was developed by Harle et al. [1999], which involved using beam elements for the side structure of the vehicle, shell elements for the car door, and non-linear spring elements to represent the floor and roof cross members. A simple finite element model of the EuroSID dummy was placed next to the shell door. The purpose of this LS-Dyna model was to develop a method to optimize the side structure (by changing the beam and spring element stiffnesses) to minimize the injury criteria measured by the dummy. Despite being presented primarily as a optimization example, this work showed that strengthening the B

pillar reduced intrusion and door velocity during the impact, strengthening the floor cross members had little effect on the rib response, (though the pelvic response was lower), the rib deflection was related to door intrusion, and that VC was related to the velocity of the door at the time of impact.

A similar attempt to develop a simplified model was developed by Malkusson and Karlsson [1998]. In this work a half vehicle model was created such that the A pillar, B pillar and C pillar along with the lower door sills and doors were modeled as shell elements, while non-linear spring elements were used to represent the cross members. Lumped masses were added to represent the non-struck side of the car. The occupant and seat were included to provide a similar response to the full car test. The velocity profile of the B pillar was found to mimic the response of a full scale test, though the model was not developed further.

More recently, full scale finite element models of both vehicles and occupants have been developed to study injury and the effects of various occupant protection measures. For example Schönpflug et al. [2004] developed a PAMcrash model of a BMW in a EuroNCAP test to compare the response of a EuroSID and a human body model (the H-model). The researchers found that in general the H-model predicted less and shorter duration rib deflection histories when compared to the EuroSID. This was partly attributed to the interaction or the H-model's arm with the door, which was not the case with the EuroSID. A model with the H-model was created with a side airbag to compare the response of the human body model with and without a side airbag. It was found that in general the presence of the airbag increased and delayed the peak rib deflection. A similar finding between a side ATD and the H-model was noted by Pyttel et al. [2007] who compared the ES-2 and the H-model in a full scale side impact without a side airbag, and again attributed the lack of chest deflection to the interaction of the H-model's arm with the intruding door panel.

In a slightly different full scale side impact simulation, Shah et al. [2005] developed a finite element model of a vehicle to vehicle impact where the target vehicle occupant suffered a rupture of the aorta in an attempt to replicate this type of injury numerically. This simulation was broken up into two portions, one that defined the motion of the vehicles and one where the interior trim (which had its motion defined by the vehicle only impact) was allowed to interact with the human body model. This method was used to aid in computational efficiency, though

this method implicitly assumes that the occupant has no effect on the intruding door and vehicle structure. Additionally no seat or belt interaction was considered in this model. The maximum stress in the aorta of the human body model occupant occurred at roughly the same position as the aortic tear in the real world occupant, but the authors caution that "no conclusion should be drawn on the models capabilities to predict injury considering the current modeling limitations."

Several other areas of side impact modeling are discussed later in Chapter 4 and Chapter 5 as they pertain to the development and validation of the full scale finite element model developed for this thesis.

Chapter 3 Review of NCAP Side Impact Test Results

3.1 Introduction

To better understand side impact testing and the response of vehicles and occupants to this type of loading a review of the NHTSA crash test database was carried out. This database provides information for every NCAP and FMVSS214 (as well as other compliance test) carried out by NHTSA. This information includes the dimensions and specifications of the vehicle, the location of the accelerometers placed on the vehicle, the response of the accelerometers on the vehicle, the response of the instrumentation installed in the ATD (including accelerometers, force transducers, potentiometers and contact switches where applicable) and the amount of deformation measured on the vehicle after impact.

A series of average lateral velocity plots were created from the accelerometers of a series of 72 side NCAP tests. These plots were used as a 'reality check' during the validation of the side impact finite element models to ensure the results from the model were reasonable. In addition to the plots used for verification of the finite element model, correlations between TTI and various other parameters (such as vehicle mass, peak lateral Y velocity, etc.) were studied. During these tests there was often a significant amount of yaw rotation, the effects of which were studied both by the occupant response and response of the vehicle. Additionally the contact time as measured by the occupants was studied to see what effect, if any this had on the response of the vehicle door.

3.2 Methodology

To obtain the vehicle response information required in this study the NHTSA Vehicle Crash Test Database [NHTSA Vehicle Crash Test Database, 2009] was surveyed. Of interest in this work were the vehicle and occupant responses in more recent crash tests using the USSID, meaning only data between model years 2005 and 2009 were studied. Additionally, to reduce any issues arising from a mismatch between the barrier and vehicle door, only 4 door sedans were studied. These criteria led to a sample size of 72 vehicles. These 72 vehicles were primarily new to the American marketplace (either new nameplates or cars previously available only in foreign markets), vehicles with major redesigns, or vehicles with the addition of new safety features

(such as the addition of side airbags). Unfortunately, for all but 12 of the vehicles in the sample set, the door mounted accelerometers were not fitted meaning lateral door intrusion velocities were captured during only these 12 tests. Additionally, these 12 vehicles were all from model year 2005, so an understanding of door intrusion is somewhat limited for newer vehicle designs.

In addition to studying the lateral velocity profiles of the vehicle accelerometers, the front seat dummy acceleration response profiles were recorded for each test. The TTI, the peak dummy pelvic acceleration, and the Head Injury Criterion were recorded along with the offset between the dummy's arm and the vehicle door (AD distance) and the maximum door crush distance after testing. These parameters were plotted against the TTI measured by the USSID to identify their importance to the predicted injury.

The accelerometer data published in the NHTSA Vehicle Crash Test Database generally begins 20 ms prior to the MDB contacting the door of the target vehicle and lasts 200 ms or 300 ms after initial contact. The maximum thoracic response, as predicted by TTI, typically occurs in the first 50 ms after the MDB contacts the door while maximum VC tends to occur roughly 10 ms after peak acceleration and maximum compression tends to occur slightly later than maximum VC [Viano, 1987]. For this reason, this study focused on occupant and vehicle response only during the first 100 ms after impact.

The data was filtered using a CFC60 class filter following the guideline laid out in SAE J-211 [SAE, 2003] stating that 'Total vehicle comparisons' should use this type of filter. For simplicity, the accelerations extracted from the dummy were also filtered using this filter rather than CFC180 suggested for spine acceleration and CFC1000 for rib acceleration. The velocity of the vehicle was found from each accelerometer by numerically integrating the acceleration trace. To actually extract the accelerometer data and perform the filtering from the NHTSA database, a piece of software developed by NHTSA in their Signal Analysis Software pack [NHTSA, 2010b] named 'Signal Browser' was used. This software essentially accesses the database and provides a graphical interface to view, filter, integrate, differentiate and export the accelerometer traces. To ensure that the method of numerical integration had no effect on the results, a simple test case was performed comparing the integrated velocity output from the Signal Browser software to output from an accelerometer trace integrated using the rectangle method, the trapezoidal method and Simpsons method. Due to the high sampling rate, there was effectively no difference

between any of the methods. Additionally whether filtering was performed before or after integration had no effect on the final velocity trace. Following integration, the time histories were subsampled such that all of the traces had a sampling rate of exactly 10000 Hz. From this subsampled data, 'average' velocity histories were determined using the mean value at each point within the velocity history as discussed in Eppinger et al. [1984], along with curves representing one standard deviation above and below the mean. In order to calculate the rotation of the vehicle, acceleration of the non struck side sill and the center of gravity were also extracted from the database.

In addition to the accelerometer traces, the mass, maximum lateral velocity of the center of gravity, the maximum deformation distance after impact of the vehicle and the arm to door distance were recorded for each test, along with front seat occupants TTI, peak pelvic acceleration, and HIC score. Finally the front seat star rating was recorded for each vehicle.

3.3 Results

Table 3.1 shows a summary of the results found in this study separated by vehicle class. The mean value, the maximum value, the minimum value and the coefficient of variation (standard deviation divided by the mean) are included in this table. By looking at the measures of injury in Table 3.1, one sees that while there may be a slight deceasing trend in the injury sustained by the occupants of larger vehicles, no definite conclusion can be drawn based simply on vehicle class. The model year of the vehicle, vehicle mass, peak pelvic acceleration, HIC, maximum lateral CG velocity, AD distance and maximum deformation were plotted against the TTI measured by the front seat occupant in each test. Figure 3.1 through Figure 3.7 show these plots. Each of these plots also shows a linear curve fit which is intended to show the general trend that increasing each characteristic has on TTI. The plots show that while the TTI tended to decline with lower pelvic acceleration, lower HIC, higher vehicle mass, lower door intrusion, and larger initial AD values, the scatter is sufficient to make generalizations difficult. It is also worth noting that TTI tended to decrease with newer vehicle models.

Table 3.1: NHTSA database study results

	Vehicle Class	Sub Compact	Compact	Mid Sized	Full Sized	All
Year	Average	2006.33	2007	2006.55	2006.33	2006.64
Stars	Average	3.67	4.39	4.48	4.67	4.42
Driver TTI [G]	Average	69.60	57.64	54.24	53.98	56.56
	CV	0.1339	0.2920	0.3082	0.1635	0.2752
	Max	85	96	100	65	100
	Min	60.5	33	33	36	33
Vehicle Mass [kg]	Average	1326.5	1572.41	1761.5	1901.42	1689.8
	CV	0.0321	0.0874	0.0579	0.0527	0.1145
	Max	1377	1809	2026	2088	2088
	Min	1274	1366	1608	1675	1274
Driver Peak Pelvic Acceleration [G]	Average	85.12	70.09	64.53	68.84	68.74
	CV	0.2304	0.2479	0.2840	0.2476	0.2677
	Max	123.5	107.1	109.5	99	123.5
	Min	71	38.9	24	48	24
HIC	Average	245	270.27	215.88	231.5	238.47
	CV	0.2506	0.4840	0.5099	0.6280	0.5054
	Max	362	673	608	539	673
	Min	195	120	72	73	72
Max Lateral CG Velocity [kph]	Average	25.57	26.30	25.47	24.18	25.55
	CV	0.1947	0.0941	0.1069	0.0791	0.1104
	Max	31.07	32.87	33.59	27.38	33.59
	Min	18.23	23.09	21.19	21.67	18.23
Max Deformation Distance [mm]	Average	317.5	287.61	297.58	298	296.13
	CV	0.1330	0.1659	0.1779	0.1503	0.1650
	Max	359	402	463	360	463
	Min	244	191	222	223	191
Driver AD [mm]	Average	104.83	104.13	109.23	129.58	110.63
	CV	0.1819	0.1543	0.2046	0.1420	0.1912
	Max	120	130	150	167	167
	Min	68	71	62	111	62

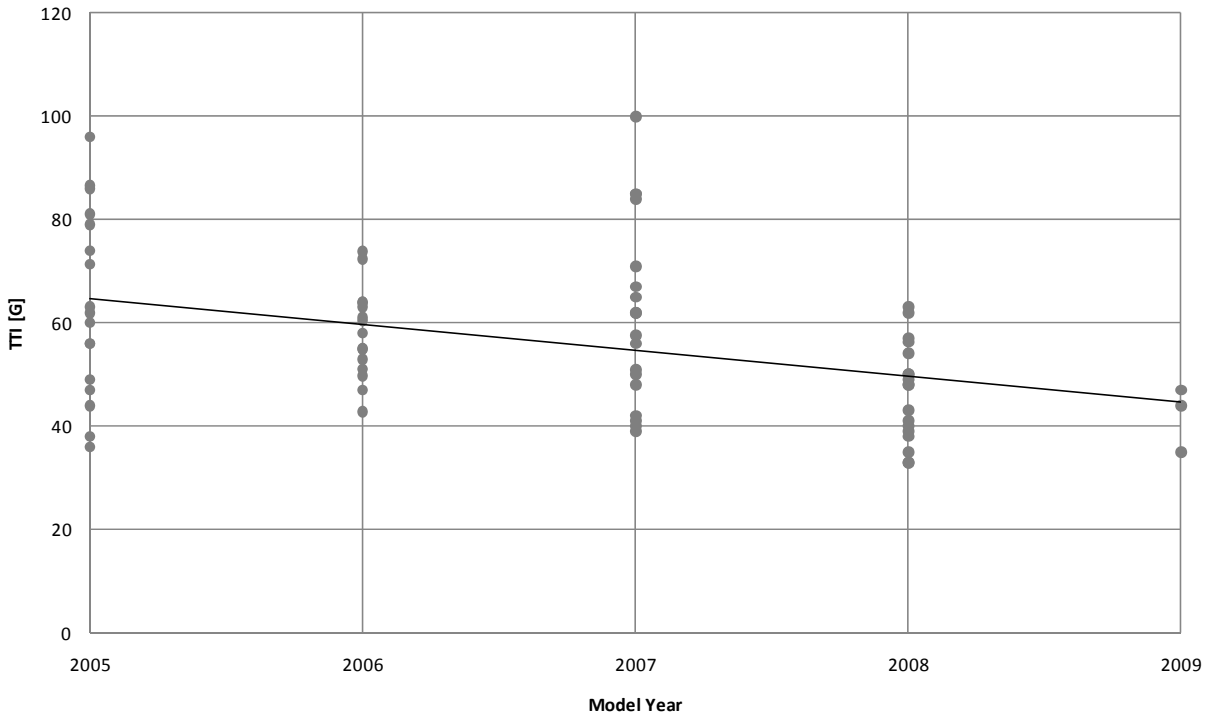

Figure 3.1: TTI as a function of model year

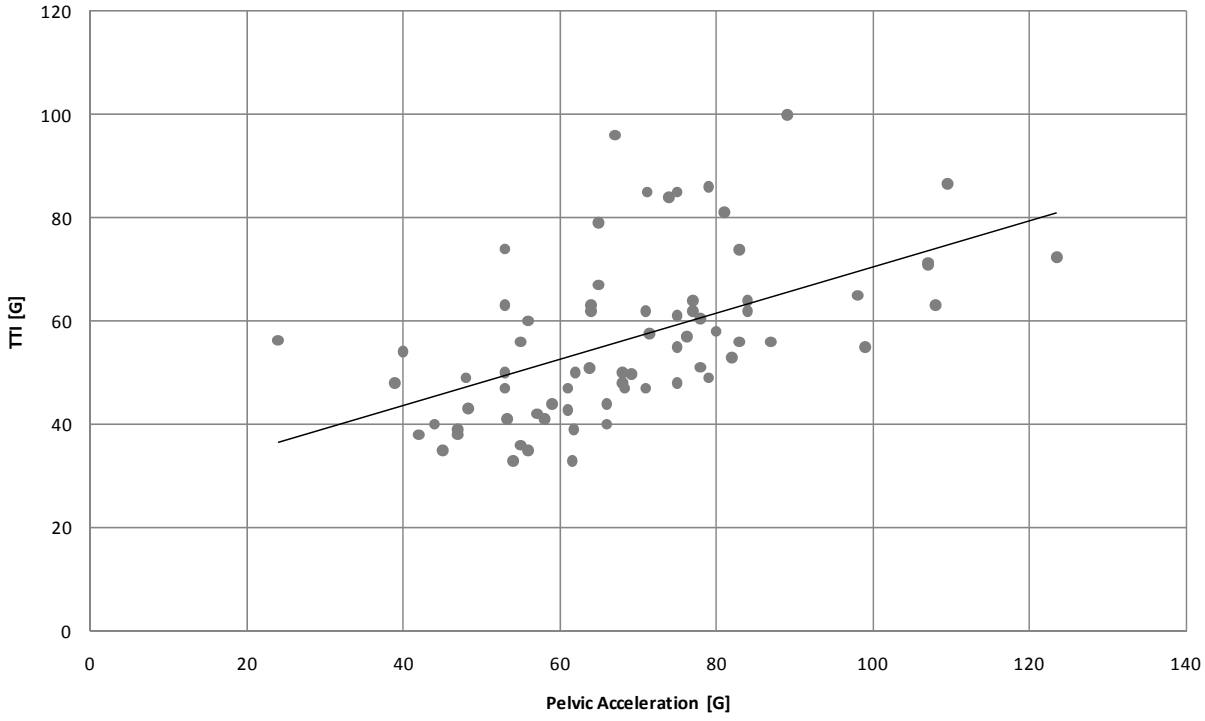

Figure 3.2: TTI as a function of pelvic acceleration

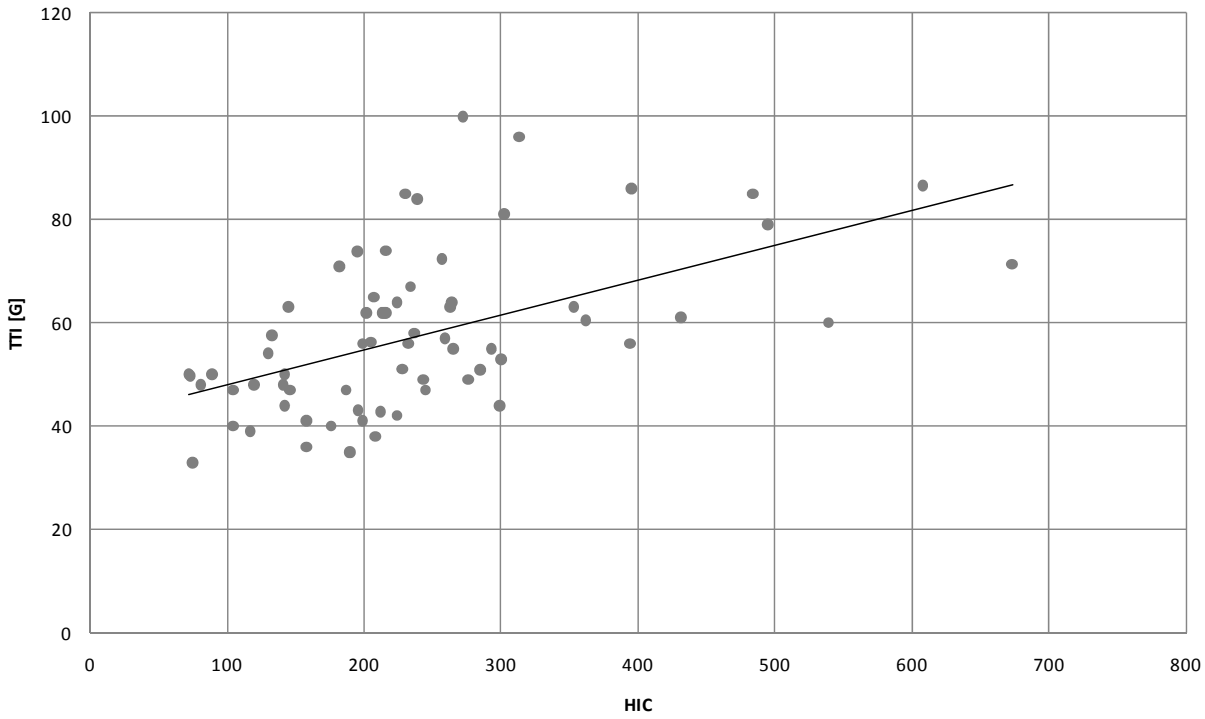

Figure 3.3: TTI as a function of HIC

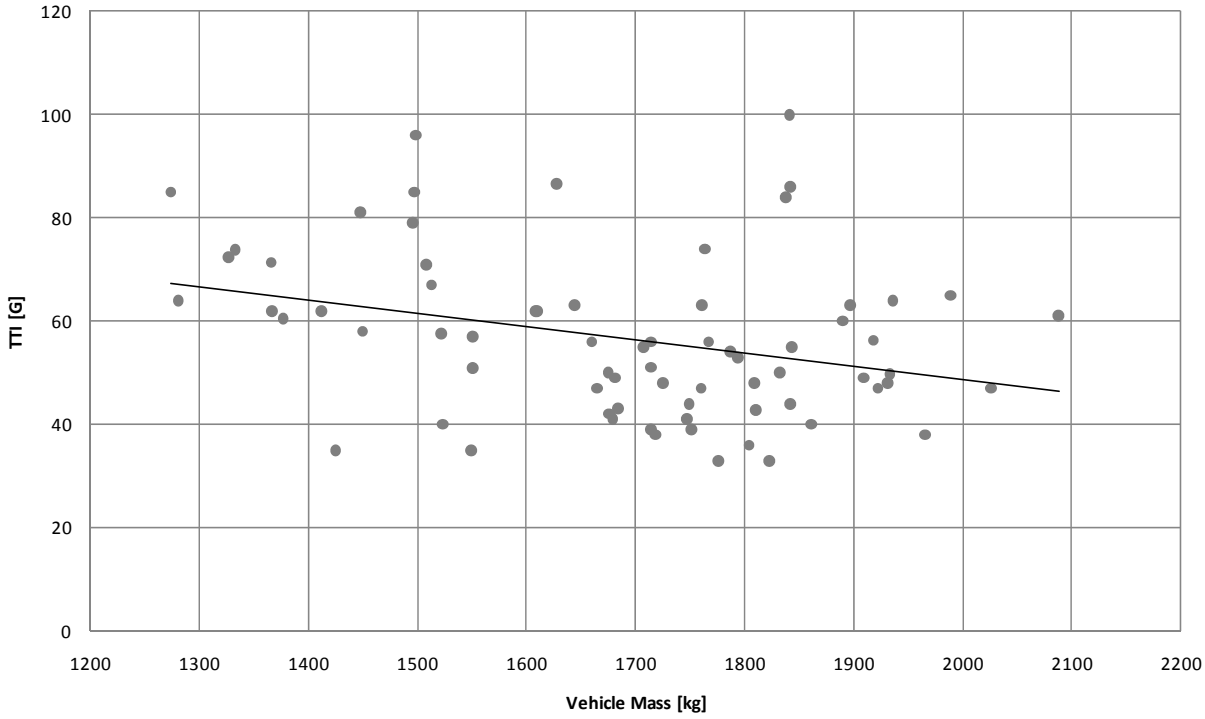

Figure 3.4: TTI as a function of vehicle mass

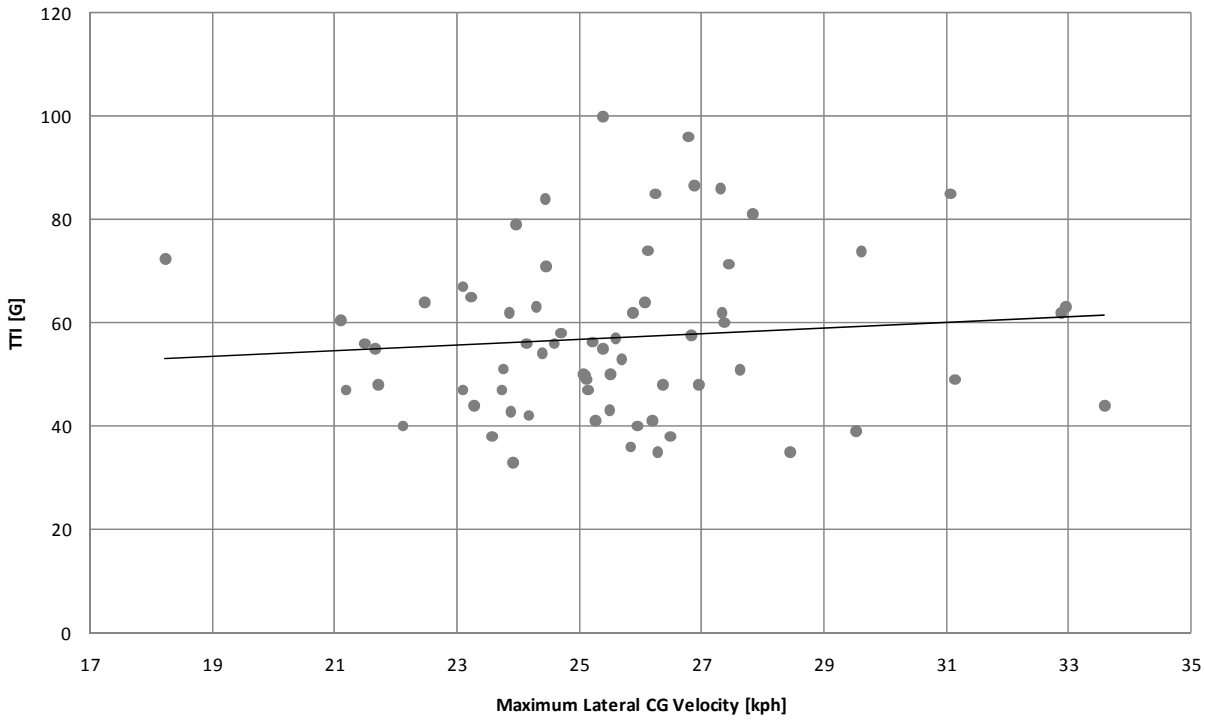

Figure 3.5: TTI as a function of maximum lateral vehicle CG velocity

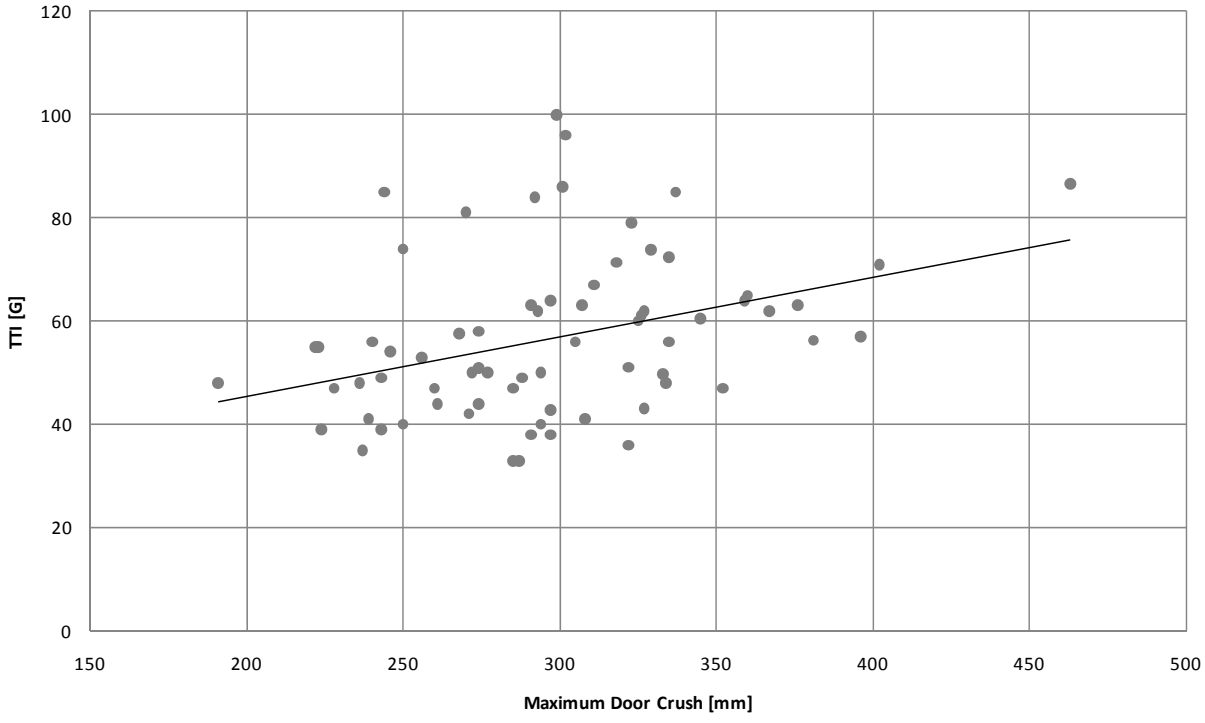

Figure 3.6: TTI as a function of door intrusion

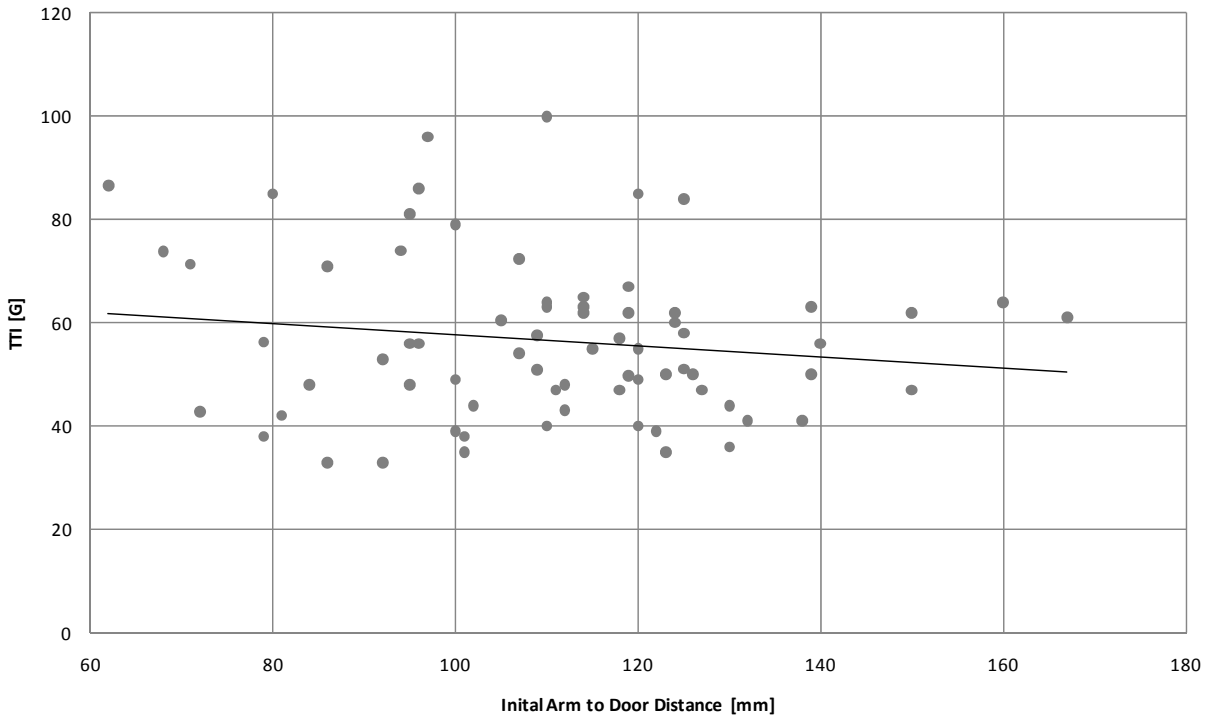

Figure 3.7: TTI as a function of AD distance

Figure 3.8 shows the test responses of the velocity for the right front sill location (a) along with the average velocity and ± 1 standard deviation above and below average (b). This figure gives a sense of the scatter that was present in these velocity profiles, though this location was found to have the lowest amount of variability between tests. The full set of average curves, along with the ± 1 standard deviation corridor and the experimental maximum and minimum corridors are included in Appendix A.

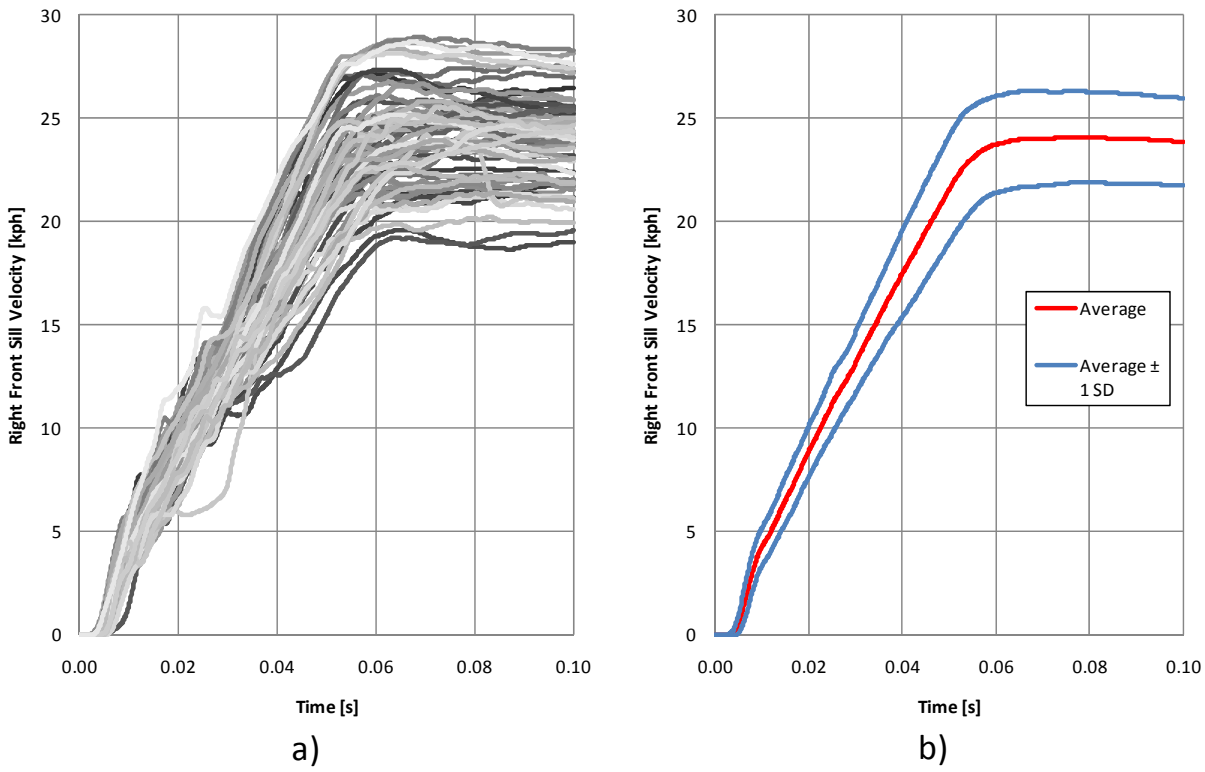

Figure 3.8: Right front sill lateral velocity traces

The average velocity profiles plots show gross trends seen from each individual curves of the data set, however some trends are not reflected in the average. The average lateral center of gravity plot is shown in Figure 3.9, along with several test traces to illustrate this point. Several of the vehicles showed a pronounced peak in velocity very early in the time history. This however is not fully captured in the average trace due to the number of tests where this peak was not present, which caused these early peaks to be "averaged out".

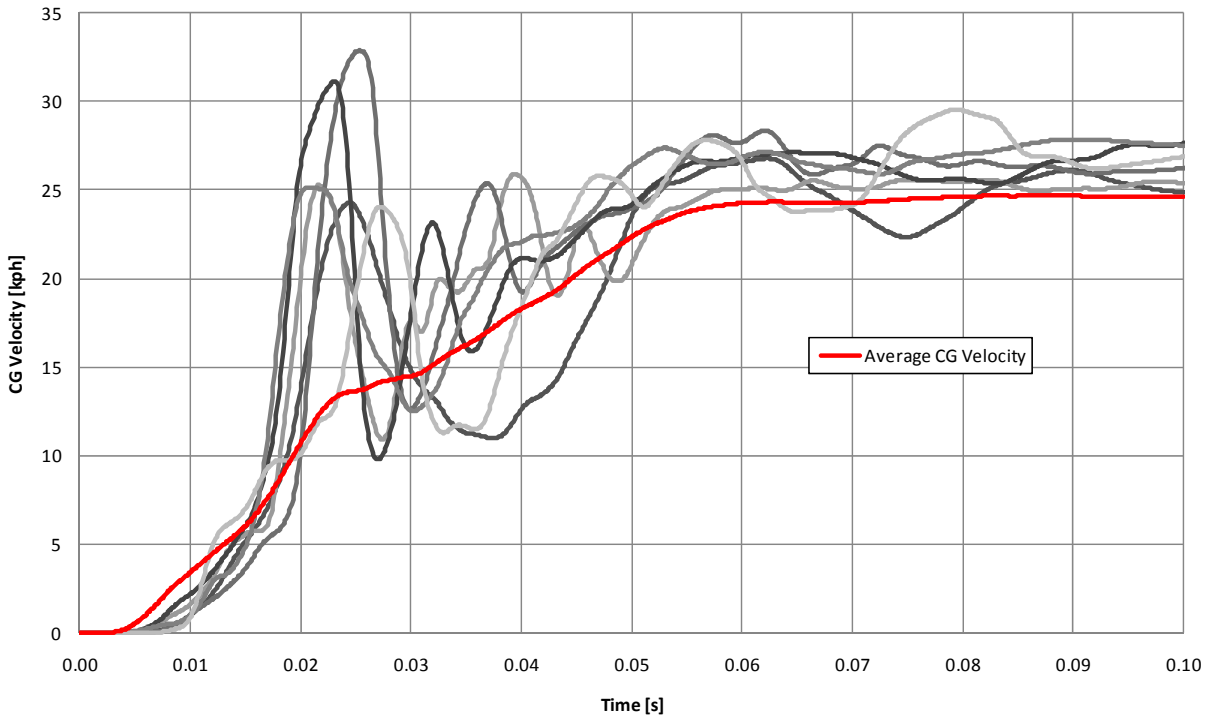

Figure 3.9: CG lateral velocity traces

Another issue with this type of averaging scheme is shown in Figure 3.10. In this profile of the mid-rear driver's door lateral velocity, the average rises for roughly 0.015 seconds at which point there is a slight dip in the average response. This dip is due primarily to the time offset of the peaks, which do not all occur at the same time after impact. This meant that while some velocity profiles were declining, some were reaching their peak. In a sense these time offsets created a sort of 'interference' when averaged, causing the behavior shown. This average curve was created from a small number of tests which exacerbates this issue due to the lower number of points to average over for each time point. If more curves were used in this averaging, the extent to which this issue occurs would diminish.

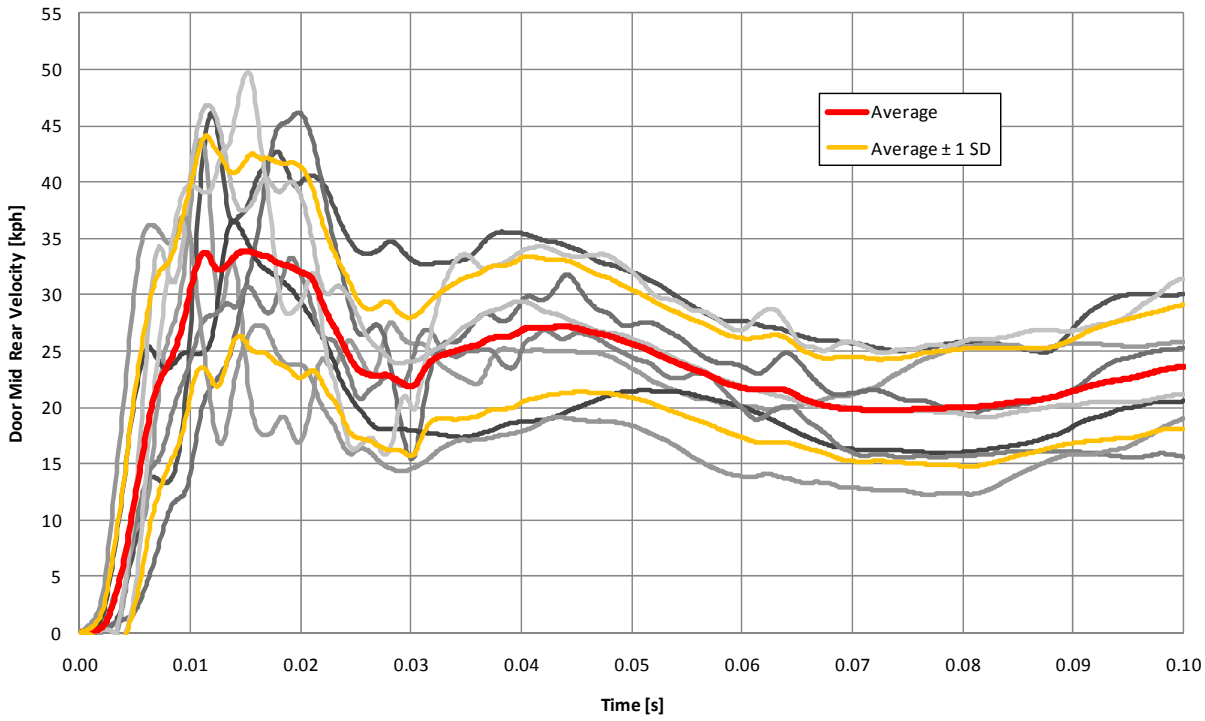

Figure 3.10: Average mid-rear door lateral velocity

During testing the target vehicle rotates, causing the orientation of the accelerometers to change relative to the ground. The angular velocity was found for all tests by performing a kinematic analysis based on the triaxial accelerometers mounted on the passenger side door sills, the center of gravity and the trunk above the axels. For each test the position of each accelerometer was recorded prior to testing. With these positions and the longitudinal and lateral acceleration from three of these accelerometers, it was possible to calculate the angular acceleration of the vehicle during the crash, assuming that the accelerometers used to calculate this rotation remain fixed in position and orientation relative to each other using the following equation at each time step:

$$\alpha = \frac{\Delta_{Rear_y}(a_{CG} - a_{Front}) + \Delta_{Front_y}(a_{Rear} - a_{CG})}{\Delta_{Front_y} \cdot \Delta_{Rear_x} - \Delta_{Rear_y} \cdot \Delta_{Front_x}}$$

(Equation 3.1)

Where 'Δ' refers to the distance between the front and rear right side sill accelerometers and the CG accelerometer location prior to testing in the x and y directions, and 'a' refers to the lateral acceleration at each time step for the front and rear right side sill and center of gravity

accelerometers. It is important to note that this equation assumes that the accelerometers remain in fixed positions relative to each other and there is no local rotation of any accelerometer during the impact. The right (non-struck) side sill and CG accelerometers were used to calculate this rotational acceleration since no damage was seen surrounding these positions (unlike the struck vehicle side). There were several tests where this method could not be used due to erroneous data from crash testing (when accelerometer channels failed, for example).

The angular acceleration traces were numerically integrated to find the angular velocity. The average rotation velocity (found in a similar fashion to the rest of the average velocity histories) of all tests is shown in Figure 3.11. One can see that the rotational velocity is on the order of 1.5 rad/s or roughly 80˚/s. To get a better idea of the meaning of this quantity, the rotational velocity curve was numerically integrated to find rotation as a function of time. This was plotted on the same graph as the dummies thoracic acceleration response for each vehicle, with a typical example being shown in Figure 3.12.

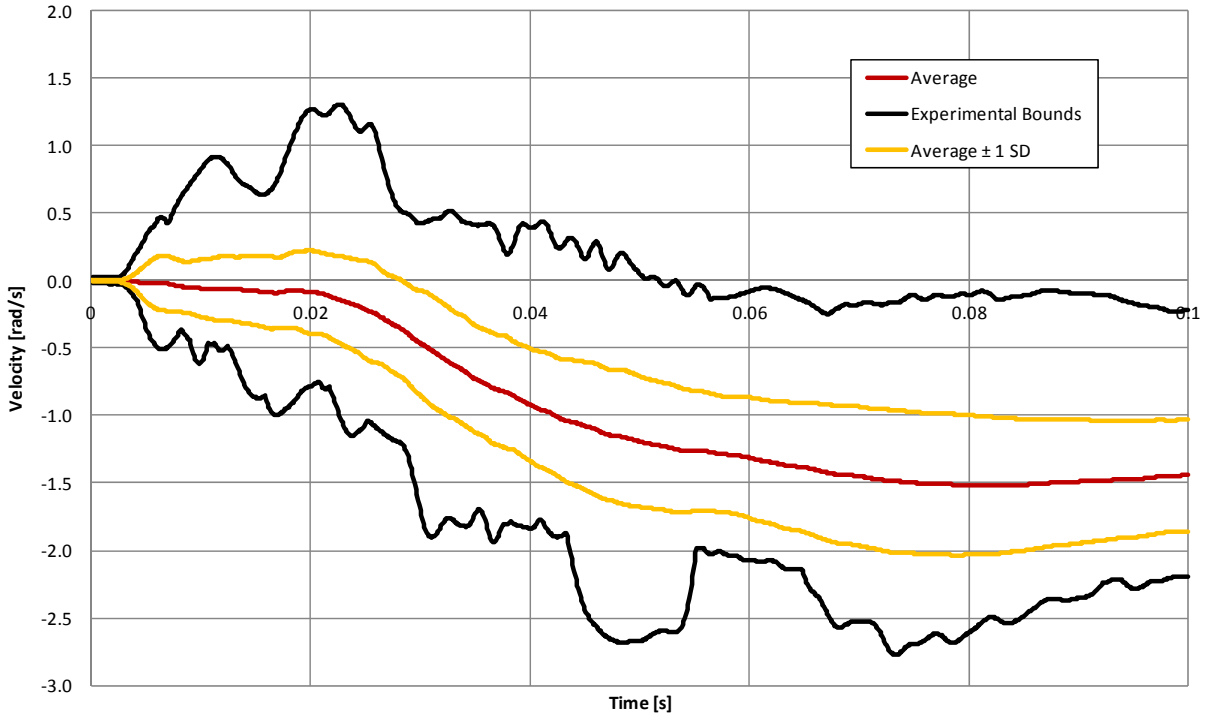

Figure 3.11: Average rotational velocity

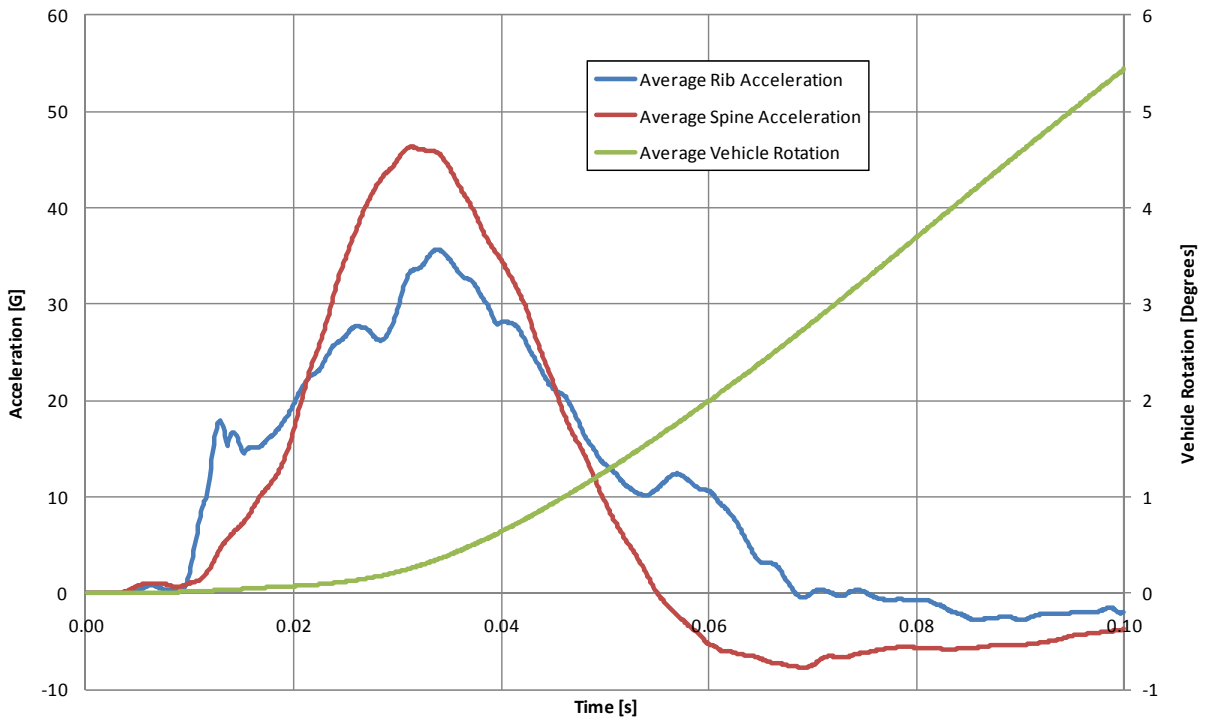

Figure 3.12: Vehicle rotation and ATD response

To study the timing of contact between the ATD and the vehicle, 6 tests were studied in which the thoraxes of the ATDs were instrumented with contact switches to measure the time at which contact with the door occurred. These 6 tests were chosen because they also included door accelerometers, allowing for the study of contact on the door velocity profile. The average time to thoracic contact as measured by these switches after contact between the barrier face and the outer skin of the side door was 0.0125 s, with all times falling between 0.092 s and .0173 s. Figure 3.13 through Figure 3.18 show the contact and door velocity responses of these tests. These plots show that all initial contact occurs prior to the door velocity plateau that is seen after roughly 0.03s though no direct effect of the contact on the door velocity can be inferred based on these plots.

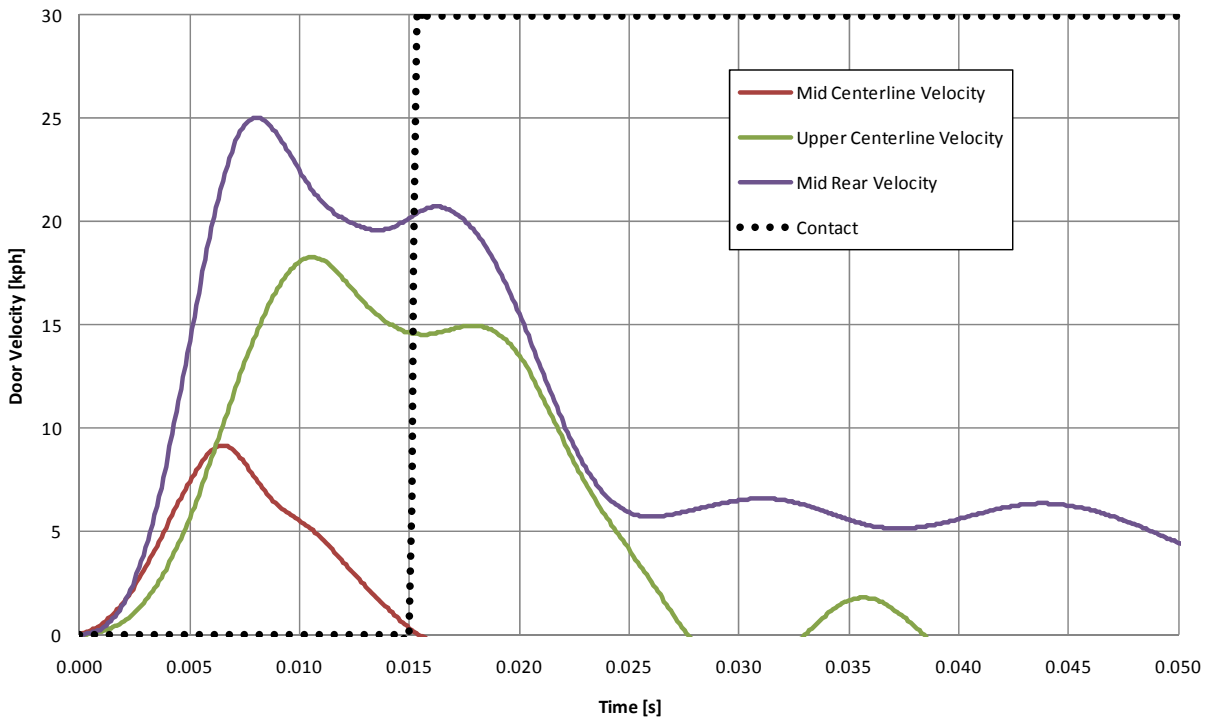

Figure 3.13: Door velocity and contact timing of 2005 Toyota Corolla side NCAP test

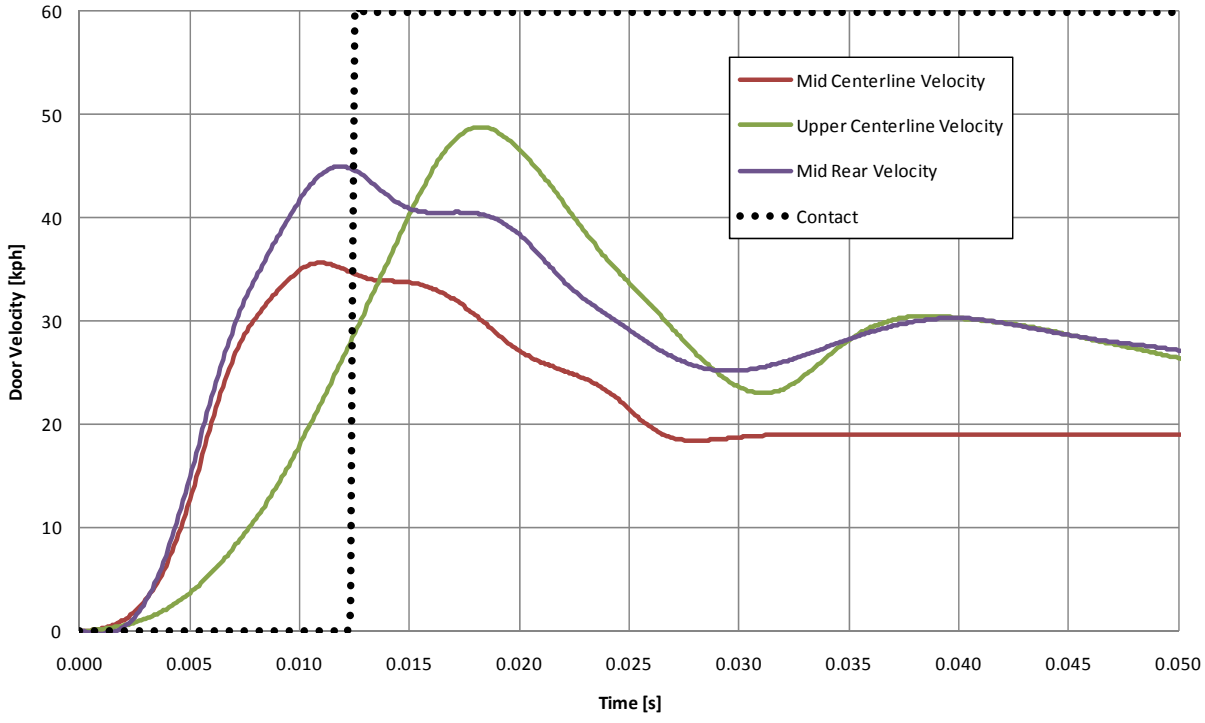

Figure 3.14: Door velocity and contact timing of 2005 Chevrolet Malibu side NCAP test

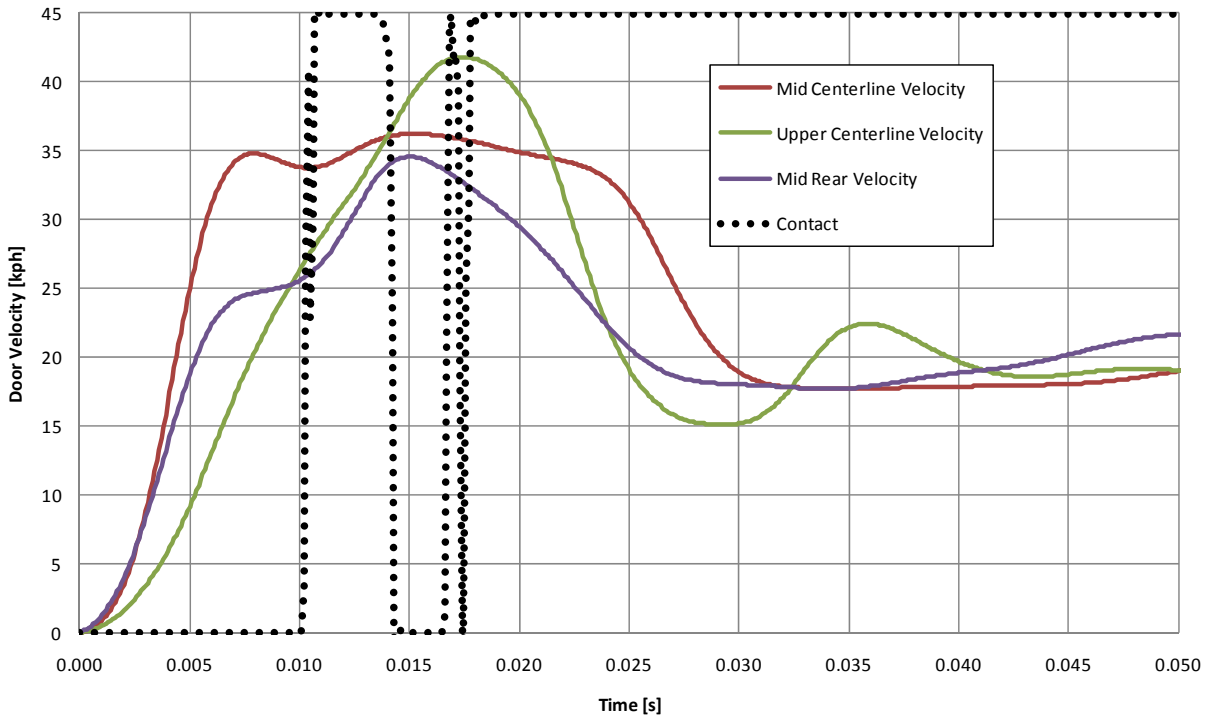

Figure 3.15: Door velocity and contact timing of 2005 Volkswagen Jetta side NCAP test

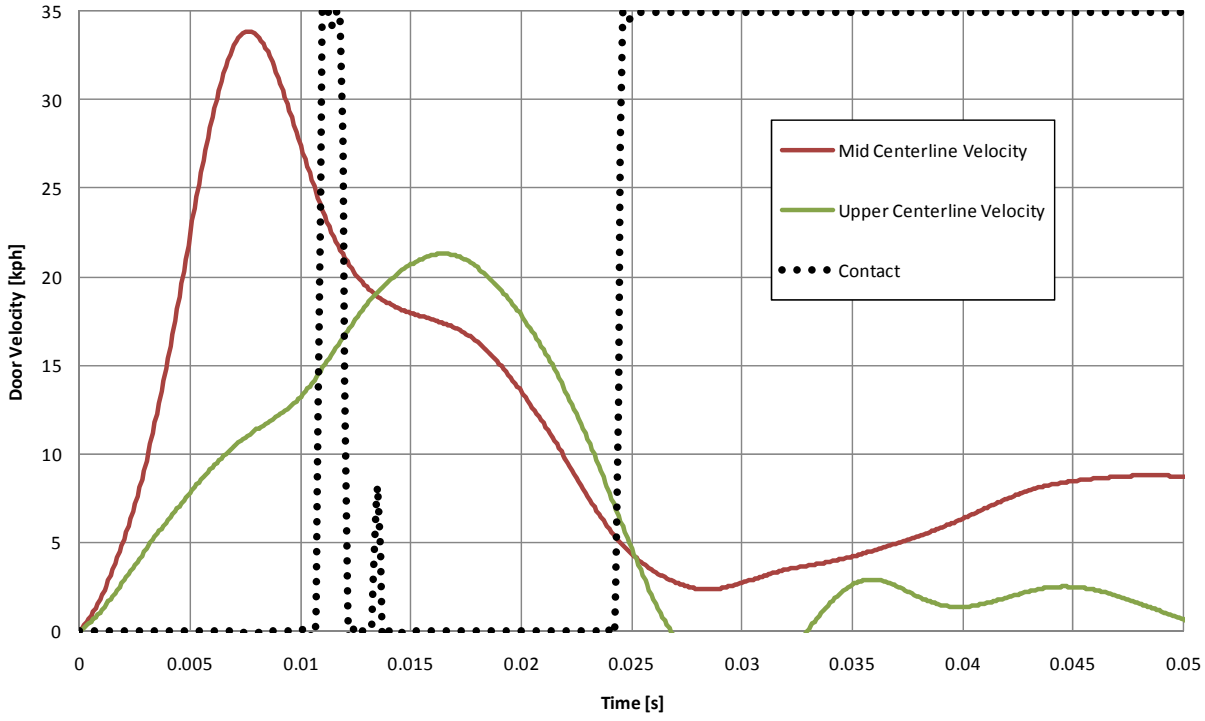

Figure 3.16: Door velocity and contact timing of 2005 Volkswagen Passat side NCAP test

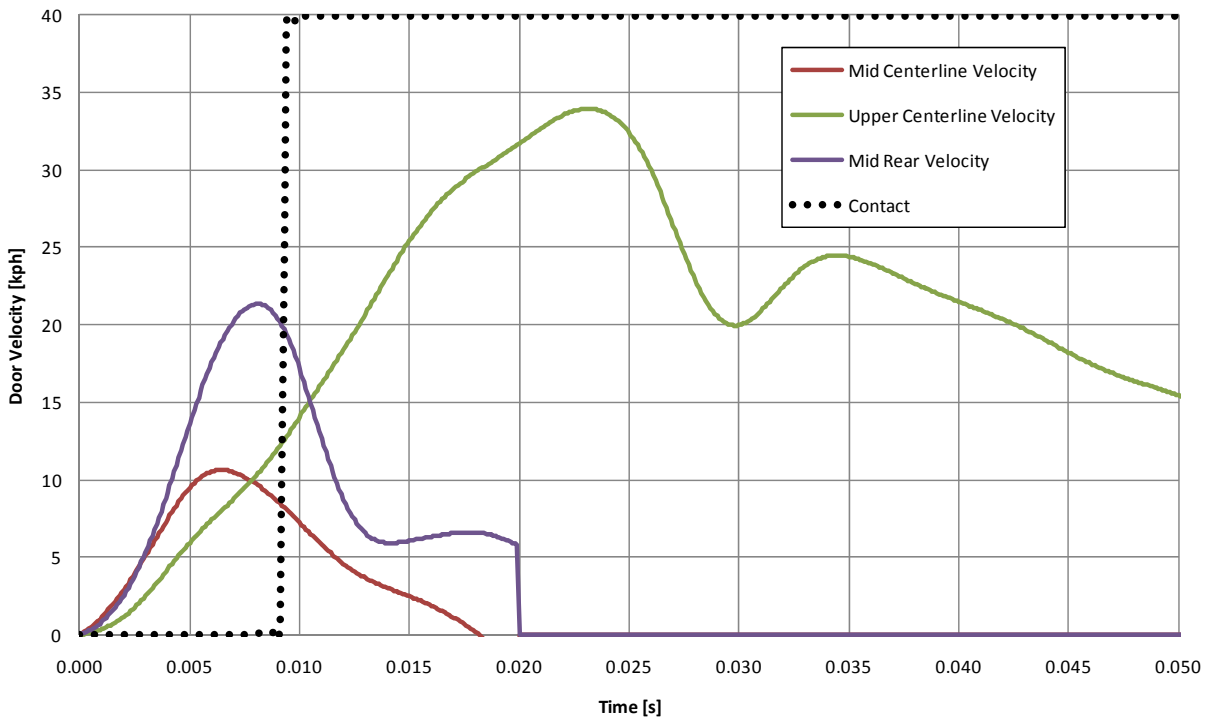

Figure 3.17: Door velocity and contact timing of 2006 Kia Rio side NCAP test

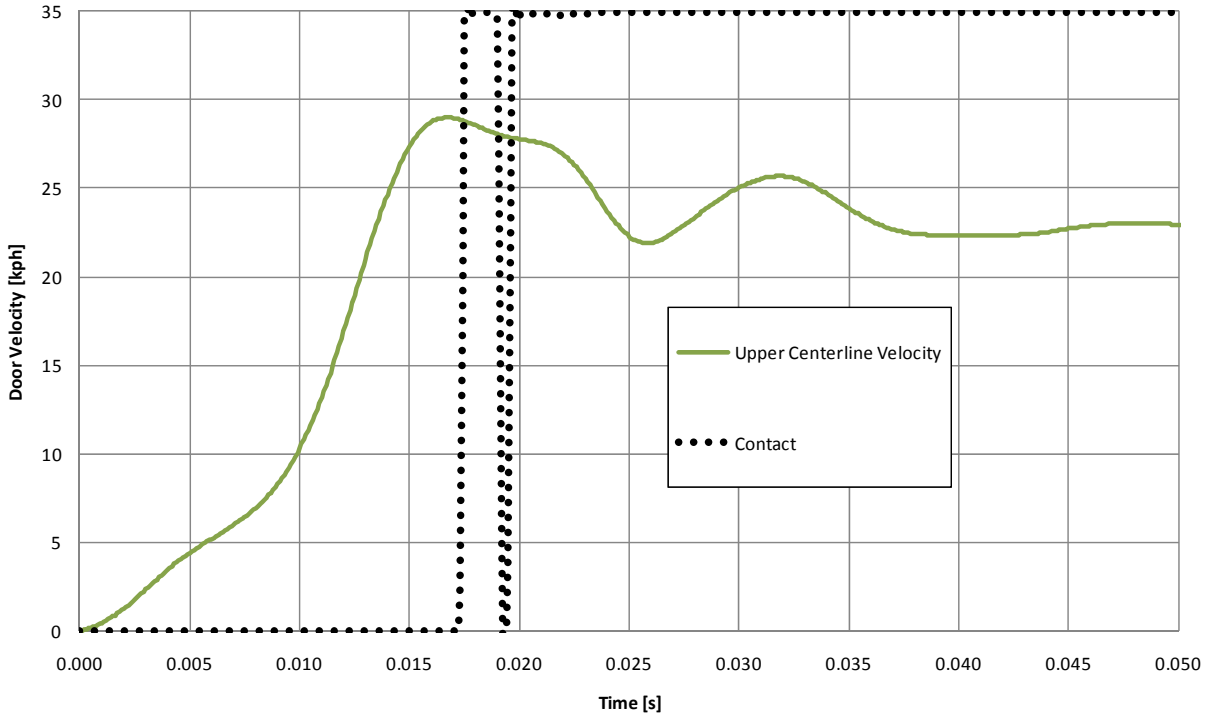

Figure 3.18: Door velocity and contact timing of 2006 Chevrolet Impala side NCAP test

3.4 Discussion

Intuitively one would assume that increasing the vehicle mass, increasing the distance between the occupant and the door, reducing the effective speed of impact and decreasing the amount of intrusion into the vehicle should lower the injury seen by the occupant. Additionally it is not unreasonable to assume that in general vehicles which protect one body region well would provide higher levels of protection to other regions as well. Figure 3.2 through Figure 3.7 show these general trends; however they also show by their lack of linear correlation, that each of these factors alone is not a good indicator of what leads to thoracic injury. The scatter present in these plots shows that there are a number of factors beyond those presented that affect thoracic injury. This is in agreement with the work of Tencer, who attempted to develop a linear relation between TTI and vehicle weight, peak door velocity, peak door acceleration and door crush distance [Tencer et al, 2005]. In this work the best correlation was found to have an 'r^2' value of 0.35.

The various velocity-time histories determined from the database are in good agreement with the existing literature. The first peak observed in the door velocity history is often attributed to the outer skin of the door collapsing. Once the barrier reaches the outer structure of the door (the A and B pillars and door sill) the door velocity decreases and equalizes with the pillar velocity. When these structures collapse the velocity of the door again increases [Payne et al., 1997]. It has also been suggested that as the door begins to collapse, the velocity is elevated until the first peak at which time the interior door contacts the occupant, slowing the door velocity until the occupant is pushed away, at which time the velocity increases again [Chan et al., 1998].

To address some of the shortcomings using the point wise average to develop the mean representation of the velocity traces, a new method of averaging was investigated. The basic idea was that each curve could be represented a series of points that each individual curve passes though. For example the door velocity profiles have a large peak early in the time history followed by a valley and another peak, then remaining nearly constant for the rest of the time history. By looking at individual curve responses in this manner it may be possible to develop a curve that represents both the velocity magnitude and the time value better than by averaging the plots at a given time. For example Figure 3.19 shows a series of door velocity profiles along with their pointwise average. A simple algorithm was developed to find the peak velocity in the

first 0.03 s (shown in red along the bottom of the graph), along with the time corresponding to that peak. Similarity the lowest velocity between 0.015 s and 0.04 s (blue) and it time were found, the highest velocity between 0.03 s and 0.06 s (orange) and it time, and the lowest point between 0.06 s and 0.1 s (grey) and its corresponding time. For each of these four points, both the time and the velocity magnitude were averaged. Using these four points, along with 0 velocity at time 0 s and the average velocity at 0.1 s, an average velocity profile was created. This is shown in Figure 3.20 along with boxes showing the maximum and minimum values for each point in time and velocity.

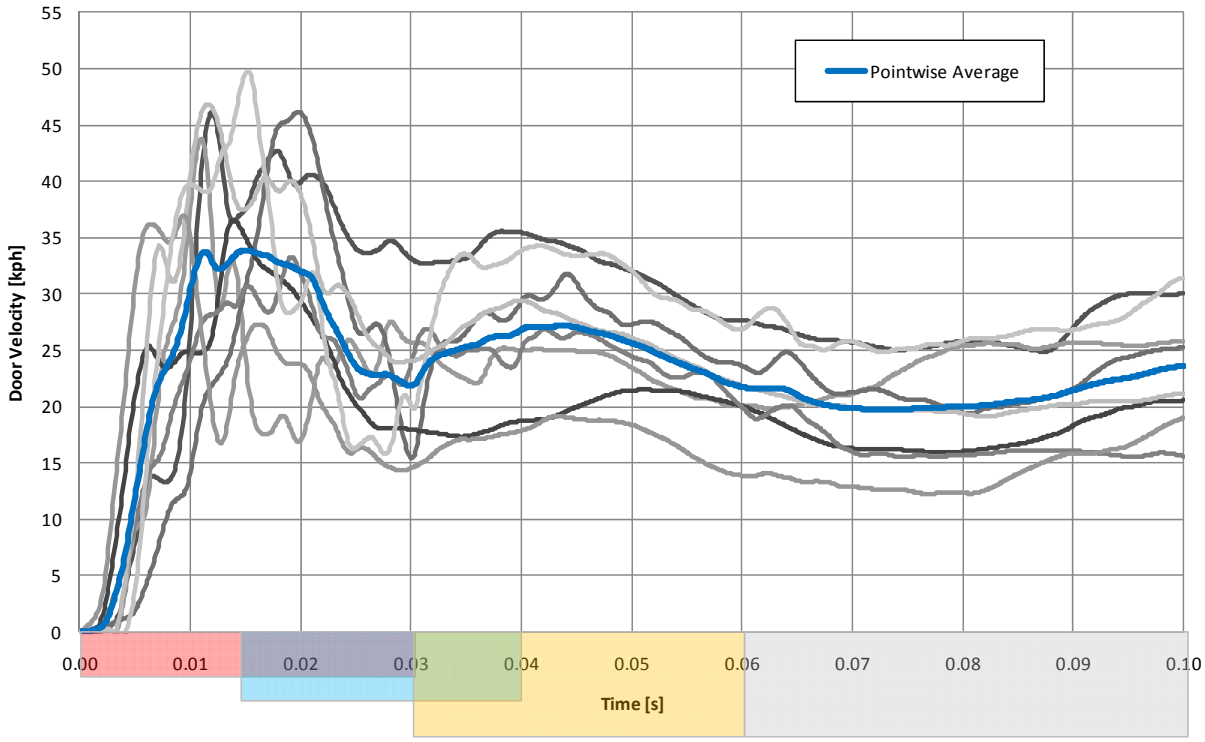

Figure 3.19: General door velocity profiles

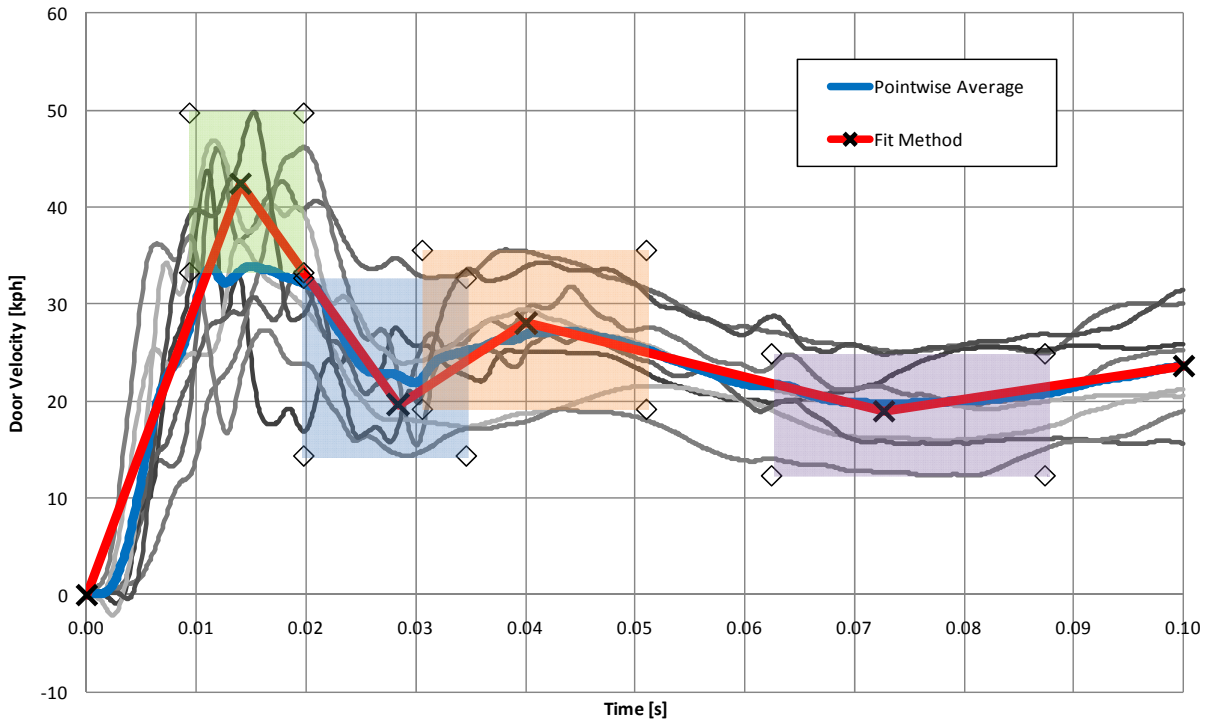

Figure 3.20: Comparison of pointwise averaging and alternative method for door velocity

Figure 3.20 clearly demonstrates the potential to use this method of curve averaging when performing studies involving the parametric study of these types of curves. For example if one chose to use these velocity curves as input into a side sled test, input curves could be developed which were taken from a large sample which are contained within the boxes shown.

A similar approach to this idea is demonstrated in Figure 3.21. To develop this curve, the 'average' curve was assumed to be bi-linear with a knee near the region shown in the green (which represents the actual corridor where this knee occurred for all tests). A least squared fit was performed for all tests to find the point for this knee which led to the optimum bi-linear representation for each curve. These points were then average in time and velocity to find the average knee point, which allowed the average curve shown in Figure 3.21 to be developed.

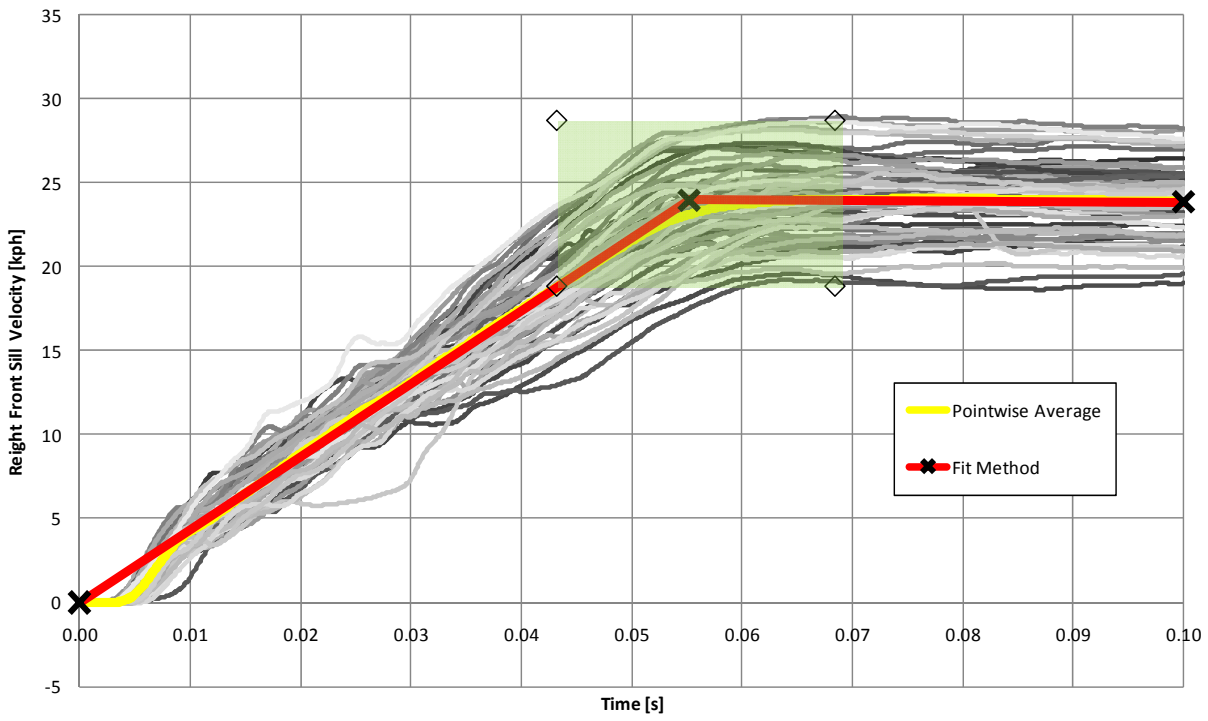

Figure 3.21: Comparison of pointwise averaging and alternative method for right front sill velocity

To assess the relative 'goodness of fit' of the box-corridor method, a cumulative sum of squares was performed. Essentially each squared difference between the response of each test curve and the average were summed for all time steps and all curves. This was repeated with the boxed corridor average. The results of these tests show that the pointwise average performed slightly better in both cases presented here. This may be due to the use of linear point to point representations of the plot. If more elaborate methods were used (sinusoidal or polynomial fits) the box method may provide a better fit. One obvious disadvantage of using this method is that a judgment is required as to what an 'average' curve should look like prior to development. If a strong knowledge of the response is not already present, it may be difficult to assess this and thus may lead to erroneous results. Additionally, curves that do not follow the general trend of what one expects must be considered outliers and cannot be used, which may lead to excessive reduction in the data used to construct these curves.

Figure 3.12 illustrates that the maximum injury to the dummy (if one considers TTI) occurs prior to 50 ms, while the vehicle has essentially not rotated. This indicates that rotation of the vehicle does not play a part in the initial loading of the dummy. The second peak seen at roughly 125

ms which occurs due to the unloading of the chest occurs after a small amount of rotation has occurred. A series of tests on the NHTSA Biomechanics Test Database [NHTSA Biomechanics Test Database, 2009] (test #'s 1246, 1247, 1248, 1249, 1256 and 1257) show that the predicted injury to USSID dummies from purely lateral pendulum strikes and from strikes rotated by 10˚ laterally are essentially the same. Additionally during this unloading period the relative difference between the rotation of the dummy and the door is very small as the acceleration traces of the dummy returns to zero prior to unloading. Thus it can be inferred that the rotation does not play a significant role in loading the dummy during LINCAP testing. This is not to say that in general rotation does not affect injury in all side impacts; at higher impact velocities which result in higher rotational velocities, this may be not be the case.

Figure 3.13 through Figure 3.18 show that the contact between the occupant and the intruding door tended to occur after the peak door velocity. This would lend credence to the notion that the drop in door velocity is not due to solely to contact with the occupant, but that the side vehicle structure begins to take the brunt of the impact leading to this drop in velocity. Unfortunately, few of these velocity profiles were typical 'double peak profiles' making any other conclusions difficult to draw.

One significant issue to consider with respect to the database is the effect of side airbags on occupant response. A review of the vehicles tested by NHTSA during the time period of interest for this study showed that there was a significant increase in side airbag installation over the time in which the study has focused. A number of the vehicles in the early part of the data set either were not equipped with side airbags or they were optional equipment for that vehicle. For cases where they were optional equipment, the LINCAP test was often performed twice on the vehicle model; once on a vehicle with side airbags, and once on a vehicle without side airbags. Of the 72 vehicle included in this survey, the average TTI score of the 60 vehicles with at least one side airbag was 53 g while the 12 without side airs scored an average of 74.5 g. The majority of the vehicles without side airbags were from the 2005 and 2006 model years. A search of all cars (sedans, coupes and wagons) tested over the same time period (a total of 119 tests) showed that this phenomena was not limited to sedans. Figure 3.22 shows that as the average number of side airbags per vehicle for the driver have steadily increased over the past 5 years, the average TTI score has decreased. A similar finding was highlighted in a NHTSA report [Kahane, 2007] which

concluded that the large drop in TTI since the inception of the FMVSS 214 regulatory test was due in large part to the inclusion of side airbags however this is not always reflected in epidemiological studies [McGwin et al., 2003].

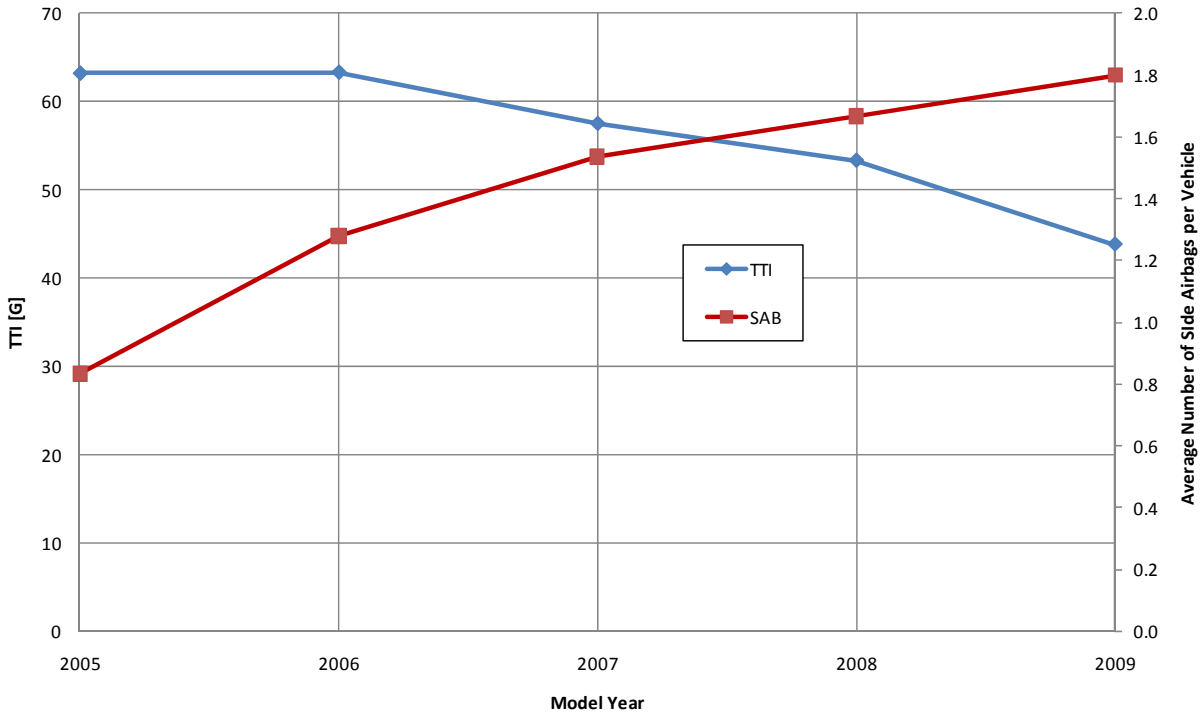

Figure 3.22: Side airbag installation and TTI score

Chapter 4 Modeling Approach and Description

4.1 Introduction

To fill some gaps in knowledge from the study of NHTSA's crash database, a set of side NCAP and FMVSS214 simulations were created. These simulations were intended to allow much more detailed analysis of side impact, particularly with regards to the response of the occupant. Additionally, using finite element modeling allowed the true effects of changes to the vehicle interior and initial occupant position to not be confounded by the variability in experimental crash testing. In these simulations, a vehicle model was impacted by a MDB model, with an occupant model in the front left driver's seat. A three point restraint system model was also included. The three occupant models (USSID, ES2-re, and WSID) were each placed in a nominally central seating position laterally and longitudinally. With the occupant models in this position, a series of simulations were carried out at two different barrier speeds 54 kph (representing the FMVSS 214 barrier speed) and 61 kph (representing the NCAP barrier speed). These simulations were compared to experimental crash test from the NHTSA car crash database [National Highway Traffic Safety Administration Vehicle Crash Test Database, 2009] as well as the experimental corridors discussed in Chapter 3 for verification and validation purposes. Following this, the occupant models were moved laterally, longitudinally, and vertically to assess the differences in the response of the models in a nominal position and out of position (OOP). Additionally several material models of interior panels were modified to assess the importance that these materials play in mitigating injury to the occupant.

The following sections outline each of the models developed for these side impact simulations and discuss the model validation which was performed on each sub-model. The single precision explicit finite element solver LS-Dyna [LSTC, 2007] Version 971 Revision 3.1 was used for all simulations.

4.2 ATD Models

The ATD models used in this research were commercially available models supplied by First Technology Safety Systems and Dynamore GmbH. The USSID and ES-2re models were developed by in conjunction with DYNAmore GmbH [Franz and Graf, 2004; Franz et al., 2002;

Franz et al., 2008; Schuster et al., 2004] while the WorldSID model was developed solely by FTSS [Liu et al., 2007]. These models were developed from either three dimensional scans of parts from and actual ATD or from CAD geometry provided by ATD manufacturer. Each part was meshed individually and then assembled. Material properties (such as foam stress-strain behavior) were found by the developers of these models by performing material characterization tests at strain rates from quasi-static to upwards of 200 s^{-1} (in both tension and compression, where applicable) on material taken from an actual ATD [Franz et al., 2008]. Throughout the development of these models, sub level components such as rib modules, head forms, and the partially assembled pelvis were tested using various impactor and drop tests to ensure that each component responded as the actual subassembly that it was modeling. With each sub-module responding properly, the full models were assembled and tested against their pertinent calibration tests and also a series of rigid side sled tests to compare the response of the models to the actual ATDs. Rigid joints were defined between the various articulating parts (ie. the arms, the knees, the feet, etc.) to allow rotation during simulation.

While a great deal of effort was put into the verification and validation of these models by the developers, to ensure consistency between the computing platforms of the developers and those used in this research, each ATD model was verified independently of developers validation and verification. The verification of the ATD models was essentially a series of simulations based on the pertinent calibration tests laid out in Title 49 Section 572 of the United States Federal Code for the USSID and ES-2re [United States Code, 2008] and the calibration tests described in the WorldSID Users Manual [WorldSID TG, 2005]. It is important to note that only those tests involving the thoracic region were performed.

4.2.1 USSID

Initial pendulum tests with this modeled showed that under heavy loading, numerical instability (ie. inverted elements leading to negative volumes) occurred in the foam arm section of this model (the foam part in quesion is shown in green in Figure 4.2). To overcome this, the foam arms were assigned an interior contact. In essence, this type of contact tends to eliminate nodes passing through the opposite face of an element which can happen with soft materials such as foam [LSTC, 2007].

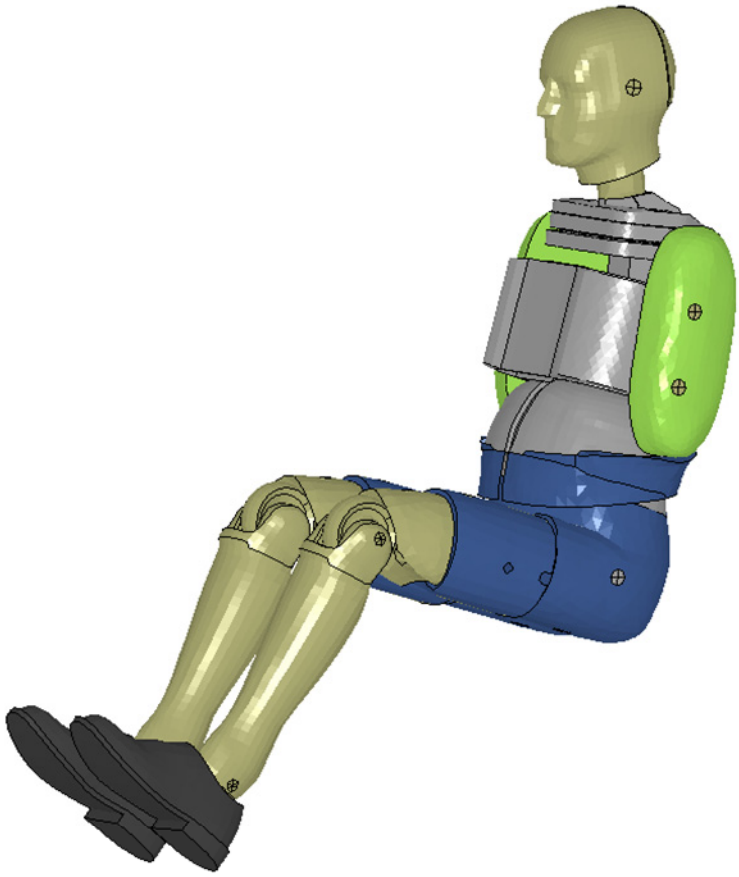

Figure 4.1: USSID model with no jacket

The thoracic calibration test for the USSID is outlined in the US Federal Code Title 49 Part 572 Subpart F. Essentially a USSID is required to undergo a 14 foot/second pendulum impact at the center of the dummies third rib prior to use in crash testing. The pendulum specifications are laid out in Title 49 Part 572.44a, which require the pendulum to be 6" in diameter with a 0.5" radius on the face and weigh 51 lb. The dummies acceleration response is filtered with an FIR100 filter and to be considered within calibration spec must fall between 37 G and 46 G for the upper and lower rib accelerometers and 15 G and 22 G for the lower thoracic spine accelerometer.

For this calibration test simulation, a 6" diameter, 150 mm long rigid pendulum model composed of shell elements with an added nodal mass in the center of the pendulum on the rear face was used. A 0.5" chamfer rather than a 0.5" radius was used on the front surface of the pendulum to simplify meshing. The dummy just prior to impact by the pendulum is shown in Figure 4.2.

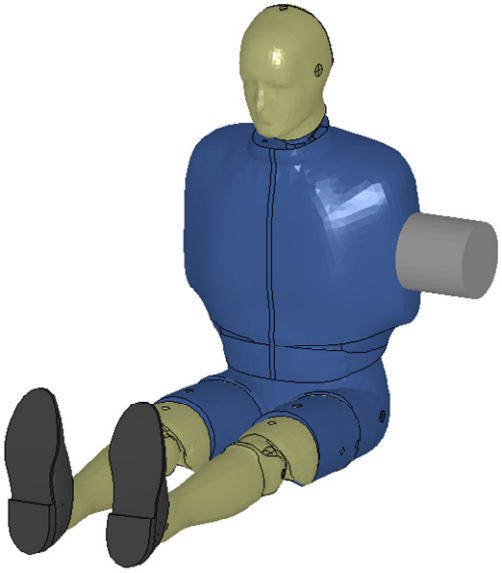

Figure 4.2: USSID calibration test

The response from the calibration simulation is shown in Figure 4.3. The peak responses of the accelerometers were 38.2 G for the upper rib, 38.1 G for the lower rib and 19.2 G for the lower spine, all of which were within the required specification.

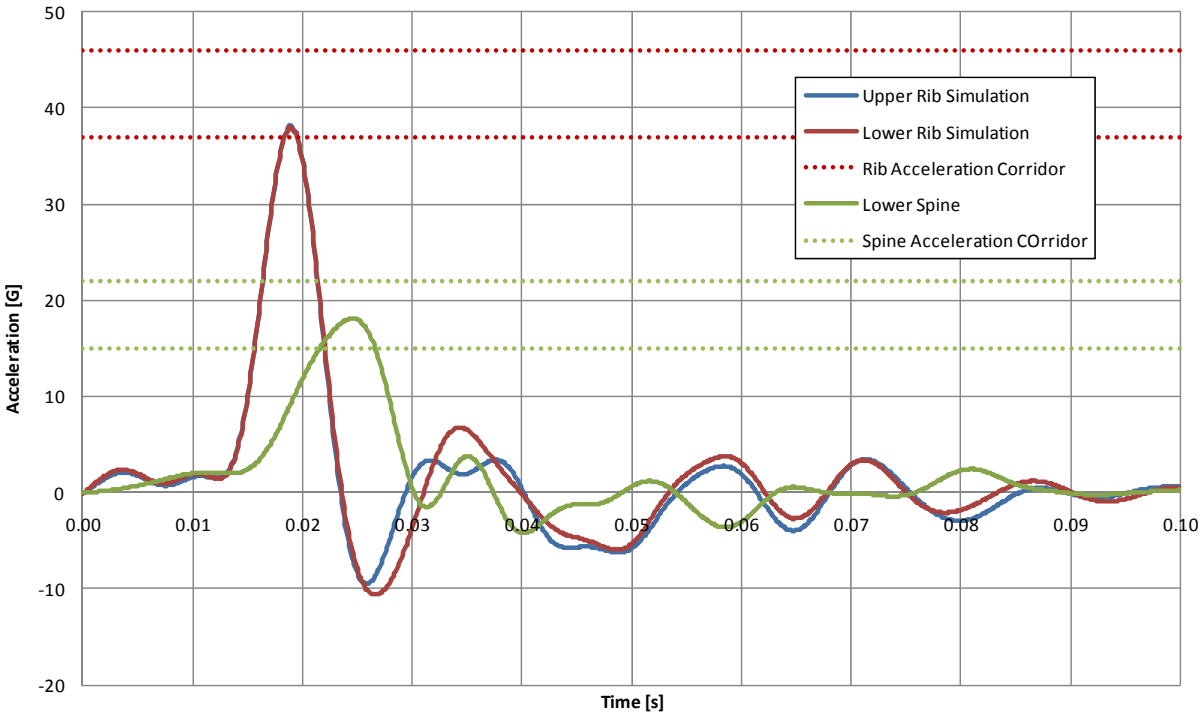

Figure 4.3: Response of USSID to federal thoracic calibration testing

4.2.2 ES-2re

In a similar manner to the foam arm in the USSID model, the foam material surrounding the ribs of the ES-2re model (shown in green in Figure 4.4) were given an interior contact definition to reduce the tendency of these elements to invert and create numerical instabilities.

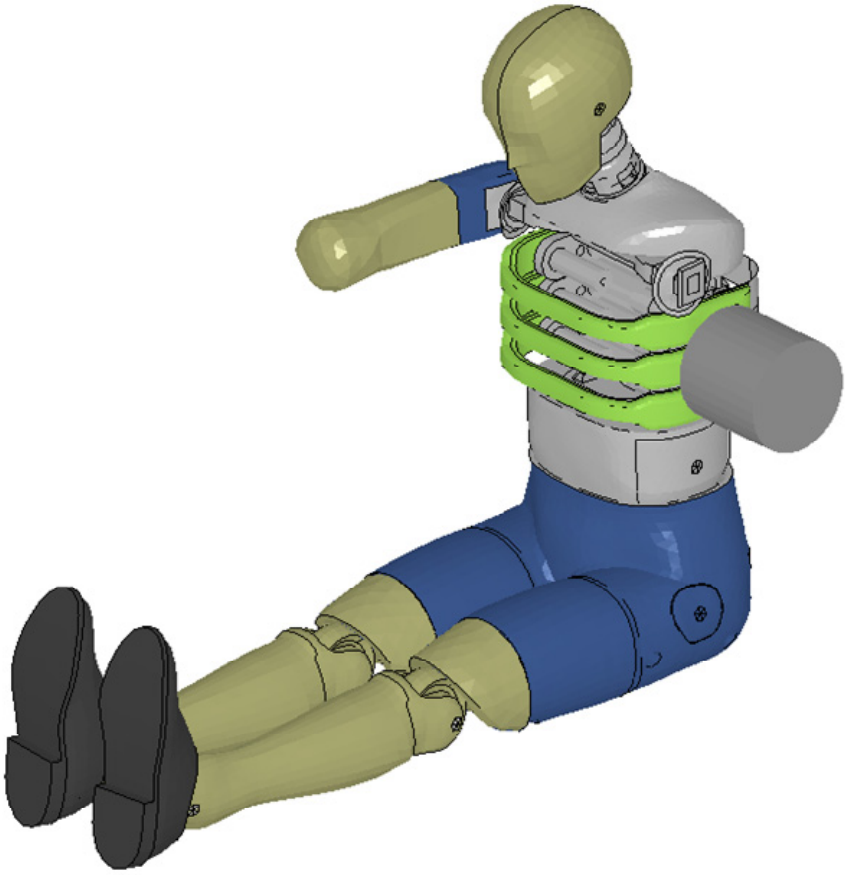

Figure 4.4: ES-2re model with thoracic region exposed

The calibration test for the ES-2re, as outlined in US Federal Code Title 49 Part 572 Subpart E, is slightly more complex than that of the USSID. The thoracic calibration is divided into component tests on each rib and a full thorax impact test. The component tests involve dropping a 7.78 kg, 150 mm diameter mass onto the rib module from heights of 459 mm and 815 mm. The rib deflection must fall between 36 mm and 40 mm for the 459 mm drop test and between 46 mm and 51 mm for the 815 mm drop test. These tests were modeled by isolating the parts of the top rib module of the ES-2re model, as shown in Figure 4.5 (along with the pendulum) while maintaining the relative contacts and constraints between the components. The large body (rib

rail assembly cover) in the center of the module was fixed in position using a rigid body constraint and the impactor was given an initial speed of 3 m/s to simulate the 459 mm drop and 4 m/s to simulate the 815 mm drop. These values were found using a simple conservation of energy balance, assuming no energy is lost in the conversion between gravitational potential energy and kinetic energy. The deflection responses of the rib at 3 m/s and 4 m/s are shown in Figure 4.6, with peak values of 34.7 mm and 46.3 mm for the 3 m/s and 4 m/s cases respectively. The later portions of these curves show a significant amount of oscillation. This behavior is due to the constraints used to fix the rib module in space which upon unloading cause numerical noise due to excessive compression of the soft material within the rib rail assembly. Because this instability did not lead to peak deflections above those seen during loading and was not present in any sled or pendulum tests, this phenomenon was not investigated further. Additional tests were performed at 1 m/s and 2 m/s as per Economic Commission for Europe Transport Regulation 95 [United Nations Economic Commission for Europe, 1995] which states that the rib deflection must be between 10 mm and 14 mm for the 1 m/s impact and 23.5 mm and 27.5 mm for the 2 m/s impact. This simulated response has been included in Figure 4.6, and the peak values recorded were 8.3 mm for the 1 m/s impact and 21.0 mm for the 2 m/s impact.

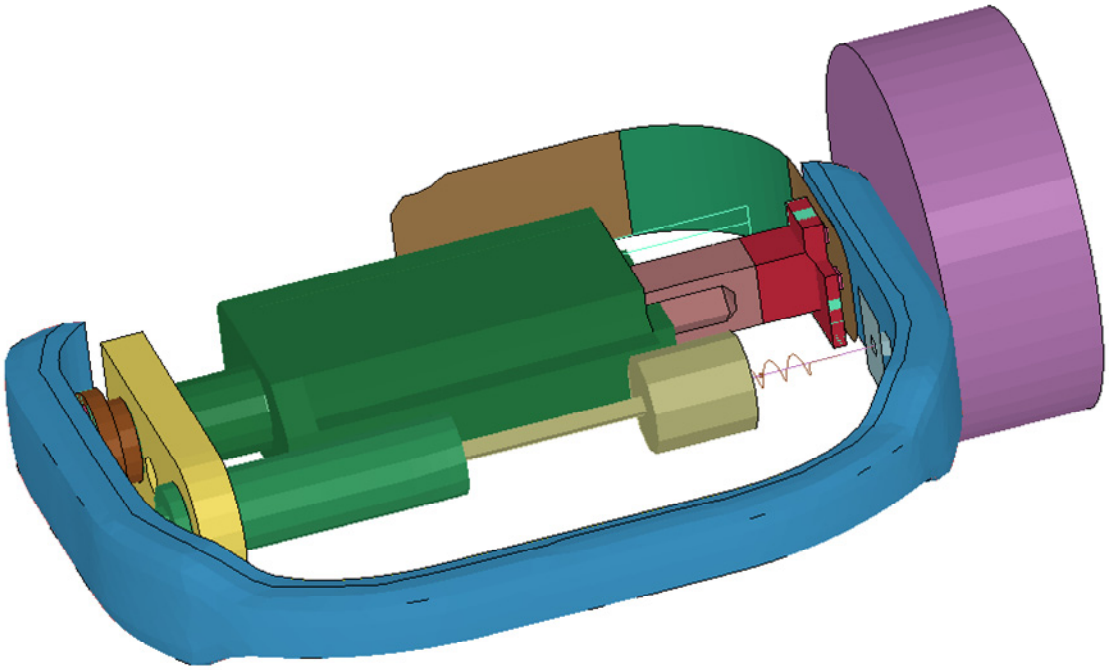

Figure 4.5: Rib module used for component testing

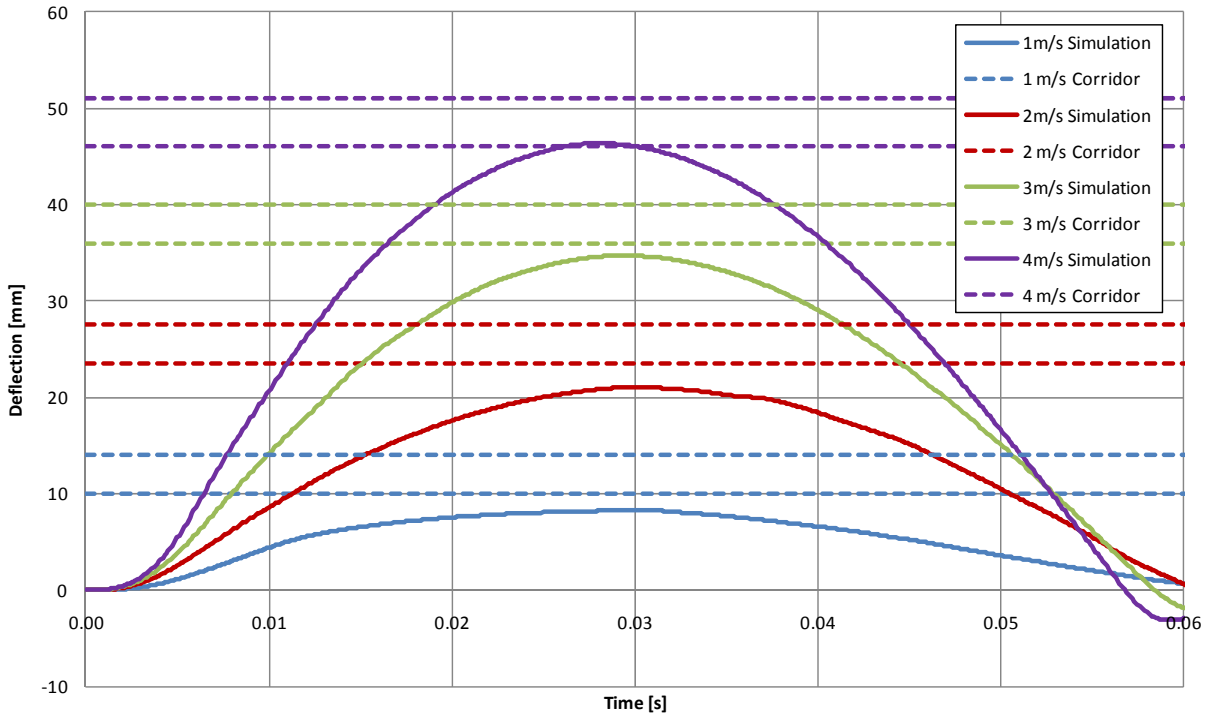

Figure 4.6: Response of rib module at differing impactor velocities

The full thorax calibration was performed on the ES-2re with the struck side (left) arm, shoulder pad and jacket removed, as indicated in Subpart U of Title 49, Part 572 of the United States Code [United States Code, 2008] and is shown in Figure 4.4. The same pendulum used to test the USSID dummy was used in this test with a speed of 5.5 m/s on the middle of the second rib module. For this test, the rib deflections must fall between 34 mm and 41 mm for the upper rib, 37 mm and 45 mm for the middle rib and 37 mm and 44 mm for the lower rib. Additionally the peak force applied by the pendulum (defined as the product of mass of the pendulum and the CFC 180 filtered acceleration of the pendulum) must be between 5100 N and 6200 N. The results of the simulation of this calibration test are shown in Figure 4.7 and Figure 4.5, with peak values of 40.6 mm upper rib deflection, 41.5 mm middle rib deflection, 42.4 mm lower rib deflection and 5798 N pendulum force. Despite responses of the individual rib components being slightly lower than their calibration corridor for the 1 m/s, 2 m/s and 3 m/s impact velocities, the rib deflections of the full thorax impact were within the acceptable response corridors.

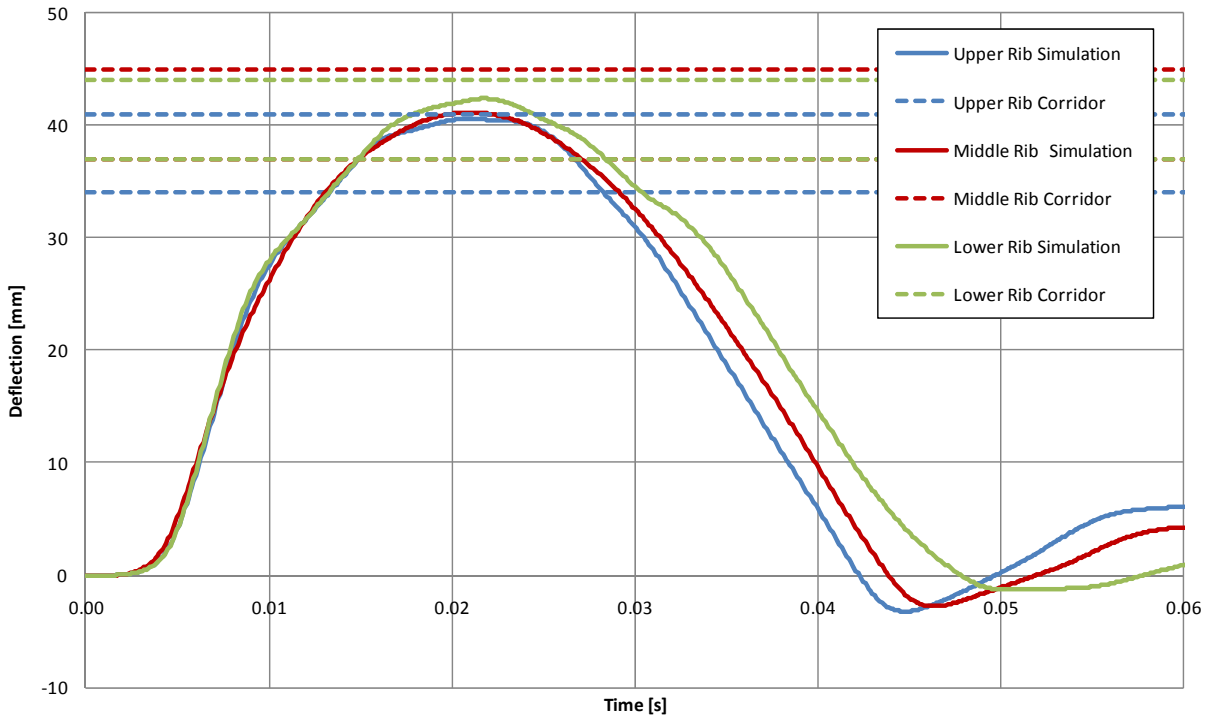

Figure 4.7: Rib deflection of ES-2re in federal calibration test simulation

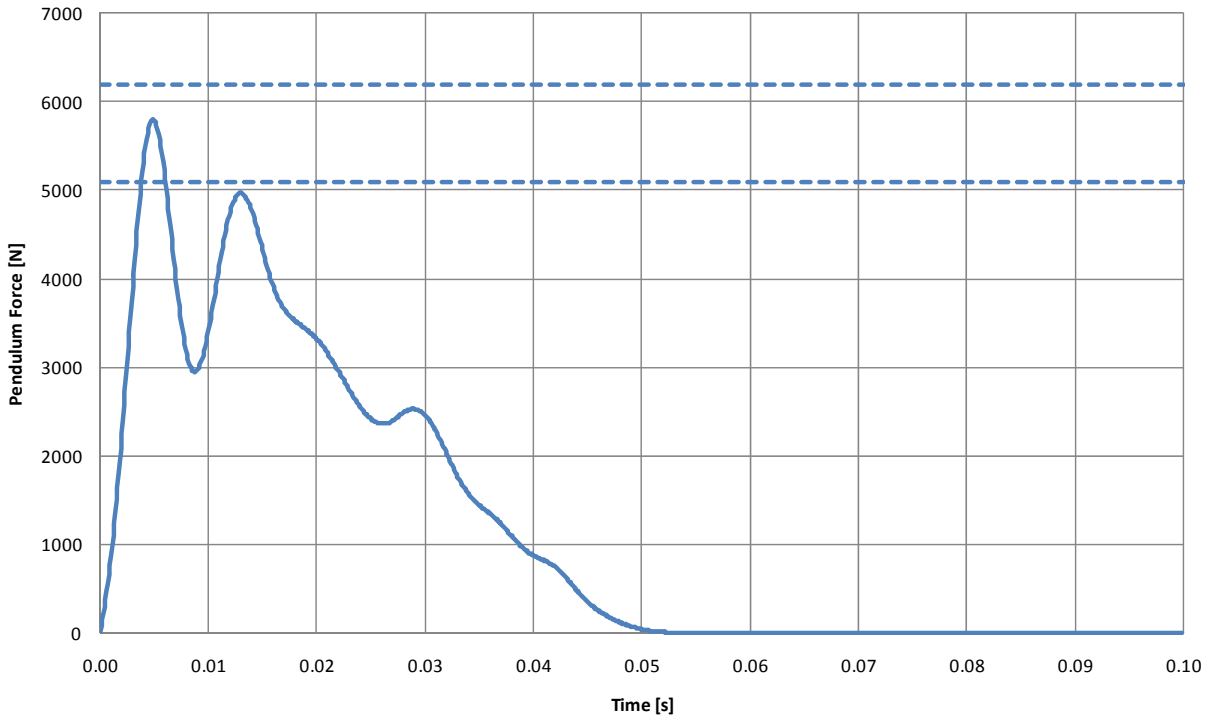

Figure 4.8: Pendulum force resulting from ES-2re thoracic federal calibration test simulation

A simulation of the shoulder impact used to test the ES-2re's calibration was also performed. In this test, the same pendulum used in the thoracic test was used to impact the center of the shoulder at 4.3 m/s (shown in Figure 4.9). The only performance criterion for this test is the peak acceleration of the pendulum which, when filtered with a CFC 180 filter, must be between 7.5 G and 10.5 G during contact with the dummy. The peak acceleration during simulation was 8.6 G. The response of this simulation is shown in Figure 4.10.

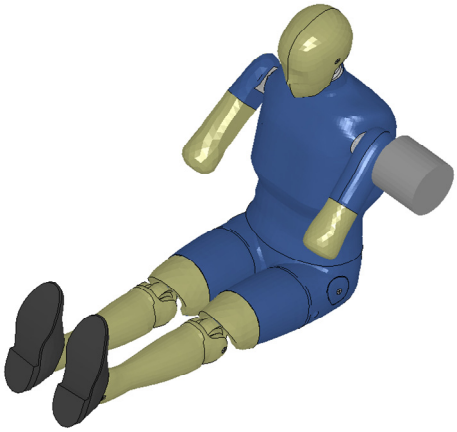

Figure 4.9: ES-2re prior to shoulder impact

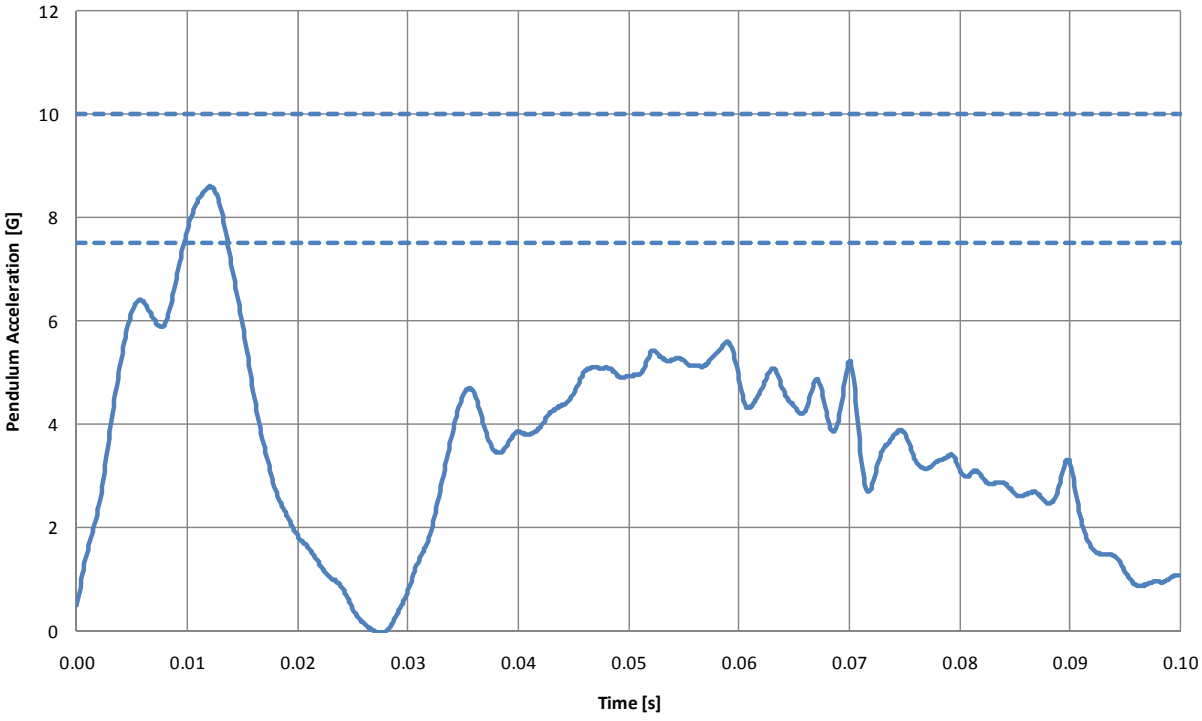

Figure 4.10: Pendulum force resulting from ES-2re thoracic federal calibration test simulation

4.2.3 WorldSID

Like the ES-2re and USSID models, during initial pendulum simulation numerical instabilities were found due to element inversion in a foam material used to surround the ribs of the WorldSID model (shown in green in Figure 4.11). Again, internal contacts were included to increase the stability of the model.

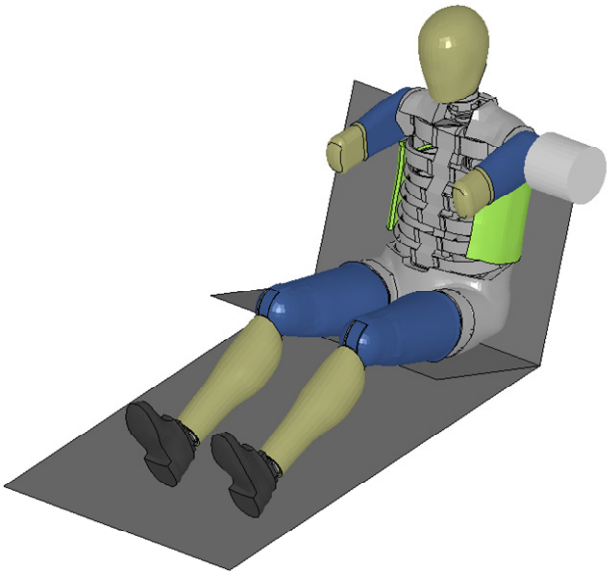

Figure 4.11: WorldSID model with jacket removed prior to shoulder impact

Three separate verification simulations were performed on the WorldSID based on the thoracic certification tests developed by the WorldSID working group. This included a shoulder impact and two thoracic impacts, one with the arm between the pendulum and the thorax (the arm being parallel to the thorax) and one direct impact to the ribcage (the arm raised towards the dummies head). In all three of these simulations, the WorldSID was seated on a rigid surface representing the test bench described in the WorldSID Users Manual. The pendulum's centerline was place coincident with the centerline of the shoulder rib of the WorldSID and was released at 4.3 m/s. The certification requires that the peak pendulum force fall between 2.6 kN and 3.3 kN and the peak deflection of the shoulder rib range between 35 mm and 44 mm. The simulations had peak force and deflection values of 3.30kN and 47.4 mm respectively as shown in Figure 4.12.

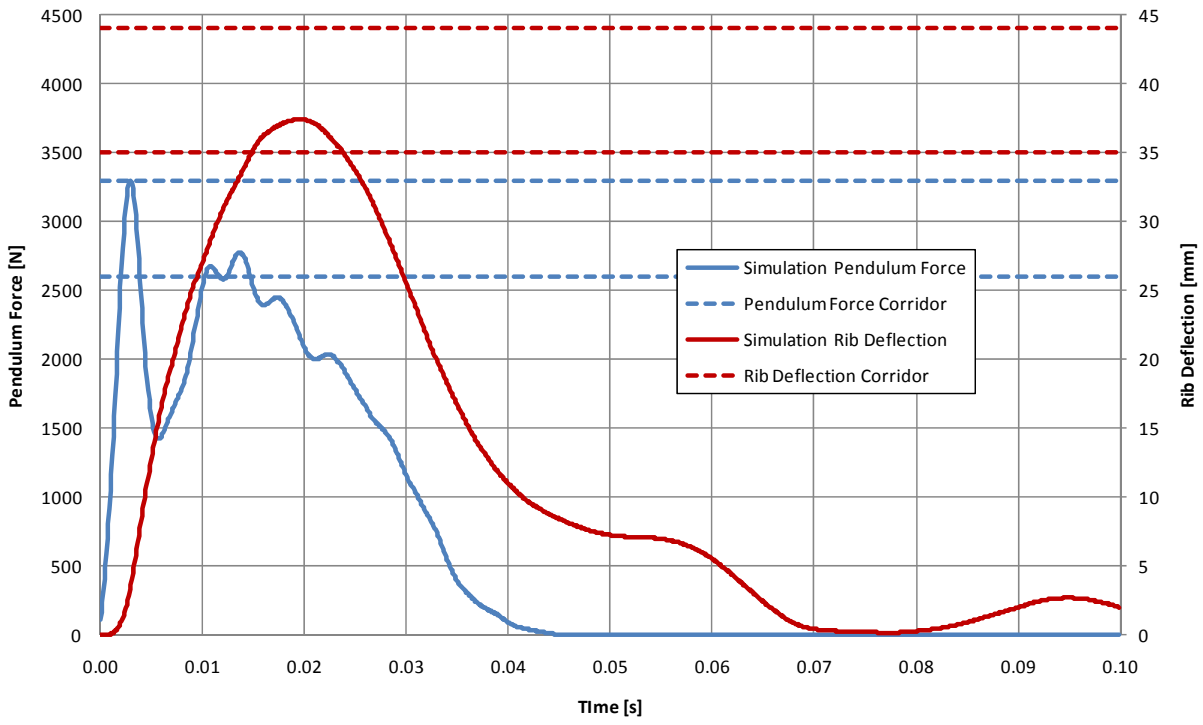

Figure 4.12: WorldSID shoulder calibration response

For the thoracic impacts, the centerline of the pendulum was aligned with the centerline of the second thoracic rib. The pendulum speed was 6.7 m/s for the impact with arm between the pendulum and rib cage and 4.3 m/s for the direct impact between the pendulum and the rib cage. These two initial conditions are shown in Figure 4.13 and Figure 4.14. The certification corridors for the dummies response are shown in Figure 4.15 through Figure 4.18 along with the response of the simulations.

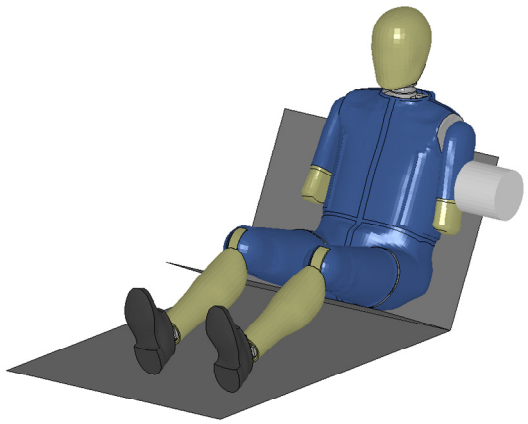

Figure 4.13: Thoracic calibration test simulation prior to impact with arm interaction

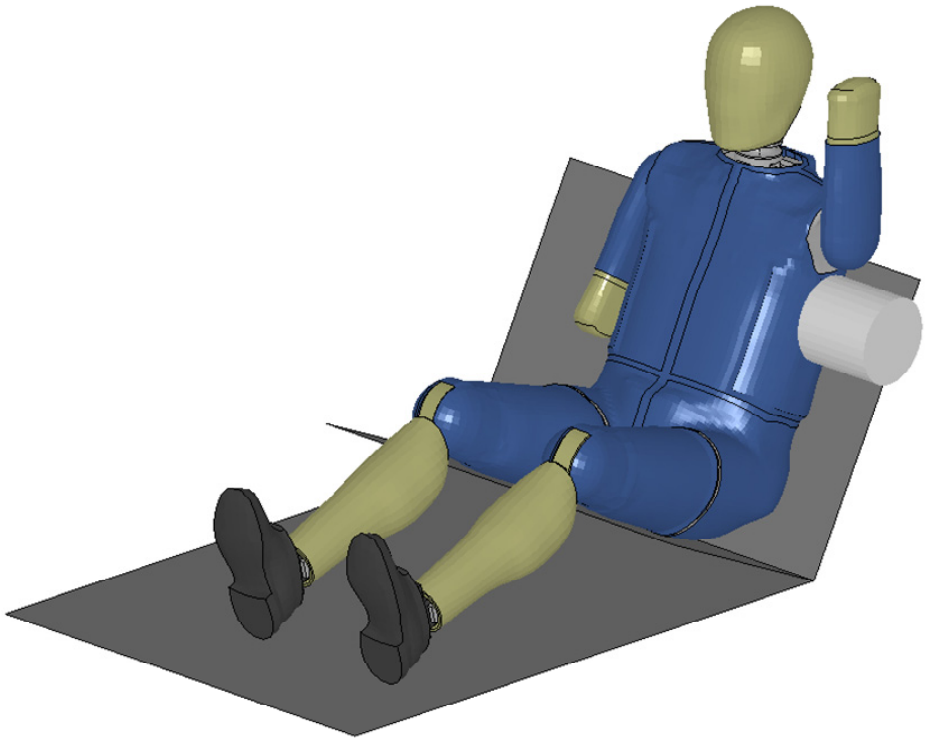

Figure 4.14: Thoracic calibration test simulation prior to impact with no arm interaction

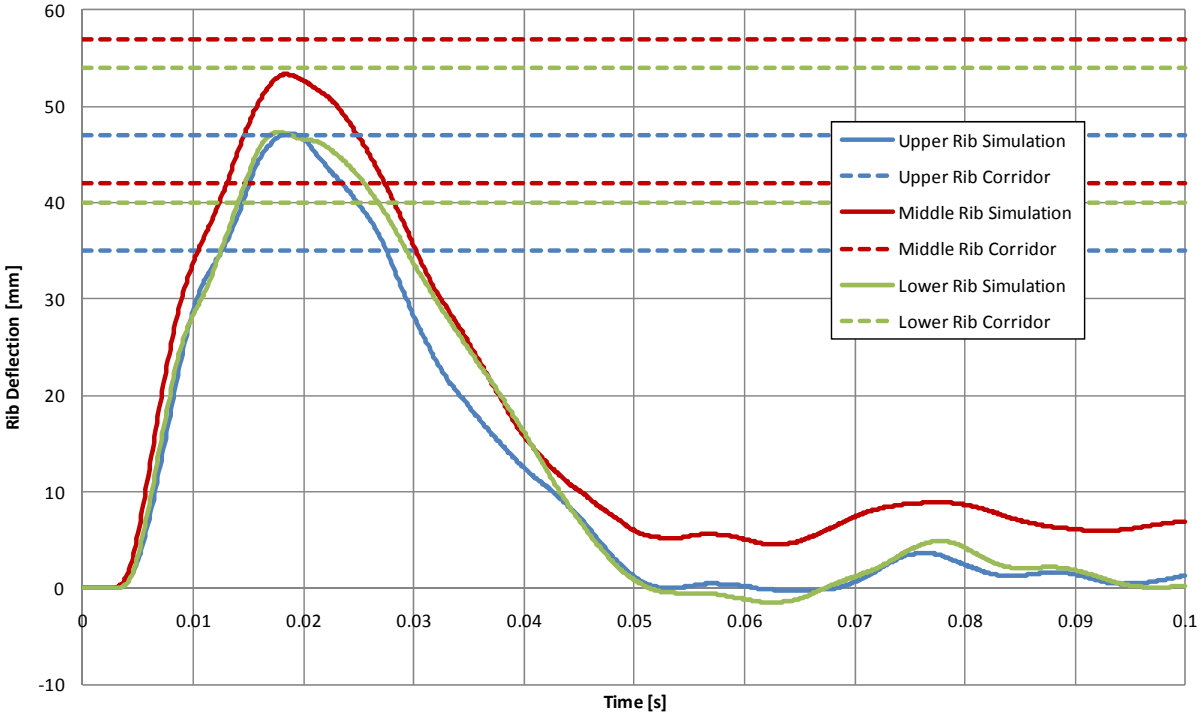

Figure 4.15: Rib deflection of pendulum simulation involving arm interaction

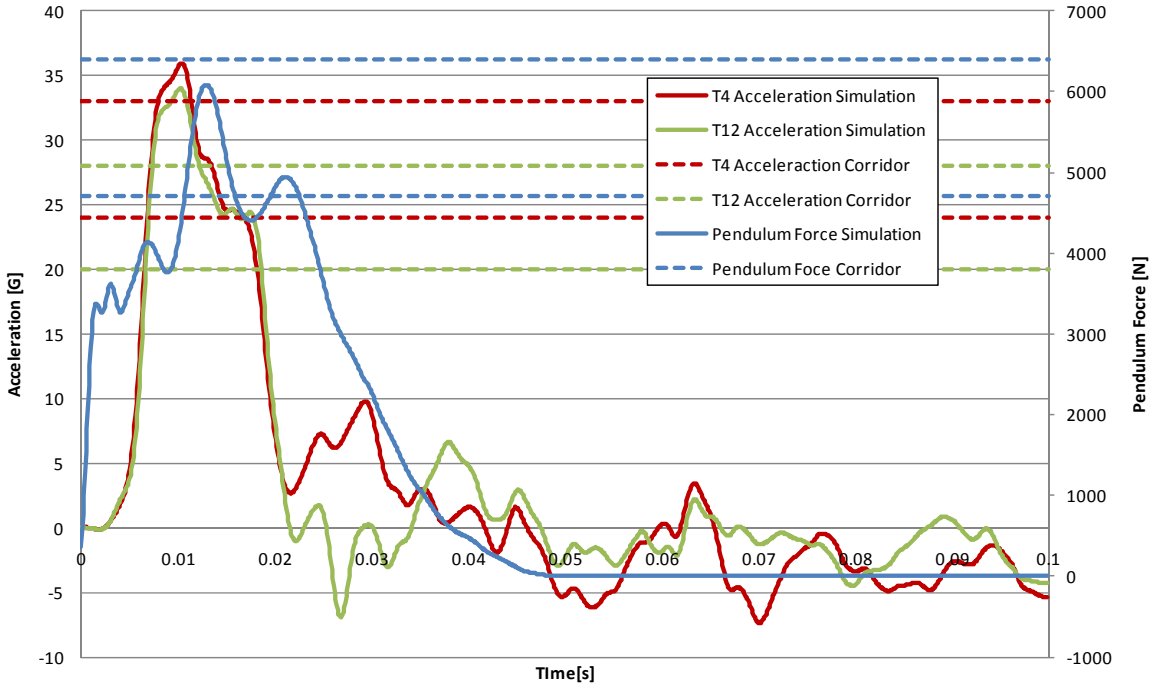

Figure 4.16: Spine acceleration and pendulum force in simulation involving arm interaction

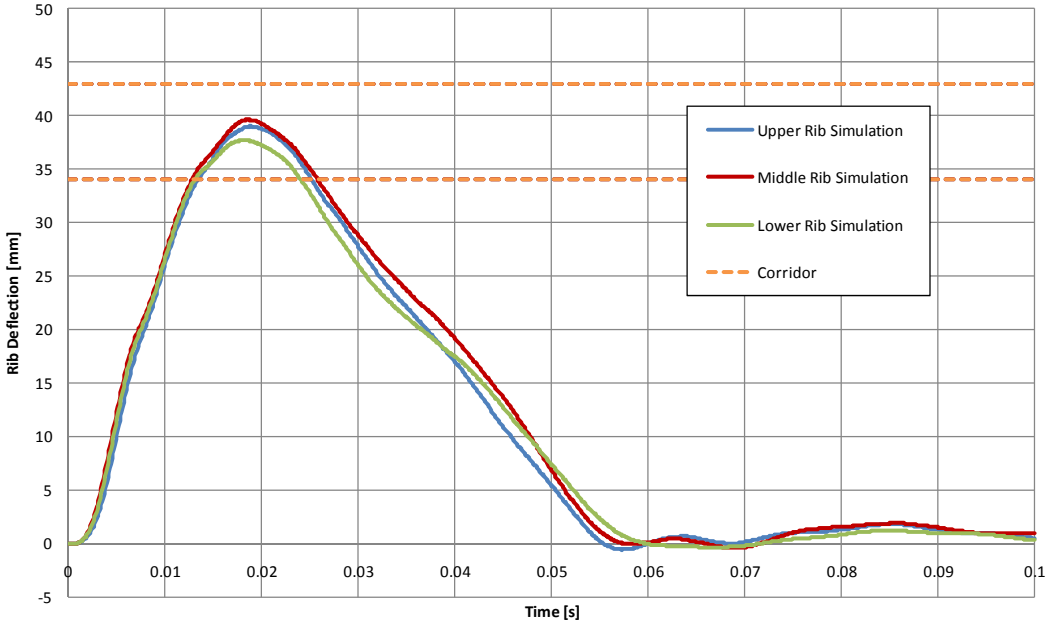

Figure 4.17: Rib deflection of pendulum simulation involving no arm interaction

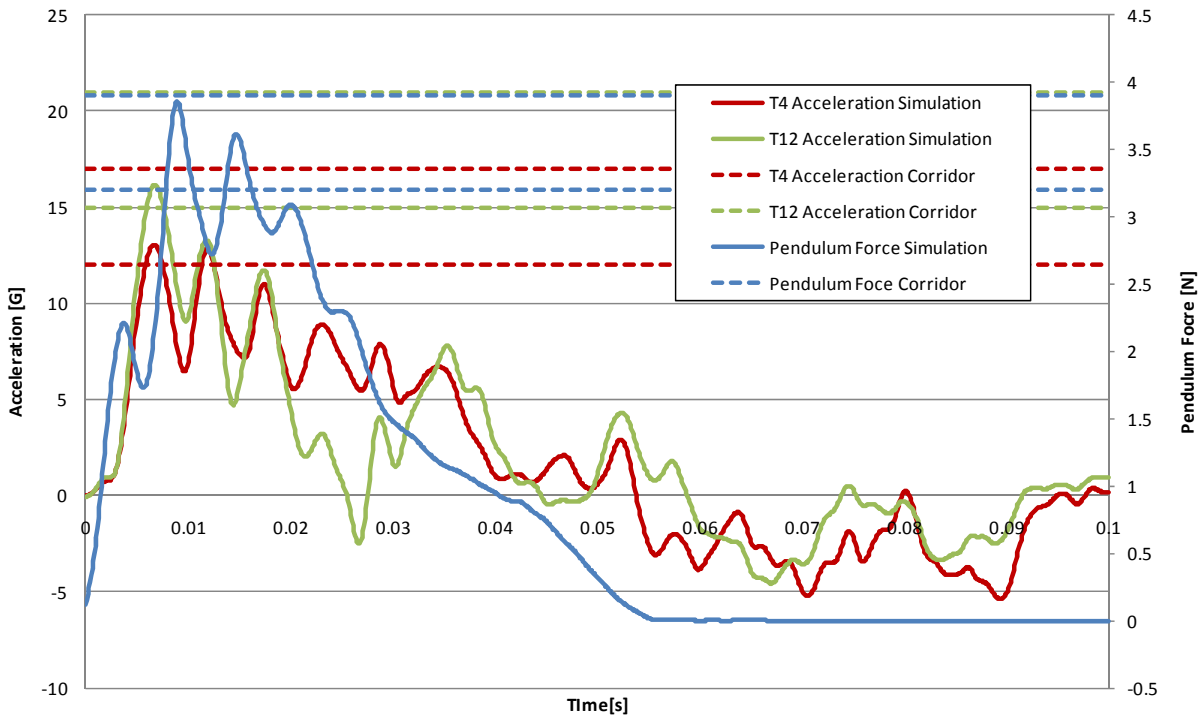

Figure 4.18: Spine acceleration and pendulum force in simulation involving no arm interaction

These simulations show that overall the WorldSID model responds as it should to calibration testing, with the exception of spinal accelerations during the test with arm interaction. However, this work is focused on using compression based criteria so the predicted accelerations were not an issue.

4.3 Ford Taurus Model

The vehicle model used in the crash test simulations was developed by the National Crash Analysis Center for use as a frontal impact model, primarily for the development of roadside highway features such as utility poles and guard rails. Over a dozen models have been developed by this center with varying degrees of detail. The 2001 Ford Taurus model is the most detailed model that has been developed to this point (in terms of the number of elements) and more importantly has the most complete interior with which the occupant can interact. The basic method used by this center in developing their vehicle models has been to disassemble a vehicle purchased from a local dealership and create the model based on 3D scans of the vehicle using material data from a series of mechanical tests. Following this, components of the vehicle are

meshed and component level modeling is performed to ensure that each component model is representative of the physical part. The model components are assembled and put through a series of full vehicle simulations to ensure the vehicle functions like their real world counterparts [Zaouk et al., 2000a; and Zaouk et al., 2000b]. Previous models developed by the NCAC in this manner have been used in full scale simulation testing, both frontal [Kan et al. 2001] and in side impact [Fang et al., 2005; Teng et al., 2007].

The vehicle used in this study was a model of a 2001 Ford Taurus, the second best selling mid-sized car and sixth bestselling vehicle in the US for that model year [Riches, 2002]. During this model's validation the developers simulated a rigid wall impact similar to the FMVSS 208 frontal collision regulatory test, and a deformable offset barrier test performed by the IIHS. In both cases the measured simulation response captured the real world crash test result for the velocity of the top and bottom of the engine and the seat cross member, and also the total force on the wall. The deformation pattern of the vehicle in the deformable offset simulation was also shown to be similar to the crash test results [Opiela, 2008].

The majority of the body in white (BIW) and other structural members, along with the body panels such as the trunk lid, doors and hood are modeled as shell elements with a piecewise linear plastic material constitutive model. The flow stress curves for these materials were taken from coupon tests performed during the development of this model. The BIW members were connected with both nodal rigid bodies (when more than two nodes were connected) and spot welds (when only two nodes were connected). In both cases failure of these joints was not considered, meaning no allowance for weld failure is present in the model. Like the sheet metal, the interior plastic trim was modeled with a linear piecewise plasticity material model with material data being taken from tensile tests. The mechanical components of the vehicle (engine, drive train, suspension, etc.) were modeled with somewhat less detail that the interior and BIW as these components do not generally contribute to the overall crashworthiness of the vehicle to the same degree, though their mass and general shape were needed to provide a reasonable representation of the crash. These components were assigned a combination of rigid, elastic, and linear piecewise plastic material models depending on the required behavior of the part during impact. The windshield glass was assigned a bi-linear material model with an element erosion strain of 0.01, however the originally side and glass parts were assigned elastic material models.

These side window constitutive models were changed in this work to utilize the same material model as the front windshield. This material model, while not ideal, was considered acceptable since the kinematics of the head, which is most often in contact with the side window in side impact, was not a focus for the research presented here. If head and neck injury were to be studied with this model this material model should be changed to reflect the brittle failure that occurs with glass.

Several additional modifications were made to the model prior to its implementation in the current set of side impact simulations. First, the front driver's seat was repositioned. This was necessary to ensure that the occupant model was located in the same position (longitudinally and vertically) as the ATD in physical testing. Initially the measurements presented in the test reports from NHTSA were used as a guideline to positioning the occupant and seat; however each position conflicted with at least one measurement provided in the test reports. Thus, to position the seat the interior photograph taken prior to the test with the ATD in position was used to compare to the model's position until the model and test were in roughly the same position. Figure 4.19 shows the nominal position of the occupant in both the test and model. Additionally a large plate inserted in the trunk to represent electrical equipment used in the frontal crash tests was removed, as were the rigid body accelerometers used for measuring the simulated response of the vehicle during the frontal crash tests, since these locations were not used to measure acceleration during side impact. Additionally the model was renumbered, to avoid duplicate numbering of parts, nodes, elements, etc. with any other portion of the model.

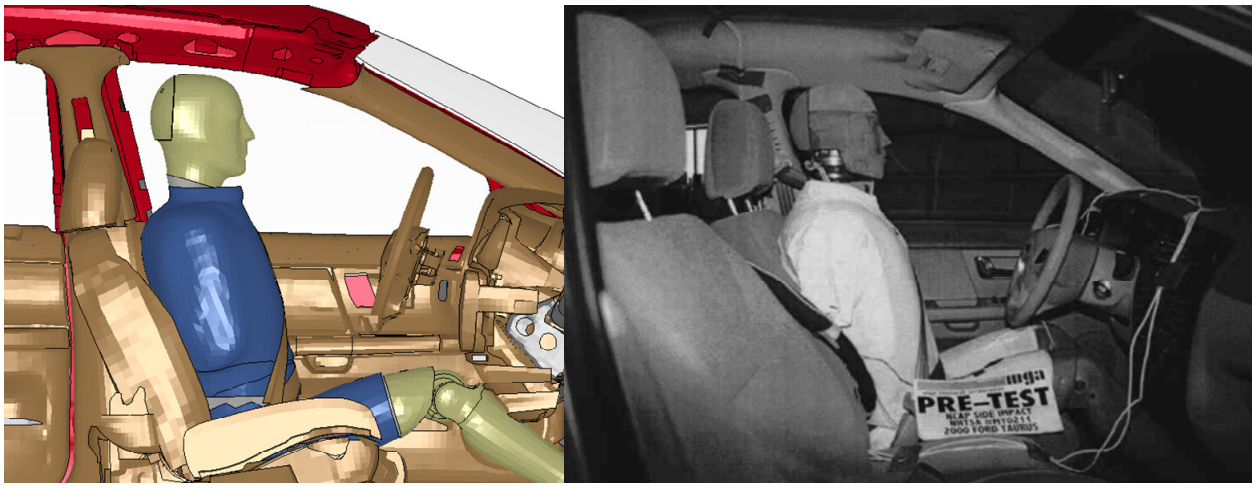

Figure 4.19: Initial occupant position in simulation and test

A series of accelerometers were added to the model at the locations where acceleration is measured during FMVSS214 and NCAP testing. These accelerometers were implemented by creating a small rigid body element at the appropriate location in the model and creating a rigid body attachment to 9 nodes surrounding the body, (an example is shown in Figure 4.20, where the rigid body is the gray cube, attached to the highlighted nodes of the red sheet metal part). This is similar to the approach that was taken during the initial validation of the mode in frontal crash. Seatbelt elements were created using the nodes of these rigid bodies to allow measurement of the local acceleration of the rigid body, as in a real crash test. In addition to the simulated rigid body accelerometers, nodes at the front, middle and rear of the driver's door at 3 levels were tracked on the door panel between the interior trim and the outer door surface (see Figure 4.21 for location). While all of these measurement points provided insight into the dynamics of the intruding door, it was found that the upper-rear location (highlighted in Figure 4.21), provided the best link to thoracic response, thus the velocity from this point was of the most interest in the results of these simulations.

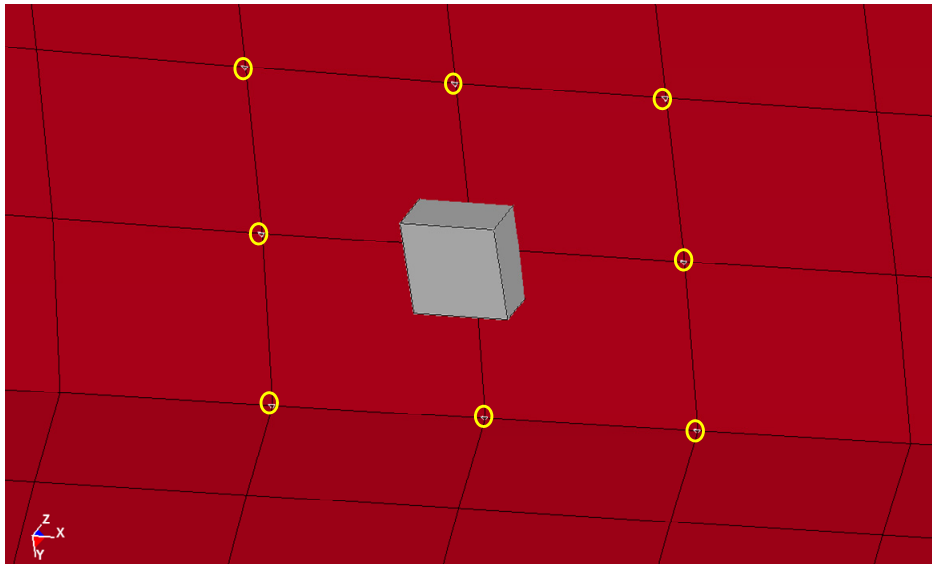

Figure 4.20: Accelerometer mounting method

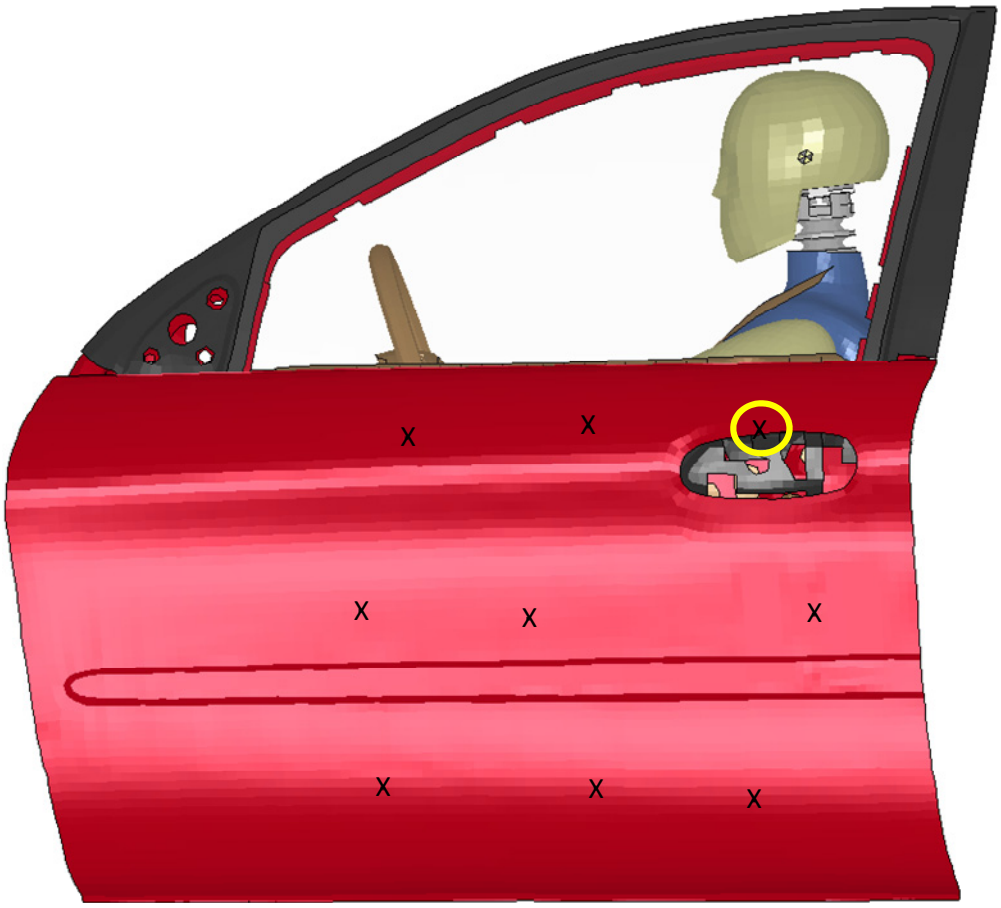

Figure 4.21: Position of door nodes tracking lateral velocity

A material model change was made to two foam blocks which were set in the door panels of the model, shown in Figure 4.22. This foam material is often used in vehicle doors to provide some cushioning to the thorax and pelvis in side impact. In the original vehicle model these parts were modeled using the same material properties as the hardened plastic used for the other interior trim pieces. To better represent these pieces actual properties, a crushable foam material model was used instead. The material properties for these parts were based on a material developed by Campbell [2008], which represented an 'average' door material in terms the force deflection characteristics when a rigid body form was pressed into the door. This crushable foam material acted as an elastic material with a Young's modulus of 300 MPa until the material yield strength, above which the material was perfectly plastic. The yield strength was defined by a material curve that defined the yield strength as a function of volumetric strain. This relation is shown in Figure 4.23.

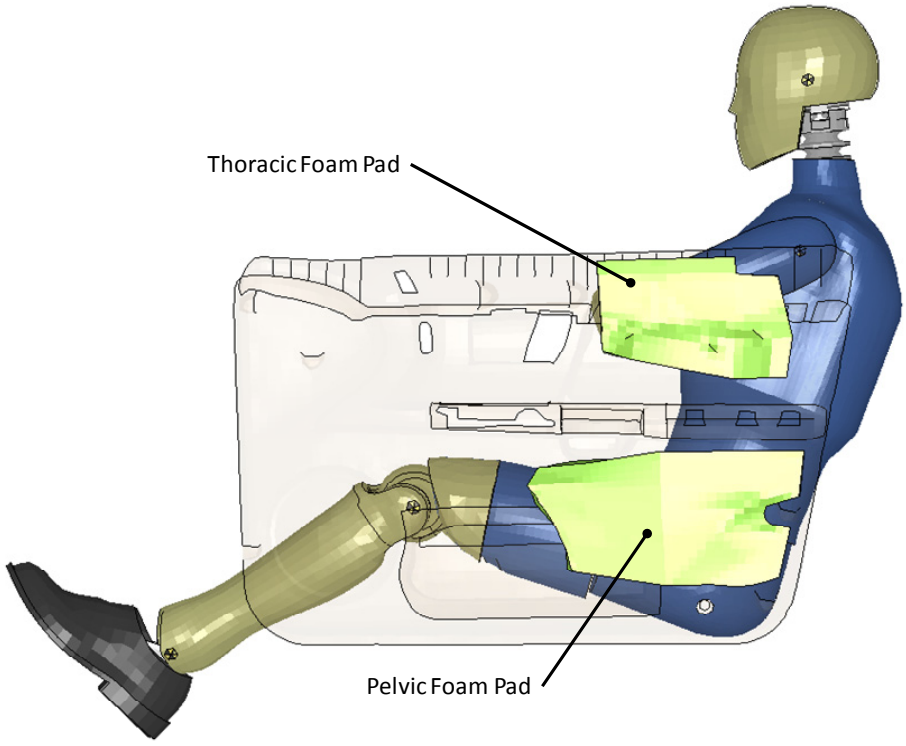

Figure 4.22: Interior foam door pads

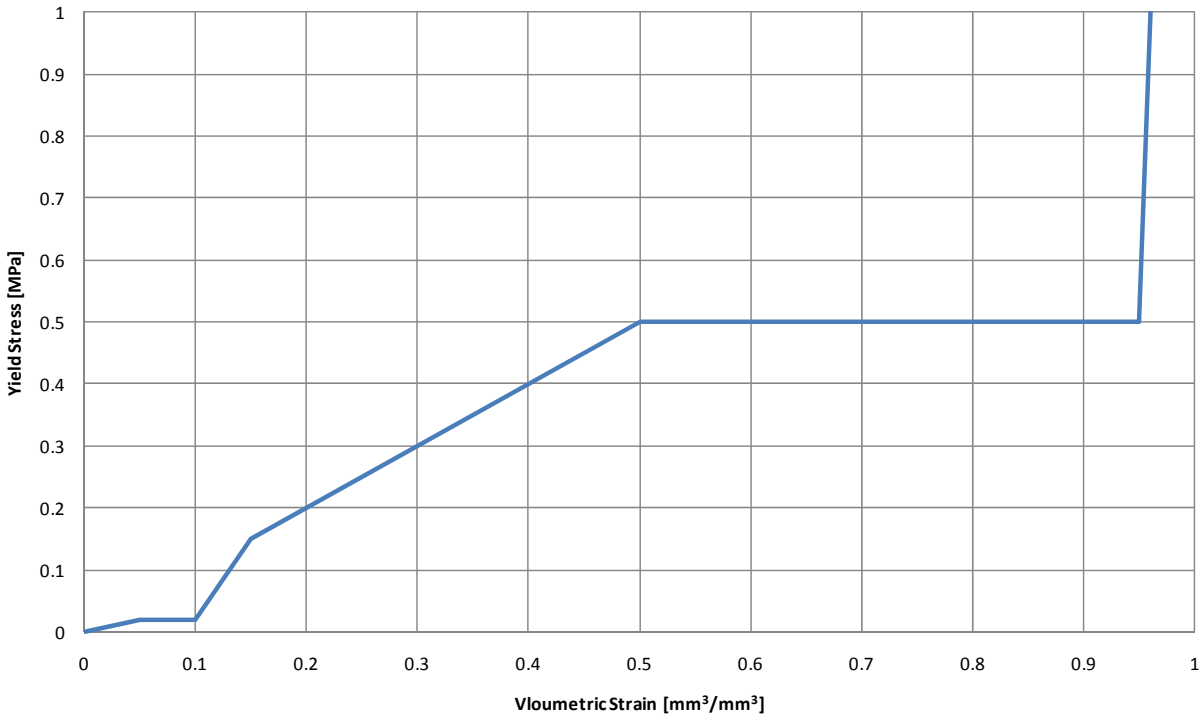

Figure 4.23: Volumetric strain - yield stress behaviour of crushable door foam [Campbel, 2008]

Though the model was validated by the developers in frontal impact, no claim was made as the applicability of the vehicle model in side impact. Thus, the first step of the simulations performed for this thesis was to ensure that the response of the vehicle model was representative of the physical crash response. The results for these simulations were compared to both the large amount of data collected and studied in Chapter 3, as well as to the individual crash tests for this particular vehicle. The results of these comparisons are presented in Chapter 5.

4.4 Seat and Restraint System Model

The seat model used in these simulations was a typical seat frame with foam covering. The frame of the seat is shown in Figure 4.24, with the seat foam superimposed in position.

Figure 4.24: Seat model

The material model for the frame of the seat was defined by a piecewise linear plasticity material model with the flow stress of the sheet metal taken from tensile testing. Each part was connected via nodal rigid bodies at positions where the actual parts would be welded. The seat foam material was modeled using a low density foam material model. This material model was essentially defined by the stress-strain curve shown in Figure 4.25. The foam material was attached to the seat frame at several location using nodal rigid bodies.

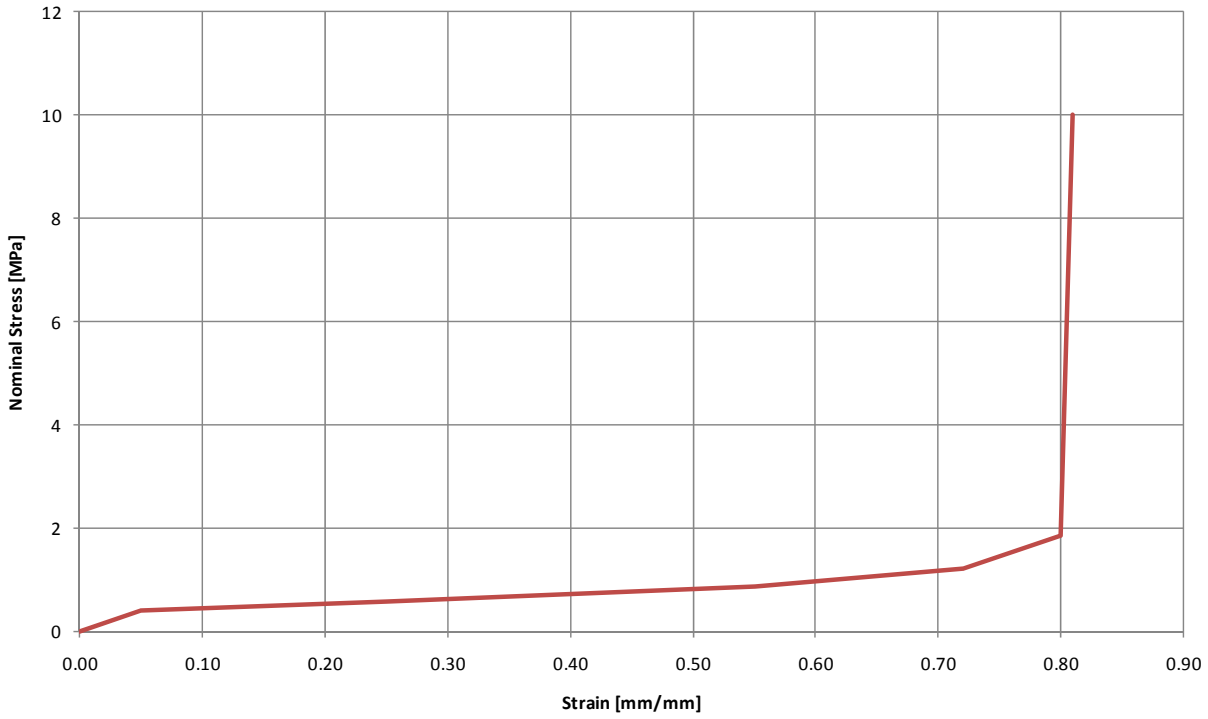

Figure 4.25: Seat foam stress-strain curve

The seat model was integrated into the car model by creating nodal rigid bodies between the lower portion of the seat frame and the cross members on the vehicle floor as shown in Figure 4.26.

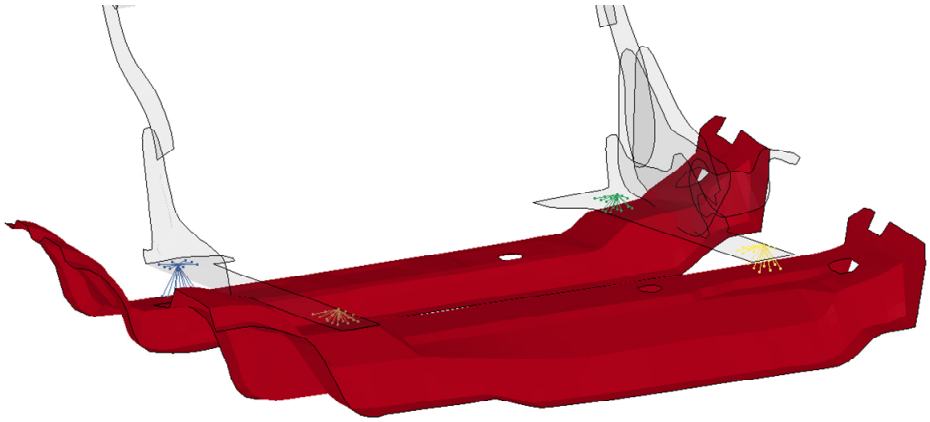

Figure 4.26: Nodal rigid bodies securing seat to floor

The belt system of the model utilized a combination of one dimensional seatbelt elements and two dimensional shell elements. The shell elements were used for portions of the belt which were in contact with the occupant models while the one dimensional seatbelt elements were used where the belt was not in contact with the occupant and near the buckle. The shell element portions of the belt system were meshed as rectangular shells, with a thickness of 1.2 mm and a total width of 47 mm, a measurement obtained from a 2000 Ford Ranger driver's seat belt. The belts were modeled using 4 elements across the width, with each element being approximately square (ie. the mesh was nominally 11.75 m square). The 1 dimensional seatbelt elements were connected to the shell element edges with nodal rigid bodies. Work presented by Baudrit et al. [1999], was used as the basis for the material properties of the shell elements and also the behavior of the 1 dimensional seatbelt elements. Baudrit et al. used a simplified Johnson-Cook material model with no rate or temperature effects as the constitutive model for the seat belts, which is contrary to the suggestion of the uses of a fabric material that is commonly used [Williamson, 2005]. For simulations presented here, the Johnson-Cook material model was used due to the slightly higher computational efficiency of this material model. An early study showed that there was essentially no difference in occupant response when the Johnson-Cook and fabric material models were compared. The loading characteristics of the 1 dimensional belt elements are shown in Figure 4.27. It should be noted that in unloading the strain path returns to 0 stress (a seat belt cannot hold a compressive load and thus does not fall below 0 MPa) along a path parallel to the initial slope of the loading curve. The force-strain curve for the shell element portion of the belts is similarly described using the Johnson-Cook material model.

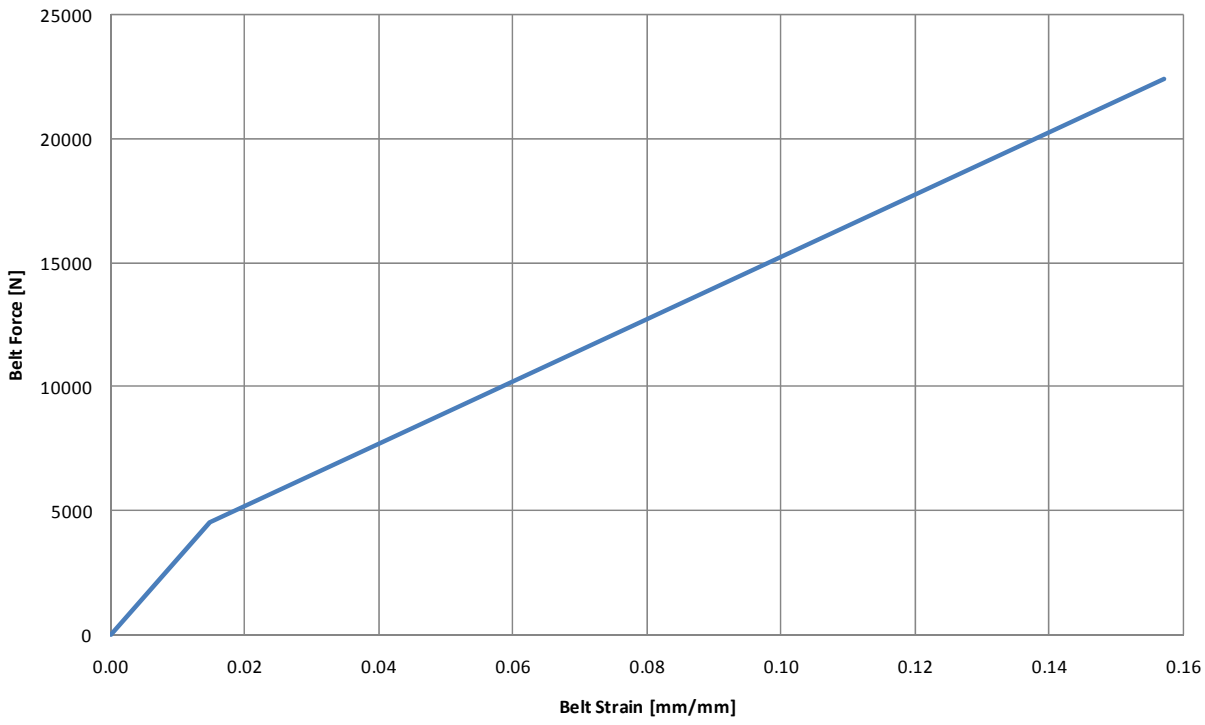

Figure 4.27: Seatbelt force-strain relationship

A seatbelt pretensioner was modeled using a simple time vs. pull in criteria (similar to a pyrotechnic retractor used on many production vehicles) where 60 mm of the seatbelt was drawn in over 7.5 ms, with a 10 ms delay after the firing of the pretensioner [Baudrit et al., 1999]. A node on the lower left seat frame was used as an acceleration sensor for the pretensioner and was fired after reaching a peak acceleration of 5 G. A force limit of 6000 N was enforced on this pretensioner, meaning that if the belt force exceeded 6000 N [Baudrit et al., 1999], the pull in stopped and the retractors behavior took over. The retractor was used to allow belt elements to be drawn in during the firing of the pretensioer and also to allow belt material to be fed out if a belt load of 6000 N was exceeded during the simulation. The loading characteristics of the retractor are shown in Figure 4.28. In the first 15 mm of the retractors pull in, there was essentially no force, though this increased as the retractor pulled in seatbelt material. As with the 1 dimensional seatbelt elements, the unloading characteristics of the retractor followed the slope of the first real portion of the load curve (the slope between 15 mm and 25 mm in Figure 4.28) from the point where unloading began to 0 force. Both the pretensioner and retractor were based on the seatbelt system described in Baudrit et al. [1999].

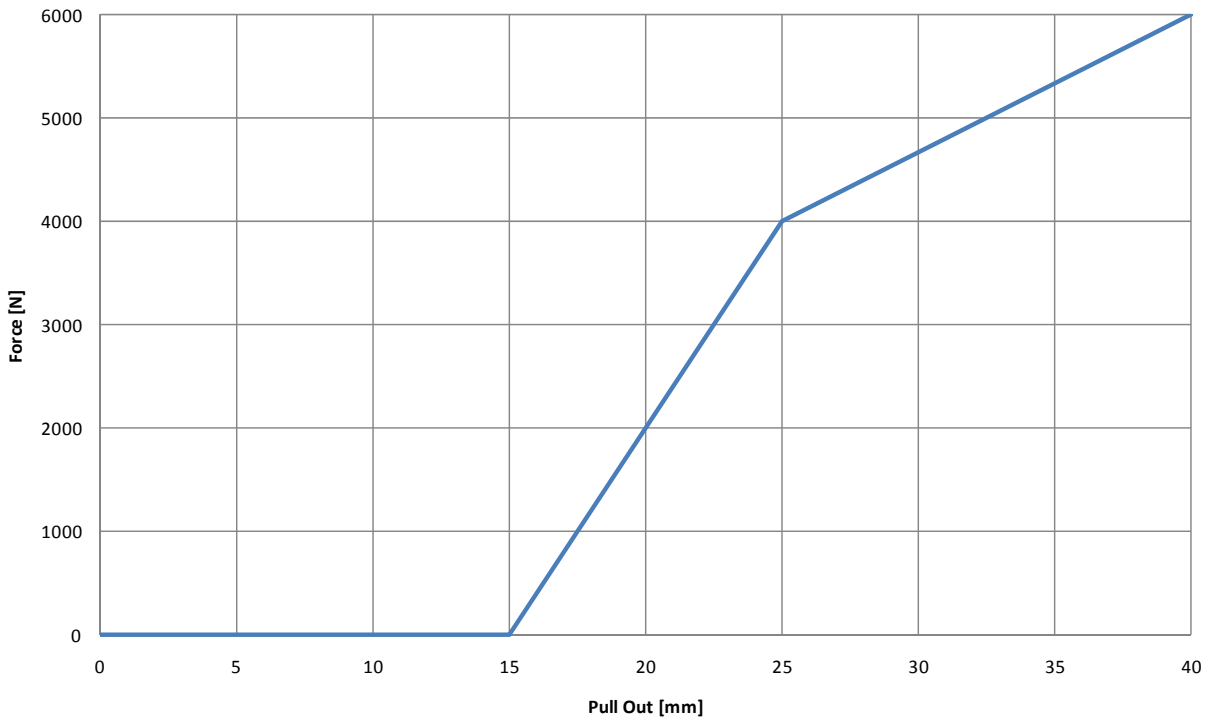

Figure 4.28: Retractor force-pull out relationship

Four anchorage points were created for the belts by defining 4 small rigid bodies placed on the floor cross member and the B pillar (highlighted in Figure 4.29). These rigid bodies were attached to the car structure in a similar manner to the accelerometers. The retractor element was placed at location A in Figure 4.29, as was the pretensioner. A slip ring was defined at B to allow material to feed from the shoulder belt towards the retractor. A simplified buckle was represented by an octagonal shell element part placed near the occupant's h-point. A series of 1D seat belt elements ran from point D to the buckle. Another slip ring was defined on the buckle to allow material to feed between the lap belt section and the shoulder belt section. The location of the mounting points of the seat belt were placed in accordance with SAE J383 [SAE, 1995] which states that the lower anchorage points of a three point harness must be 165 mm apart and provide a angle between 30^0 and 75^0 from horizontal for the pelvic belt. This specification also states that the anchorage for the shoulder belt is required to be positioned behind and above the shoulder point of the occupant.

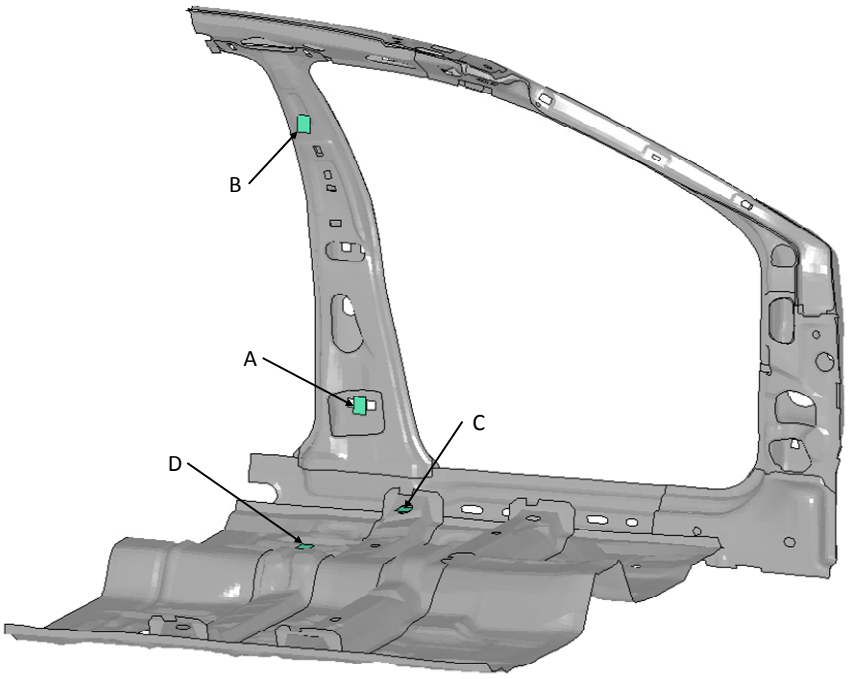

Figure 4.29: Anchorage points for safety belts

An example of the geometry of the complete belt system is shown in Figure 4.30 along with the outline of the seat frame. The location of the node used as a sensor for the retractor is also highlighted.

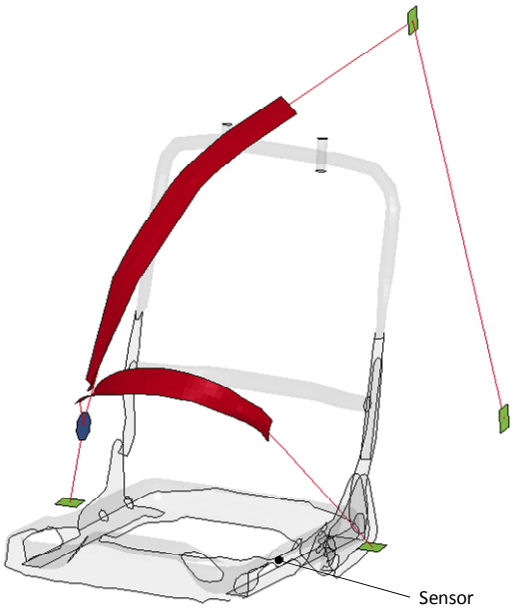

Figure 4.30: Seatbelt geometry

4.5 Moving Deformable Barrier Model

The US NCAP / FMVSS214 barrier model used in this study was developed by Livermore Software Technology Corporation (LSTC) for it LS-Dyna finite element package. The chassis of the MDB was composed of rigid solid elements. The mass and inertial properties of this structure were explicitly defined in part card and not calculated from the element and material data. Revolute joints were defined between the chassis and the tire rim to allow the MDB to roll forward. The crushable structure of the MDB was composed mainly of solid elements with a honeycomb material constitutive model for both the main crush structure and the lower front bumper. A series of shell elements surrounded these solid blocks with material properties simulating the sheet aluminum used on the physical MDB. The MDB model is shown in Figure 4.31.

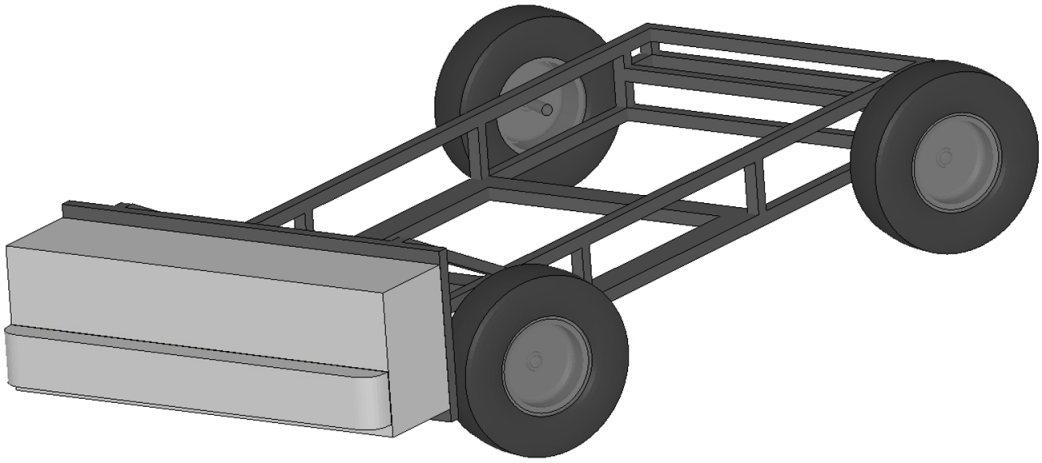

Figure 4.31: Model of MDB

During the development of this model by LSTC, the barrier model was compared to a pair of physical tests, one with the barrier impacting a flat rigid wall at 35 kph, and one against a 300 mm diameter rigid pole at 25 khp. The velocity of the barrier center of gravity and the force displacement characteristics of the barrier in the physical tests were compared to the model. The developers of the model showed that the model mimics the behavior of the physical tests quite closely [Bhalsod and Krebs, 2008]. To ensure consistent results with the developers, these test cases were re-run and their results are shown in Figure 4.32 and Figure 4.33, along with the experimental results presented by the model developers.

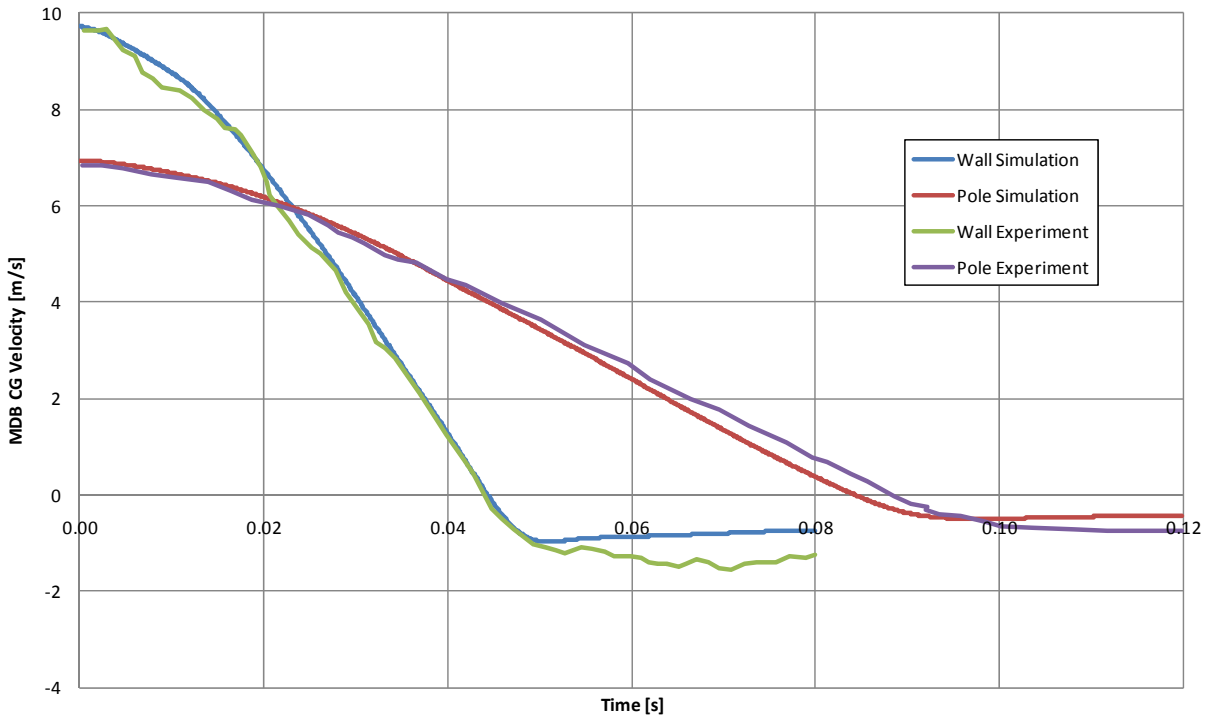

Figure 4.32: Barrier validation simulation - CG velocity profile

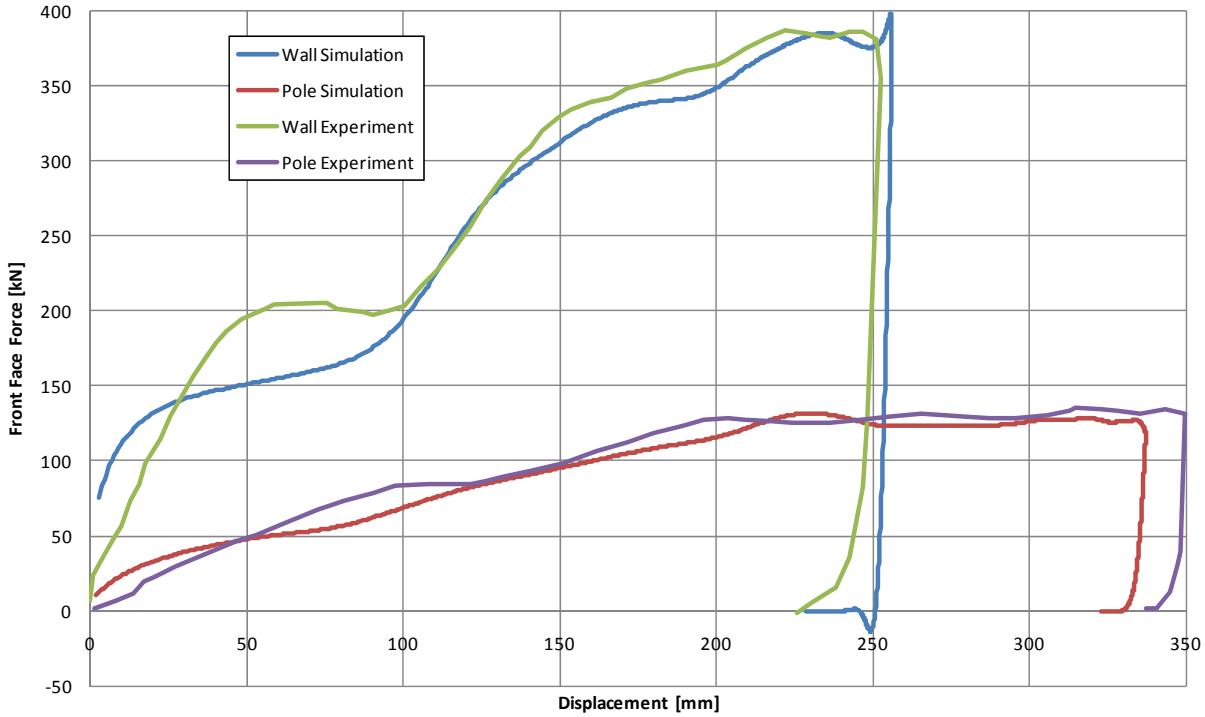

Figure 4.33: Barrier validation simulation – force-displacement characteristics

4.6 Integration of Models

The first step in integrating these models involved sinking the occupant models into the seat model. This step was done to create a profile in the seat foam that matched the occupant's body as a real seat would. The method which was chosen to sink the dummy is essentially the same as that described by Vemulakonda et al. [2007]. A 'pre crash' simulation was carried out in which only the occupant and seat were present. The occupant was changed to a rigid shell representation of the exterior elements of the ATD model. The rigid occupant was assigned the mass and inertia properties of the deformable occupant model and was subject to a load equal to that the force of gravity. During this simulation, the rigid occupant modal was constrained such that no motion was allowed in the lateral direction. Additionally no rotation in any direction was allowed. These constraints were implemented to ensure the deformable occupant model would fit the depression left by the rigid model. These simulations were run until the magnitudes of the oscillations of the CG velocity of the occupant model were less than 0.00075 m/s. The nodal coordinates of the foam parts were extracted from these models and were input into the crash model. Using both the nodal coordinates from the sinking models, as well as the original nodal positions, a stress initialization card was used to allow the solver to compare the position of each node to its original position. This allowed the stress of each element in the seat to be calculated based on the material models stress-strain definition. It should be noted that using this method ignored any deformation that would have occurred to the dummy from the seat, however to perform the sinking simulations with a full deformable dummy was deemed to be too computationally expensive as these models needed roughly 4 seconds to reach equilibrium, which took roughly 300 hours of computational time with the rigid occupant.

The next step in integrating these models was to position each submodel into the integrated model in its proper relation to the rest. The origin of the crash model was selected to be the ground level, on the center plane of the vehicle, below the most reward piece of the rear bumper. The vehicle model was placed such that this point on the model corresponded to the origin. The coordinate system was set such that the direction of travel of the vehicle was aligned with the positive X direction, the direction laterally from passenger side to driver's side was the positive Y direction, and the direction from the ground upward was the positive Z direction. With the vehicle placed in the proper position for the selected coordinate system, the barrier was placed

such that the bottoms of the tires on the barrier were at the same vertical position as the tires of the vehicle model. The position on the car side was dictated by the NCAP test procedure as discussed in Section 2.7.1. The front of the barrier was placed within 1 mm of the door of the Taurus to initiate contact as quickly as possible in the simulation while ensuring that there were no initial penetrations. The seat was positioned in the car as outlined in Section 4.4. With the seat in position, the occupant models were placed such that the h-point of the deformable model was in the same relative position in the seat as the rigid model h-point at the end of the sinking simulation. The lower extremities of the occupant models were repositions to avoid inference with the floor and firewall of the vehicle model. In some cases no position could be found to avoid interference with the pedals of the vehicle. To remedy this, the pedals were removed from the part set used to define contact in the model. This was acceptable since the pedals did not affect the side impact response, particularly of the thorax.

With the occupant and seat models in their proper location in relation to the vehicle, the geometries of the seat belts were created using the seatbelt generation module of LS-PrePost.

Part sets containing all parts all parts of each sub model were created. These part sets were then used in the contact definitions of the full crash simulation. A contact definition was defined between the vehicle and barrier, the vehicle and occupant, the vehicle and seat, the seat and occupant, and the occupant and the restraint system. Automatic surface-to-surface contacts were used to define the contact between each sub model.

To simulate a road surface, an infinite, fixed rigid plane was defined on the $Z = 0$ plane in the simulation. A contact was defined between the tires of both the barrier and Taurus model and the rigid plane using a coefficient of friction used by the developers of the Taurus model in their frontal impact verification simulation. A gravity load was also defined for all parts in the model.

Every node of the barrier was given an initial velocity forward and to the right to simulate the motion of the crabbed MDB during NCAP and FMVSS214 testing. These velocities were the same as the component velocities shown in Figure 2.18.

It is important to note that no side airbag systems were implemented in these models. The reason for this was threefold. First, airbags were not present in a number of the individual experimental crash tests used for verification and validation of this model. Second, despite a great deal of

research into the area, there does not appear to be a consensus as to the best method to implement these devices into crash models [Chawla et al., 2007; Gai and Zhang, 2005; Hayashi et al., 2008; Pyttel et al, 2007]. Unlike frontal air bags (which are often numerically represented by uniform pressure models) side air bags tend to not be fully inflated prior to the occupant contacting them. This means that the inflation of side airbags and the interaction of the inflating air bag with the occupant are vital to the overall load placed on the occupant. The arbitrary Lagrange-Eulerian (ALE) element formulation and smooth particle hydrodynamics (SPH) method have been proposed as alternative methods to simulate side airbag inflation and research has shown that these methods generally provide better inflation characteristics than uniform pressure methods, but these methods are quite computationally expensive. The final reason that these secondary restraints were not included was that their presence would confound the results, meaning that instead of the interaction between the occupant and the intruding door being studied, the results would rather describe the interaction between the door, the airbag and the occupant.

Chapter 5 Simulation Validation

5.1 Introduction

With any finite element model it is critical to compare the results against experimental work to ensure that the model predicts the actual phenomena being studied with a reasonable degree of accuracy. In an ideal situation, one would be able to perform experimental work that is exactly the same as the model one is developing, however in the case of side impact testing this is often financially unfeasible. Due to the high cost associated with these types of tests, it is usually necessary to use existing data to validate large scale crash models. For the case of the model developed in this work, these previous experiments took the form of the NCAP tests described in pervious chapters. Two approaches were taken in the validation of this model. First, the response was compared to the set of data presented in Chapter 3 to ensure that the response of the vehicle was in reasonable agreement with a large set of NCAP tests. The second approach was to compare the response of the vehicle and driver seat occupant to the response of Taurus models of a similar era to ensure that the specific vehicle models side NCAP crash test was adequately reproduced with the finite element model.

5.2 Comparison to NCAP Database Review

The primary focus for this series of validation comparisons was to ensure that the simulated dynamic (lateral velocity) response of the vehicle was similar to what one could expect from real world crash tests. The response corridors developed in Chapter 3 were compared to the simulated lateral velocity response of each accelerometer location in a NCAP barrier speed simulation with a SID occupant in the front seat. A pair of examples of these results are shown in Figure 5.1 and Figure 5.2, with the full set of these simulation results being included with the corridors presented in Appendix A.

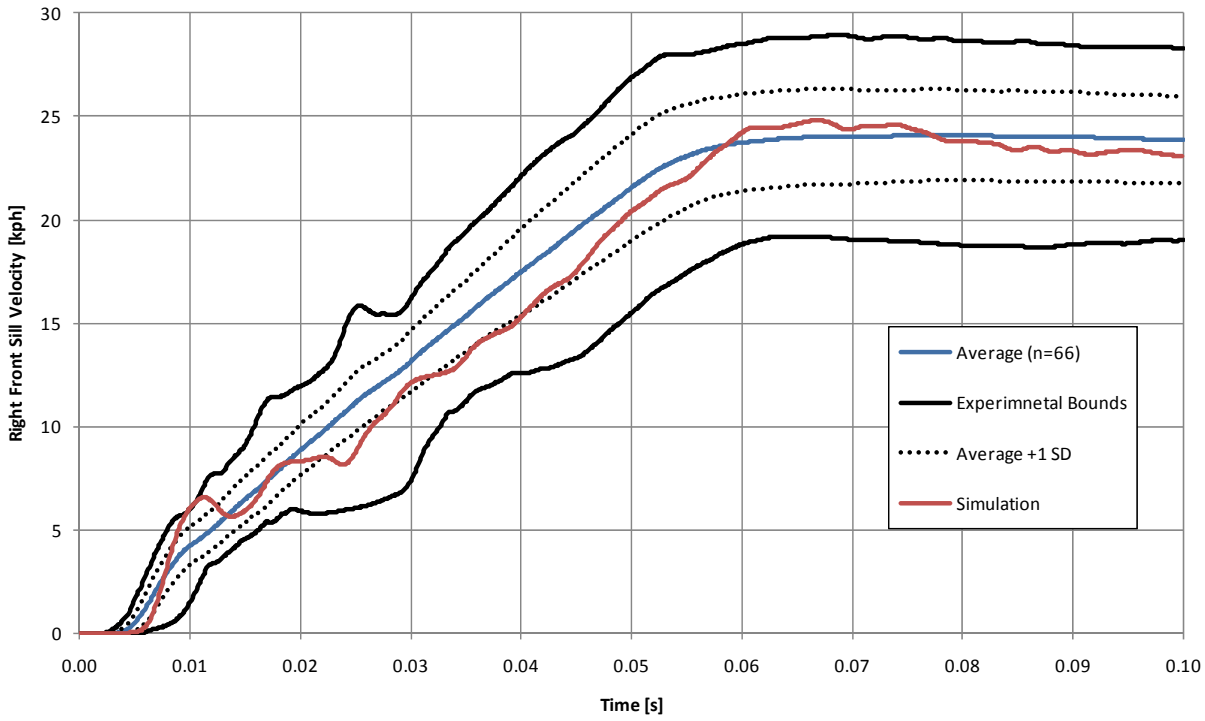

Figure 5.1: Simulated vehicle velocity compared to experimental corridors of right front sill

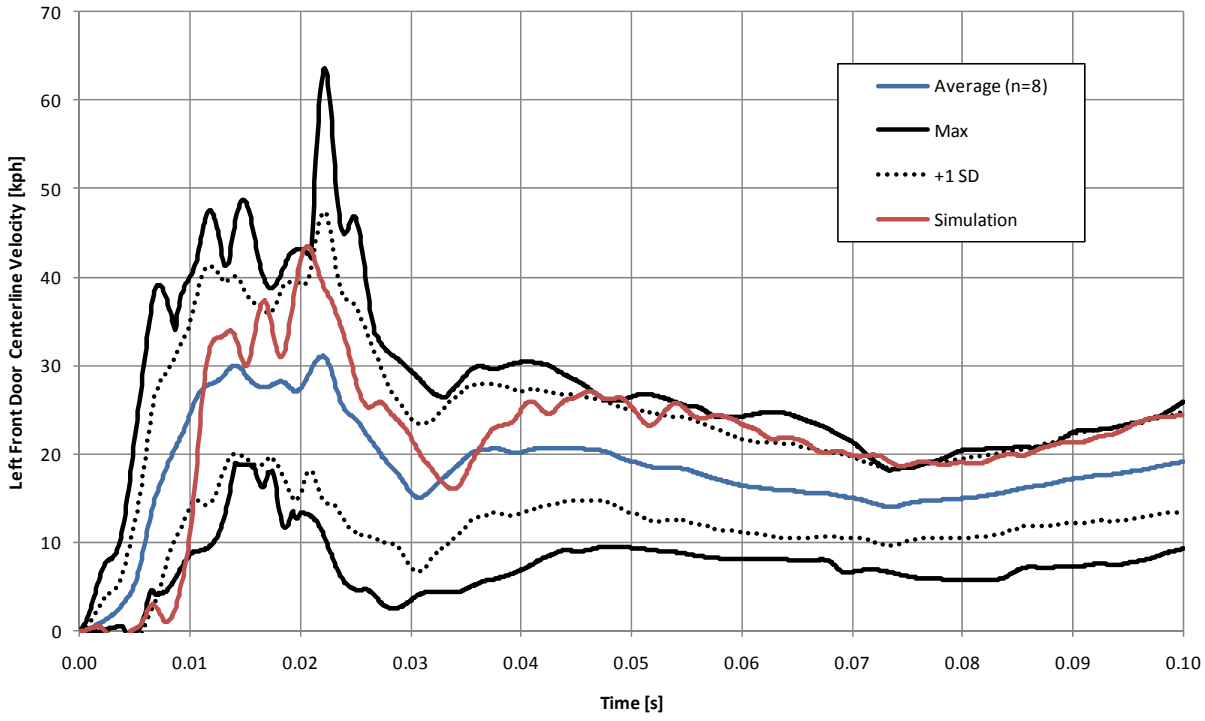

Figure 5.2 : Simulated vehicle velocity compared to experimental corridors of left front door

In nearly all cases the velocity response as measured by the accelerometers, fell within the maximum and minimum corridors developed from the experimental testing. At several locations (such as the floor pan, center of gravity, left rear sill, and lower B pillar response) the simulated response moved outside of the corridor, but in regions where several experimental curves had peaks in their velocity profiles.

Of major importance to this work was the velocity response of the intruding door. Unfortunately, these velocity responses were also the most underrepresented with only 12 vehicles in these tests contributing to the development of the front door velocity corridors. Due to the low number of tests used to develop the front door corridors there are several areas where the simulated response extends beyond the experimental corridors. This is seen in Figure 5.1 at 0.02 s and 0.073 s.

One area where there is a significant deficit in the model is in the response of the rear doors. As with the front doors, the number of tests with these accelerometers is limited, but more importantly the lack of a rear occupant in the simulation led to an elevated velocity response in the model. If an occupant were present this velocity would be somewhat lower due to interactions between the intruding door and the rear seat occupant. Because the front door response was similar to the experimental tests, this effect was considered to be minimal with regard to the front seat occupant, and thus no rear seat occupants were included in any subsequent work.

One challenge that arose during this validation involved the response of the accelerometers mounted on the left (struck) side sills. During impact these accelerometers rotated about the direction of travel (X axis) a great deal. This is illustrated in Figure 5.3, showing that prior to impact (time = 0 s) the accelerometer element was aligned with the global system, while at time = 0.1 s the accelerometer had rotated a great deal as the local Z axis was nearly aligned with the global negative Y axis.

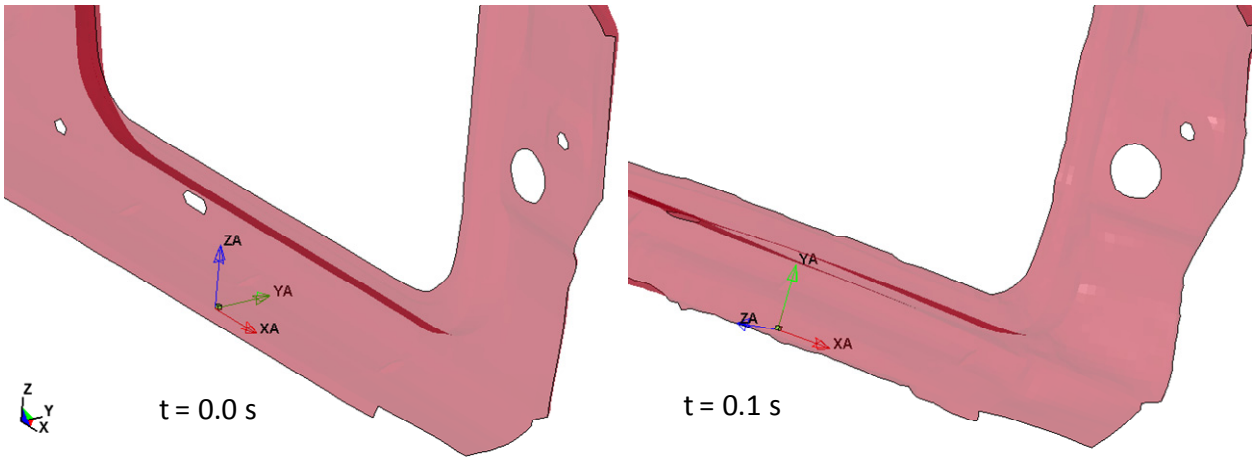

Figure 5.3: Rotation of left side sill accelerometer

The result from this rotation is shown in Figure 5.4. This plot shows that the velocity measured from this accelerometer (Local Co-Ord Sys) was well under the average response, though relatively close to the lower corridor, indicating that this phenomenon may be occurring in actual NCAP tests. The global response is also shown in this figure and is shown to better predict the average response. For this reason the global response from the left front and left rear sills has been presented throughout this work. It is important to note that for the rest of the accelerometers, the local response has been presented, which the is response one would measure in physical testing.

Part of the reason for this behavior may be due to the use of non-deformable spotwelds in this region. The spot welds were subjected to a large amount of shear stress and may fail in actual testing (or deform to allow some rotation between the weldments creating the side sill). This rigid connection may have led to non-physical deformation in this region, leading to the rotation causing odd local velocity response. This type of connection may also have led to the high spike in velocity seen at roughly 0.01 s in the simulated response.

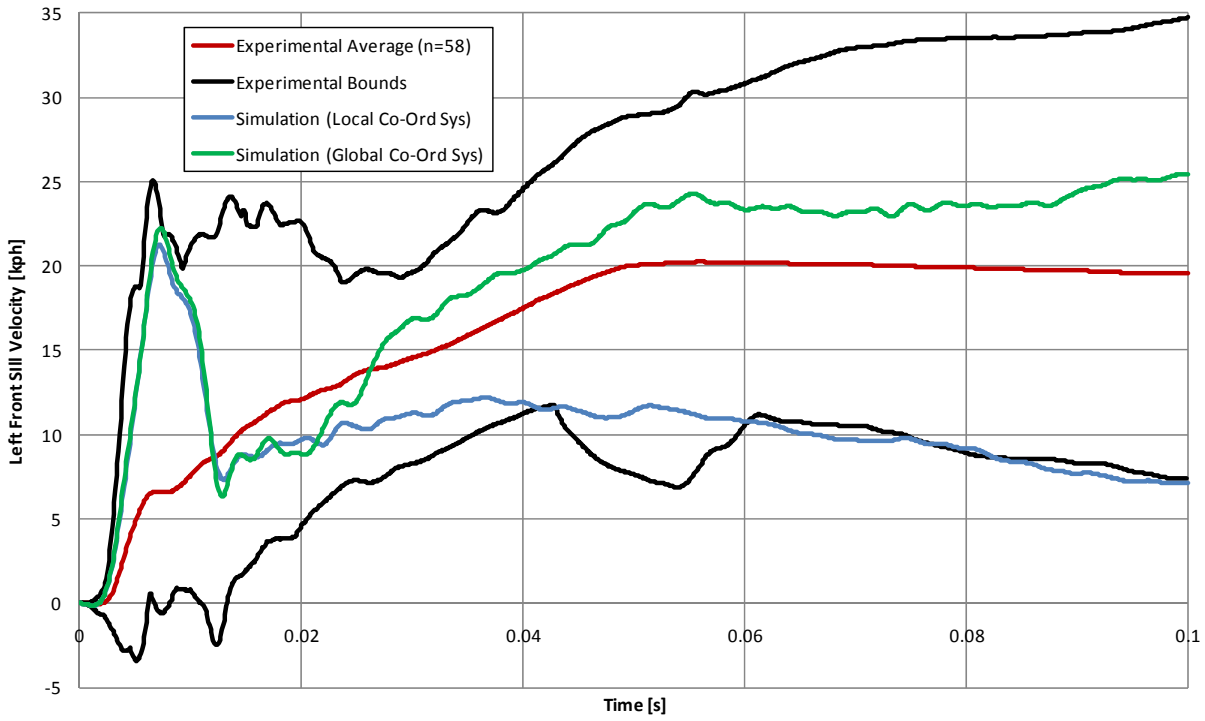

Figure 5.4: Left front sill velocity response in local and global co-ordinate systems

5.3 Ford Taurus Testing Validation Results

To further validate the model, the simulated vehicle response was compared to crash tests performed by NHTSA on the specific Ford Taurus models represented by the finite element model to better understand the ability of the FE model to predict real world crash responses. Five tests were used in this more specific validation case. Four of these tests were carried out at 54 kph (FMVSS 214 speed) and one at 61 kph (NCAP speed). The NCAP test (NHTSA Test # 3263) was a standard NCAP test on a 2000 Ford Taurus with SID occupants in the front and rear seats. Of the 4 FMVSS 214 speed tests, two were performed with SID occupants (NHTSA Tests # 2340 and 2975), and two with prototype ES-2re occupants (NHTSA Tests # 3522 and 3482). Three of these tests were performed on model year 1996 vehicles and one (a SID occupant test) was performed on a 1999 vehicle. Unfortunately all of these vehicles were from the generation previous to model on which the finite element model was based, which is similar to the NCAP test model. The main structure of the vehicle was very similar between these generations, with the primary differences being changes to the body panels of the vehicle and an updating of the interior. With these validation cases, both the vehicle and occupant response were studied.

5.3.1 Vehicle Response

The simulated vehicle response was compared to both the velocity response of the Ford Taurus crash tests, as well as the deformation pattern. After comparing the simulated response of the vehicle with both the SID and ES2-re occupants, very little difference was noticed in either the vehicles velocity response or deformation pattern. For the sake of clarity, only the responses of the simulations with the SID are presented here.

The predicted velocity response was extracted from the accelerometer locations as discussed in Section 5.2. These velocities were then plotted along with the response from the tests carried out by NHTSA to provide a qualitative comparison. These plots are included in Appendix B for both the NCAP and FMVSS 214 response. It should be noted that the NHTSA test cases used for this portion of the model validation were not included in those used to develop the corridors used to evaluate the model in Section 5.2.

The model tended to respond in a manner congruent with the experimental tests. There are several areas to note, however. In general the lateral velocity of the rear portions of the vehicle towards the non-struck side (rear floor pan, right rear sill and rear occupant compartment) were over-predicted in the model. This is in part due to the lack of a rear seat occupant, which would provide additional inertia (a SID having a mass of 80 kg in a roughly 1500 kg vehicle) to the model to reduce the rotation and thus the lateral velocity of the rear portion of the vehicle. Another point of interest is a fairly large peak in the simulated velocity traces of the struck side sills and lower A pillar, which is not seen in the experimental results. This may be attributed to the issues with the rotation of the sill previously discussed. Despite the large peak in velocity not appearing in any of the responses for this set of validation cases, these peaks did occur in some other tests used to develop the response corridors (Section 5.2).

To obtain the measurements required to compare the deformation of the simulated impact to the experimental impact, the vehicle side geometry (doors, front and rear bumpers, front quarter panel, A, B and C pillars, door sill, roof rail and rear quarter panel) was exported at the final time step of a the simulation and rotated such that the center line of the crushed vehicle was in the same position as the vehicle prior to impact. The longitudinal position was dictated by the centerline of the front and rear axles which were found after impact by exporting the front brake

rotors and rear brake drums and using the centers of these parts to define the axels. The position of the node on the vehicle body closest to the intersection of the 5 measurement heights and the longitudinal measurement points were recorded for each position and subtracted from the initial position of the node closest to a given intersection point to obtain the vehicle crush at that location. In nearly all cases the node post impact was different than the node pre impact, due to the deformation on the vehicle. Figure 5.5 shows an example of the vehicle model before and after impact, along with the measurement points.

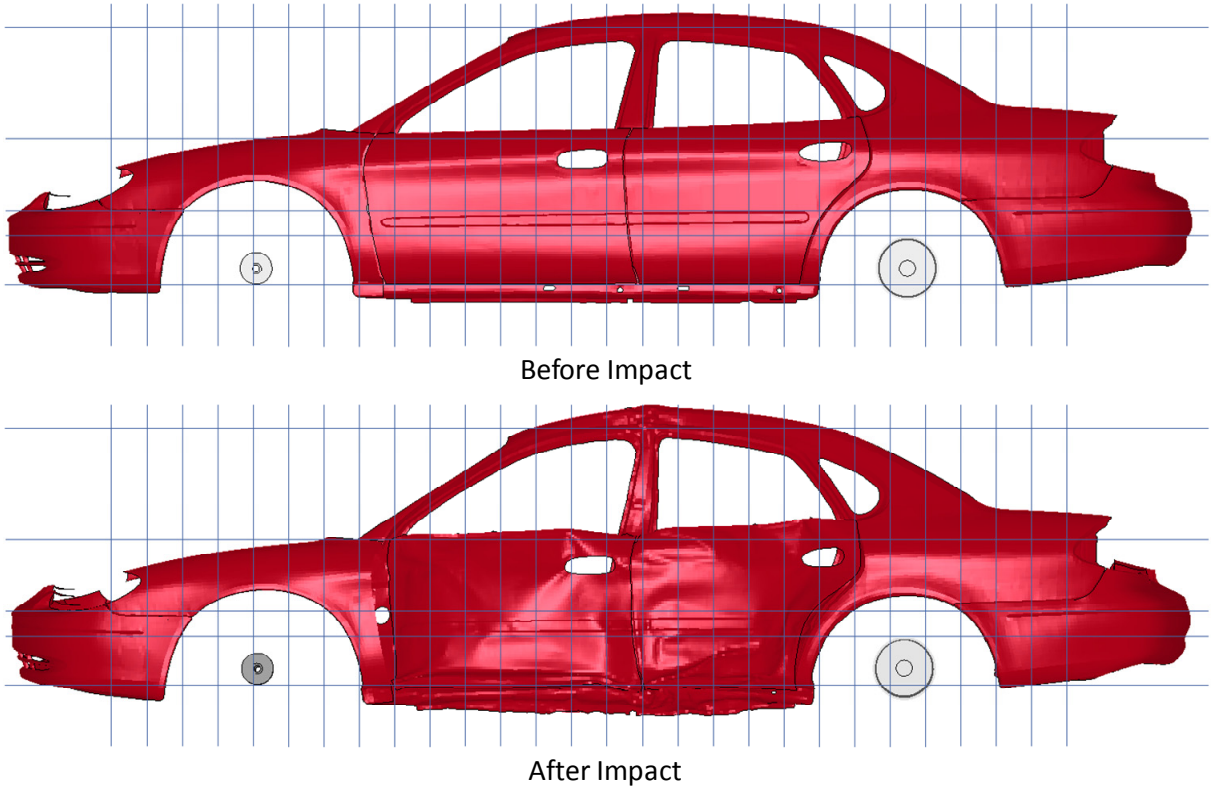

Figure 5.5: Deformation measurement points for validation

The results of these deformation measurements, along with the results from the NHTSA tests are presented in Figure 5.6.

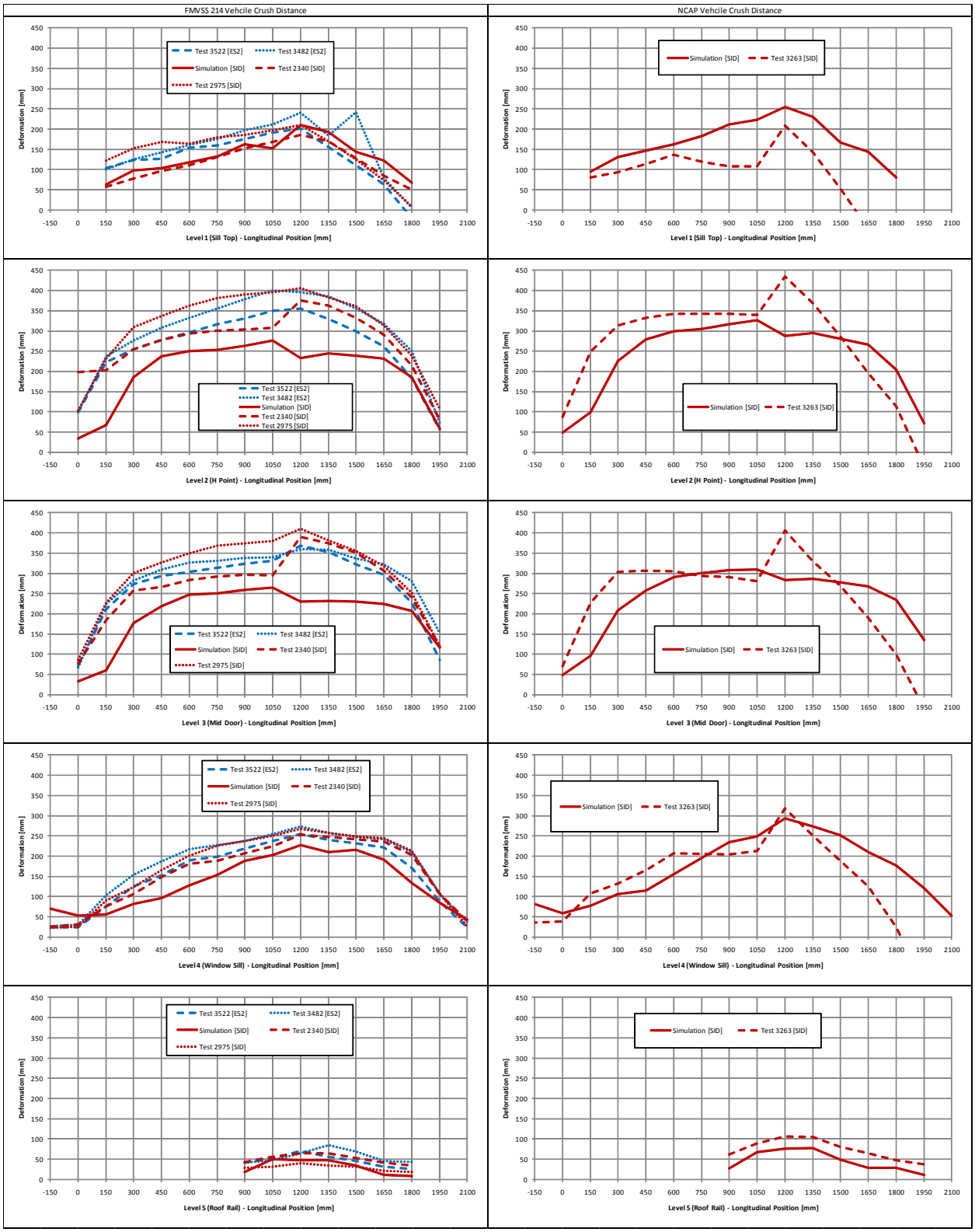

Figure 5.6: Taurus deformation validation

Figure 5.6 shows that the deformation characteristics for the model are in good agreement for the NCAP impact speed both in terms of magnitude and general shape. The large spike in the experimental results at the 2nd (H-point) and 3rd (mid-door) heights 1200 mm behind the zero point can be explained by results of the impact depicted in Figure 5.7. At the longitudinal position of 1200 mm, which corresponds to the rear portion of the front door, there is a large gap between the front door and rear door, which is not present in the model due to the door latch in the model being represented by a nodal rigid body which did not allow for failure. This excessive deformation to the rear door caused a large deformation measurement at this location in the experimental test which was not captured in the model. Nevertheless, aside from this location, the deformation predicted by the model is quite accurate for the NCAP barrier speed. The FMVSS 214 barrier speed model tended to slightly under predict the deformation at most levels. It is worth noting that experimental deformation distances are comparable between the FMVSS214 test and the NCAP test, while there is a noticeable difference between the simulated results. This may be explained by the differences in body panels between the different generations of vehicle, given that all the FMVSS barrier speed tests were performed on the generation of vehicle pervious to the generation tested at NCAP speeds. Overall the response of the finite element model predicted the intrusion of the experimental test of the same vehicle generation quite well.

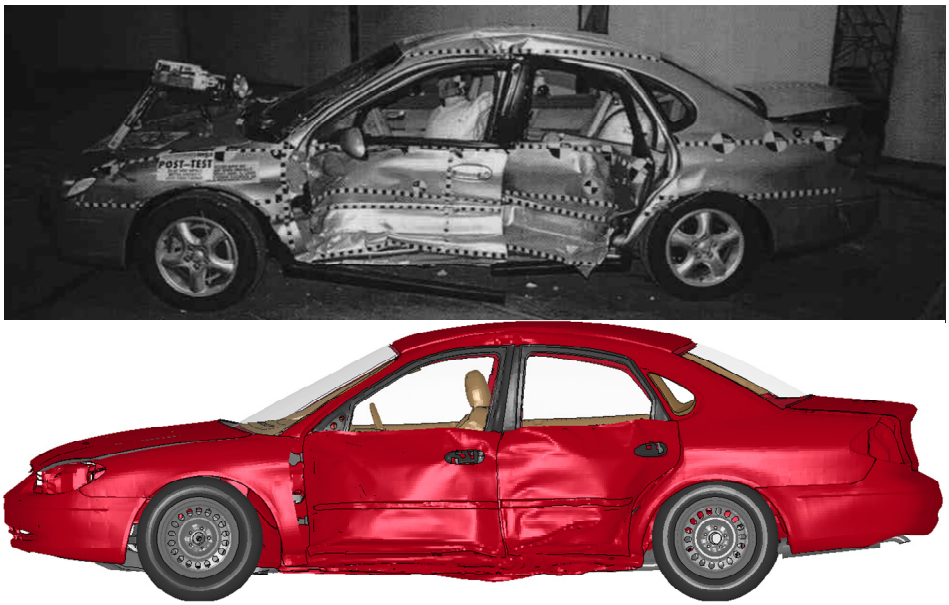

Figure 5.7: Side view of post impact vehicle test and simulation

5.3.2 Occupant Response

With an understanding of the ability of the model to predict vehicular response, the validation efforts turned to the response of the occupant. The response of the occupant was essentially split into two categories. The first dealt with only the kinematics of the occupant, while the second dealt more specifically with the injury criteria predicted by the occupant. The primary method of comparing the motion of the occupants was to use the lateral velocity obtained experimentally from the accelerations mounted inside the ATD's. These values were compared to those predicted numerically. Of primary interest were those locations in the thoracic region; the lower spine, the upper rib, and the lower rib. In addition, from the two FMVSS214 barrier speed tests performed on the prototype ES2 models, the lateral velocities of the upper spine were compared as well. In all cases, the head CG velocity and pelvic velocity were also compared. Obviously, unlike the vehicle response, the occupant response was dependent on the type of ATD used in the test. Though both the SID and ES-2re represent a 50^{th} percentile male, the differing construction and design of each dummy provide different response, so the results of both the 51 kph barrier speed simulation involving the SID and ES2 occupant models are presented. These response velocities are shown in Figure 5.8. To numerically compare the curves, the r^2 values were calculated comparing the simulated response to each experimental response. These values are provided in Table 5.1, with values below 0.75 highlighted in yellow and values below 0.5 highlighted in red.

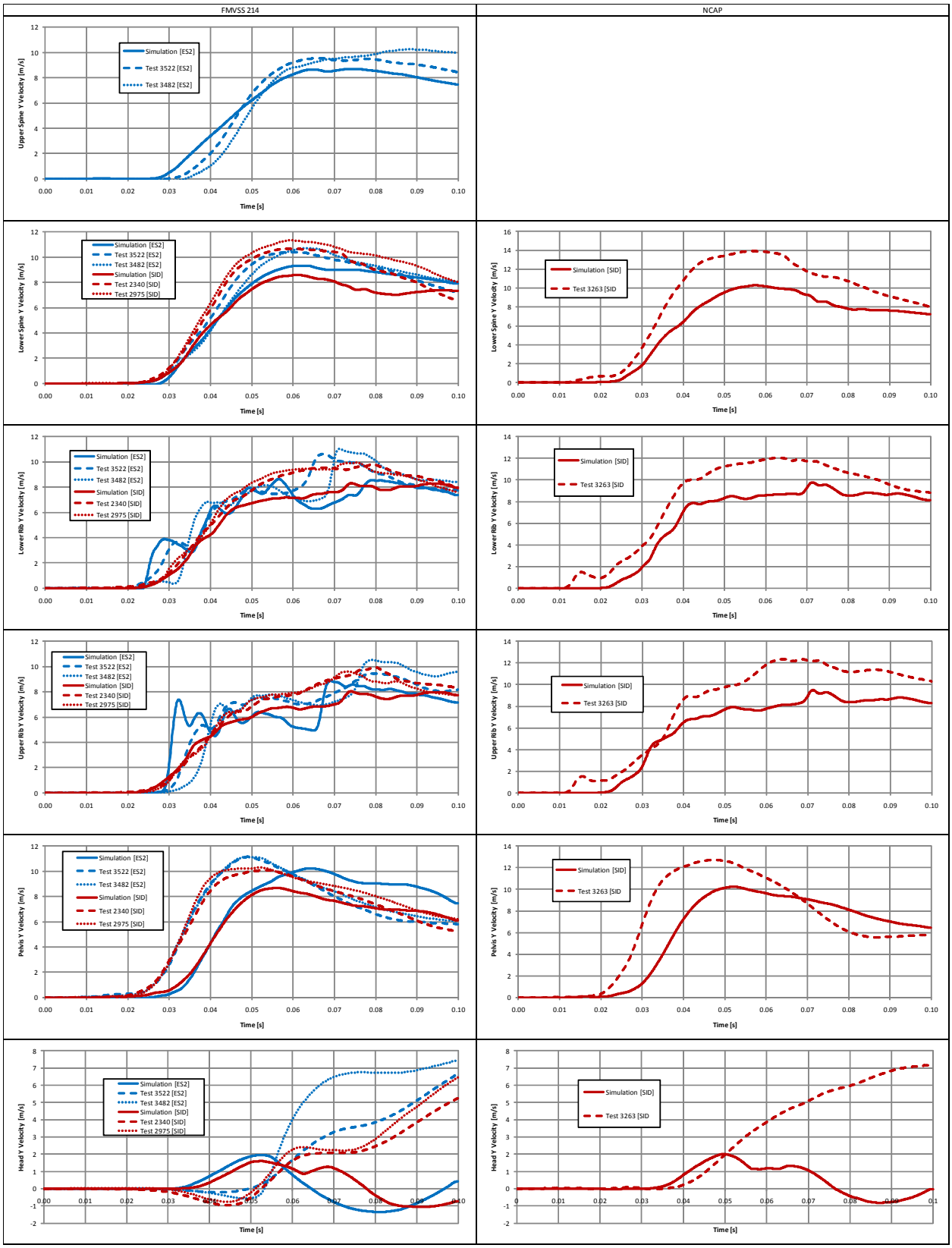

Figure 5.8: Occupant velocity response validation

Table 5.1: R^2 values comparing occupant velocity simulation and test

Barrier Speed	ATD	Test	Upper Spine	Lower Spine	Lower Rib	Middle Rib	Upper Rib	Pelvis	Head
54 kph	ES2-re	3522	0.985	0.983	0.898	0.921	0.874	0.703	0.329
		3482	0.943	0.993	0.886	0.824	0.766	0.740	0.413
	SID	2340		0.974	0.984		0.983	0.855	0.236
		2975		0.989	0.974		0.978	0.852	0.237
61 kph	SID	3263		0.971	0.962		0.973	0.704	0.044

The response in the thoracic region showed very good agreement in nearly all cases while the pelvis response was in poorer agreement and the head response was extremely poor. The head response may be explained by interaction with the side window. Generally the window shatters during impact; however this was not accounted for in the model where the glass remained intact during the entire impact. Due to the high degree of correlation between the numerical and experimental responses in the thoracic region, the inability of the model to capture the kinematics of the head was deemed to be acceptable for this study, which focused on thoracic injury. The load transferred between the head and thorax was quite modest when compared to the loads required to cause rib deflection.

TTI and rib deflection were used to validate the model. As the SID ATD was not originally designed to measure rib deflection, none of the SID ATDs used in the tests of this validation study included this response, meaning only the tests of the prototype ES-2re ATDs were used. The peak response values are included in Table 5.2, along with the average of the two experimental cases and the difference between this average and the numerical result. The rib deflection time-responses for both the experimental and simulated cases are shown in Figure 5.9.

Table 5.2: Validation peak rib response and comparison

	Upper Rib Deflection [mm]	Middle Rib Deflection [mm]	Lower Rib Deflection [mm]
Test 3522	34.6	33.0	24.5
Test 3482	39.2	39.8	37.2
Experimental Average	36.9	36.4	30.8
Simulation	40.7	34.3	35.6
Difference	3.9	-2.1	4.8

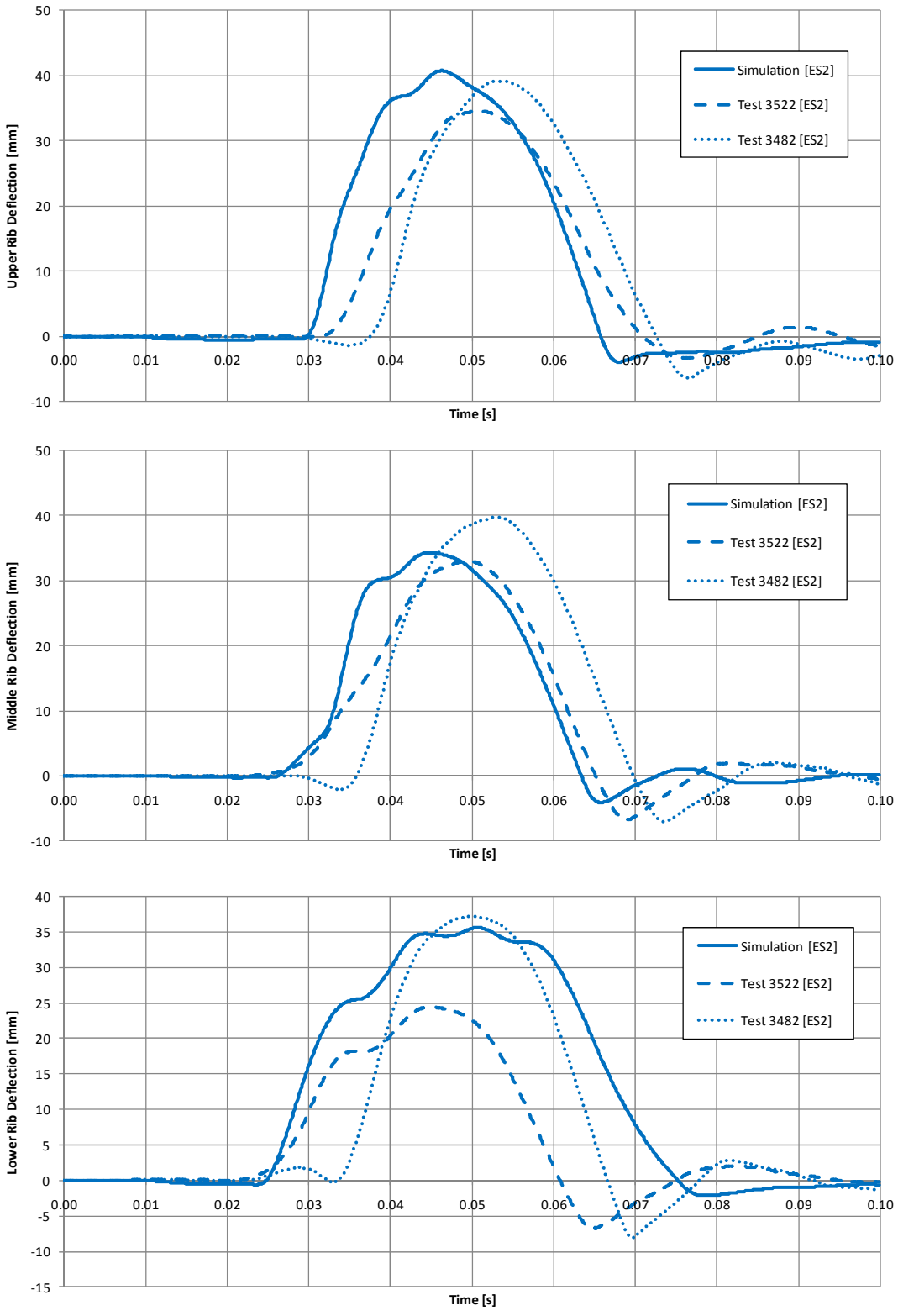

Figure 5.9: Rib deflection validation time response

Table 5.2 shows that there is a good agreement between the experimental and numerical results, with an average difference of 2.2 mm between the predicted numerical result and the experimental average. The largest difference is seen by the lower rib, however in the test cases the upper and middle ribs dictated the peak rib deflection and therefore dictated the injury criteria that would be calculated for their respective crash tests. The numerical curves had a faster rise time and earlier peak than the experimental curves, though there is a noticeable phase shift between the two experimental curves. This phase shift may be due to slight positioning differences were one occupant may have been positioned slightly further from the door, leading to a delayed contact with the interior door trim. Also the differences between the interior of the two generations of vehicles may account for some of this discrepancy.

The TTI criterion was also investigated in this validation study. Table 5.3 shows both the experiment and simulated responses. A time history evolution of TTI was also created for these responses and is shown in Figure 5.10. These plots were created by exporting the TTI score at each time step as if the crash had ended at that time, allowing the progression of TTI to be graphically represented.

Table 5.3: Validation TTI response

Barrier Speed	ATD	Test	TTI [G]
FMVSS 214 (54 kph)	ES2-re	3522	76
		3482	93
		Simulation	129
	SID	2340	50
		2975	59
		Simulation	50
NCAP (61 kph)	SID	3263	85
		Simulation	67

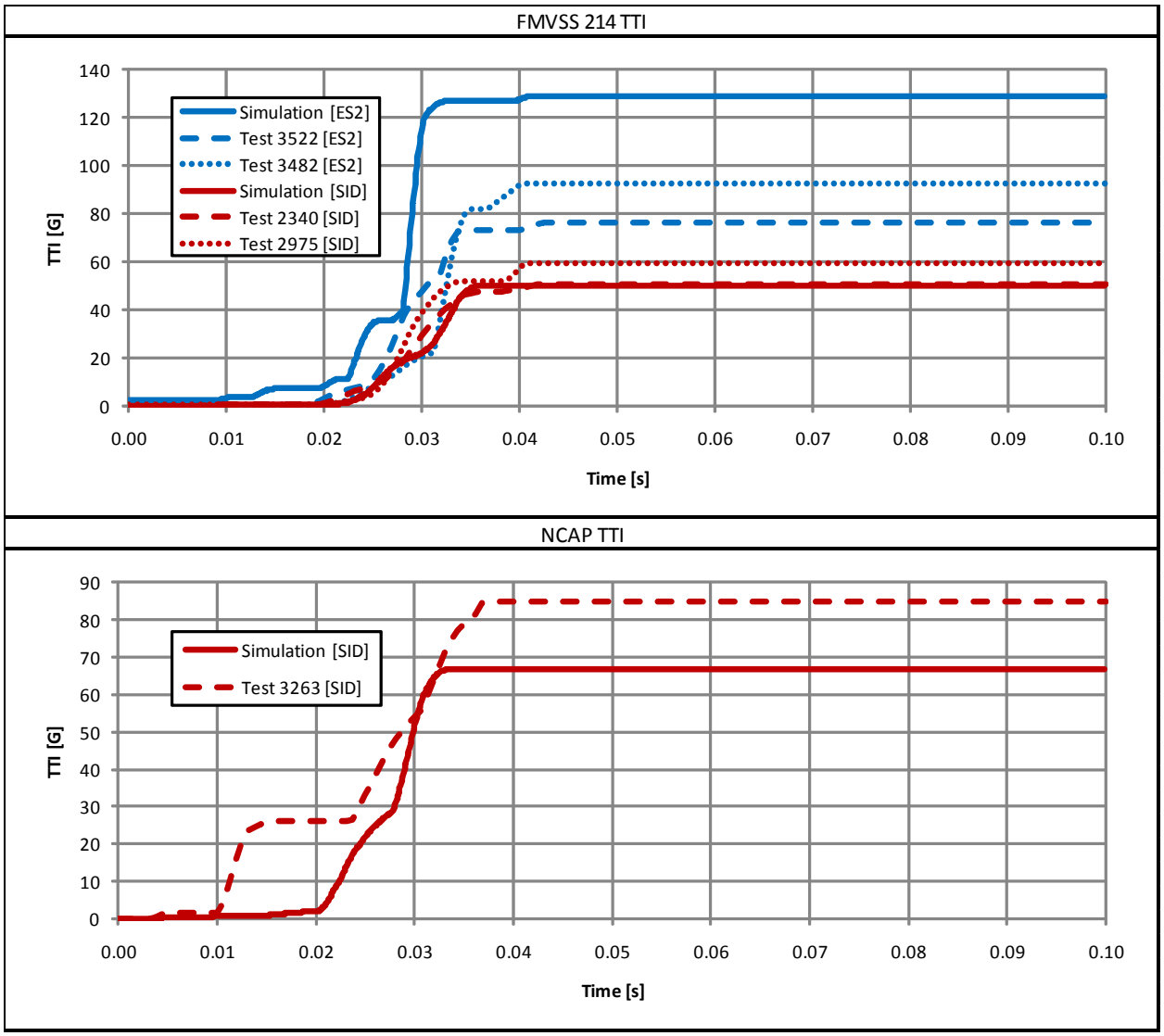

Figure 5.10: TTI validation time response

Due to the TTI response being based on acceleration and the inherent difficulties in extracting acceleration data from an explicit finite element code due to numerical noise, TTI is a difficult criterion to assess with the methods used here. Additionally to ensure that the accelerations are monitored in a local coordinate frame, small portions of the otherwise deformable parts must be made rigid, which can affect the acceleration results. Filtering and numerically integrating can 'even out' some of this noise, but raw nodal acceleration data is often difficult to interpret [LSTC, 2007]. For example in one side impact FE analysis [Teng et al., 2007], the experimental and numerically predicted TTI score were 77 G and 78 G respectively. The experimental lower rib acceleration was 70.5 G while the simulation predicted 80.1 G. Additionally, the peaks of the

rib accelerations were roughly 10 ms out of phase. Theses discrepancies show the difficulty in capturing the occupant's true response using only TTI. It is also worth stating that TTI was developed primarily with the SID ATD in mind. To date no other ATD has used this criterion. The results presented in Table 5.3 show that at the FMVSS 214 barrier speed, the SID model seemed to predict TTI quite well, while the ES-2re model severely overpredicted TTI, though this ATD was not designed to use this criterion to predict injury. Additionally, the changes in the interior between the two generations make it difficult to draw a firm conclusion on the ability of the model to predict TTI. The NCAP barrier speed simulation is in poorer agreement with the experimental test. It is interesting to point out that the vehicle used in this experimental test was equipped with a side air bag, while the simulation with no air bag predicted a considerably lower TTI score.

Chapter 6 Effect of Occupant Position and Interior Trim Properties

6.1 Introduction

With a thorough understanding of the response of the model and how it compared to crash tests carried out by NHTSA, a study was performed to assess the effect of a number of items thought to have an effect on the overall response of the vehicle and the occupant during side impact. The initial position of the occupant, the use of different material properties in the vehicle interior, and the use of seat belts were all studied. For each set of simulations carried out in this chapter, the injury criteria response curves (rib deflections, VC and TTI) have been included in Appendix C for reference. This chapter begins with a section qualitatively describing, step-by-step, the progression of a typical side impact which is followed by a description of each aspect of the study performed and the parameters which were altered followed by the changes in response of the model to each of these changes. The changes to the vehicle velocity and deformation response were examined in the portions of this study dealing with the presence of the occupant and the initial lateral position of the occupant. These changes in vehicle response were found to not vary significantly with changes to the interior trim of the vehicle, and thus are not presented.

6.2 General Description of Side Impact Occupant Response

The following section outlines the progression of a typical side impact with particular attention paid to the response of the occupant and the factors that strongly affect the dynamic response of the occupant. The top view of the impact shown in Figure 6.1, depicts the gross motion of the vehicle during the crash. This image shows that there was very little gross vehicle motion until approximately 0.06 s after initial impact, due to the deformation of the front end of the NHTSA MDB, as well as the deformation of the vehicle side structure. After 0.06 s there was a noticeable amount of rotation of the vehicle; however this was typically after peak injury predicted by the occupant rib deflection, TTI, and VC. An isometric view of the same impact is show in Figure 6.1.

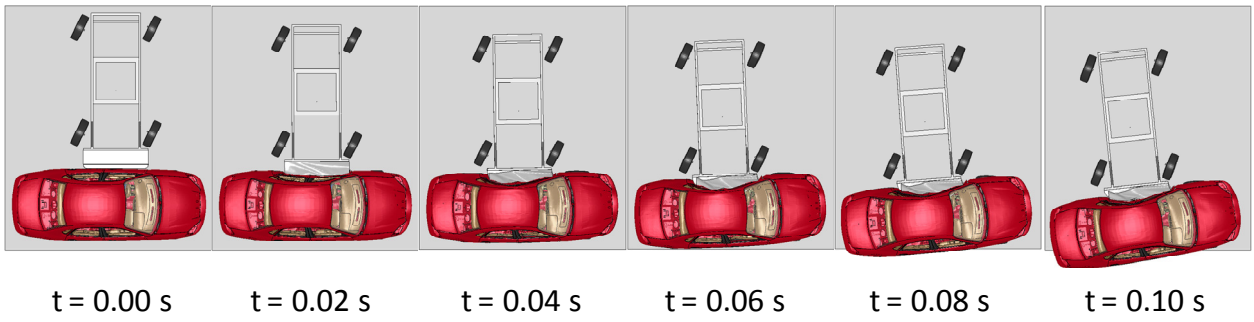

Figure 6.1: Top view of simulated NCAP side impact

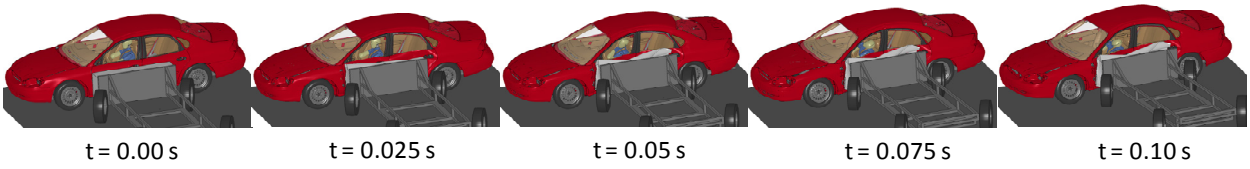

Figure 6.2: Isometric view of simulated NCAP side impact

A detailed image of the impact progression of the NCAP barrier speed impact on the ES-2re model is shown in Figure 6.3. In this image the seat, belts, occupant, door and front portion of the barrier have been isolated to illustrate the occupant response during the impact. The ATD jacket has also been removed for clarity.

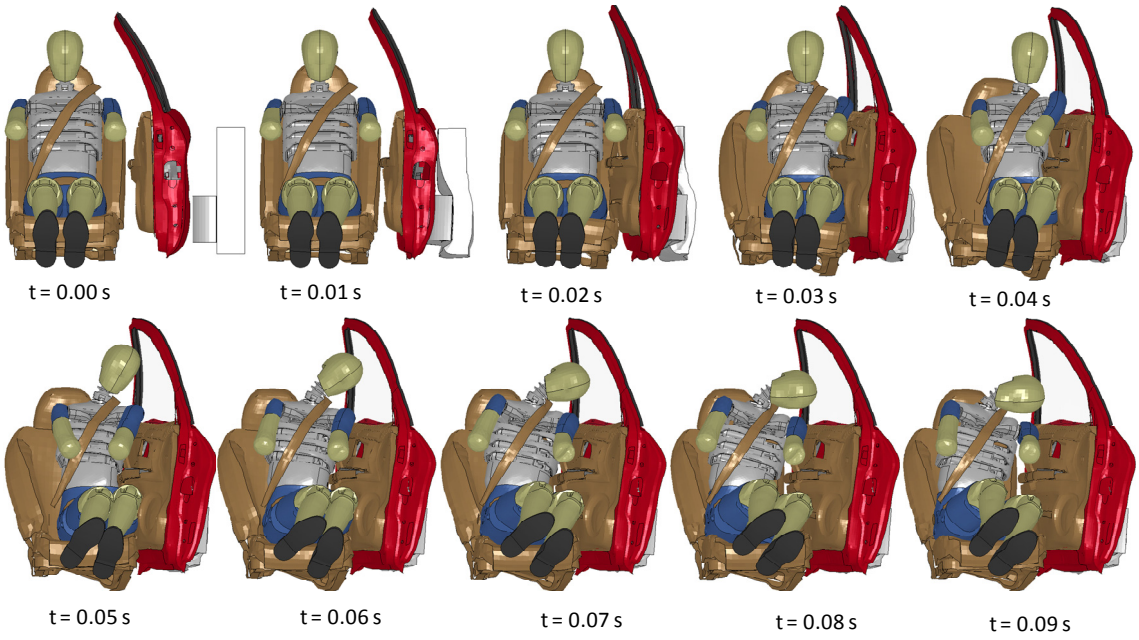

Figure 6.3: ES-2re, seat and door during impact

During the first stage of the impact shown above (t = 0.01 s), the lower portion of the barrier began to consolidate in the area of the lower bumper, which also began to deform the door, as well as the side sill / upright structure of the vehicle (not shown). In the next time step shown (t = 0.02 s), the barrier had begun to push the B pillar into the vehicle causing side sills and roof rails to bow into the vehicle. At this point the arm was engaged by the intruding door, though the thorax was not engaged at this time. At t = 0.03 s the armrest was in contact with the abdomen and the lower rib was beginning to contact the flat portion of the door above the arm rest. Between the times of 0.03 s and 0.06 s there was a noticeable change in the angle of the mid-sagittal plane of the occupant, which began vertically and ended with the shoulders rotated towards the impacting door. This change was primarily due to the impact of the arm rest to the abdomen which caused the top of the thorax to rotate towards the door. This rotation, along with the top rib interaction with the arm, would explain why the top rib generally exhibited the largest deflection. At t = 0.05 s the ribs reached their maximum deflection and began to unload. After this time the occupant began to move away from the door towards the center of the vehicle and no further primary injury was predicted, though impacts with other structures of the vehicle and / or other occupants could cause further injury. Injuries of this type are commonly referred to as secondary injuries.

One important observation that should be made from Figure 6.3, is that there was a significant amount of motion between the ATD and the seat. This phenomenon is shown clearly between 0.02 s and 0.06 s showing the space between the ATD and the inboard side of the seat changing dramatically. Three point restraint systems were primarily designed to protect occupants in front end collisions, and do not significantly restrain the occupant laterally in the event of a side impact [Morris et al., 1997]. This means that while the seat begins to move away from the intruding door due to deformation of the floor of the vehicle where the seat is mounted, the occupant, which is not firmly fixed to seat, remains in position until it is impacted by the door. This phenomenon was observed in a review of high speed video of several recent model side impact tests provided by NHTSA as shown in Figure 6.4, the rear view from an onboard camera used during a side NCAP test of a 2005 Ford 500.

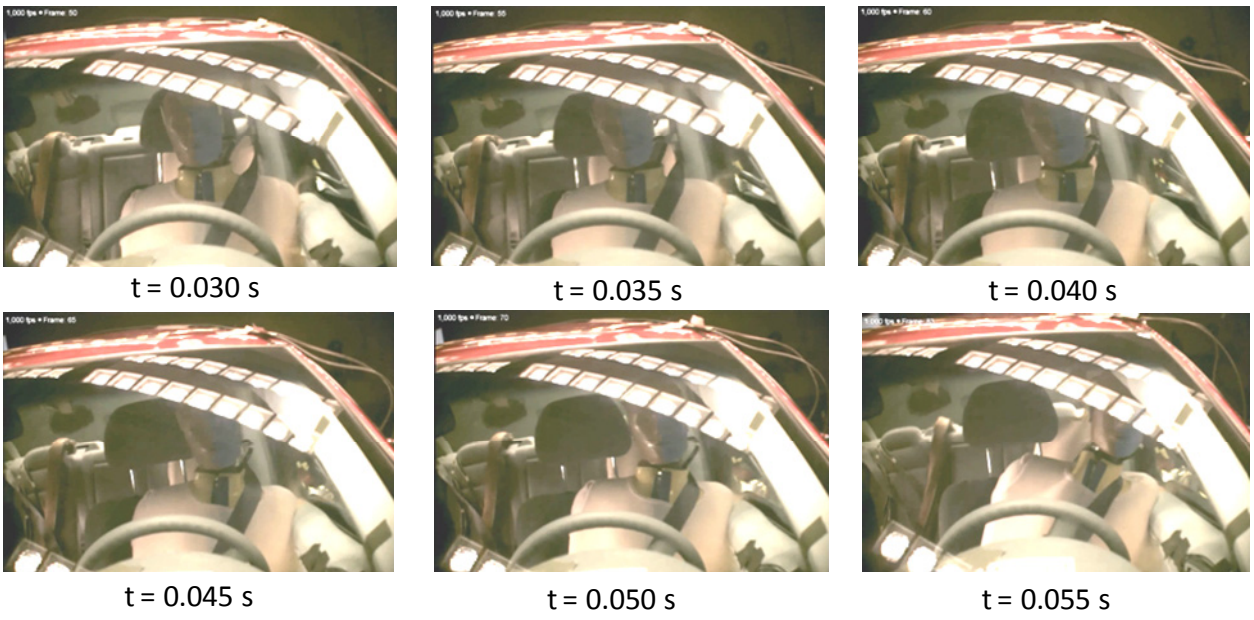

Figure 6.4: Rearview of occupant compartment during 2005 Ford 500 NCAP test

6.3 Effect of the Presence of an Occupant on Vehicle Response

In this portion of the study, the three ADT models (USSID, ES2-re and WorldSID) were placed in the nominal seating position and the impact simulations were run with the barrier having initial velocities of 54 kph (FMVSS 214 speed) and 61 kph (NCAP speed). Additionally, two other simulations were run, one at each speed, with no occupant in the driver's seat. The reasoning behind doing so was to assess the importance of the occupant in determining the door velocity and crush characteristic of the vehicle. It is important to note that the 'door velocity' mentioned here and in subsequent discussion is the lateral velocity of the inner sheet metal panel of the driver's side door and does not necessarily capture the velocity of the interior door trim which contacts the occupant. Some comment has been made on the importance of the occupant on controlling the door velocity by Kent and Crandall [2000]. They reviewed the NHTSA crash test database and found a single case where a vehicle was impacted with and without an occupant. They found that there was a noticeable difference in the vehicle door velocity trace, though as with all crash testing, the results were somewhat clouded by the inherent variability present in the test. They also performed a finite element analysis, which had similar findings, though very little detail was given with regards to validation or model description.

6.3.1 Changes to Response due to Presence of an Occupant

The lateral velocity of the door in the region of the occupant's thorax is shown in Figure 6.5 for the NCAP barrier speed simulation and in Figure 6.6 for the FMVSS 214 barrier speed simulations.

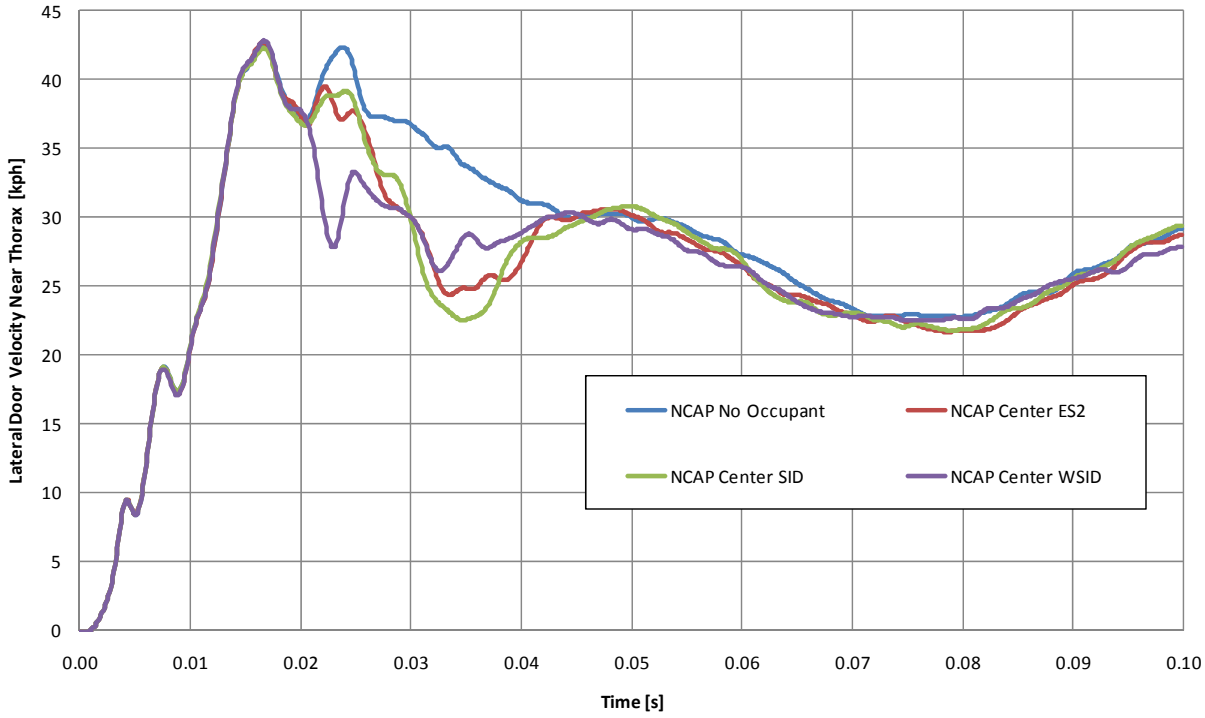

Figure 6.5: Lateral door velocity for central occupant impacts - NCAP Barrier Speed

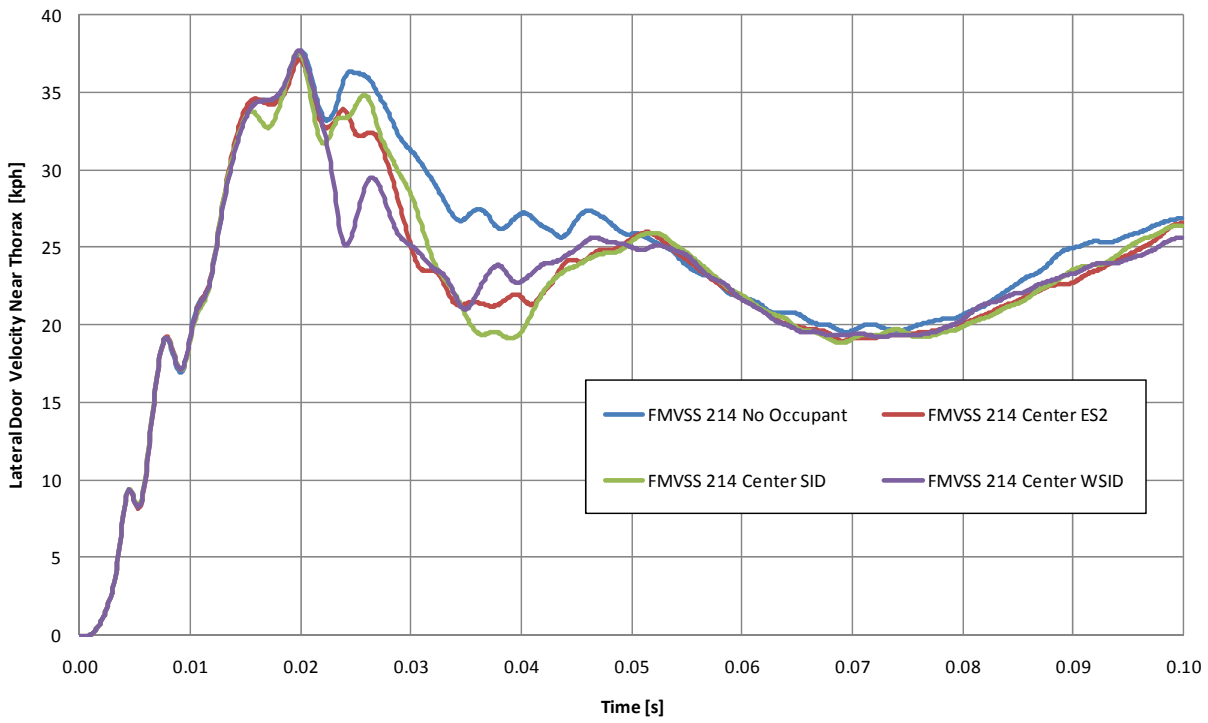

Figure 6.6: Lateral door velocity for central occupant impacts – FMVSS 214 Barrier Speed

These figures show very clearly that the presence of the occupant does have a noticeable effect on the intruding door velocity. The trough in velocity response at 0.035 s in the responses with occupants was missing in the two responses with no occupant. Figure 6.7 shows the rib velocity of the SID model during the NCAP simulation along with the lateral door velocity for both that simulation and the simulation with no occupant. This figure shows that up to the point of contact with the ATD (where the rib velocity began to increase) the velocity of the door followed the door velocity of the simulation with no occupant. After that time, the door velocity decreased at a greater rate than the no occupant scenario, until it reached equilibrium with the rib velocity at approximately 0.035 s. The door and occupant then travelled at the same velocity until separation at roughly 0.06 s. For the later portion of this time period the door velocity from the simulation with no occupant matched the door velocity from the simulation with the SID, which corresponded to the time after the occupant was pushed away from the door. This figure shows the extent to which the door velocity was coupled to the occupant. While the vehicle structure dominated the initial and final stages of the impact, the time period during contact was dominated by the occupant.

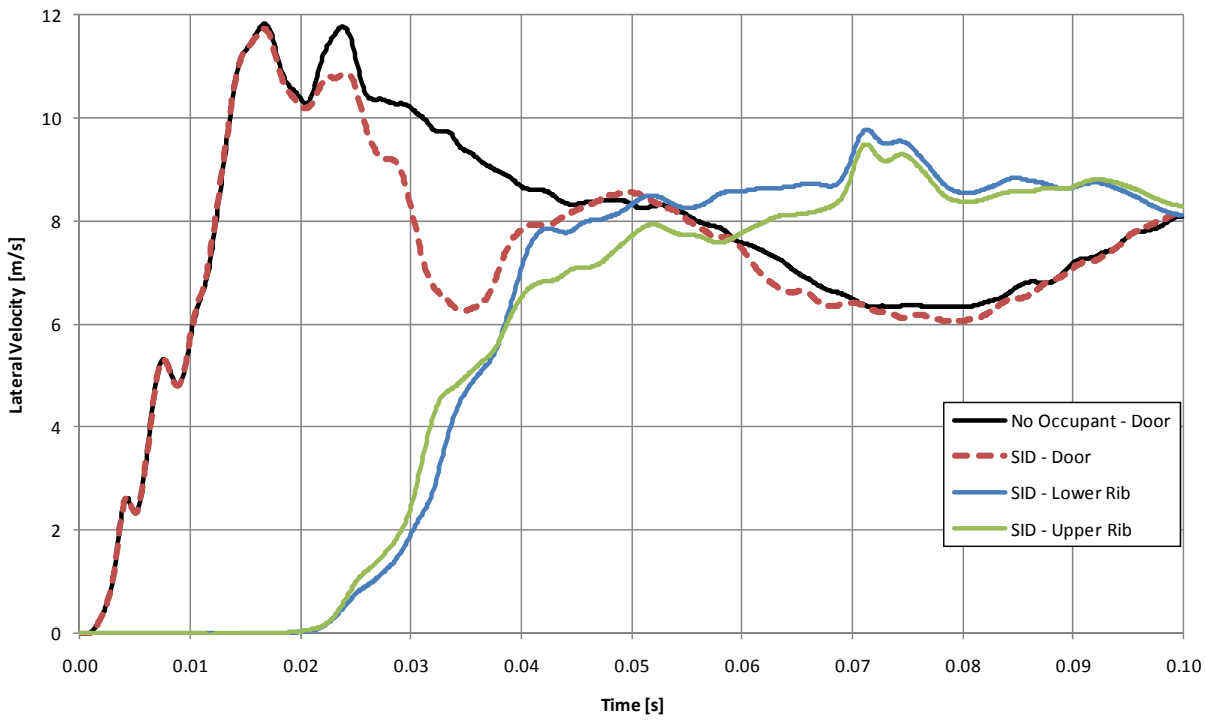

Figure 6.7: Door and rib velocity of NCAP simulation with SID

While the occupant had a strong effect on the door velocity, and to a lesser degree the B pillar, the remaining velocity profiles were relatively unchanged. An example is shown in Figure 6.8, which shows the vehicle center of gravity lateral velocity for those simulations with and without an occupant at both the FMVSS 214 and NCAP barrier speeds. This figure shows that while the final lateral velocity was slightly higher for those simulations without an occupant, there is not a noticeable difference in the velocity time histories, and the change in velocity can be attributed to the reduction in total mass of the model when the occupant was removed.

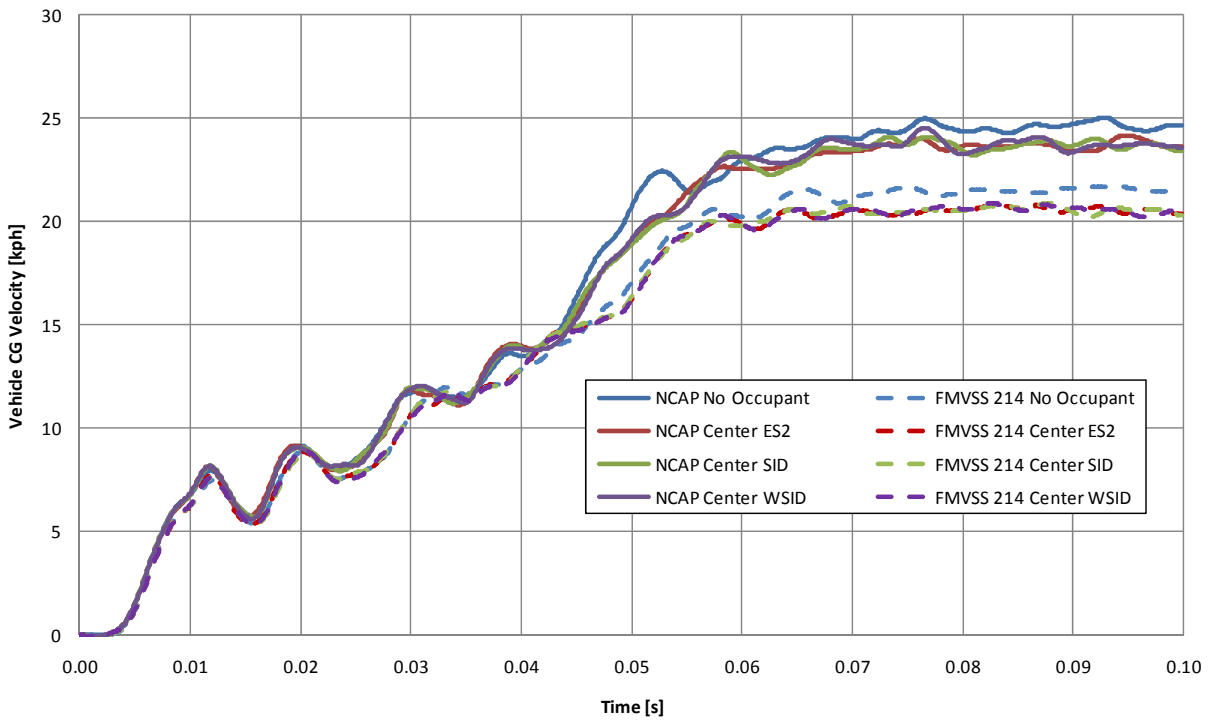

Figure 6.8: Vehicle center of gravity velocity for central occupant impacts

In addition to the changes in the door velocity, the deformation pattern of the vehicle was slightly changed in the simulation with no occupant. Figure 6.9 shows the vehicle deformation pattern for both the NCAP and FMVSS 214 cases. For both barrier speeds the maximum deformation with no occupant was larger (37 mm for the NCAP case and 24 mm for the FMVSS 214 case) than the next largest deformation. Also of note from this figure is the small scatter among the different ATDs. This indicates that the type of occupant had little determination on the deformation pattern of the vehicle, as long as an occupant was present. This result was not unexpected since, in general, the compliance and inertia properties of each ATD are similar due to all three ATDs representing a 50th percentile male occupant.

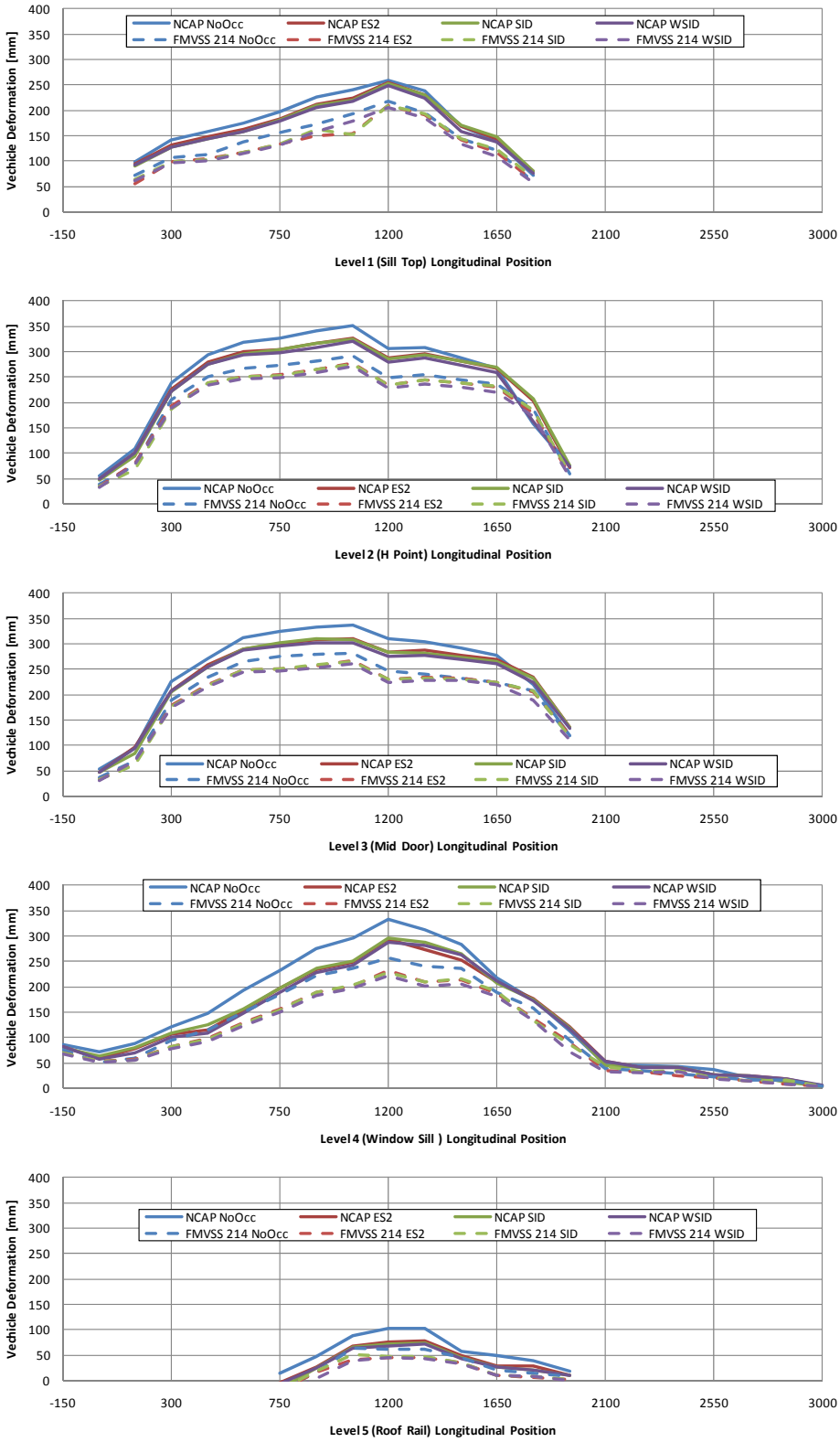

Figure 6.9: Vehicle deformation profile for impacts with occupant in central position

6.4 Effect of Initial Lateral Position of Occupant

In this portion of the study, the initial lateral position of the occupant was varied to assess the effect of the occupant initial position on the injury response measured by the ATD models. The dummy models were re-sunk in positions 40 mm to either side of the nominally central position of the seat with the new seat foam meshes exported as described in Section 4.6. The three lateral positions of the ES-2re models after the sinking process are shown in Figure 6.10 along with the approximate distances from the center sagittal plane of the occupant to the arm rest. For the three ATD models these offset distances remained fixed, however the distance between the point of contact for the ATD and the door panel (the AD distance) was variable depending on the geometry of the ATD. The three ATD's in their central seating location are shown in Figure 6.11. The 40 mm offset was chosen to avoid interference between the arm of the SID model, which had the largest breadth across the chest, and the interior door panel. In a study carried out to assess the ability to repeatedly position an occupant in a vehicle, the scatter in the position of the H-point from a well controlled setup was found to be within a 26 mm distance in the longitudinal direction and 8 mm in the vertical direction [Adalian et al., 2009]. Unfortunately, no mention was made regarding the lateral position; however given the size of the corridors presented in that study it is unlikely that the corridor would be above 40 mm.

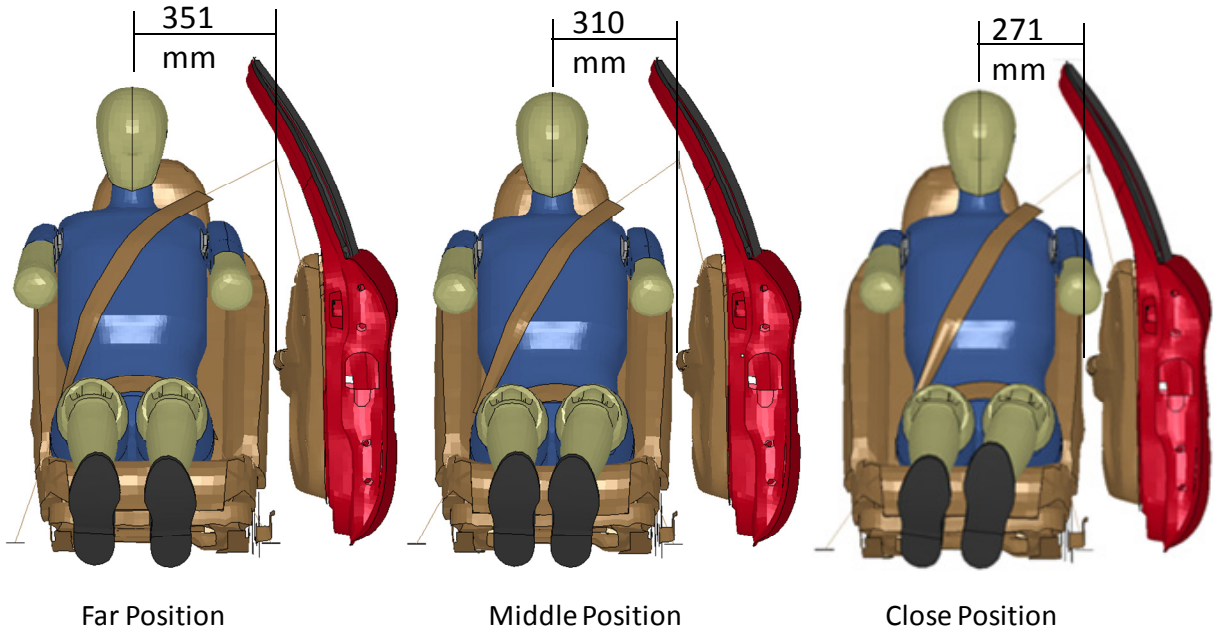

Figure 6.10: Initial position of occupants at three lateral offsets

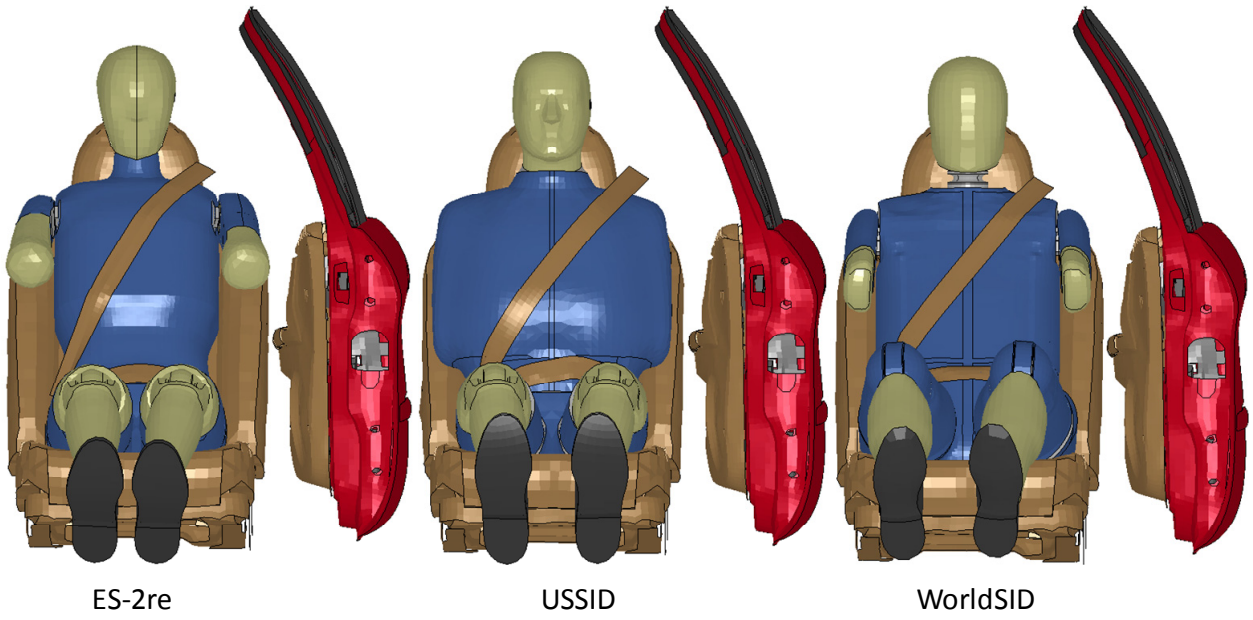

Figure 6.11: ATD models in central seating position

6.4.1 Changes to Response due to Initial Lateral Position of Occupant

The primary changes in vehicle response to occupant initial position were seen in the door velocity. Figure 6.12 shows the door velocity response from the USSID simulations along with the door velocity with no occupant present. In each case, the velocity trace of the door followed the case with no occupant to the point at which contact was made between the door and the occupant. At this point the velocity began to decrease as momentum was transferred to the stationary occupant. The trough velocity was consistent for each initial offset, though there was a shift in the time of the trough. This illustrates the effects the occupant and the time of contact have on the lateral door velocity and reinforces the importance of the proper seating position of the occupant at the start of the simulation.

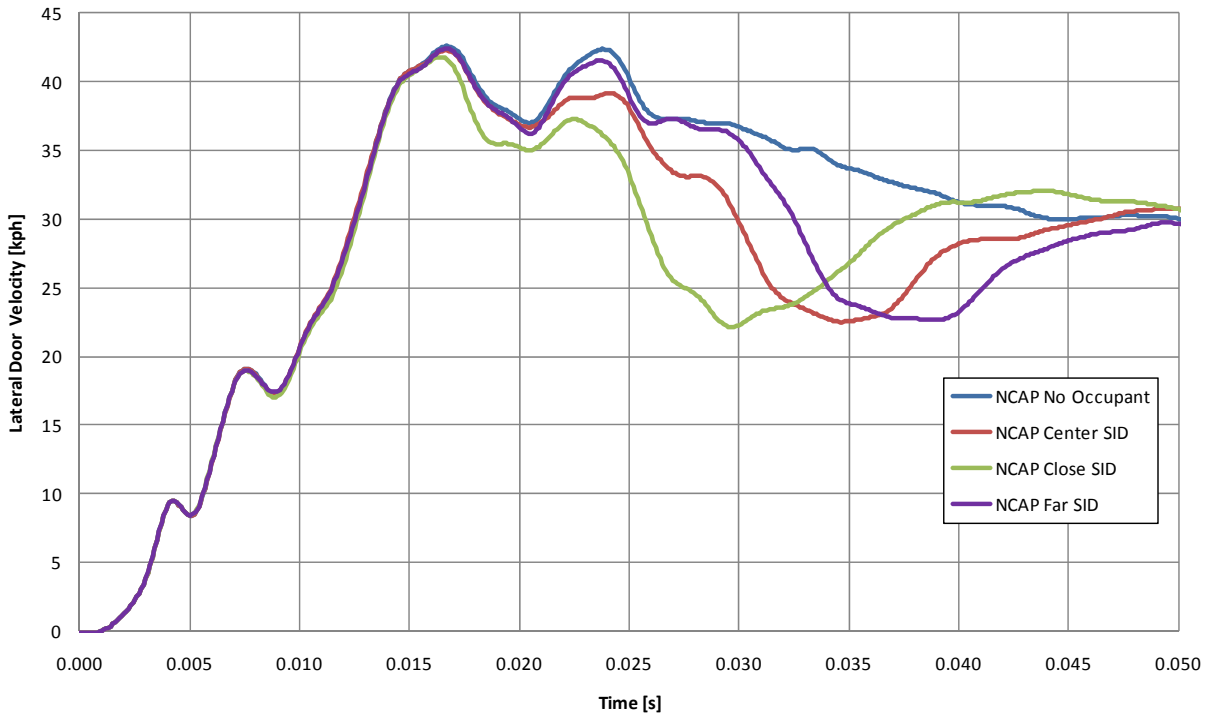

Figure 6.12: Changes to door velocity profile with differing initial lateral offset

The deformation pattern from each of these simulations is shown in Figure 6.13. This figure highlights that there was very little difference between the final vehicle deformations of any occupant - location combination.

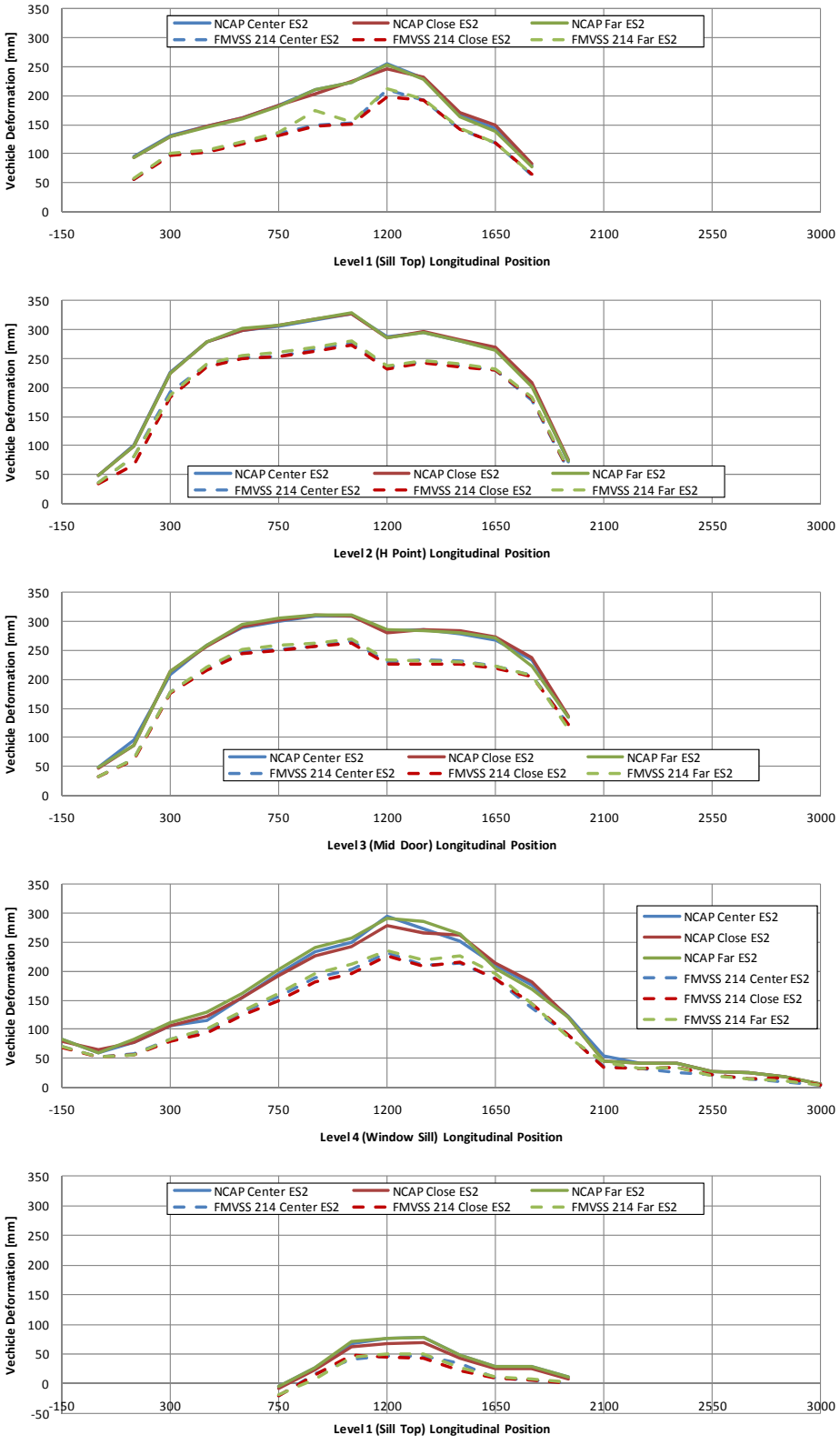

Figure 6.13: Vehicle deformation profile for differing initial lateral offset

The rib deflection, VC and TTI scores from each occupant, position and barrier speed combination is shown in Table 6.1.

Table 6.1: Injury criteria response for differing initial lateral seating positions

			Rib Deflection [mm]				VC [m/s]				TTI [G]
Barrier Speed	ATD Model	Lateral Position	Upper	Middle	Lower	Max	Upper	Middle	Lower	Max	
NCAP (61 kph)	ES-2re	Close	51.6	43.4	38.3	51.6	1.15	1.35	0.87	1.35	158
		Center	50.1	43.1	41.8	50.1	1.11	1.56	0.77	1.56	152
		Far	49.2	43.0	24.3	49.2	1.16	1.12	0.39	1.16	146
	SID	Close		29.5		29.5		0.25		0.25	68
		Center		29.0		29.0		0.26		0.26	67
		Far		24.8		24.8		0.24		0.24	56
	WSID	Close	45.7	26.2	27.5	45.7	1.08	0.36	0.41	1.08	156
		Center	46.8	27.5	68.5	68.5	1.21	0.40	1.37	1.37	168
		Far	43.2	29.3	30.3	43.2	0.83	0.41	0.43	0.83	136
FMVSS 214 (54 kph)	ES-2re	Close	43.4	36.2	31.2	43.4	0.80	1.02	0.47	1.02	124
		Center	40.7	34.3	35.6	40.7	0.72	0.84	0.44	0.84	129
		Far	41.0	34.9	18.4	41.0	0.58	0.64	0.23	0.64	121
	SID	Close		26.2		26.2		0.15		0.15	54
		Center		24.5		24.5		0.16		0.16	50
		Far		21.1		21.1		0.15		0.15	45
	WSID	Close	37.2	18.7	22.3	37.2	0.79	0.14	0.30	0.79	158
		Center	37.8	20.1	57.1	57.1	0.92	0.20	0.92	0.92	142
		Far	31.5	20.1	22.9	31.5	0.52	0.16	0.15	0.52	106

Typical rib deflection, VC and TTI responses are shown in Figure 6.14, which were generated from the simulation performed with the ES-2re model at NCAP barrier speed. The time shift in the responses due to differing contact time is clearly visible in this figure.

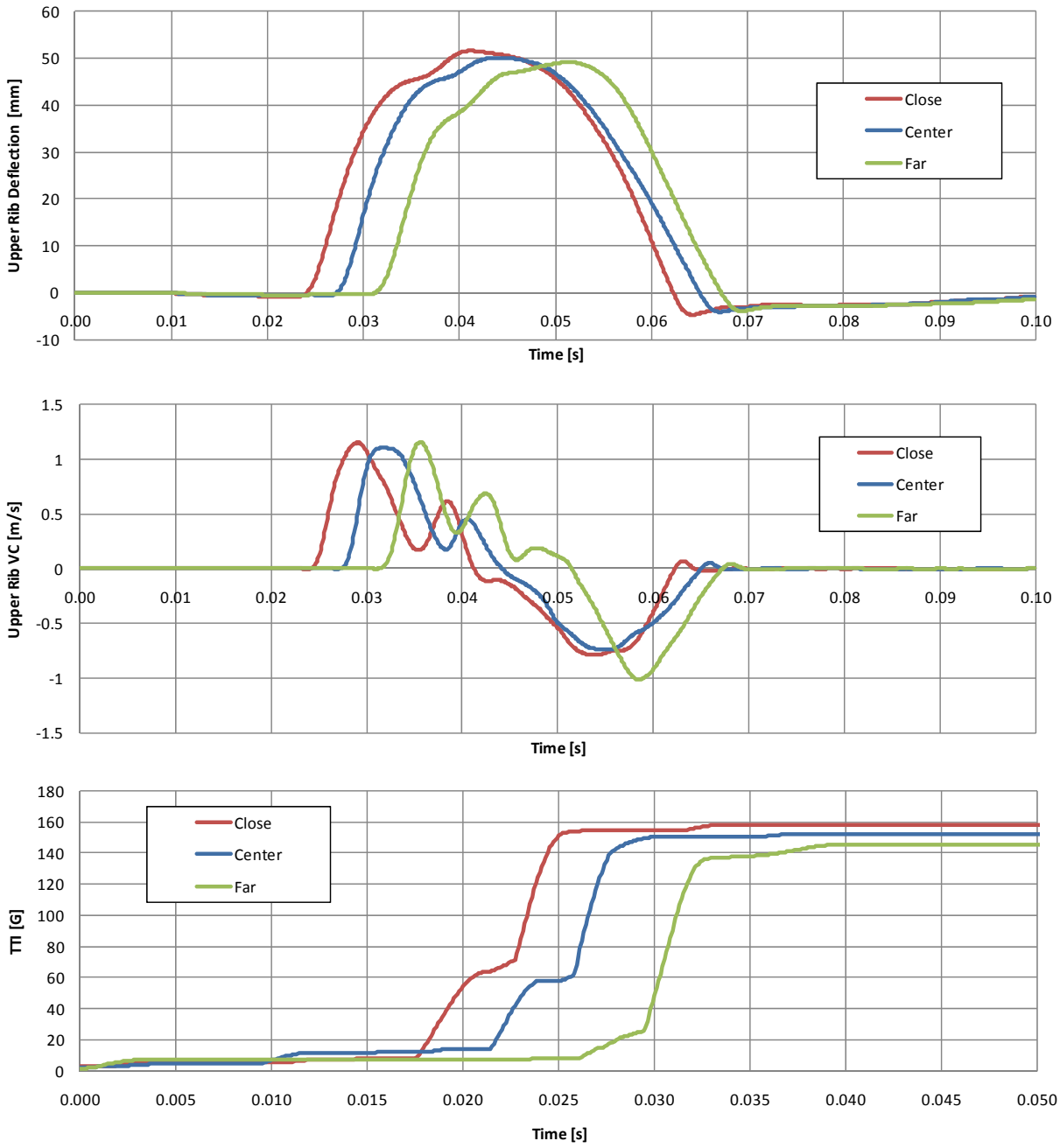

Figure 6.14: Injury criteria responses for ES-2re in NCAP tests at three initial lateral offsets

The results in Table 6.1 show a general trend in the slight reduction of rib deflection as the occupant was moved further towards the center of the vehicle for the ES-2re and USSID models. The WSID model showed the greatest rib deflection in the middle position. This was due to the armrest in the vehicle model directly impacting the lowest thoracic rib in this position rather than the abdominal region, as with the other cases. When the occupant was sunk in the seat, the H-

point was slightly lower (roughly 15 mm) in the center position than on either side. This was due to structure of the seat which provided more structural support on the exterior edges of the seat and thus allowed for more deformation in the center position, causing to the H-point to be slightly lower. This slight difference in height made little difference in the response of the USSID and ES-2re models; however this changed the impact point for the WSID model enough to cause significant difference in the thoracic response. Figure 6.15 shows the point of impact for the WSID in the center and far positions to illustrate this point. Other than these two cases the top rib showed the maximum deflection in all other cases for the ES-2re and WSID. This was primarily due to the effect of the armrest causing the rotation of the mid-sagittal plane as discussed in Section 6.2. In side impacts with actual human bodies, the deflection characteristics would be different between the top and bottom ribs, unlike the ATD thorax which respond similarly at each level. In the human body, the top (true) ribs are attached to both the sternum and the spine, while the lower (false) ribs are only attached at the spine. As stated earlier, a fracture of the top rib is an indication of extraordinarily high levels of trauma, while false ribs can be fractured relatively easily. This means that in an actual side impact, focusing on loading the top ribs may be advantageous as they are less likely to fracture, but this should not be at the expense of exposing the lower ribs to higher levels of trauma as these ribs are more easily damaged. It is worth noting that the magnitude of the rib deflection predicted by each occupant model varied a great deal. In general the ES-2re predicted rib deflections 5 mm to 10 mm higher than the WSID and 15 mm to 20 mm higher than the USSID. This discrepancy made drawing comparisons between the ATD models difficult. The rib deflection responses were normalized to the middle rib response of the middle seating position model for each ATD/barrier speed combination. These results are presented in Table 6.2 which shows that the upper rib response was higher in roughly the same proportion (1.2 times the middle response) for the ES-2re for both barrier speeds and that this differential was slightly higher for the lower speed impact with the WSID. In nearly all cases the middle rib response was fairly consistent throughout the range of seating positions and barrier speeds. The lower rib response was significantly lower for the ES-2re in the far seating position when compared to the other two positions, while the response of the WSID was much higher in the center position as described previously.

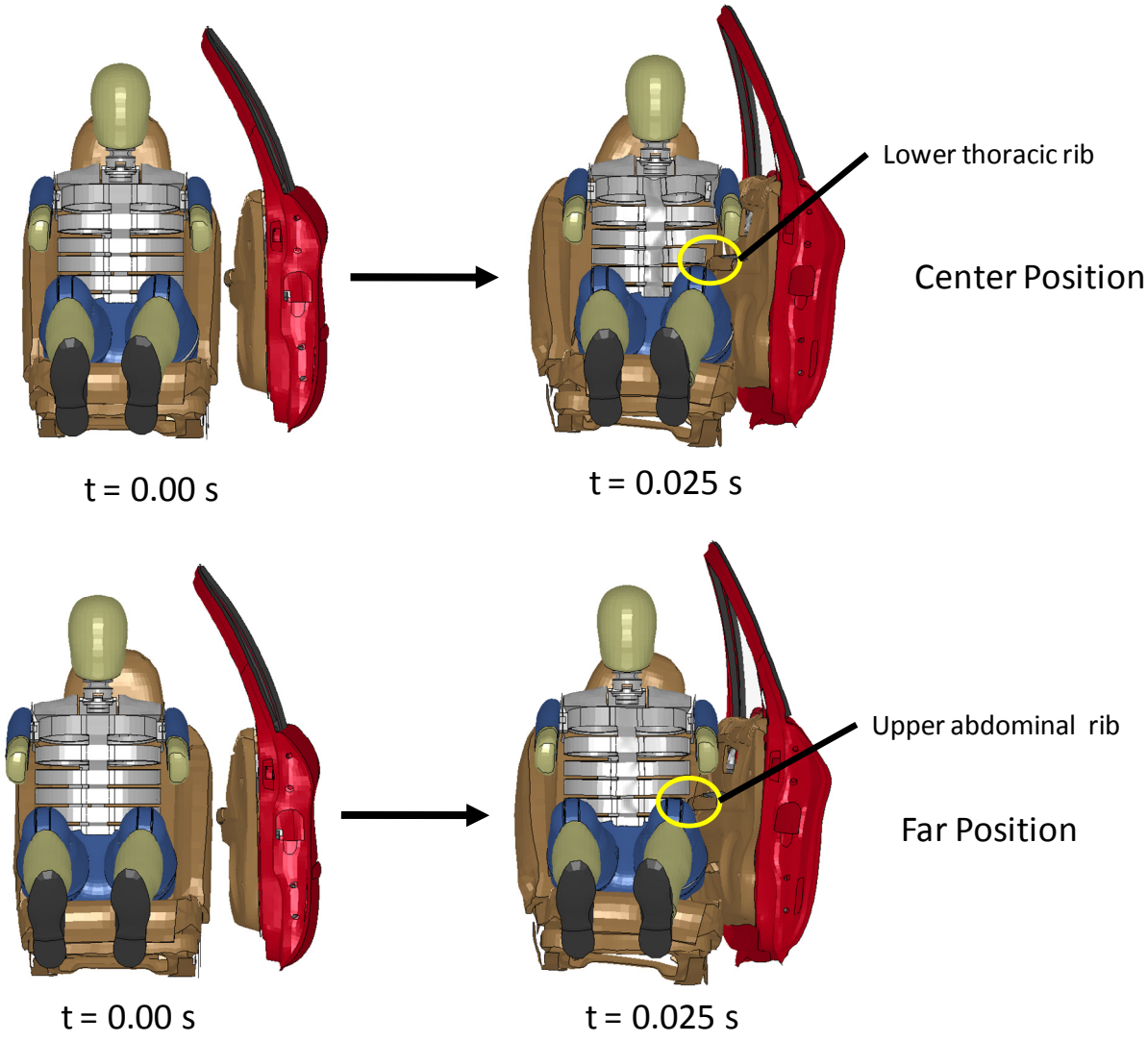

Figure 6.15: Armrest impact point on WorldSID

Table 6.2: Normalized rib deflection response for differing initial lateral seating positions

Barrier Speed	ATD	Lateral Position	Upper Rib	Middle Rib	Lower Rib
NCAP (61 kph)	ES-2re	Close	1.1955	1.0060	0.8867
		Center	1.1623	1	0.9698
		Far	1.1396	0.9959	0.5632
	SID	Close		1.0192	
		Center		1	
		Far		0.8548	
	WSID	Close	1.6599	0.9511	0.9969
		Center	1.6971	1	2.4853
		Far	1.5691	1.0652	1.0986
FMVSS 214 (54 kph)	ES-2re	Close	1.2662	1.0561	0.9105
		Center	1.1874	1.0000	1.0376
		Far	1.1940	1.0166	0.5371
	SID	Close		1.0666	
		Center		1	
		Far		0.8609	
	WSID	Close	1.8486	0.9300	1.1086
		Center	1.8760	1	2.8362
		Far	1.5638	0.9966	1.1378

It was found that the VC response varied more than the rib deflection response. In most cases with the ES-2re the middle rib provided the maximum VC response and the velocity component of VC dominated the response. This was contrary to the response of the WSID, where the rib which exhibited the most deflection provided the maximum VC response in all cases. As with rib deflection, the ES-2re generally exhibited a higher VC prediction than the WSID or the SID, which predicted low VC responses. Unlike the rib deflection response, the there was no clear reduction in VC as the occupant was moved further from the intruding door, with the middle position providing the highest response for several ATD-barrier speed combinations, though this results is somewhat confounded by the WSID response.

The TTI scores of the USSID show a downward trend as the occupants was moved further inboard. The ES-2re and WSID were less clear and both ATDs exhibited much higher TTI scores than the USSID. It must be reiterated that both the ES-2re and WSID were not designed to utilize this injury prediction.

6.5 Effect of Initial Vertical Position of Occupant

To study the effect of the vertical position on the occupant's injury response, the position of the seat and ATD were moved upward 50 mm in the vertical position, referred to as the 'high position'. This position was used as it provided a clearly elevated seating position while still being a realistic driving position. Additionally this position was used to avoid contact between the occupant's thighs and the steering wheel. To avoid confounding issues, only the center seating position of the three lateral positions was studied. The ES-2re model in both positions is shown in Figure 6.16. Because the seat in the nominal case was nearly as low as possible without interference between the seat structure and the vehicle floor, no seating position lower than the baseline was investigated. The seat foam profile would not change due to the entire seat being moved so no additional sinking models were required to study the effect of these positions; however each simulation required specific seat belt geometry to be generated.

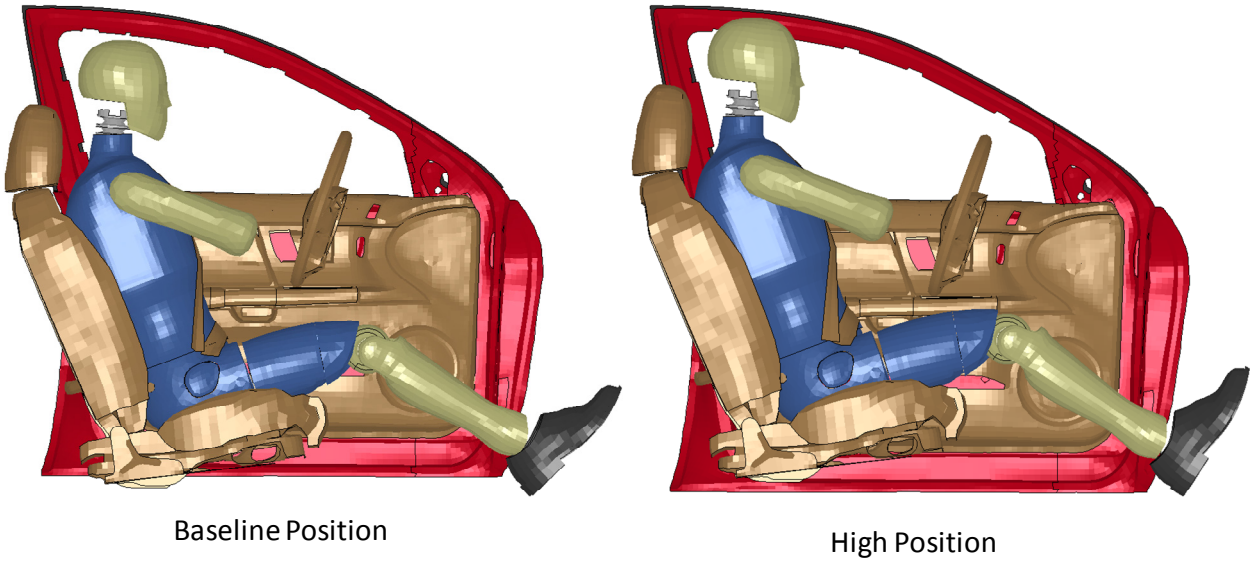

Figure 6.16: Initial vertical position of occupant

6.5.1 Changes to Response due to Initial Vertical Position of Occupant

The injury criteria responses for each ATD, barrier speed, and vertical position combination are shown Table 6.3.

Table 6.3: Injury criteria response for differing initial vertical seating positions

			Rib Deflection [mm]				VC [m/s]				TTI [G]
Barrier Speed	ATD Model	Vertical Position	Upper	Middle	Lower	Max	Upper	Middle	Lower	Max	
NCAP (61 kph)	ES-2re	Nominal	50.1	43.1	41.8	50.1	1.11	1.56	0.77	1.56	152
	ES-2re	High	53.8	47.6	33.8	53.8	1.47	1.33	0.84	1.47	154
	SID	Nominal		29.0		29.0		0.26		0.26	67
	SID	High		25.4		25.4		0.20		0.20	67
	WSID	Nominal	46.8	27.5	68.5	68.5	1.21	0.40	1.37	1.37	168
	WSID	High	39.3	26.2	23.7	39.3	0.75	0.29	0.22	0.75	130
FMVSS 214 (54 kph)	ES-2re	Nominal	40.7	34.3	35.6	40.7	0.72	0.84	0.44	0.84	129
	ES-2re	High	46.8	37.5	26.4	46.8	0.88	0.89	0.46	0.89	138
	SID	Nominal		24.5		24.5		0.16		0.16	50
	SID	High		20.1		20.1		0.11		0.11	50
	WSID	Nominal	37.8	20.1	57.1	57.1	0.92	0.20	0.92	0.92	142
	WSID	High	29.1	18.4	16.7	29.1	0.45	0.14	0.11	0.45	113

Figure 6.17 shows the point of contact between the armrest and the abdomen of the ES-2re model in both seating positions.

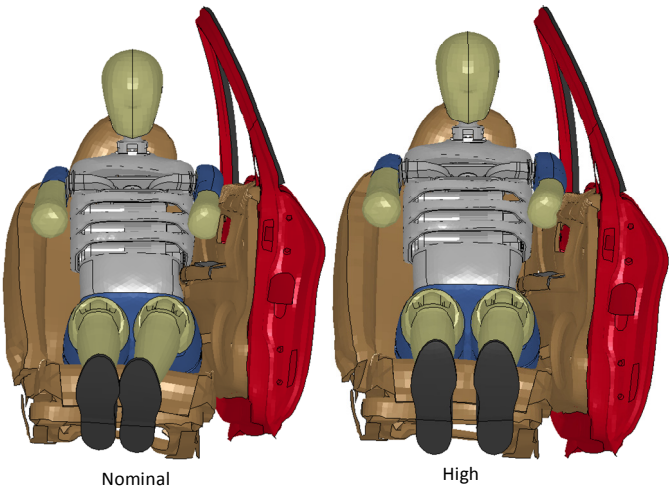

Figure 6.17: Armrest impact point for differing vertical initial positions

The most obvious outcome from these simulations was the large reduction in the rib deflection and VC predicted by the WSID model. This was an expected result since the increase in seating position height was enough to move lower thoracic rib above the point of impact of the armrest. The two simulations with the WSID in the high position predicted the highest rib deflection and VC measurements from the top rib which was similar to the results from the ES-2re model. The rib deflection predicted by the ES-2re at both barrier speeds was higher in the elevated seating position than the baseline positions. This was due to the impact point of the abdomen providing a larger moment, causing the thorax to rotate and forcing the top rib to impact the door panel harder than in the lower baseline condition. No change was seen in the TTI scores for the USSID model. However, the ES-2re predicted higher TTI scores in the higher seating position while the WSID predicated lower.

Due the contact with the armrest being centered lower on the abdomen, one would expect the probability of injury in this body region to increase. For example in the NCAP barrier speed test the maximum deflections of the two abdominal ribs of the WSID were 68 mm and 34 mm for the upper and lower abdominal ribs respectively. With the occupant was shifted upwards, these deflection increased to 70 mm and 69 mm.

6.6 Effect of Initial Longitudinal Position of Occupant

The focus of this portion of the study was to assess the implications of the thorax impacting the B pillar rather than the interior door trim. To study the effect of the longitudinal position the occupant and seat models were moved 150 mm rearward in the vehicle. This position was used to ensure that the center of the ATD rib would be contacted by the B pillar during impact, while still maintaining a reasonable driving position. The baseline condition from this set of models was the same as for the models studying the vertical position, and no change was made in either the vertical or horizontal position between the baseline and the rear position. As with the vertical position models, the seat foam geometry did not change, but new seatbelt geometry was created. The initial position of the ES-2re model in the baseline and rear seating position are shown in Figure 6.18.

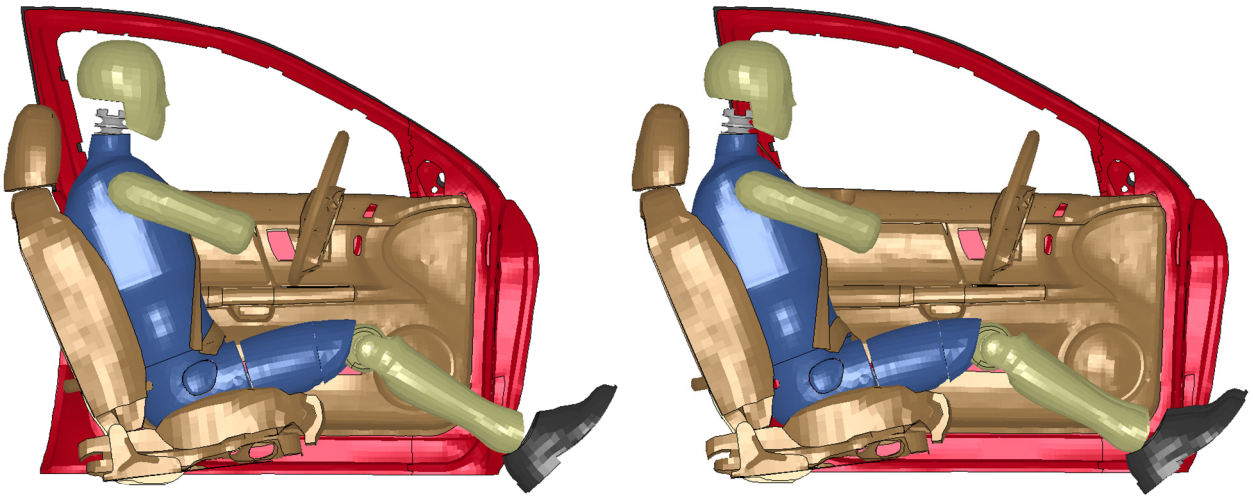

Figure 6.18: Initial longitudinal position of occupants

6.6.1 Changes to Response due to Initial Longitudinal Position of Occupant

The injury criteria responses for each ATD, barrier speed, and longitudinal position combination are shown in Table 6.4.

Table 6.4: Injury criteria response for differing initial longitudinal seating positions

			Rib Deflection [mm]				VC [m/s]				TTI [G]
Barrier Speed	ATD Model	Lonitudinal Position	Upper	Middle	Lower	Max	Upper	Middle	Lower	Max	
NCAP (61 kph)	ES-2re	Nominal	50.1	43.1	41.8	50.1	1.11	1.56	0.77	1.56	152
	ES-2re	Rear	46.1	42.6	44.4	46.1	1.21	0.64	0.82	1.21	127
	SID	Nominal		29.0		29.0		0.26		0.26	67
	SID	Rear		36.6		36.6		0.64		0.64	121
	WSID	Nominal	46.8	27.5	68.5	68.5	1.21	0.40	1.37	1.37	168
	WSID	Rear	76.3	43.0	44.4	76.3	2.03	0.75	0.98	2.03	176
FMVSS 214 (54 kph)	ES-2re	Nominal	40.7	34.3	35.6	40.7	0.72	0.84	0.44	0.84	129
	ES-2re	Rear	34.4	29.8	33.7	34.4	0.75	0.29	0.64	0.75	106
	SID	Nominal		24.5		24.5		0.16		0.16	50
	SID	Rear		36.0		36.0		0.53		0.53	94
	WSID	Nominal	37.8	20.1	57.1	57.1	0.92	0.20	0.92	0.92	142
	WSID	Rear	62.2	31.2	32.2	62.2	1.50	0.27	0.53	1.50	152

Figure 6.19 shows the occupant at the point of impact along with interior trim part covering the B pillar and the steering wheel for reference. This image clearly shows the distinction between the point of thoracic impact for the two cases.

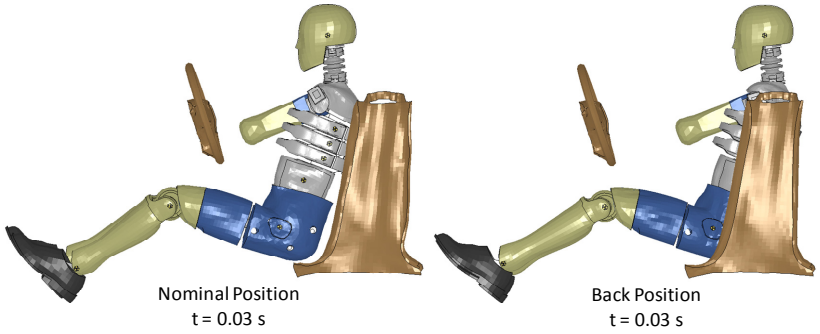

Figure 6.19: Position of occupant at impact for differing initial longitudinal positions

For both the USSID and the WSID, the rib deflections were higher in the rear seating position while the response of the ES-2re was higher in the baseline seating position. This was due to an effect of the arm interaction which can be explained with the aid of Figure 6.20 and Figure 6.21. The upper rib response of the ES-2re during the NCAP barrier speed impact is shown in Figure 6.20, for both seating positions, while Figure 6.21 shows a front view of those models between the times of 0.03 s and 0.04 s.

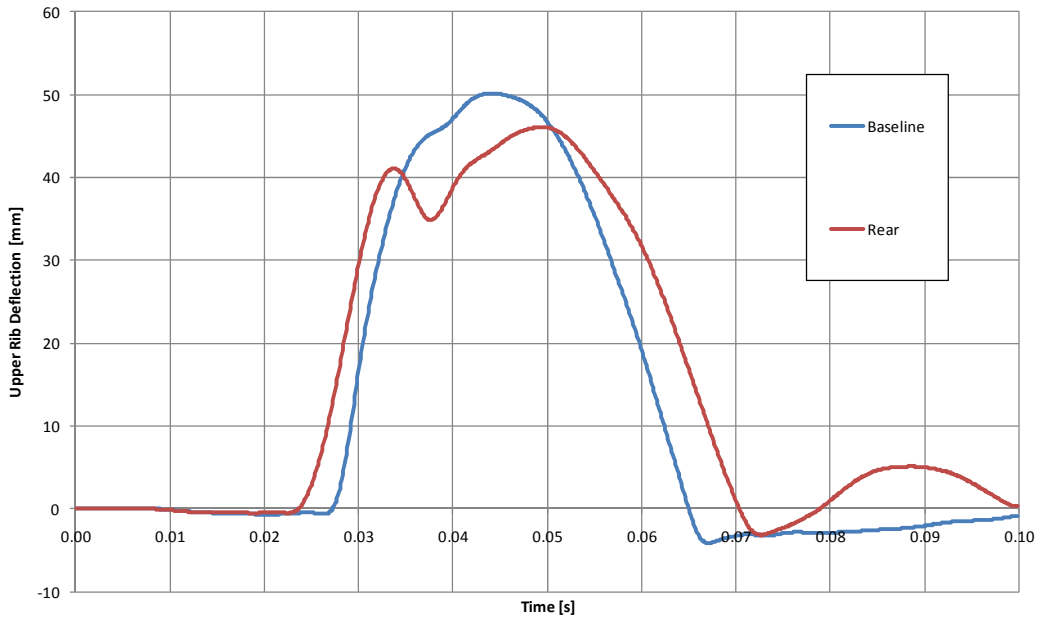

Figure 6.20: Upper rib deflection of ES-2re in baseline and rear positions at NCAP barrier speed

Figure 6.21: Front view of ES-2re in baseline and rear positions at NCAP barrier speed

At 0.03 s the arm of the ES-2re was at roughly the same position in both cases, however after this time the arm of the occupant in the rear position began to rotate upwards, which allowed some room for the rib to unload, which is seen between 0.03 s and 0.04 s in Figure 6.20. In the baseline case, the arm stayed in position, causing the rib deflection to increase monotonically to the peak. This small amount of unloading in the rear position led to a lower overall rib deflection. A similar trend was seen with the FMVSS 214 barrier speed impacts. Without this arm effect, one would expect the response to be higher (as with the WSID) due to the rear seated occupant being impacted by the B pillar, which is less forgiving than the door structure, which itself crushes a great deal during impact, absorbing energy.

6.7 Effect of Interior Plastic Trim Materials

This study was continued by examining the effect of several interior part material properties. For this portion of the study, only the centrally positioned ES-2re model was used with the NCAP barrier speed.

The material properties of the interior plastic trim pieces highlighted in green in Figure 6.22 were varied to study the outcome of these changes on the occupant's response.

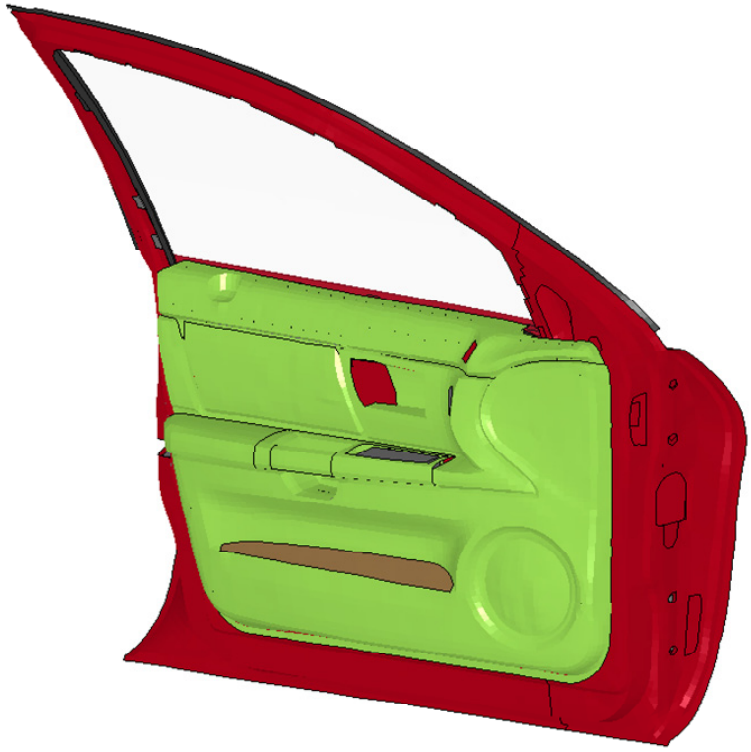

Figure 6.22: Interior panels changed to study effect of interior materials

In the as-delivered state of the vehicle model, these interior trim pieces were modeled using a piecewise linear plasticity material model. After yield stress the material behaved according to a flow stress curve supplied in the material input deck. ABS was a common material used for the plastic trim pieces during the 2000 model year and thus these parts were assumed to be ABS. A search of a materials database, found that the density, Young's modulus and yield strength of material in the as-delivered model were within the range show in that database [MatWeb, 2010]. To assess the effect that the material properties had for these parts, a series of upper and lower bounds were created. The highest Young's modulus, density and yield strength were used to

create a 'high strength' ABS material model, while the lowest Young's modulus, density and yield strength were used to create a 'low strength' ABS material model. The baseline model utilized the as-delivered material model. The flow stress was scaled by applying a scale factor based on the ratio of the yield stress to the as-delivered yield stress. The material properties used for each model are shown in Table 6.5, with the stress-strain response of each material shown in Figure 6.23.

Table 6.5: Interior door trim material properties

	Density [g/cm3]	Young's Modulus [Mpa]	Yield Strength [Mpa]	Flow Stress Scale Factor
Baseline	1.2	2800	45	1
High Strength	1.26	6100	65	1.44
Low Strength	0.35	1520	27.6	0.61

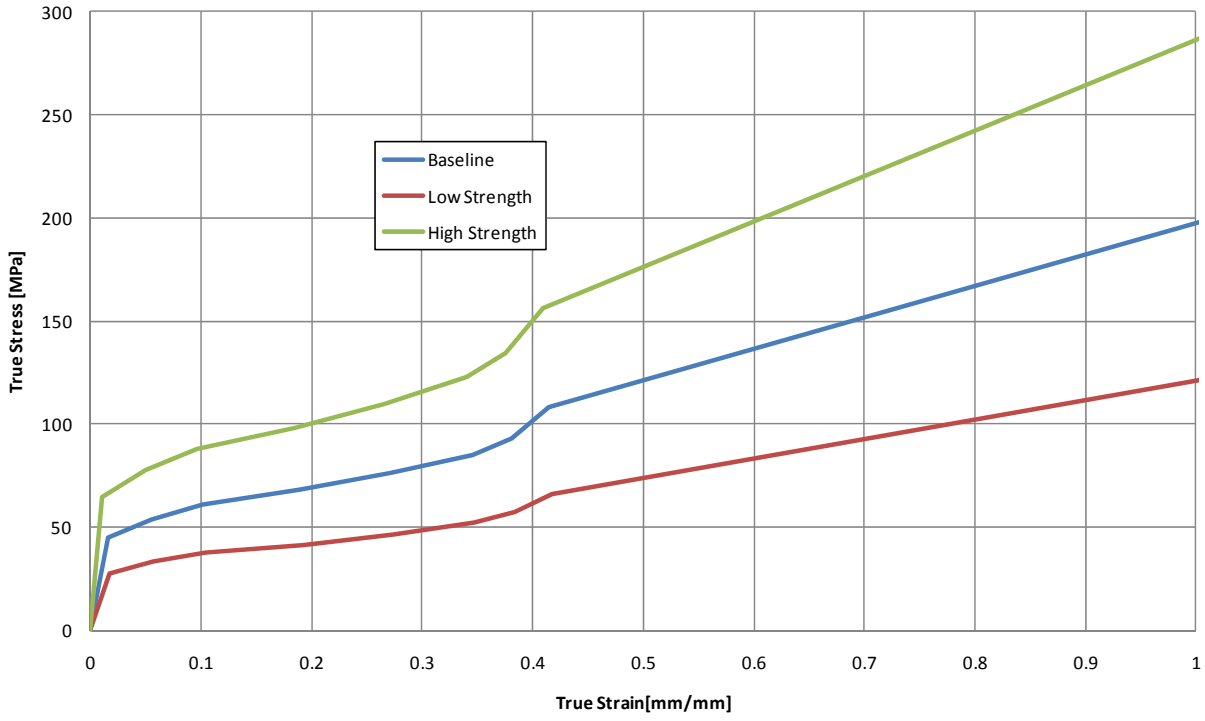

Figure 6.23: Interior trim material curves

6.7.1 Changes to Response due to Changes in Trim Material Properties

Table 6.6 shows the response of the ES-2re model for each simulation performed for this section of the parametric study.

Table 6.6: Injury criteria response for differing interior trim material strength

	Rib Deflection [mm]				VC [m/s]				TTI [G]
	Upper	Middle	Lower	Max	Upper	Middle	Lower	Max	
Baseline	50.1	43.1	41.8	50.1	1.11	1.56	0.77	1.56	152
High Strength Interior	48.9	40.2	38.8	48.9	1.04	1.42	0.72	1.42	167
Low Strength Interior	51.5	46.2	39.6	51.5	1.16	1.52	0.90	1.52	138

Table 6.6 shows that for both rib deflection and VC, lower injury was predicted as the material strength increased, while the converse was true for the TTI prediction. This was due to the higher strength material interior door panel providing slightly better resistance to collapsing, which reduced the amount of contact between the inner steel door panel and the occupant once the door had consolidated. Obviously there is an upper limit to the effectiveness of an increased panel stiffness to prevent injury and the gains to occupant protection by increasing the stiffness of the door are modest.

6.8 Effect of a Collapsible Arm Rest

Due to some of the issues associated with the armrest impacting the abdomen noted previously, the effect of a collapsible armrest was investigated. The material model of the part highlighted in green in Figure 6.24 was changed to the foam material used for the seat in the vehicle model. The stress strain response of the both the original arm rest and the foam material model are shown in Figure 6.25, which highlights the foam material response being an order magnitude below the ABS plastic.

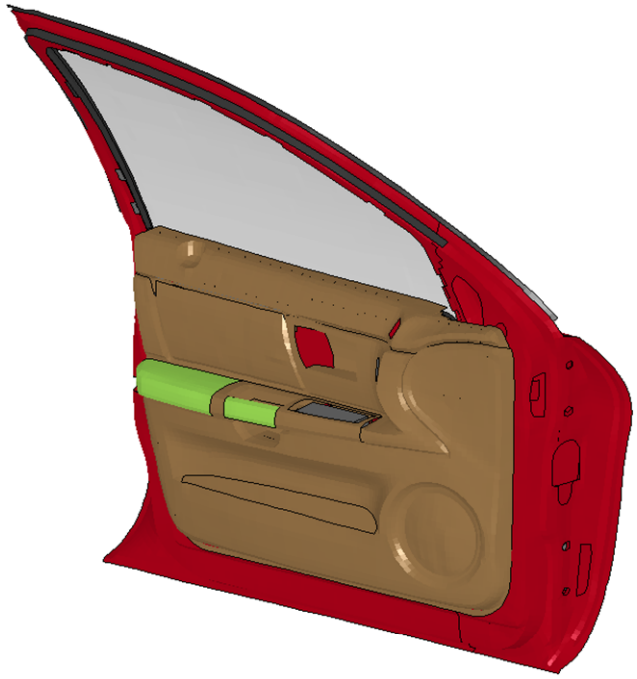

Figure 6.24: Portion of armrest changed to collapsible material

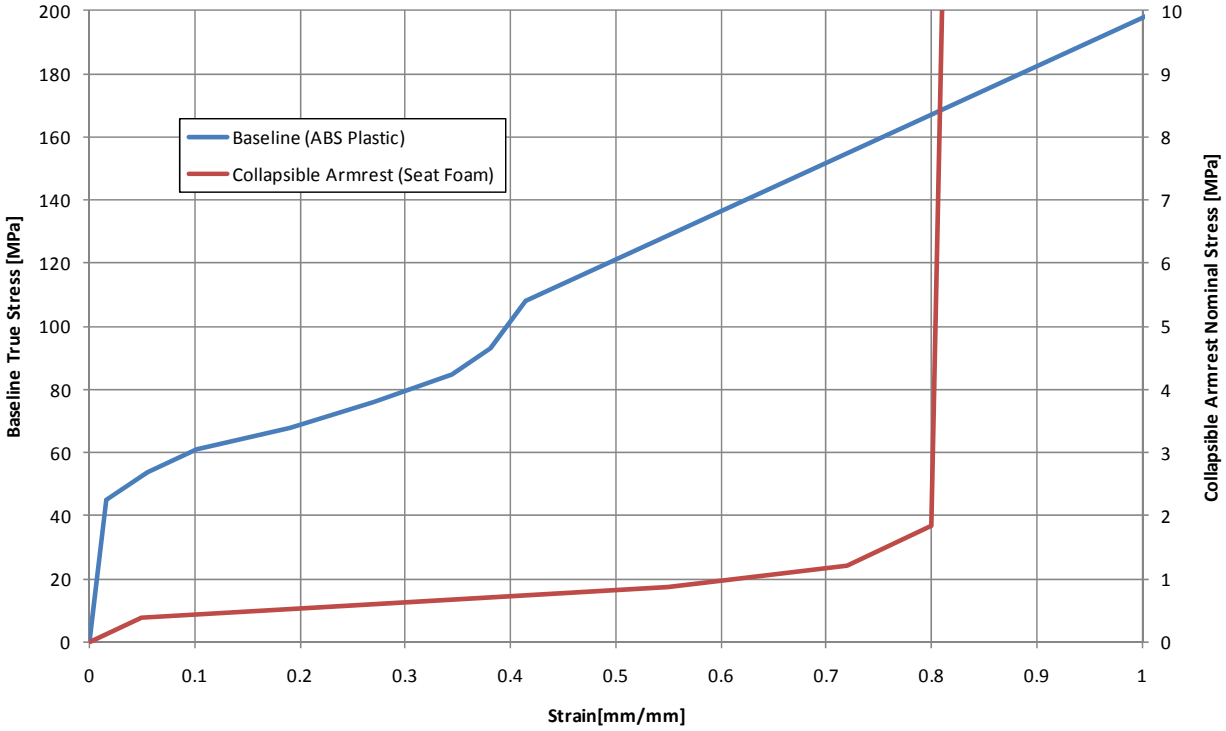

Figure 6.25: Armrest material properties

6.8.1 Changes to Response due to Changes in Armrest Properties

The ES-2re model's responses to this part of the study are shown in Table 6.7.

Table 6.7: Injury criteria response for collapsible armrest

	Rib Deflection [mm]				VC [m/s]				TTI [G]
	Upper	Middle	Lower	Max	Upper	Middle	Lower	Max	
Baseline	50.1	43.1	41.8	50.1	1.11	1.56	0.77	1.56	152
Collapsible Armrest	55.8	53.4	43.3	55.8	1.49	1.83	1.12	1.83	146

The VC and rib deflections were higher at all levels in the simulation with the collapsible armrest. The stiffer armrest provided a means to slightly push the occupant away from the door early in the impact which reduced rib deflection. Figure 6.26 shows the models with the standard and crushable armrest at t = 0.04 s. This figure shows the lower and middle rib of the baseline case were not in contact with the door at this time due to the armrest forcing the abdomen away from the door. In the case with the collapsible armrest, the ribs were in contact with the inner panel of the door throughout the impact.

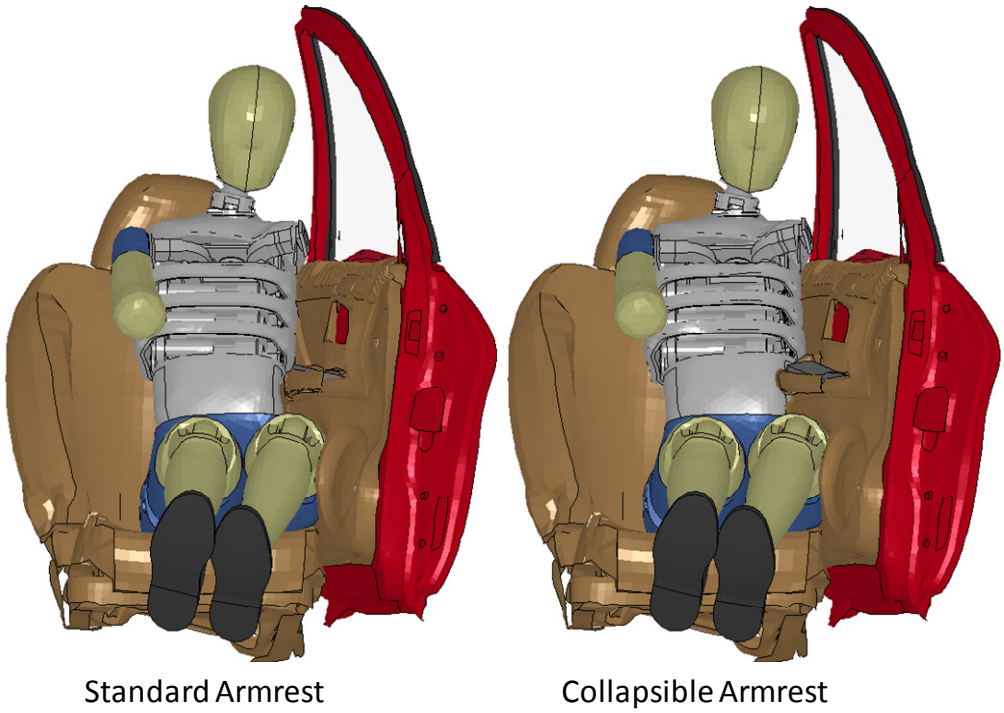

Figure 6.26: Effect of collapsible arm rest

6.9 Effect of Door Foam Material

The final portion of the material parametric study assessed the effect of the material of the foam inserts placed in the door discussed earlier and shown in Figure 4.22. The material model of these blocks was changed from the baseline, crushable foam material to an ABS plastic block of material (from the as-delivered material model and used throughout the rest of the model as the interior trim material model) and the foam used in the vehicle's seat. Additionally a model was run with no door foam.

6.9.1 Changes to Response due to Changes in Door Foam Material Properties

Table 6.8 shows the effect of the door foam material on the occupant. There was very little difference in the rib deflection response, and only a slight variation in the occupants predicted VC. The response of the ribs showed essentially no difference as seen in Figure 6.27.

Table 6.8: Injury criteria response for different door foams

	Rib Deflection [mm]				VC [m/s]				TTI [G]
	Upper	Middle	Lower	Max	Upper	Middle	Lower	Max	
Baseline	50.1	43.1	41.8	50.1	1.11	1.56	0.77	1.56	152
ABS Plastic Door Foam	50.1	42.9	43.1	50.1	1.11	1.41	0.80	1.41	169
Seat Door Foam	50.5	42.6	41.6	50.5	1.11	1.48	0.88	1.48	146
No Door Foam	51.7	44.1	41.1	51.7	1.07	1.53	0.80	1.53	147

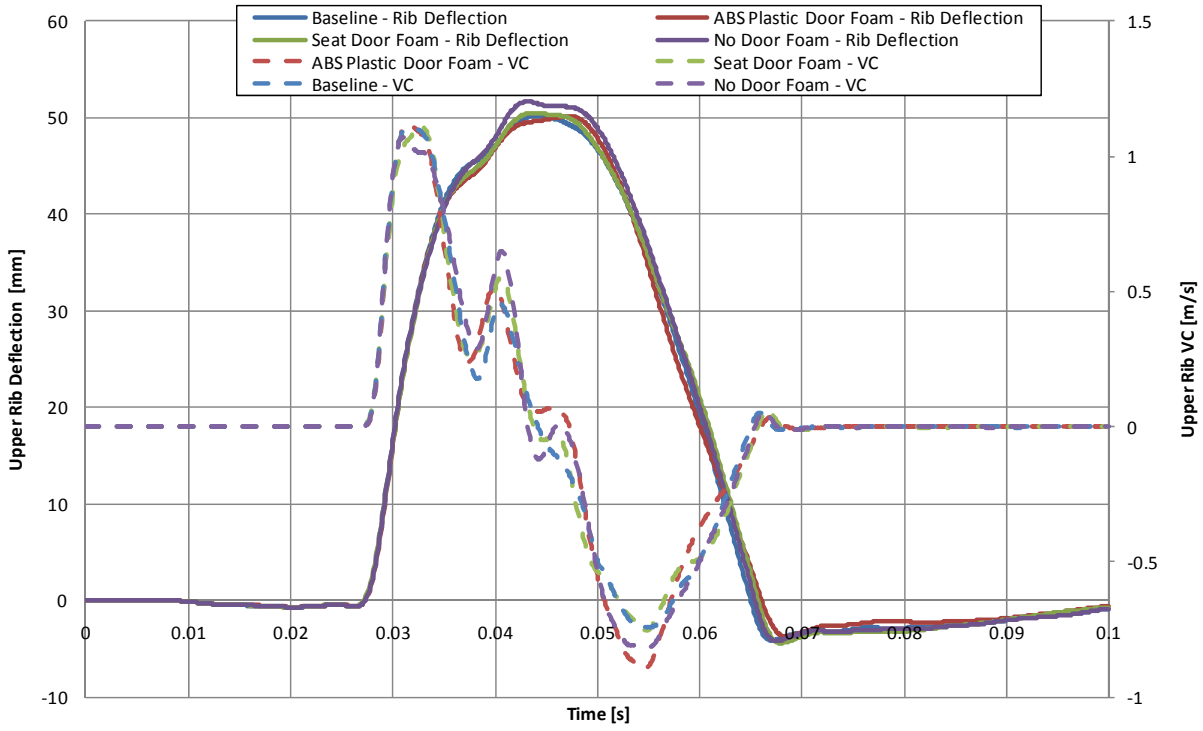

Figure 6.27: Rib deflection and VC response of ES-2re model with different door foam materials

6.10 Effect of Seatbelts

The final portion of this study involved examining the effect of seatbelt use in side impact. It has been shown that the use of seat belts in side impact does not have the same relation to survivability as frontal impact scenarios [Morris et al., 1997]. To study this in more detail, the seatbelt geometry was removed from the model with the ES-2re in the nominally central position.

6.10.1 Changes to Response due to Use of Seatbelts

The results of the simulations with and without seatbelt use are shown in Table 6.9. Somewhat surprisingly, the injury criteria responses are slightly higher for the model where the seatbelt was used.

Table 6.9: Injury criteria response for seatbelt use and no seatbelt use

	Rib Deflection [mm]				VC [m/s]				TTI [G]
	Upper	Middle	Lower	Max	Upper	Middle	Lower	Max	
Baseline	50.1	43.1	41.8	50.1	1.11	1.56	0.77	1.56	152
No Seatbelts	48.2	40.9	34.5	48.2	1.12	1.45	0.74	1.45	131

Figure 6.28 shows the model progression from the point of impact to the time when the occupant disengages from the intruding door. There is very little difference in the kinematic response between the two models. This provides further evidence that the standard three point belt does not significantly contribute to the response in a side impact to hold an occupant in the seat. If a system were developed to better contain the occupant in a side impact there may be a slight improvement in performance since currently the seat is moved away from the intruding door early in the impact, while the occupant remains essentially stationary. This concept was investigated by Melvin and Gideon [2004] who were studying race seats for oval track stock cars. Their solution was to create a composite material bolster system where the shoulder, head, pelvis and lower extremities were contained in a system that allowed less than half an inch (12.7 mm) of deflection in a nominally 40 G side impact while restraining the occupant in a six point harness.

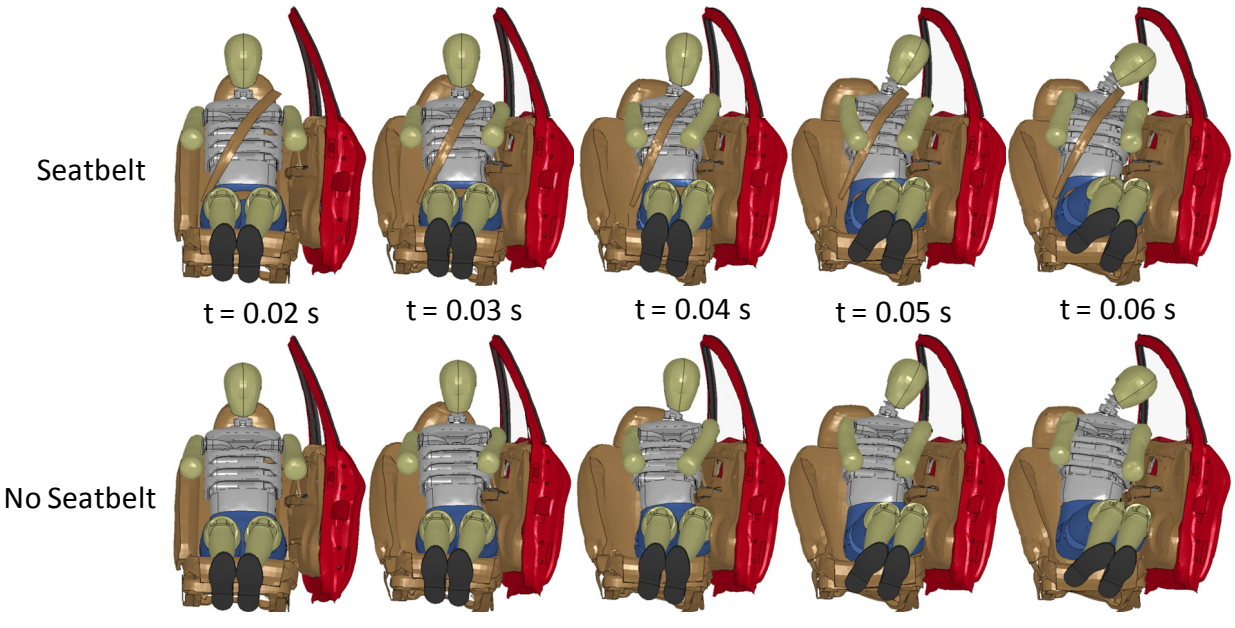

Figure 6.28: Effect of seatbelt use

Chapter 7 Discussion, Conclusions and Recommendations

7.1 Discussion and Conclusions

This study began by reviewing a series of recent side impact New Car Assessment Program (NCAP) crash tests performed by NHTSA. A series of average-velocity profiles and velocity profile corridors were created along with comparisons between vehicle parameters such as mass and occupant arm-to-door (AD) distance and TTI measured by the driver's seat occupant. None of these comparisons showed a strong correlation to thoracic injury, although certain expected trends emerged with initial arm to door distance, vehicle model year, and vehicle mass, showing negative correlations to thoracic injury; while peak lateral door velocity, door intrusion distance, and head and pelvis injury metrics were positively correlated with thoracic injury, as predicted by TTI. The effect of rotation of the vehicle during impact on the injury response of the occupant was also studied. It was found that contact time between the ATD and the door, as well as the time at which the occupant injury criteria was predicted to occur, were well before the vehicle had begun to rotate significantly, and thus rotation was not considered significant in the injury outcome of these side impacts. Due to the importance of the door velocity in controlling injury in side impact, the velocity of the door was also investigated in this study. The findings in this study are in agreement with previous research showing a 'double peak' in the door velocity response, with a peak velocity of roughly 35 kph 0.015 s after the barrier first impacted the vehicle. This velocity then dropped to roughly 20 kph at 0.03 s followed by the velocity profile leveling off at 25 kph at which point the vehicle began to rotate significantly.

A finite element model was developed by combining a full-scale 2000 Ford Taurus model, a NHTSA crash test barrier and side impact Anthropometric Test Devices (ATDs) (US Side Impact Dummy (USSID), the EuroSID-2 with rib extensions (ES-2re) and the WorldSID (WSID)). The occupant models were sunk into the vehicles driver's seat, and a three point harness was integrated. To validate the model, each ATD was simulated against its respective calibration tests and the barrier model was compared to tests performed using a rigid wall and rigid pole. Full scale crash tests were simulated with the vehicle model using initial barrier velocities of 54 khp (FMVSS 214 barrier speed) and 61 kph (Side NCAP barrier speed). The simulated vehicle component velocities (as determined from accelerometer data) were compared

to the corridors developed from the previous NHTSA database survey, and were found to fall within the corridors in most cases. The absence of a rear seat occupant did cause some simulated velocity responses outside of these corridors, particularly the rear door velocity. Following this validation, the vehicle component velocities, final vehicle deformation patterns, occupant component velocity, and occupant injury criteria were compared to testing in the NHTSA database of several Ford Taurus vehicles. The validation simulations were found to favorably compare to the test results.

With the vehicle model validation performed, a parametric study was carried out to assess the effect of the initial occupant position and the effect of the materials with which the occupant interacts during a side impact. The vehicle velocity response was investigated throughout this study and it was found that the door velocity, and to a lesser degree the B pillar velocity were altered based on the presence of an occupant and the initial lateral position of the occupant. The velocity of the door in models with an occupant were found to follow the velocity profile of the simulations with no occupant until the time the occupant model was engaged by the intruding door, at which time the door velocity began to decrease as the velocity of the occupant increased due to momentum transfer. The velocities eventually equalized until the occupant began to move away from the intruding door at roughly the same time the vehicle began gross translation and rotation, rather than local deformation. Other vehicle location velocities were essentially unchanged, and no other parametric changes to the model had a major effect on the vehicle's response. It was also found that in the absence of an occupant the trough of the 'double peak' in the door velocity response, which is often used to characterize the intruding door velocity, was not present. Furthermore, the lateral position of the occupant shifted the time of this trough without changing the magnitude. The first peak of the door velocity was not changed significantly with the absence of an occupant, or changes to the initial occupant position.

The occupant response was focused primarily on rib deflection, the viscous criterion, and, to a lesser extent, the TTI. It was found that there was a general trend in the reduction of injury to an occupant the further the initial position of the occupant was from the impacting door. The initial vertical position was important inasmuch as it dictated the position at which the armrest impacted the occupant. This vertical position was found to have a strong effect on the response of the ATD particularity if there was direct contact with between the lower rib and the arm rest.

This could be an important consideration for abdominal injury. A cursory analysis showed that there was an appreciable effect in this region when changes were made to the point of impact. It was found that when the occupant was moved reward in the vehicle such that the thorax was contacted by the B pillar, the predicted injury criteria tended to increase, though some interaction effects between the occupants arm, thorax and the vehicle B pillar were noted. The material portion of the parametric study showed that stiffer door trim material tended to reduce occupant injury by reducing the ease at which the door tended to consolidate. Additionally the use of a collapsible armrest was found to increase the injury criteria predicted by the occupant by not imparting a lateral velocity on the occupant early in the impact through the armrest. Very little difference was found when the foam door insert material was changed from crushable foam, to seat foam, a solid ABS plastic part, or removed entirely. A final study was carried out comparing the effect of seat belt use. The use or lack of use of seatbelts made very little difference to the injury criteria predicted by the occupant model. In fact, the injury criteria were predicted to be higher by the model using seatbelts rather than not. This highlights the finding that, in general, three point harnesses used in vehicles do not significantly couple the occupant to the vehicle for side impact loading conditions. Video analysis of several recent model side impact tests performed by NHTSA show that while the driver's seat begins to move laterally away from the impacted door early in an impact due to its connection to the vehicle floor structure, the inertia of the occupant forces it to remain in place. If the occupant was held in the seat during impact, there is potential to decrease the differential velocity between the occupant and the impacting door.

7.2 Recommendations

There are several areas where the current model could be improved. First, a number of material properties in the Taurus model could be improved to provide improved crash response. Specifically, the material model used for the windows of the vehicle could be improved to provide better failure response than the current strain based element erosion, which provided very little visible failure. Additionally, the interior plastic trim pieces and seat foam do not exhibit viscoelastic properties, and could be made to do so. The addition of spot weld failure may also improve the validation response of the model.

Further validation of the ATD models would allow for comment on the likelihood of injury to other body regions, such as the head, neck, abdomen and lower extremities. In the present models, the head velocity responses were significantly different from several test cases to which they were compared. The focus of this thesis was thoracic injury, and these differences were not investigated in detail. The difference in head response was not expected to affect the thoracic injury prediction. It would also be beneficial to expand the validation of these models beyond the standard calibration tests to include non-standard pendulum and side sled tests performed in the literature to better assess the ability of the occupant models to predict the injury response of their real world counterparts.

One area that this thesis did not address that has become increasingly important recently is the subject of side air bags. It may be beneficial to include these devices in the current model to assess their ability to reduce injury. The inclusion of these devices may not currently be feasible due to the relative lack of validation information and the potentially significant increase in computational cost associated with incorporating these devices. Additionally, the current vehicle model may not be conducive to the inclusion of these devices due to geometry considerations.

The next step in this work should be to include the detailed thoracic model used by Campbell [Campbell, 2008] and further developed by Yuen [Yuen, 2008]. This would provide a measure of occupant response to evaluate the thoracic model as well as possibly provide insight into what, if any, differences exist between the response of the ATD models and a more human-like occupant model.

Chapter 8 References

Adalian C, Nowakowski N, Zeitouni R (2009) 'Quantification of the Scattering Due to the Dummy Set-Up in Side Pole Impact' Proceedings of the 21st ESV Conference

Advanced Information Engineering Services (2005) 'New Car Assessment Program Side Impact Test, 2005 Suzuki Verona 4 Door Sedan', NHTSA Test #5285

Aekbote, K., Sobick, J., Zhao, L., Abramczyk, J., Maltarich, M., Stiyer, M., Bailey, T. (2007) 'A Dynamic Sled-to-Sled Test Methodology for Simulating Dummy Responses in Side Impact' SAE 2007-01-0710

Aekbote, K., Sundararajan, S., Chou, C., Lim, G., Prater, J., (1999) 'A New Component Test Methodology Concept for Side Impact Simulation' SAE 1999-01-0427

Allan-Stubbs, B. (1998) 'The Effect of Changes in Seating Position and Door Velocity Time History on Side Impact Dummy Response' SAE 980911

Baudrit, P., Hamon, J., Song,E., Robin, S., Le Coz, J. (1999) 'Comparative Studies of Dummy and Human Body Models Behavior in Frontal and Lateral Impact Conditions' 43rd Stapp Car Crash Conference Proceedings, SAE 99SC05

Bendjellal, F., Tarriere, C., Brun-Cassan, F., Foret-Bruno, J., Callibot, P, Gillet, D. (1988) 'Comparative Evaluation of the Biofidelity of EuroSID and SID Side Impact Dummies' SAE 881717

Bhalsod, D and Krebs, J. (2008) '214 Solid Barrier Documentation', Livermore Software Technology Corporation

Campbell, B.M. (2008) 'A Numerical Side Impact Model to Predict Thoracic Injury in Lateral Impact Scenarios', MASc Thesis, University of Waterloo, Waterloo, Ontario, Canada

Campbell, B, Cronin, D., Deng, Y.C. (2009) 'Coupled human body side impact model topredict thoracic injury' Proceedings of the 21st Internation Enhanced Safety of Vehicles Conference

Canada Gazette (2002) 'Regulations Amending the Motor Vehicles Safety Regulations (Fuel System Integrity)' Canada Gazette, December 14, 2002, Vol. 135, No 50, pp. 3768

Canadian Department of Justice (2009) ‘Motor Vehicle Safety Regulations’ Section 214 http://www.tc.gc.ca/eng/acts-regulations/regulations-crc-c1038-sch-iv-214.htm

Carhs (2009) *Safety Companion 2009 – Knowledge for tomorrow’s automotive engineer*, Chars Training GMBH, Alzenau, Germany

Cavanaugh, J.M. (1993) ‘Biomechanics of Thoracic Trauma’ in Accidental Injury - Biomechanics and Prevention, Nahum, A.M. and Melvin, J.W. Ed., Spinger-Verlag, New York

Cavanaugh, J.M. (2000) 'The Biomechanics of Thoracic Trauma', http://ttb.eng.wayne.edu/~cavanau/ucsdout.html

Cavanaugh, J.M., Walilko, T., Malhotra, A., Zhu, Y., King, A. (1990) 'Biomechanical Response and Injury Tolerance of the Thorax in Twelve Sled Side Impacts' SAE 902307

Chan, H., Hackney, J.R., Morgan, R.M., Smith, H.E. (1998) ‘An analysis of NCAP Side Impact Crash Data’ 16th International Technical Conference on the Enhanced Safety of Vehicles Proceedings, Paper 98-S11-O-12

Chawla, A., Mukherjee, S., Jangra, J. and Nakatani, T. (2007) 'Issues in ALE simulation of airbags', International Journal of Crashworthiness, Vol. 12:5, pp. 559 - 566

Chou, C.C., Aekbote, K., Le, J.J. (2007) ‘A review of side impact component test methodologies’ International Journal of Vehicle Safety, 2:1/2, 141-183

Chung, J., Cavanaugh, J.M., King, A.I., Koh, S.W., Deng, Y.C. (1999) 'Thoracic Injury Mechanisms and Biomechanical Responses in Lateral Velocity Pulse Impacts' 43rd Stapp Car Crash Conference Proceedings, SAE 99SC04

Chung, J., Cavanaugh, J., Mason, M., King, A. (1997) 'Development of a Sled-to-Sled Subsystem Side Impact Test Methodology' SAE 970569

Cichos, D., de Vogel, D., Otto, M., Zolsch, S. (2006) 'Crash Analysis Criteria Description' Ver. 2, Workgroup for Processing Measured Data in Vehicle Safety, 'http://www.ni.com/pdf/products/us/crash_functions_descriptions.pdf'

Deng, Y.C. (1988) 'Design Considerations for Occupant Protection in Side Impact - A Modeling Approach' SAE 881713

Deng, Y.C. and Ng, P. (1993) 'Simulation of Vehicle Structure and Occupant Response in Side Impact' SAE 933125

ECE (1995) ‘Agreement Concerning the Adoption of Uniform Conditions of Approval and Reciprocal Recognition of Approval for Motor Vehicle Equipment and Parts – Addendum 95: Regulation N0. 95’ Economic Commission for Europe

EEVC (2006) 'Technical Note on the EuroSID-2 with Rib Extensions (ES-2re)' www.eevc.org

Eiband, A.M. (1959) ‘Human Tolerance to Rapidly Applied Accelerations’ NASA Memo No. 5-19-59E

Eppinger, R.H. (1989) 'On the development of a deformation measurement system and its application toward developing mechanically based injury indices', 33rd Stapp Car Crash Conference, SAE 892426

Eppinger, R.H., Marcus, J., Morgan, R. (1984) 'Development of Dummy and Injury Index for NHTSA's Thoracic Side Impact Protection Research Program', SAE 840885

EuroNCAP (2009a) 'Assessment Protocol - Overall Rating' Version 5.0, May 2009, http://www.euroncap.com/files/Euro-NCAP-Assessment-Protocol---Overall-Rating---v5.0---0-c19221a7-e500-447b-8691-3fb3b400671f.pdf

EuroNCAP (2009b) 'Side Impact Testing Protcol' Version 5.0, Octorber 2009, http://www.euroncap.com/files/Euro-NCAP-Side-Protocol-Version-5.0---0-9085b76b-b02c-4308-9bfd-e410f0706e55.pdf

Fang, H., Solanki, K. and Horstemeyer, M. F. (2005) 'Numerical simulations of multiple vehicle crashes and multidisciplinary crashworthiness optimization', International Journal of Crashworthiness, 10:2, 161 - 172

Franz, U. and Graf, O. (2004) 'Accurate and Detailed LS-DYNA FE Models of the US- and EUROSID: A Review of the German FAT Project', 6th International LS-DYNA Users Conference Proceedings

Franz, U., Schmid, W., Schuster, P. (2002) 'Observations During Validation of Side Impact Dummy Models - Consequences for the Development of the FAT ES2 Model', Nordic LS-DYNA Users' Conference 2002

Franz, U., Stahlscmidt, S., Schelkle, E., Frank, T. (2008) "15 Years of Finite Element Dummy Model Development within the German Association for Research on Automotive Technology (FAT)", JRI Japanese LS-Dyna Conference, Nagoya, Japan

FTSS (2005) 'ES-2re Side Impact Crash Test Dummy Product Catalog Revision B', First Technology Safety Systems, http://www.ftss.com/sites/default/files/PC-ES2re.pdf

FTSS (2007) 'WorldSID 50th Percentile Dummy Product Catalog Revision A', First Technology Safety Systems, http://www.ftss.com/sites/default/files/PC-WorldSID-50th.pdf

FTSS (2010) 'US DOT SID Side Impact Dummy', First Technology Safety Systems, http://www.ftss.com/crash-test-dummies/side-impact/us-dot-sid

Gai, E. and Zhang, H. (2005) 'Finite point method: a new approach to model the inflation of side curtain airbags', International Journal of Crashworthiness, Vol. 10:5, pp. 445 - 450

Geddes, L.A. and Roeder, R.A. (2005) 'Evolution of our knowledge of sudden death due to commotio cordis' American Journal of Emergency Medicine, Vol. 23, pp 67-75

Gennarelli, T.A. and Wodzin, E. (2005) *Abbreviated Injury Scale, Association for the Advancement of Automotive Medicine*, Barrington, Illinois

Gennarelli, T.A. and Wodzin, A. (2006) 'AIS 2005: A contemporary injury scale', Injury, Int. J. Care Injured, 37, 1083-1091

Gray, H., (1918) *Anatomy of the Human Body*, Lea & Febiger, Philadelphia; Bartleby.com, 2000

Hardy, W.N., Shah, C.S., Mason, M.J., Kopacz, J.M., Yang, K.H., King, A.I., Van Ee, C.A., Bishop, J.L., Banglmaier, R.F., Bey, M.J., Morgan, R.M., Digges, K.H. (2008) 'Mechanisms of

Traumatic Rupture of the Aorta and Associated Peri-isthmic Motion and Deformation' Stapp Car Crash Journal, 52: 233-265, SAE 2008-22-0010

Harle, N., Brown, J. and Rashidy, M. (1999) 'A feasibility study for an optimizing algorithm to guide car structure design under side impact loading', International Journal of Crashworthiness, Vol. 4:1, pp. 71-92

Hayashi, S., Yasuki, T., Kitagawa, Y. (2008) 'Occupant Kinematics and Estimated Effectiveness of Side Airbags in Pole Side Impacts Using a Human FE Model with Internal Organs' Stapp Car Crash Journal, Vol. 52, pp. 363-377, SAE 2008-22-0015

Hobbs, C. (1995) 'Dispelling the Misconceptions about Side Impact Protection' SAE 950879

Hobbs, C.A. and McDonough, P.J (1998) 'Development of the European New Car Assessment Programme (EURO NCAP)' 16th International Technical Conference on the Enhanced Safety of Vehicles Proceedings, SAE 98-S11-O-06

Huang, Y., King, A.I., Cavanaugh, J.M., (1994), 'A MADYMO Model of Near-Side Human Occupants in Side Impacts' Journal of Biomechanical Engineering, 116, 228-235

Hultman, R.W., Laske, T.G., Chou, C.C., Lim, G.G., Chrobak, E.I., Vecchio, M.T. (1991) 'NHTSA Passenger Car Side Impact Dynamic Test Proceedure - Test-to-Test Variability Estimates' SAE 910603

IIHS (2010) 'IIHS vehicle ratings' http://www.iihs.org/ratings/default.aspx

ISO (International Organization for Standardization) (1999) 'Lateral impact response requirements to assess the biofidelity of the dummy', ISO 9790

Kahane, C.J. (2007) 'An Evaluation of Side Impact Protection - FMVSS 214 TTI(d) Improvements and Side Air Bags', DOT HS 810 748

Kallieris, D., Mattern, R., Schmidt, G., Eppinger, R. (1981) 'Quantification of Side Impact Responses and Injuries' SAE 811990

Kan, C.D., Marzougui, and Bahouth, G. (2001) 'Integrated Crashworthiness Evaluation Using Vehicle and Occupant Finite Element Models' International Journal of Crashworthiness, Vol. 6:3, pp 387-398

Kent, R.W. and Crandall, J.R. (2000) 'Structural Stiffness, Elastic Recovery, and Occupant Inertial Effects on Measured Door Response in a Laterally Struck Vehicle', International Journal of Crashworthiness, 5:3, 235 – 248

Kent, R., Crandall, J., Butcher, J., Russell M. (2001) 'Sled System Requirements for the Analysis of Side Impact Thoracic Injury Criteria and Occupant Protection' SAE 2001 World Congress, SAE 2001-01-0721

King, A.I. (2000) 'Fundamentals of Impact Biomechanics: Part I - Biomechanics of the Head, Neck, and Thorax', Annual Review of Biomedical Engineering, Vol. 2, pp. 55 – 81

Kroell, C.K., Allen, S.D., Warner, C.Y., Perl, T.R. (1986) 'Interrelationship of Velocity and Chest Compression in Blunt Thoracic Impact to Swine II' SAE 861881

Kroell, C.K., Pope, M.E., Viano, D.C, Warner, C.Y., Allen, S.D. (1981) 'Interrelationship of Velocity and Chest Compression in Blunt Thoracic Impact to Swine' SAE 811016

Kroell, C., Schneider, D., Nahum, A. (1971) 'Impact Tolerance and Response of the Human Thorax' SAE 710851

Kroell, C., Schneider, D., Nahum, A. (1974) 'Impact Tolerance and Response of the Human Thorax II' SAE 741187

Kuppa, S. (2006) 'Injury Criteria for Side Impact Dummies' National Highway Traffic Safety Administration

Kuppa, S., Eppinger, R.H., McKoy, F., Nguyen, T., Pintar, F.A., Yoganandan, N. (2003)' Development of Side Impact Thoracic Injury Criteria and Their Application to the Modified ES-2 with Rib Extensions (ES-2re)' Stapp Car Crash Journal Vol. 47, SAE 2003-22-0010

Lau, I.V., Capp, J.P., Obermeyer, J.A. (1991) 'A Comparison of Frontal and Side Impact: Crash Dynamics, Countermeasures and Subsystem Tests' SAE 912896

Lau, I.V. and Viano, D.C. (1981) ‘Influence of impact velocity and chest compression on experimental pulmonary injury severity in an animal model’ Journal of Trauma, Vol. 21, pp. 1022-1028

Lau, I.V. and Viano, D.C. (1986) 'The Viscous Criterion - Bases and Applications of an Injury Severity Index for Soft Tissues' SAE 861882

Livermore Software Technology Corporation (LSTC) (2007) ‘LS-Dyna Keyword Users Manual’

Liu, Y., Zhu, F., Wang, Z., van Ratingen, M. (2007) 'Side impact injury prediction with FE simulations of the new advanced world SID FE dummy models' Proceedings of the 20th International Enhanced Safety of Vehicles Conference

Malkusson, R. and Karlsson, P. (1998) 'Simulation Method for Establishing and Satisfying Side Impact Design Requirements' International Body Engineering Conference & Exposition, SAE 982358

Marcus J.H., Morgan, R.M., Eppinger, R.H., Kallieris, D., Mattern, R., Schmidt, G. (1983) 'Human response to injury from lateral impact' 27th Stapp Crash Conference, SAE 831634

MatWeb (2010) ‘Overview of materials for Acrylonitrile Butadiene Styrene (ABS), Molded’ http://www.matweb.com/search/DataSheet.aspx?MatGUID=eb7a78f5948d481c9493a67f0d089646

McGwin, G., Metzger, J., Porterfield, J.R., Moran, S.G., Rue, L.W. (2003) ‘Association between side airbags and risk of injury in motor vehicle collisions with near-side impact’ Journal of Trauma, 55:430-436

Melvin, J.W. and Gideon, T. (2004) 'Biomechanical Principles of Racecar Seat Design for Side Impact Protection' SAE 2004-01-3515

Miller, P.A. and Gu, H. (1997) 'Sled Testing Procedure for Side Impact Airbag Development' SAE International Congress and Exposition, SAE 970570

Miller, P.M., Nowak, T., Macklem, W. (2002) ' A Compact Sled System for Linear Impact, Pole Impact and Side Impact Testing' 2002 SAE World Congress, SAE 2002-01-0695

Morgan, R.M., Marcus, J.H., Eppinger, R.H. (1981) 'Correlation of Side Impact Dummy/Cadaver Tests' SAE 811008

Morgan, R.M., Marcus, J.H., Eppinger, R.H. (1986) 'Side Impact - The Biofidelity of NHTSA's Proposed ATD and Efficacy of TTI', SAE 861877

Morris, R.A., Crandall, J.R., Pilkey, W.D. (1999) 'Multibody modelling of a side impact test apparatus', International Journal of Crashworthiness,4:1, 17-30

Morris, A.P., Hassan, A.M., Mackay, M. (1997) 'Chest Injuries in Real-World Side Impact Crashes - An Overview' Proceedings of the 1997 IRCOBI Conference

Moss, S., Wang, Z., Salloum, M., Reed, M., van Ratingen, M., Cesari, D., Scherer, R., Uchimura, T., Beusenberg, M. (2000) 'Anthropometry for WorldSID A World-Harmonized Midsize Male Side Impact Crash Dummy' SAE 2000-01-2202

Mertz, H. (1984) 'A Procedure for Normalizing Impact Response Data' SAE 840884

Nader, R. (1972) *Updated - Unsafe at Any Speed: The designed-in dangers of the American automobile*, Grossman Publishers, New York

NHTSA (1997) 'Laboratory Test Procedure for New Car Assessment Testing Side Impact Testing', Docket No. NHTSA-1998-3835, Document 0001

NHTSA (2004) 'Federal Motor Vehicle Safety Standards; Side Impact Protection; Side Impact Phase-In Reporting Requirements; Proposed Rule', Federal Register, Part IV, Department of Transportation 49 CFR Parts 571 and 598, Docket No. NHTSA-2004-17694.

NHTSA (2006) 'Laboratory Test Procedure for FMVSS No. 214 'Dynamic' Side Impact Protection, Document Number TP214D-08 Part 1', Washington.

NHTSA (2008a) 'Revision to the New Car Assessment Program', Docket No. NHTSA-2006-26555, Document 0116

NHTSA (2008b) 'Revision to the New Car Assessment Program', Docket No. NHTSA-2006-26555, Document 0115

NHTSA (2008c) ‘Revision to the New Car Assessment Program’, Docket No. NHTSA-2006-26555, Document 0114

NHTSA (2009) ‘Traffic Safety Facts 2006 (Early Edition)’, DOT HS 811 170

NHTSA (2010a), Fatality Analysis Reporting System, http://www-fars.nhtsa.dot.gov/Main/index.aspx

NHTSA (2010b) ‘Signal Analysis Software for Windows’ http://www.nhtsa.gov/Research/Databases+and+Software/Signal+Analysis+Software+for+Windows, Accessed April 29, 2010

NHTSA Biomechanics Test Database (2009) http://www-nrd.nhtsa.dot.gov/database/nrd-51/bio_db.html

NHTSA Vehicle Crash Test Database (2009) http://www-nrd.nhtsa.dot.gov/database/nrd-11/veh_db.html

Neathery, R.R., Kroell, C.K., Mertz, H.J. (1975) 'Prediction of Thoracic Injury from Dummy Responses' Proceedings of the 1975 Stapp Car Crash Conference, SAE 751151

Opiela, K.S (2008) 'Finite element model of Ford Taurus' FHWA / NHTSA Finite Element Model Archive, http://www.ncac.gwu.edu/vml/archive/ncac/vehicle/taurus-v3.pdf

Patrick, L.M., Mertz, H.J., Kroell, C.K. (1967) 'Cadaver Knee, Chest and Head Impact Loads' Proceedings of the 1967 Stapp Car Crash Conference, SAE 670913

Patrick, L.M. and Sato, T.B. (1970) ‘Methods of Establishing Human Tolerance Levels: Cadaver and Animal Research and Clinical Observations’ in Impact Injury and Crash Protection, Gurdjian, E.S., Lange, W.A., Partick, L.M., Thomas, L.M. Ed., Charles C Thomas Publisher, Springfield

Payne, A.R., Mohacsi, R., Allan-Stubbs, B. (1997) ‘The Effects of Variability in Vehicle Structure and Occupant Position on Side Impact Dummy Response Using the MIRA M-SIS Side Impact Technique’, SAE International Congress and Exhibition 1997, SAE 970571

Peters, R.M. (1985) ‘Biomechanics of Chest Trauma’ in *The Biomechanics of Trauma*, Nahum, A.M. and Melvin, J.W. Ed., Appleton-Century-Crofts, Norwalk

Pike, J.A. (1990), *Automotive Safety*, Society of Automotive Engineers, Warrendale

Pintar, F.A., Yoganandan, N., Hines, M.H., Maltese, M.R., McFadden, J., Saul, R., Eppinger, R., Khaewpong, N., Kleinberger, M. (1997) 'Chest band Analysis of Human Tolerance to Side Impact' Proc. 41st Stapp Car Crash Conference, pp. 63-74, SAE 973320

Pintar, F.A., Yoganandan, N., Sances, A., Eppinger, R.H. (1996) 'Instrumentation of Human Surrogates for Side Impact' SAE 962412

Pyttel, T., Floss, A., Thibaud, C. and Goertz, C. (2007) 'Realistic simulation models for airbags and humans-new possibilities and limits of FE simulation', International Journal of Crashworthiness, Vol. 12:5, pp. 481 - 492

Rhule, H.H., Maltese, M.R., Donnelly, B.R., Eppinger, R.H., Brunner, J.K., Bolte, J.H. (2002) 'Development of a New Biofidelity Ranking System for Anthropomorphic Test Devices' Stapp Car Crash Conference Journal, Vol. 46, pp. 477-512, SAE 2002-22-0024

Riches, E. (2002) 'Top 10 Best Selling Vehicles in 2001' edunds.com, Retrieved Feb. 25, 2010 from http://www.edmunds.com/reviews/list/top10/49547/article.html

Richens, D., Kotidis, K., Neale, M., Oakley, C., Fails, A. (2003) 'Rupture of the aorta following road traffic accidents in the United Kingdom, 1992–1999. The results of the Cooperative Crash Injury Study' Eur J Cardiothoracic Surg, 23:143–8

Roberts, V.L., and Beckman, D.L. (1970) 'Mechanisms of Chest Injury' in Impact Injury and Crash Protection, Gurdjian, E.S., Lange, W.A., Partick, L.M., Thomas, L.M. Ed., Charles C Thomas Publisher, Springfield

Romanes, G.J. (1981) *Cunningham's Textbook of Anatomy*, Twelfth Ed., Oxford University Press, Oxford.

Saari, B., Ellis, R., Burguillo, S. (2004) 'New Methods of Side Impact Simulation for Better Waveform Reproduction and Door Interaction' Proceeding of the 2004 SAE World Congress, SAE 2004-01-0474

Safercar.gov (2009) 'NCAP FAQs' http://www.safercar.gov

Samaha, R.R., Maltese, M.R., Bolte, J. (2001) 'Evaluation of the ES2 Dummy in Representative Side Impacts' Proceedings of the 17th ESV Conference

Samaha, R.R., Molino, L., Maltese, M. (1998) 'Comparative performance testing of passenger cars relative to FMVSS 214 and the EU 96-ED-27 impact regulations Phase I' Proceedings of the 16th International Enhanced Safety of Vehicles Conference

Scherer, R., Bortenshlager, K., Akiyama, A., Tylko, S., Hartlieb, M., Harigae, T. (2009) 'WorldSID production dummy biomechanical response' Preceedings of ESV 2009

Scherer, R., Cesari, D., Uchimura, T., Kostyniuk, G., Page, M., Asakawa, K., Hautmann, E., Bortenschlager, K., Sakurai, M., Harigae, T. (2001) 'Design and evaluation of the WorldSID Prototype dummy' Proceedings of the 17th International Enhanced Safety of Vehicles Conference

Schönpflug, M., von Merten, K., Meister, M. and Wernicke, P. (2004) 'Numerical Simulation of Human Kinematics and Injuries in Side Crash Scenarios' Digital Human Modeling for Design and Engineering Symposium, SAE 2004-01-2161

Schuster, P., Franz, U., Stahlschmidt, S., Pleshberger, M., Eichberger, A. (2004), 'Comparison of ES-2re with ES-2 and USSID Dummy - Consideration for ES-2re model in FMVSS Tests' LS-DYNA Forum 2004 Proceedings

Shah, C.S. (2007) 'Investigation of traumatic rupture of the aorta (TRA) by obtaining aorta material and failure properties and simulating real-world aortic injury crashes using the whole-body finite element (FE) human model' Ph.D. Dissertation, Wayne State University

Shah, C.S., Maddali, M., Mungikar, S.A., Beillas, P., Hardy, W.H., Yang, K.H., Bedewi, P.G., Digges, K., Augenstein, J. (2005) 'Analysis of a Real-World Crash Using Finite Element Modeling to Examine Traumatic Rupture of the Aorta' SAE 2005-01-1293

Society of Automotive Engineers (SAE) (1995) 'SAE J383 - Motor Vehicle Seat Belt Anchorages--Design Recommendations'

Society of Automotive Engineers (SAE) (2003) 'SAE J211-1 - Instrumentation for Impact - Test Part 1 - Electronic Instrumentation'

Stapp, J. (1957) 'Human Tolerance to Deceleration' American Journal of Surgery, Vol 93, pp. 734-740

Statistics Canada (2007) 'Canadian Motor Vehicle Traffic Collision Statistics 2006' Catalogue no. T45-3/2006

Stein, D.J. (1997) 'Apparatus and Method for Side Impact Testing' 1997 International Congress and Expo, SAE 970572

Sundararajan, S., Chou, C., Lim, G., Prater, J., Clements, R. (1995) 'Dynamic Door Component Test Methodology' SAE 950877

Tencer, A.F., Kaufman, R., Mack, C., and Mock, C. (2005) 'Factors affecting pelvic and thoracic forces in near-side impact crashes: a study of US-NCAP, NASS, and CIREN data', Accident Analysis and Prevention, Vol 37, pp 287-293

Teng, T.L., Chang, K.C. and Wu, C.H. (2007) 'Development and validation of side-impact crash and sled testing finite-element models', Vehicle System Dynamics, 45:10,925 – 937

Thomas, P. and Frampton, R. (1999) 'Injury Patterns in Side Collisions - A New Look with Reference to Current Test Methods and Injury Criteria' 43rd Stapp Car Crash Conference Proceedings, 350, SAE 99SC01

Tortora, G.J. (1999) *Principles of Human Anatomy 8th Ed*., Wiley and Sons, New York

Transport Canada (1996) 'Test Method 214 Side Door Strength' Canadian Motor Vehicle Safety Standards, Schedule IV, Section 214, http://www.tc.gc.ca/roadsafety/safevehicles/mvstm_tsd/tm/pdf/2140_e.pdf

Trinkle, J.K, and Richardson, J.D. (1981) 'Thoracic Injuries' in Trauma, Carter, D.C., and Polk, H.C. Ed., Butterworths International Medical Reviews, London

United Nations Economic Commission for Europe, (1995) 'Regulation No. 95 - Uniform provisions concerning the approval of vehicles with regard to the protection of the occupants in the event of a lateral collision' Retrieved May 6, 2009 from http://www.unece.org/trans/main/wp29/wp29regs81-100.html

United States Code (2008) 'Title 49 : Transportation, Part 572 - Anthropometric Test Devices', United States Code of Federal Regulations, Retrieved May 6, 2009 from http://www.access.gpo.gov/nara/cfr/waisidx_08/ 49cfr572_08.html

van Ratingen, M. (2001) 'Development and evaluation of the ES-2 side impact dummy' Proceedings of the 17th International Enhanced Safety of Vehicles Conference

Vemulakonda, G., Tang, B., Jayachandran, R., Wan,D., Thakurta,S., Chang, J.M., Tyan, T., Cheng, J., Doong, J., Shaner, L., Bhalsod, D. (2007) 'Approaches to Modeling the Dynamic Interaction for an Automotive Seat and Occupant System' 2007 SAE World Congress, SAE 2007-01-0988

Versace, J. (1971) 'A review of the severity index', Proceedings of the 15th Stapp Conference, SAE 710881

Viano, D. C. (1983) 'Biomechanics of non-penetrating Aortic Trauma: A review' Stapp Car Crash Journal, 27:109-114

Viano, D.C. (1987) 'Evaluation of the SID Dummy and TTI Injury Criterion for Side Impact Testing' SAE 872208

Viano, D.C. (1989) 'Biomechanical Responses and Injuries in Blunt Lateral Impact' SAE 892432

Viano, D.C. and Lau, I.V. (1985) 'Thoracic Impact: A Viscous Tolerance Criterion' Proceedings of the 10th Experimental Safety of Vehicles Conference

Viano, D.C., Lau, I.V., Andrezejak, D.V., Asbury, C. (1989b) 'Biomechanics of Injury in Lateral Impacts' Accident Analysis and Prevention, 21:6, 535-551

Viano, D.C., Lau, I.V., Asbury, C., King, A.I., Begeman, P. (1989a) 'Biomechanics of the Human Chest, Abdomen, and Pelvis in Lateral Impact' Accident Analysis and Prevention, 21:6, 553-574

Watson, B, Cronin, D., Campbell, B. (2009) 'Study of vehicle dynamics and occupant response in side impact crash tests' Proceedings of the 21st International Enhanced Safety of Vehicles Conference

Williamson, P. (2005) 'Aspects of Simulation of Automobile Seating Using LS-Dyna 3D' http://www.dynamore.de/download/af05/papers/G-II-53.pdf

World Health Organization (2004) *World report on road traffic injury prevention - Main messages*

WorldSID TG (2005) 'User's manual for the WorldSID 50th Percentile male side impact dummy' Retrieved May 6, 2009 from http://www.worldsid.org/TechDocumentation.htm

Yoganandan, N., Pintar, F.A., Gennarelli, T.A., Martin, P.G., Ridella, S.A. (2008) 'Chest Deflections and Injuries in Oblique Lateral Impacts', Traffic Injury Prevention, Vol. 9-2, pp. 162-167

Yuen, K., Cronin, D., Deng, Y. (2008) 'Lung Response and Injury in Side Impact Conditions' Proceeding of IRCOBI Conference 2008

Zaouk, A. K., Marzougui, D. and Bedewi, N. E. (2000a) 'Development of a Detailed Vehicle Finite Element Model Part I: Methodology', International Journal of Crashworthiness, 5:1,25 – 36

Zaouk, A. K., Marzougui, D. and Kan, C.D. (2000b) 'Development of a Detailed Vehicle Finite Element Model Part II: Material Characterization and Component Testing', International Journal of Crashworthiness, 5:1, 37 - 50

Appendix A – NHTSA Database Survey of Side NCAP Test Results

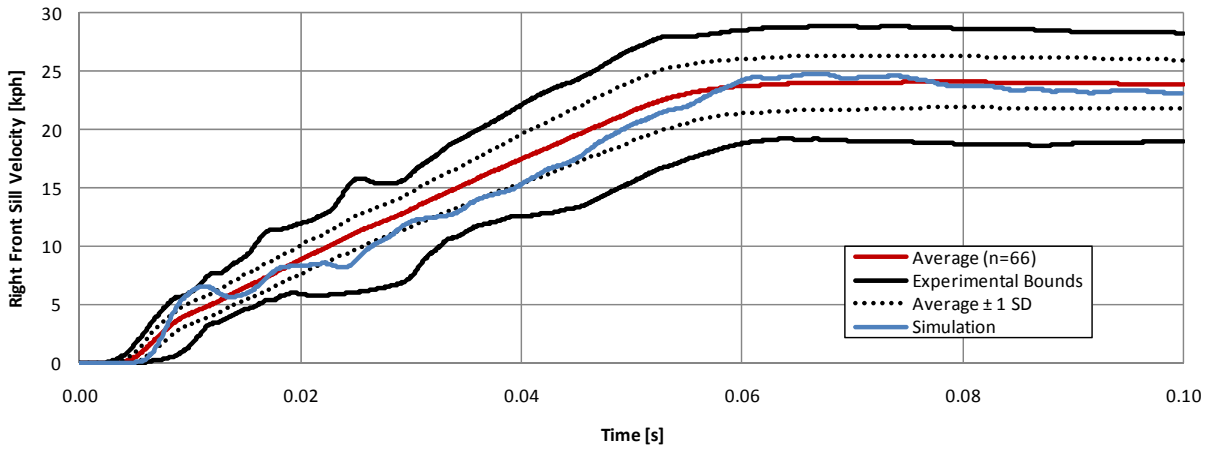

Figure A.1: NHSTA database survey – Right Front Sill Velocity

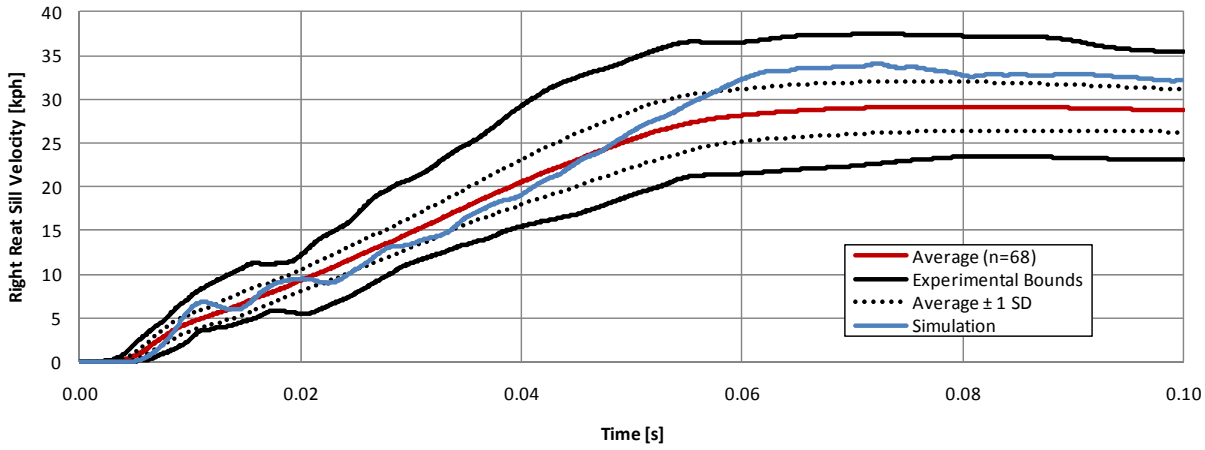

Figure A.2: NHSTA database survey – Right Rear Sill Velocity

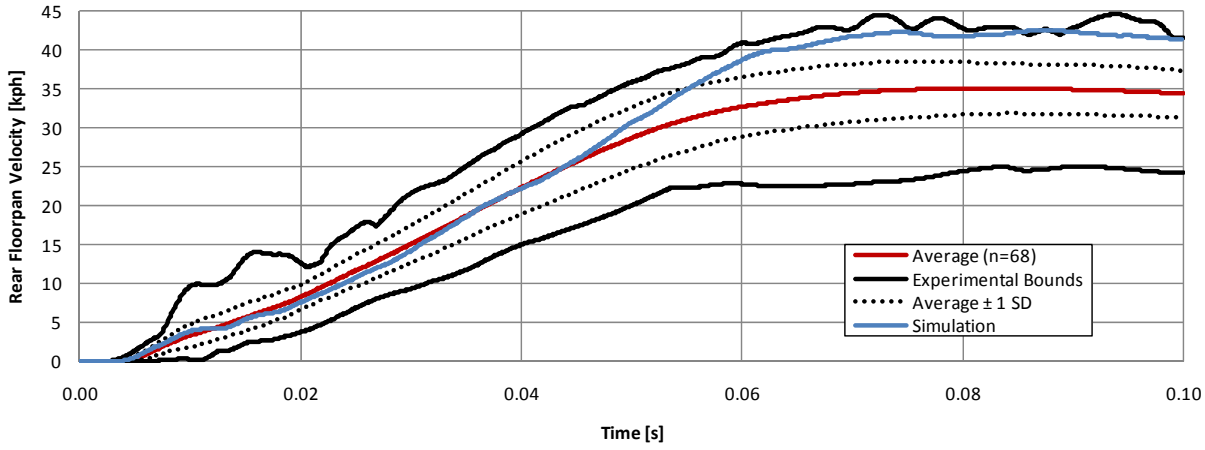

Figure A.3: NHSTA database survey – Rear Floorpan Velocity

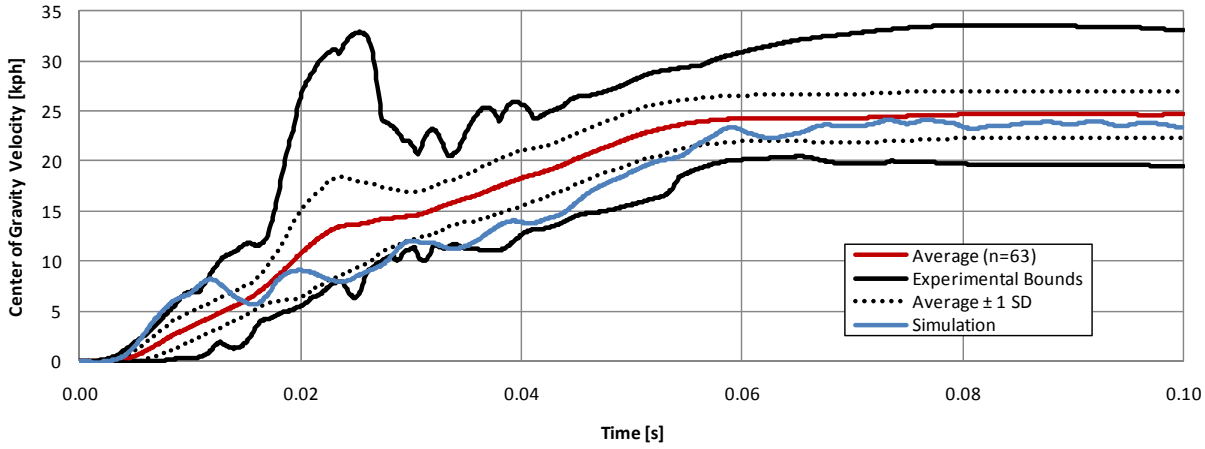

Figure A.4: NHSTA database survey – Center of Gravity Velocity

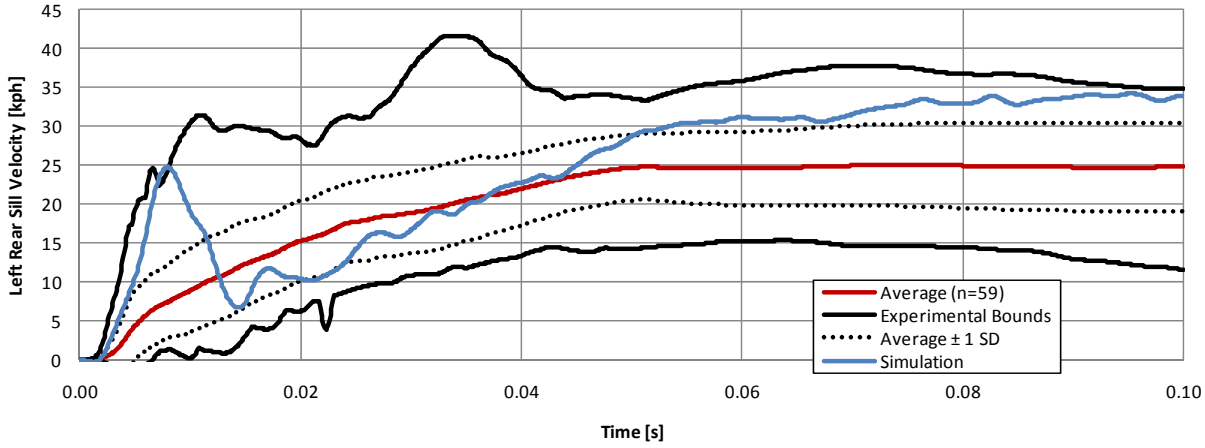

Figure A.5: NHSTA database survey – Left Rear Sill Velocity

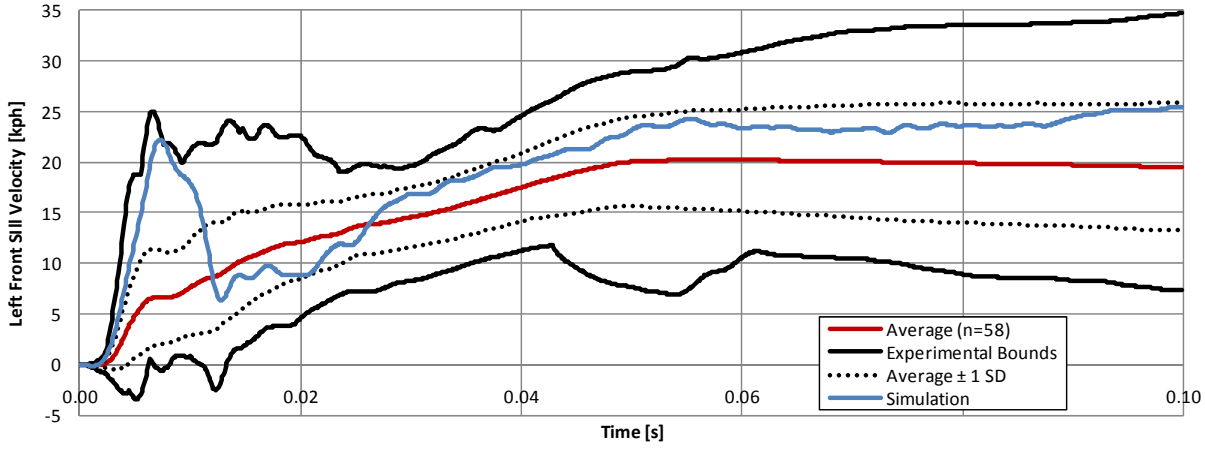

Figure A.6: NHSTA database survey – Left Front Sill Velocity

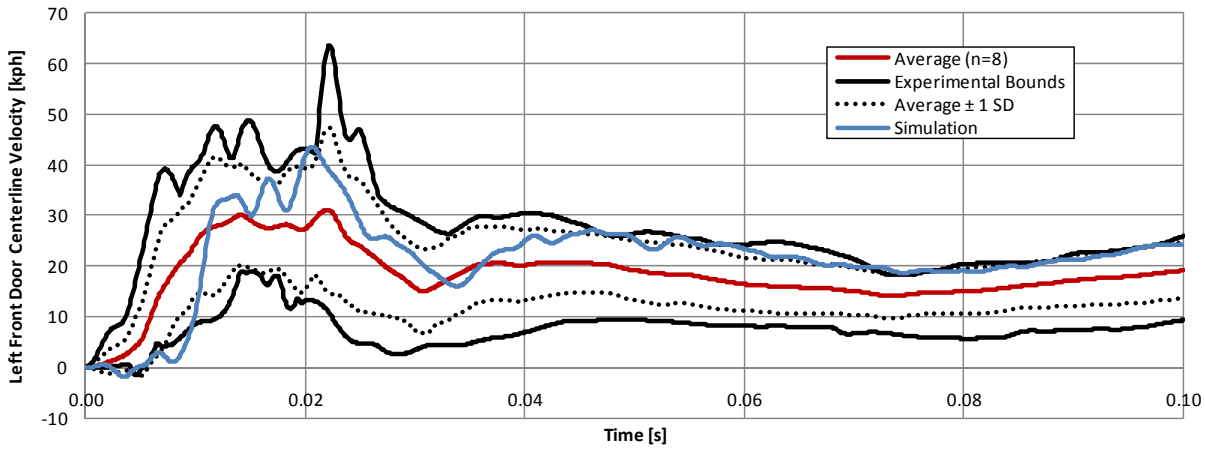

Figure A.7: NHSTA database survey – Left Front Door Upper Centerline Velocity

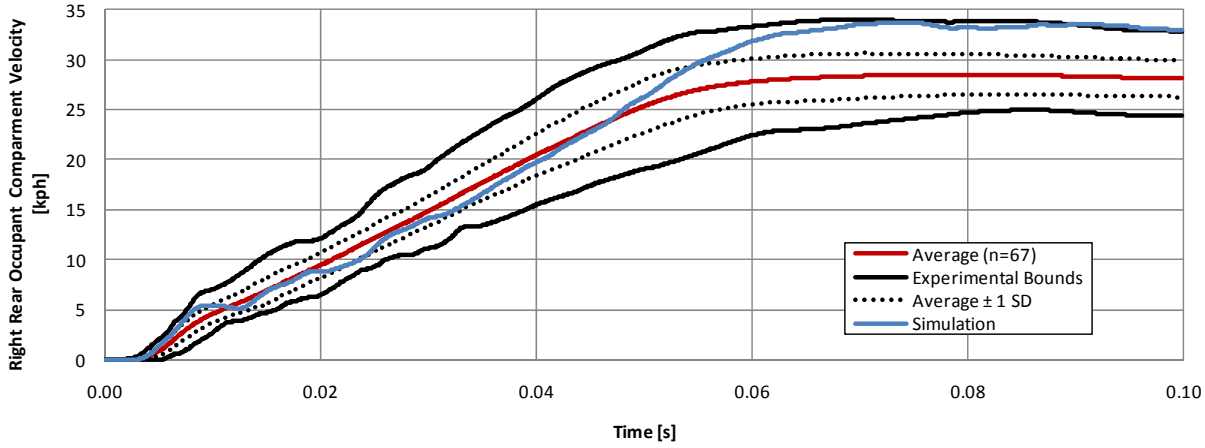

Figure A.8: NHSTA database survey – Right Rear Occupant Compartment Velocity

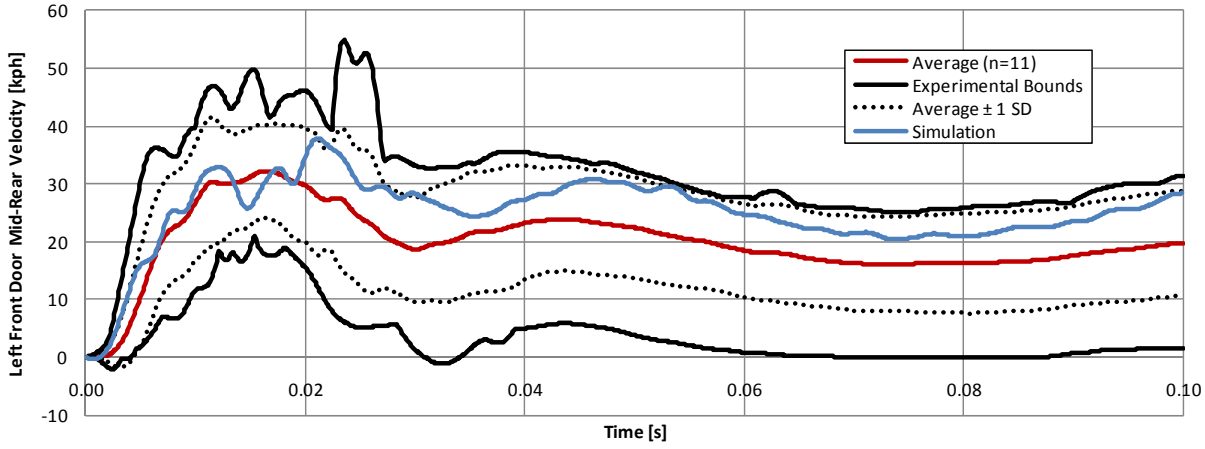

Figure A.9: NHSTA database survey – Left Front Door Mid-rear Velocity

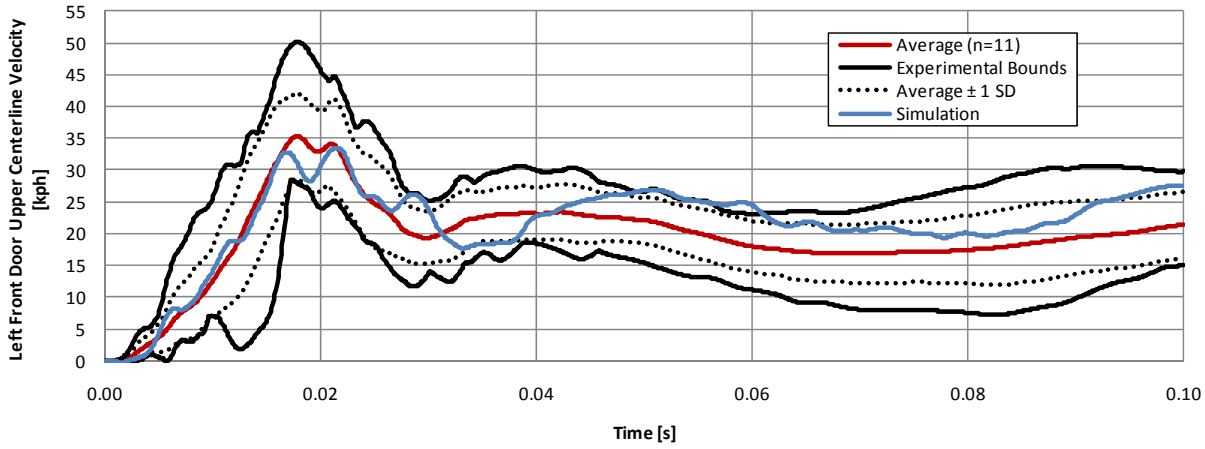

Figure A.10: NHSTA database survey – Left Front Door Upper Centerline Velocity

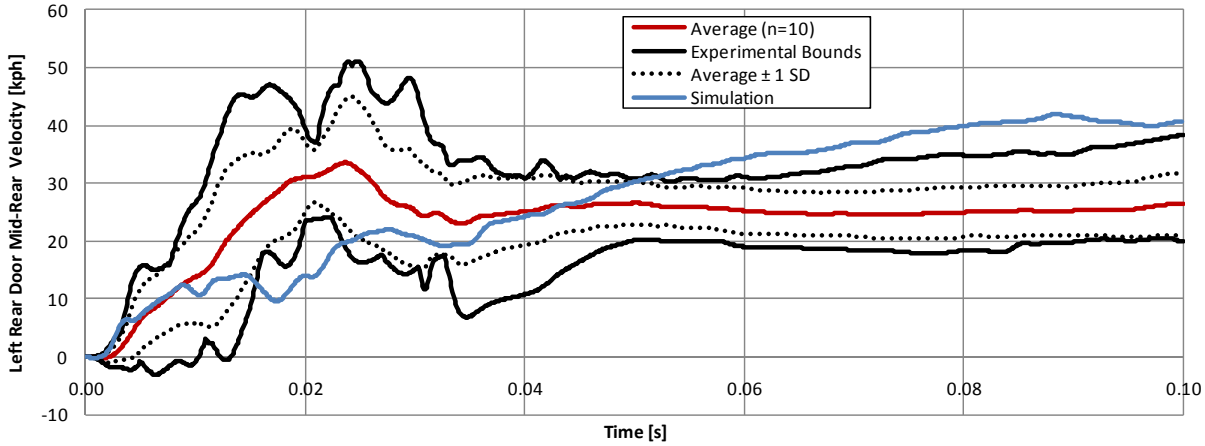

Figure A.11: NHSTA database survey – Left Rear Door Mid-rear Velocity

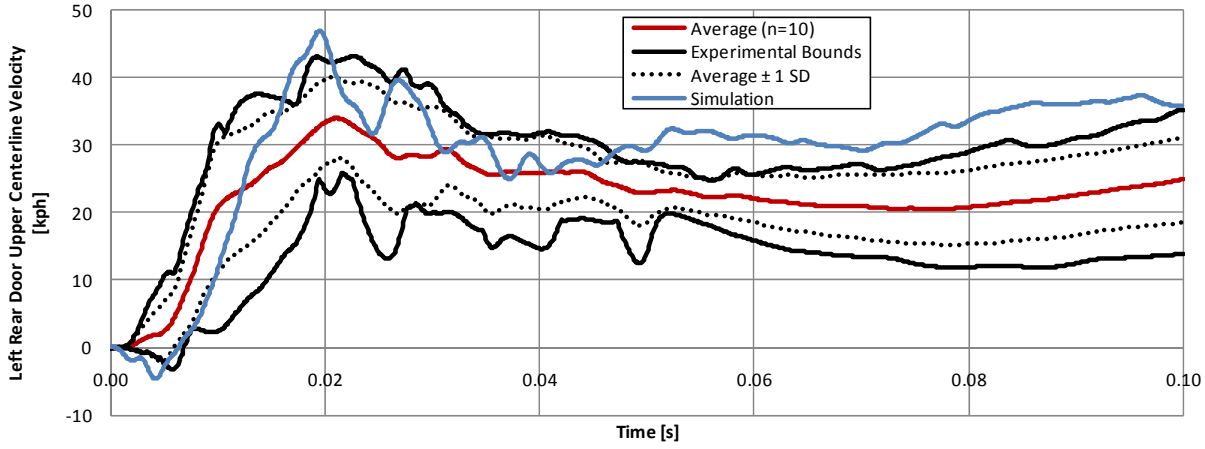

Figure A.12: NHSTA database survey – Left Rear Door Upper Centerline Velocity

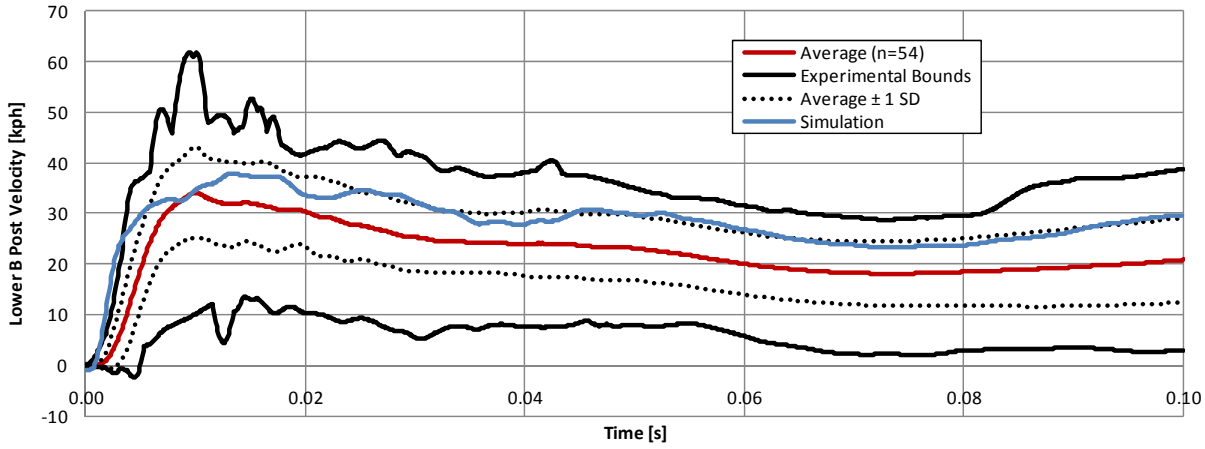

Figure A.13: NHSTA database survey – Lower B Post Velocity

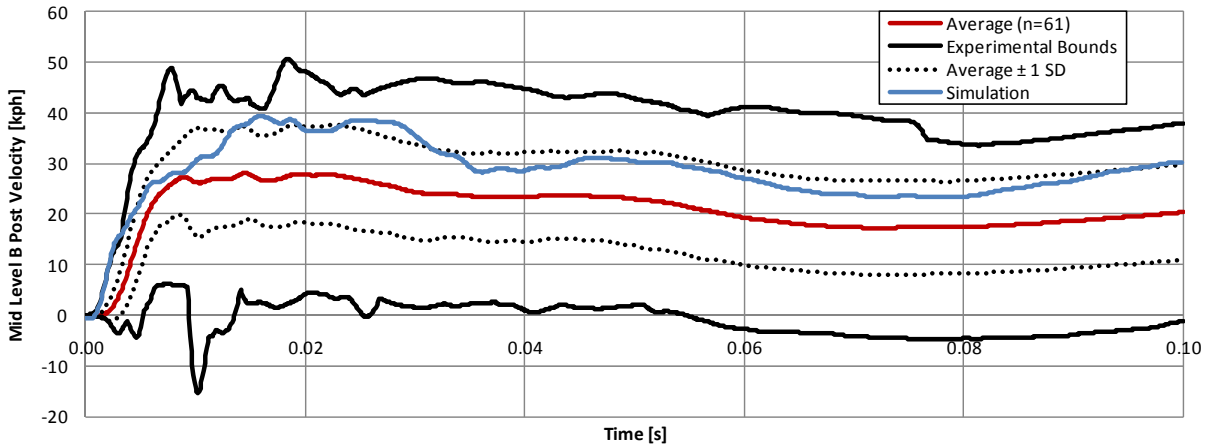

Figure A.14: NHSTA database survey – Middle B Post Velocity

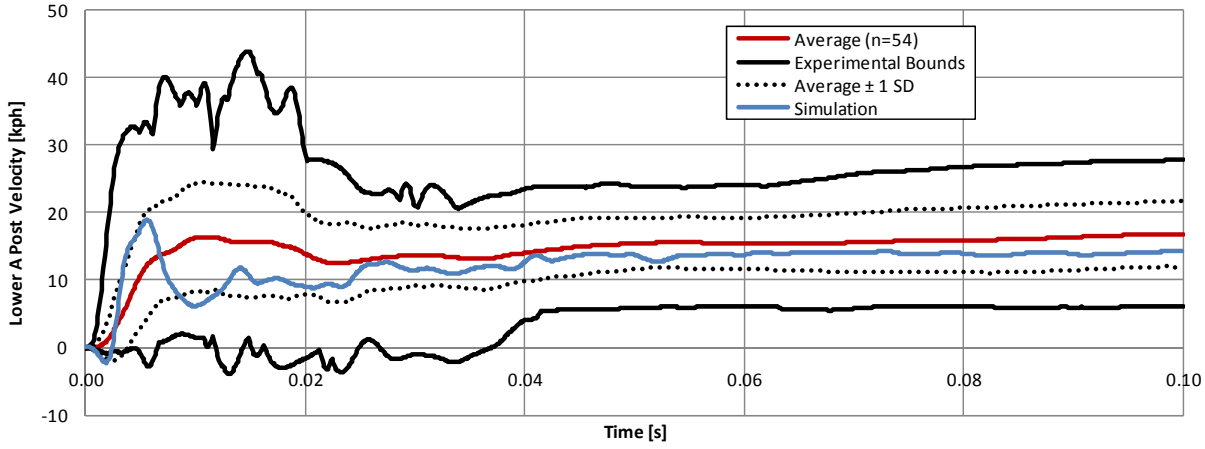

Figure A.15: NHSTA database survey – Lower A Post Velocity

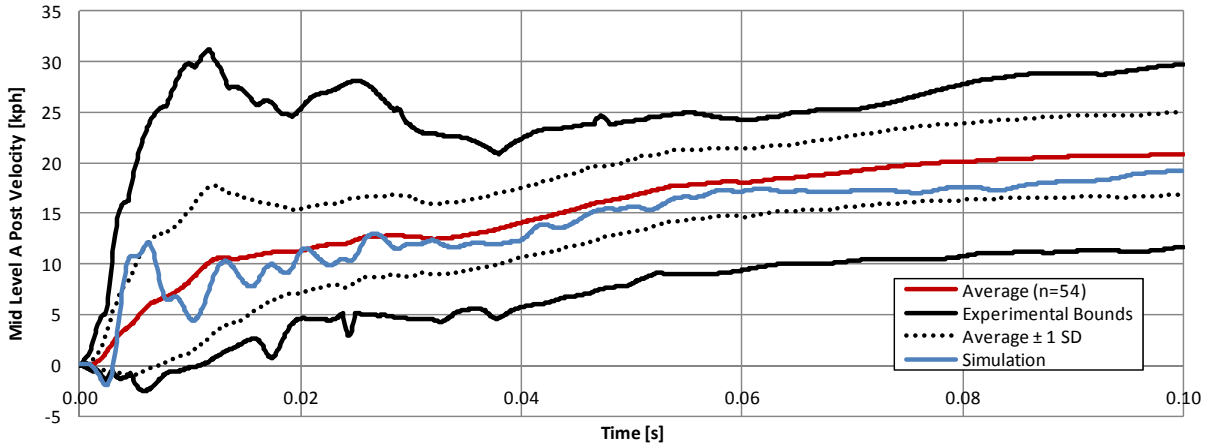

Figure A.16: NHSTA database survey – Middle A Post Velocity

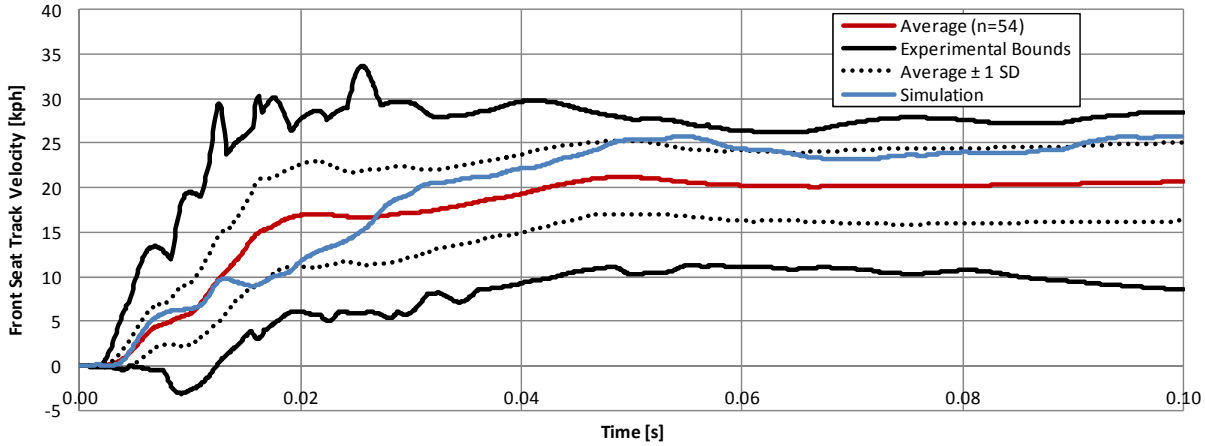

Figure A.17: NHSTA database survey – Front Seat Track Velocity

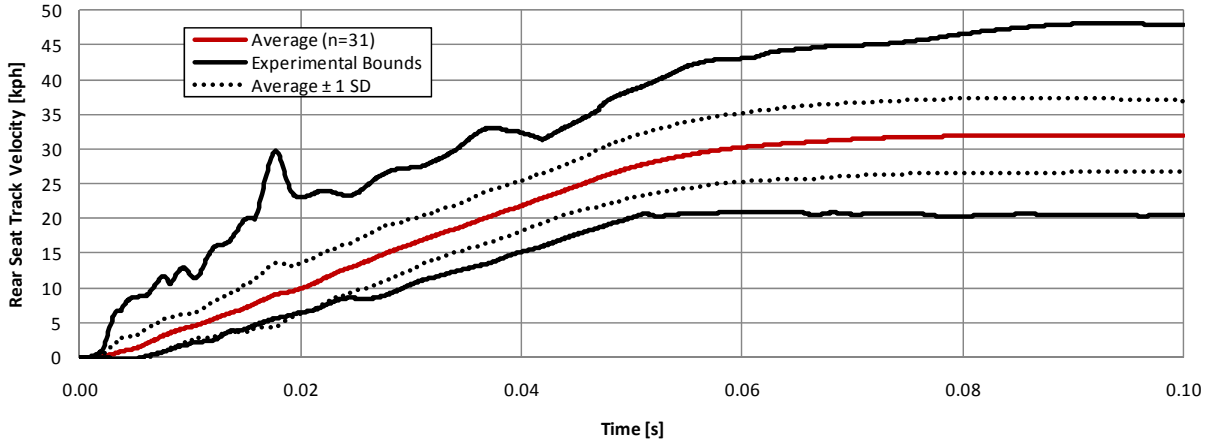

Figure A.18: NHSTA database survey – Rear Seat Track Velocity

Appendix B – Vehicle Velocity Validation Results

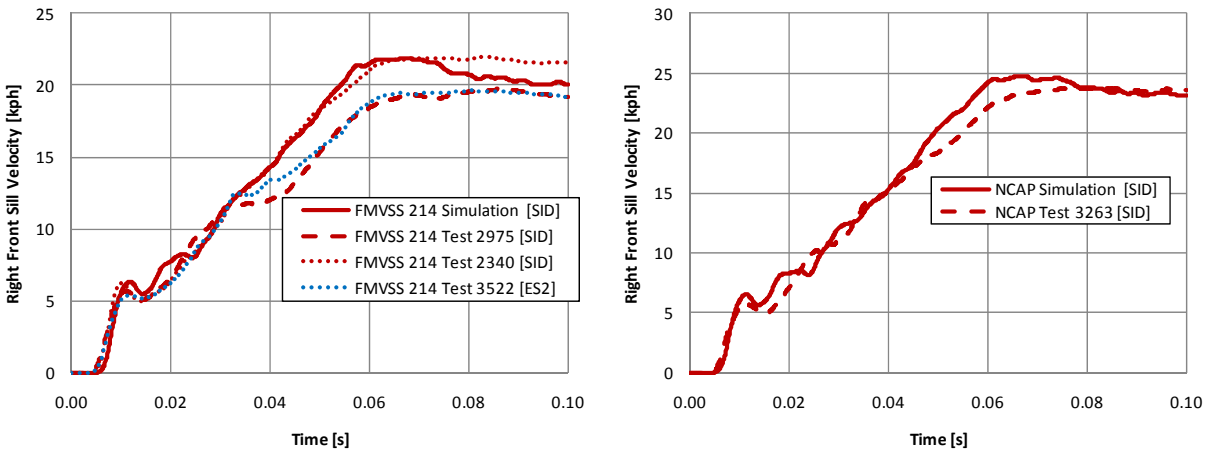

Figure B.1: Taurus Validation – Right Front Sill Velocity

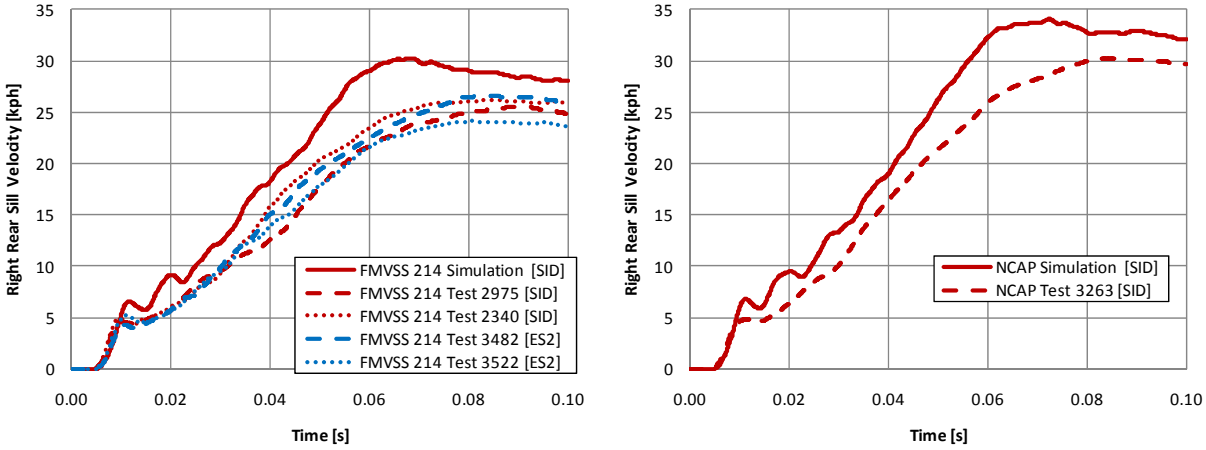

Figure B.2: Taurus Validation – Right Rear Sill Velocity

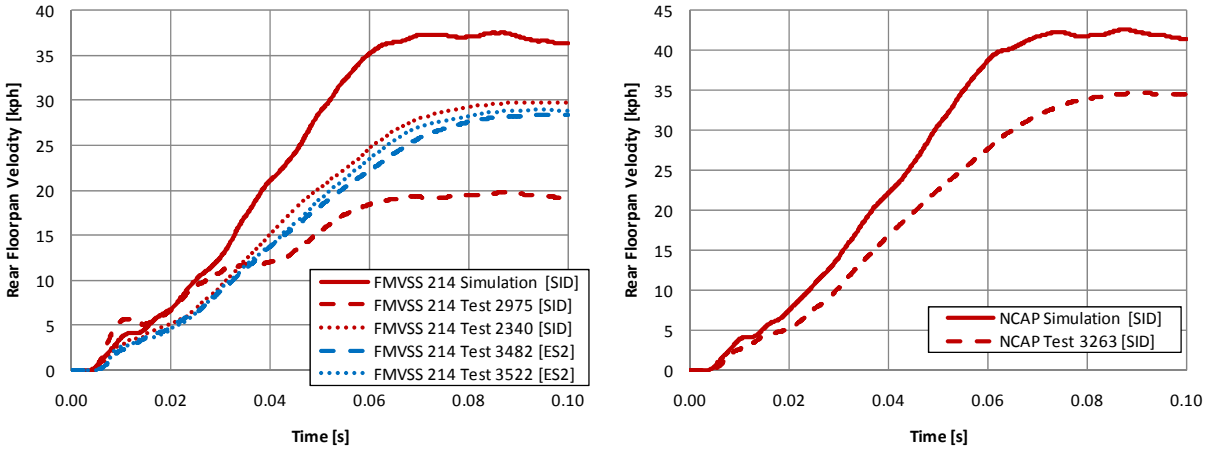

Figure B.3: Taurus Validation – Rear Floorpan Velocity

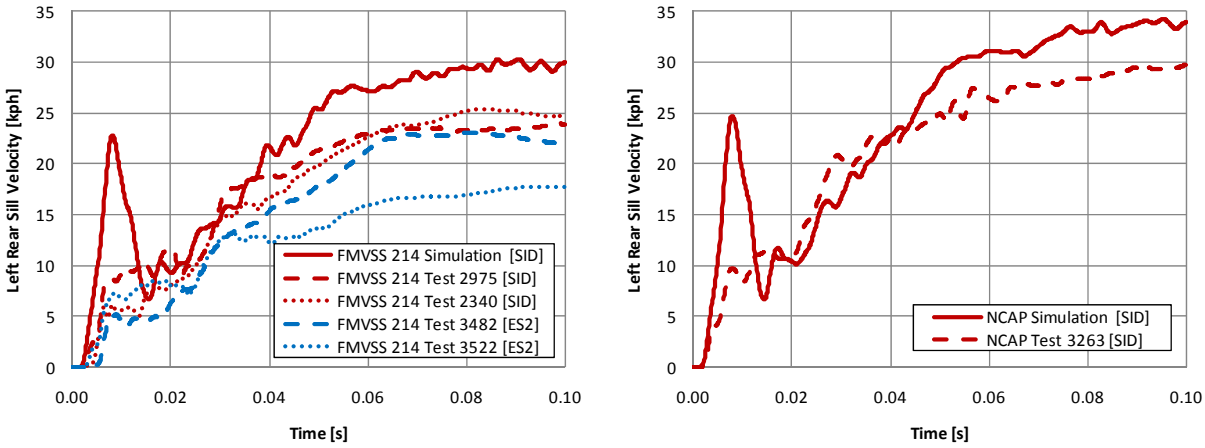

Figure B.4: Taurus Validation – Left Rear Sill Velocity

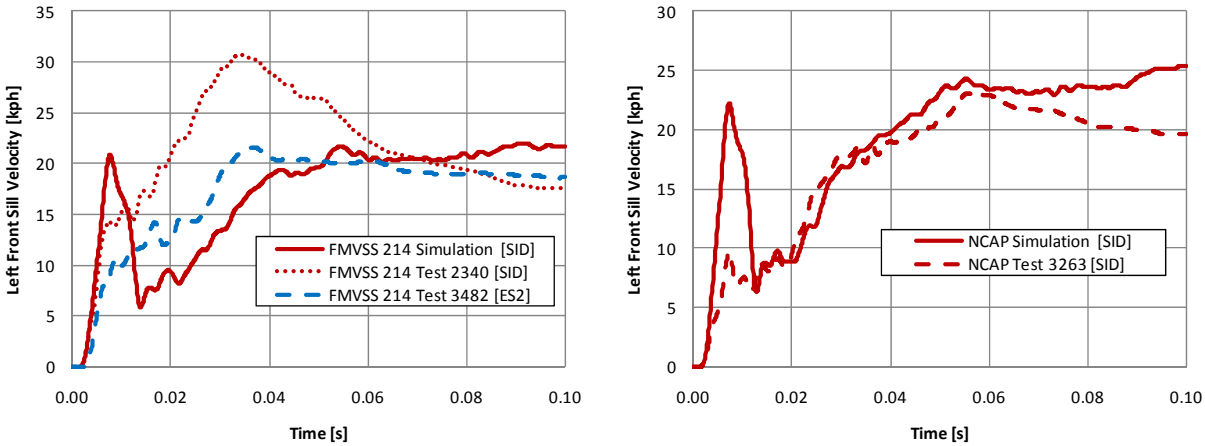

Figure B.5: Taurus Validation – Left Front Sill Velocity

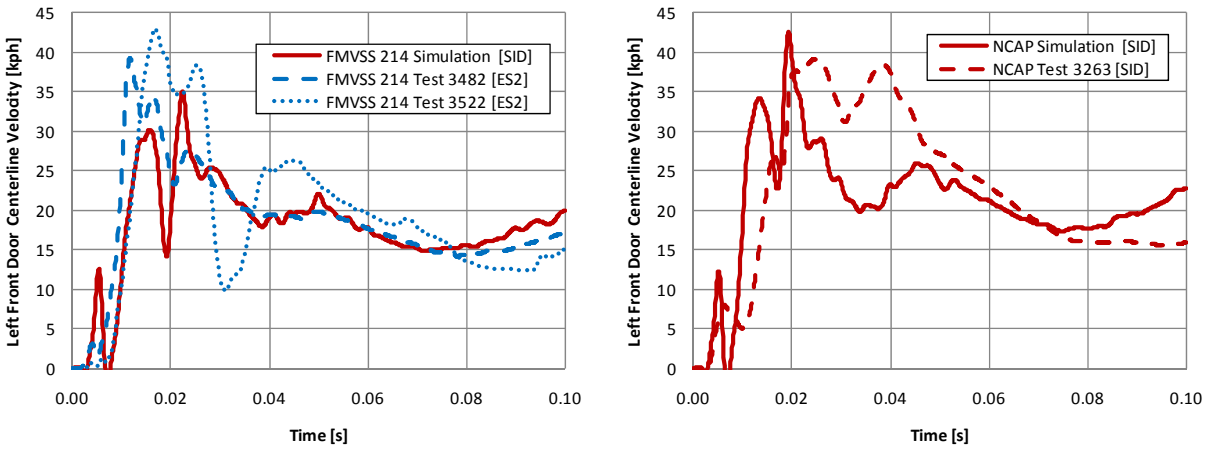

Figure B.6: Taurus Validation – Left Front Door Centerline Velocity

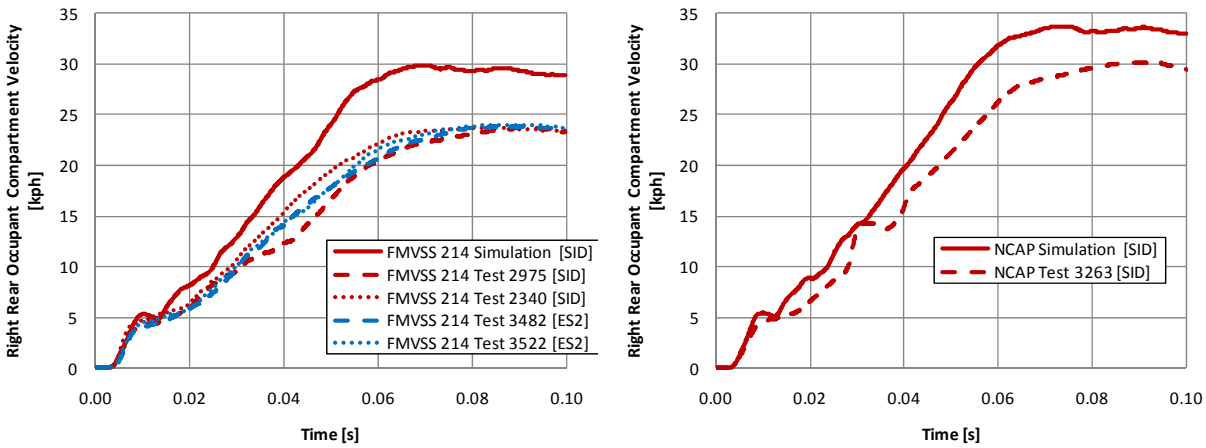

Figure B.7: Taurus Validation – Right Rear Occupant Compartment Velocity

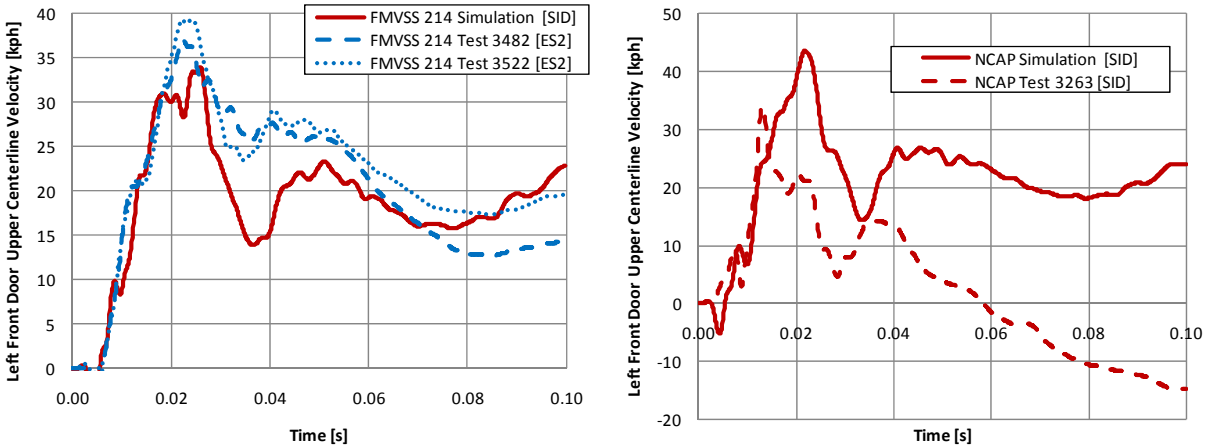

Figure B.8: Taurus Validation – Left Front Door Upper Centerline Velocity

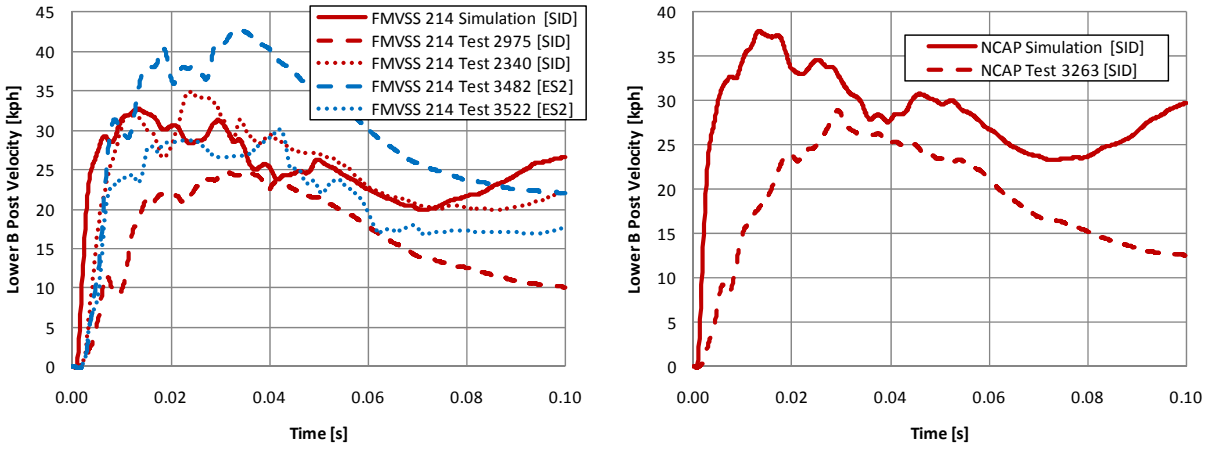

Figure B.9: Taurus Validation –Lower B Post Velocity

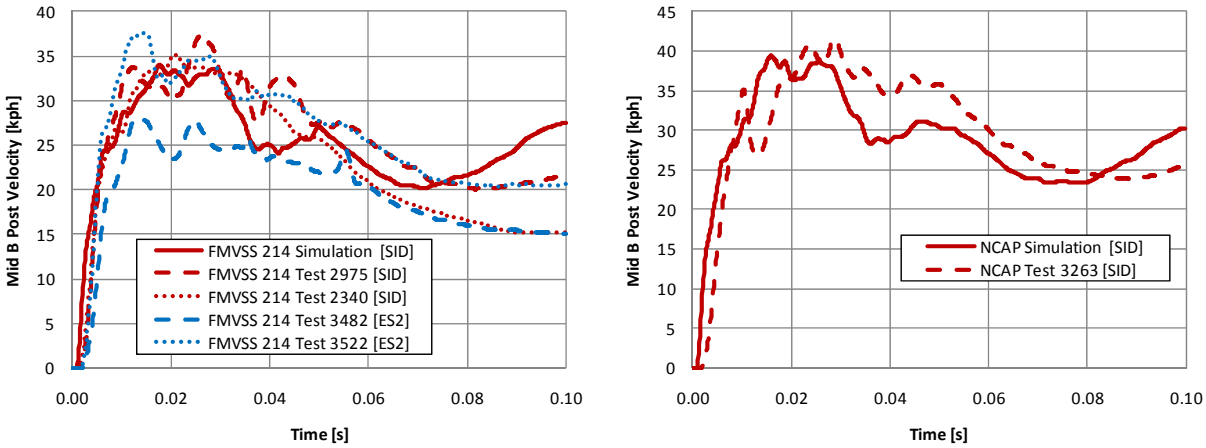

Figure B.10: Taurus Validation – Middle B Post Velocity

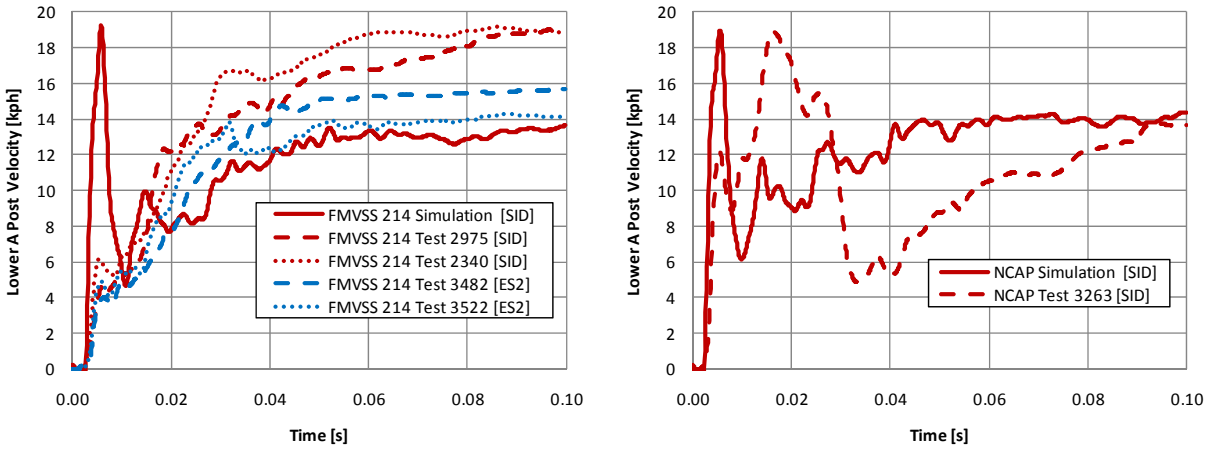

Figure B.11: Taurus Validation –Lower A Post Velocity

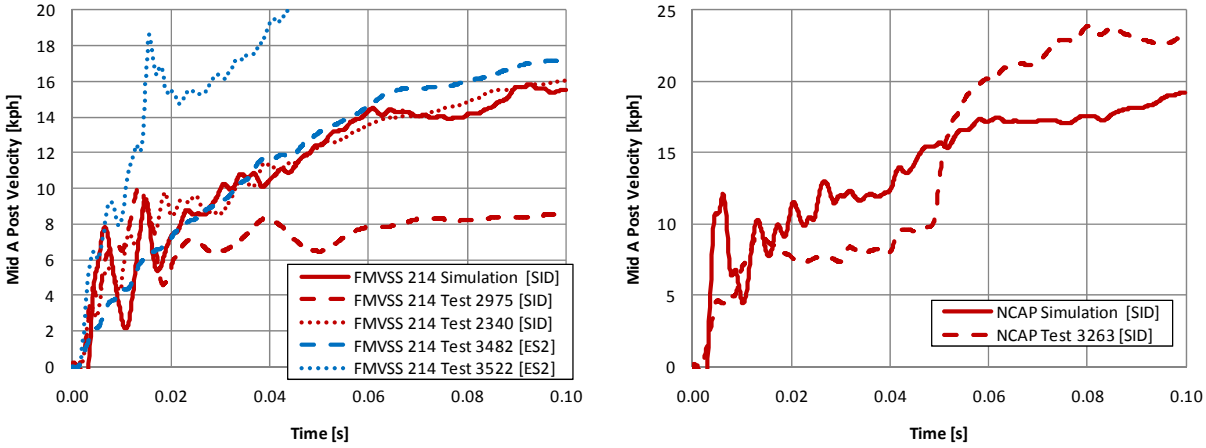

Figure B.12: Taurus Validation – Middle A Post Velocity

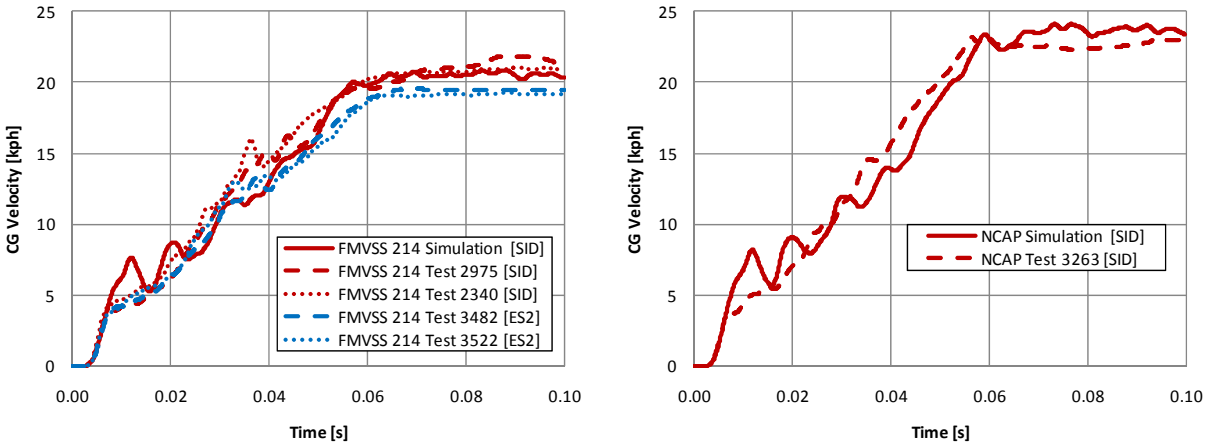

Figure B.13: Taurus Validation – Center of Gravity Velocity

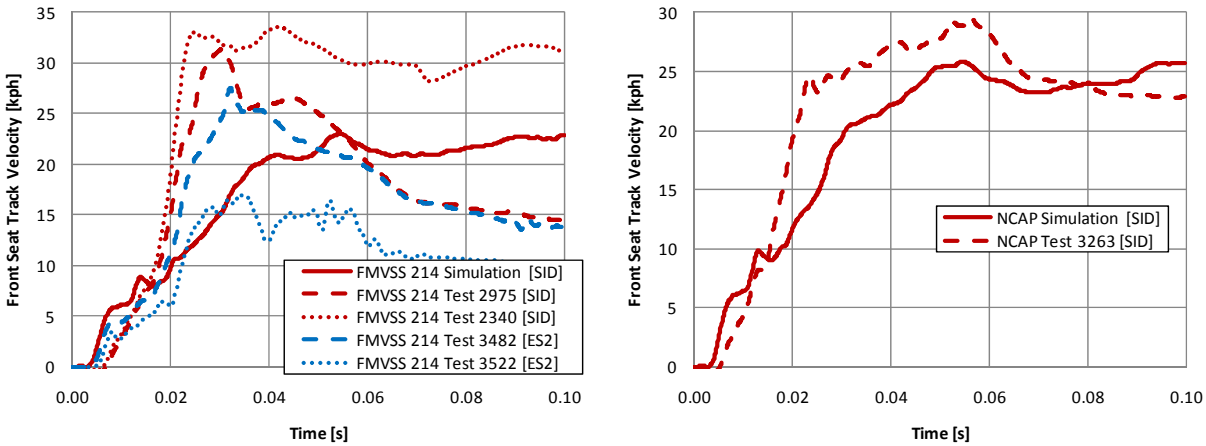

Figure B.14: Taurus Validation – Front Seat Track Velocity

Appendix C – Parametric Study Occupant Injury Criteria Response Curves

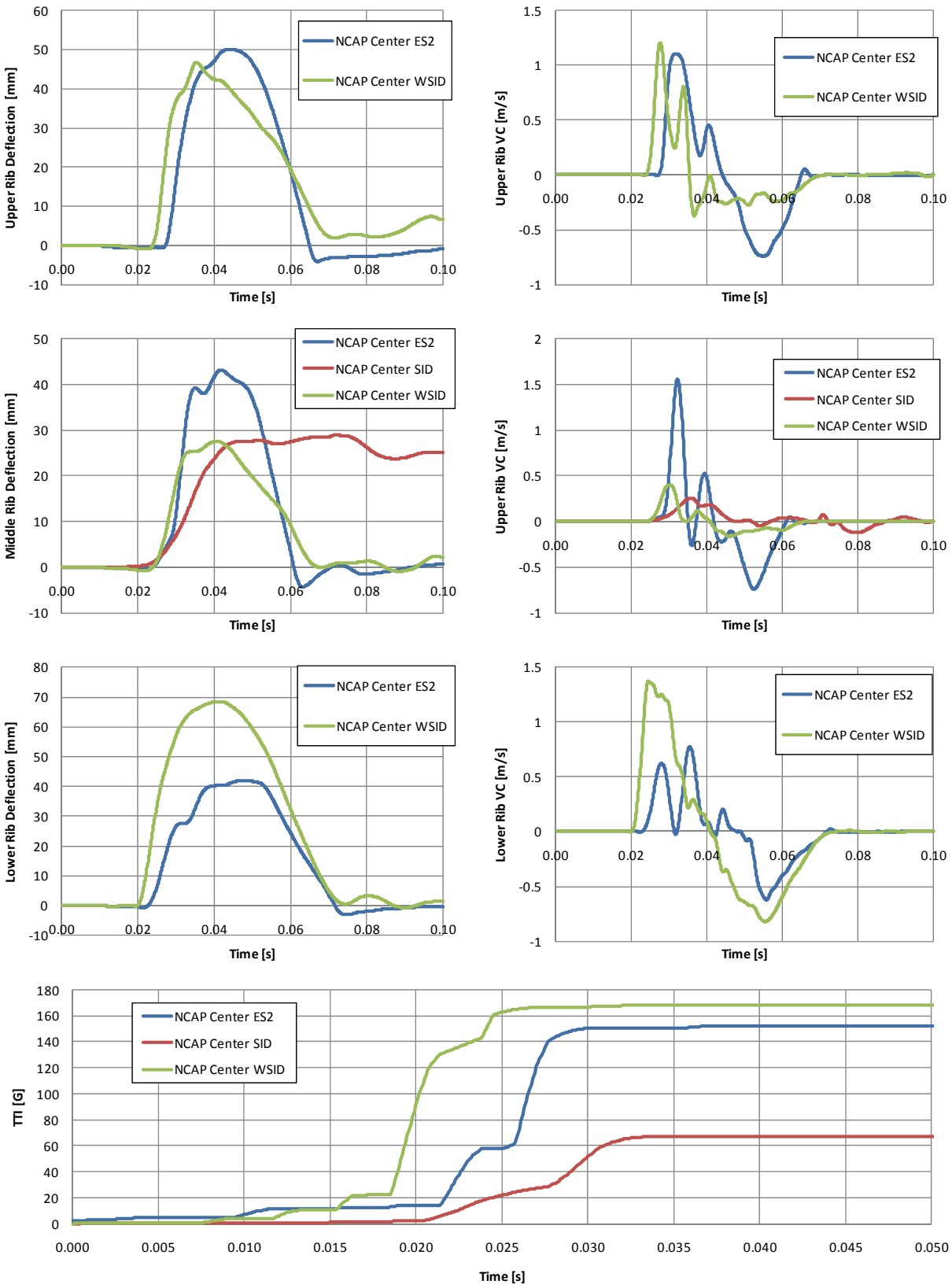

Figure C.1: Occupant Response – ATDs in Center Position – NCAP Barrier Speed

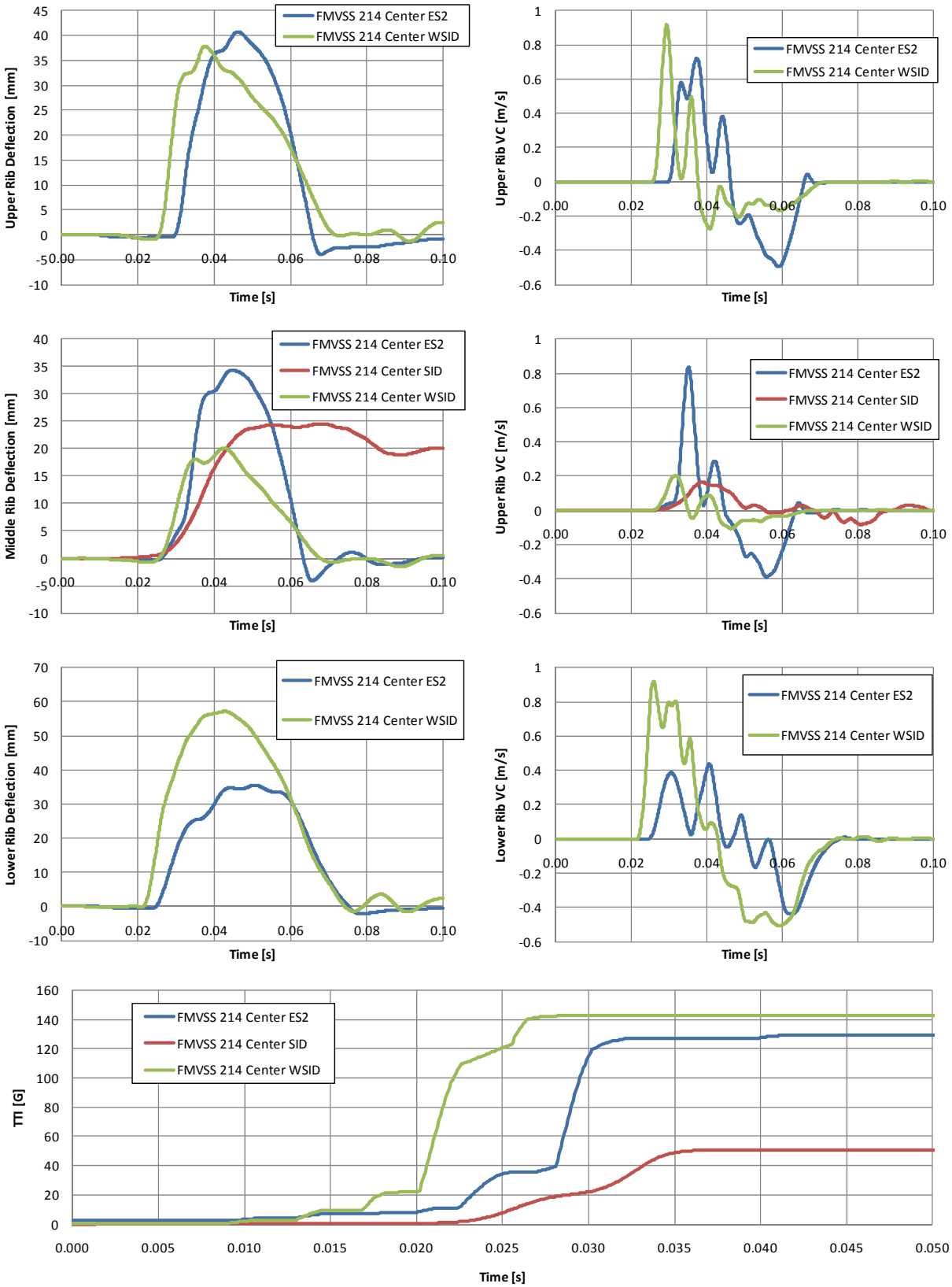

Figure C.2: Occupant Response – ATDs in Center Position – FMVSS 214 Barrier Speed

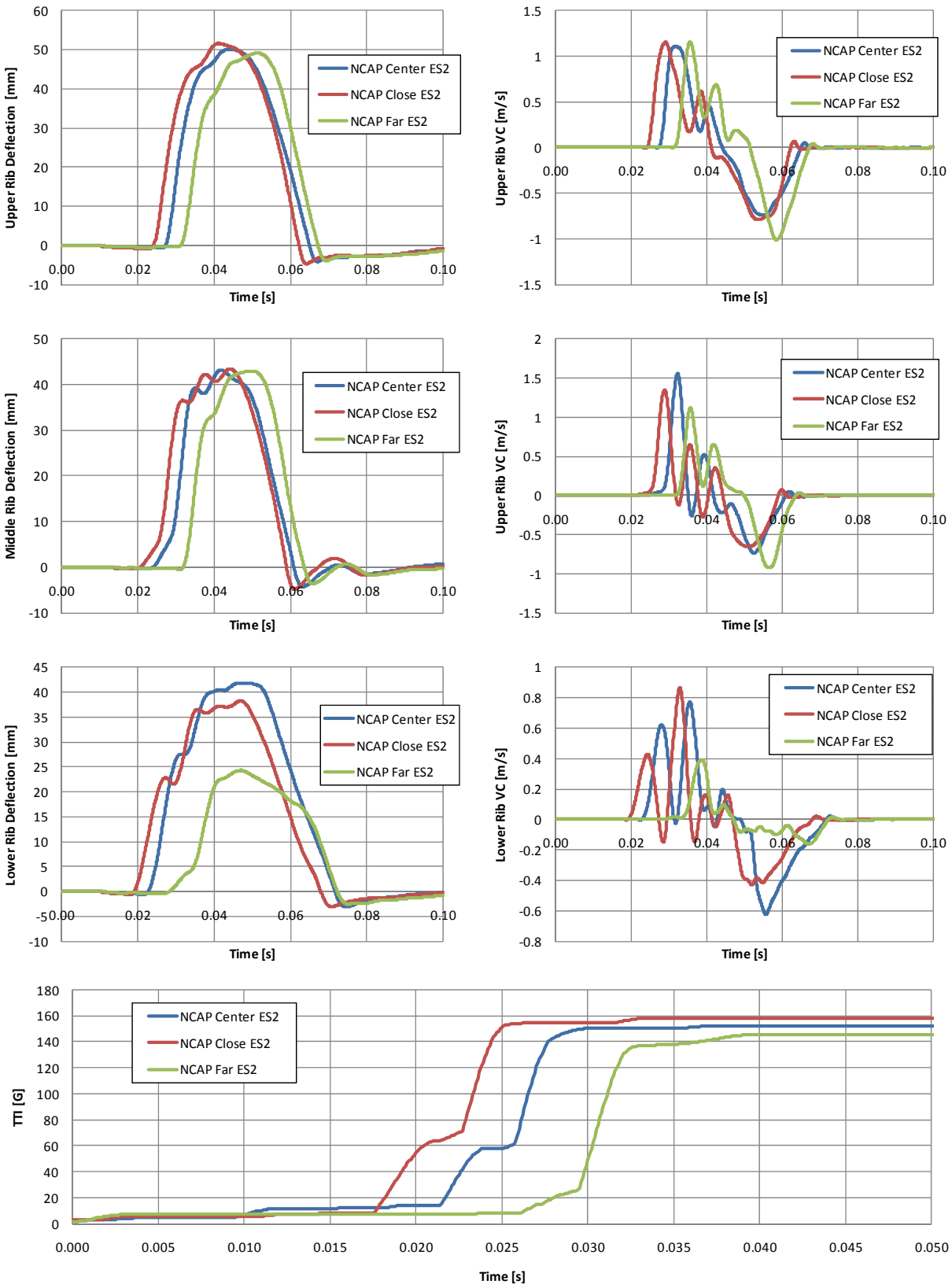

Figure C.3: Occupant Response – ES-2re at 3 Lateral Positions – NCAP Barrier Speed

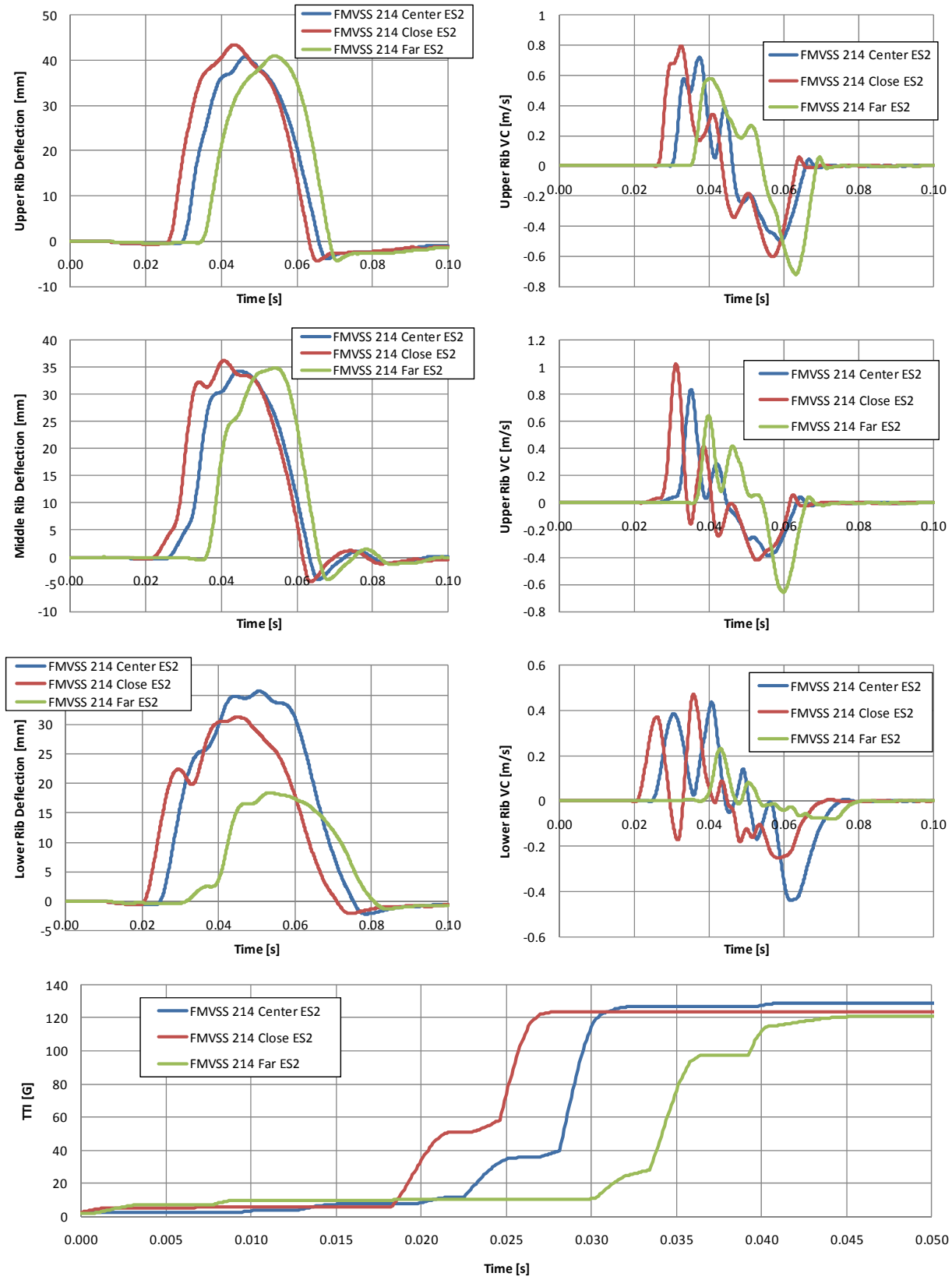

Figure C.4: Occupant Response – ES-2re at 3 Lateral Positions – FMVSS 214 Barrier Speed

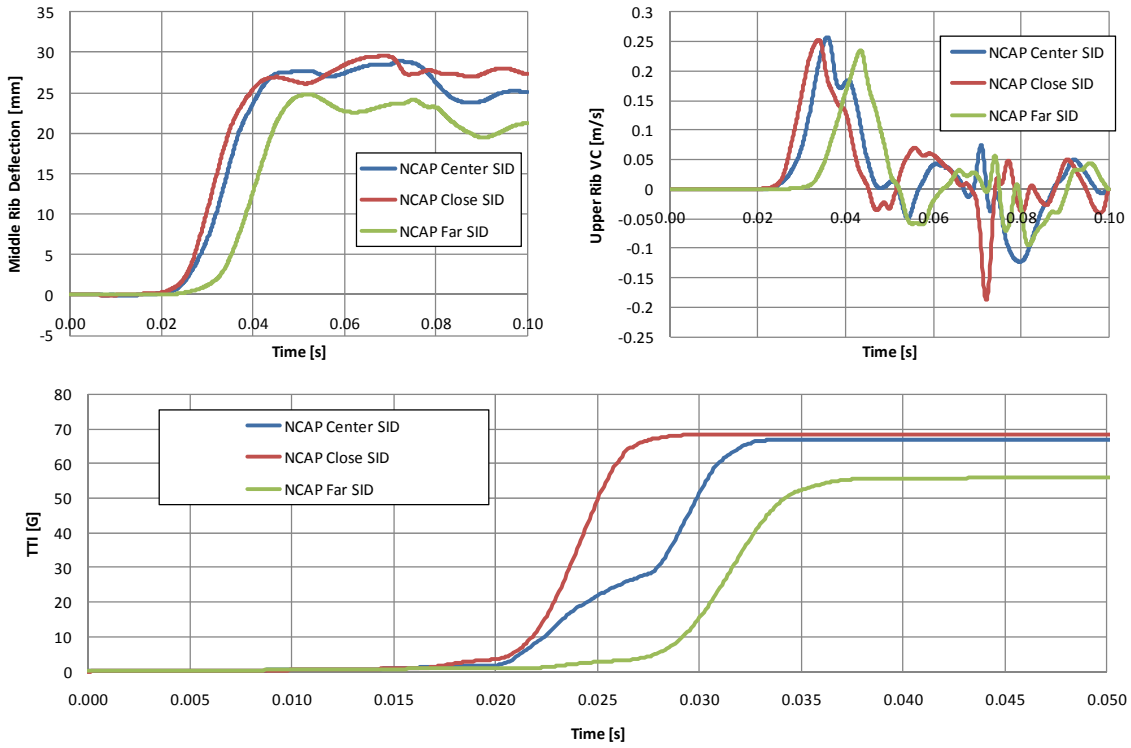

Figure C.5: Occupant Response – SID at 3 Lateral Positions – NCAP Barrier Speed

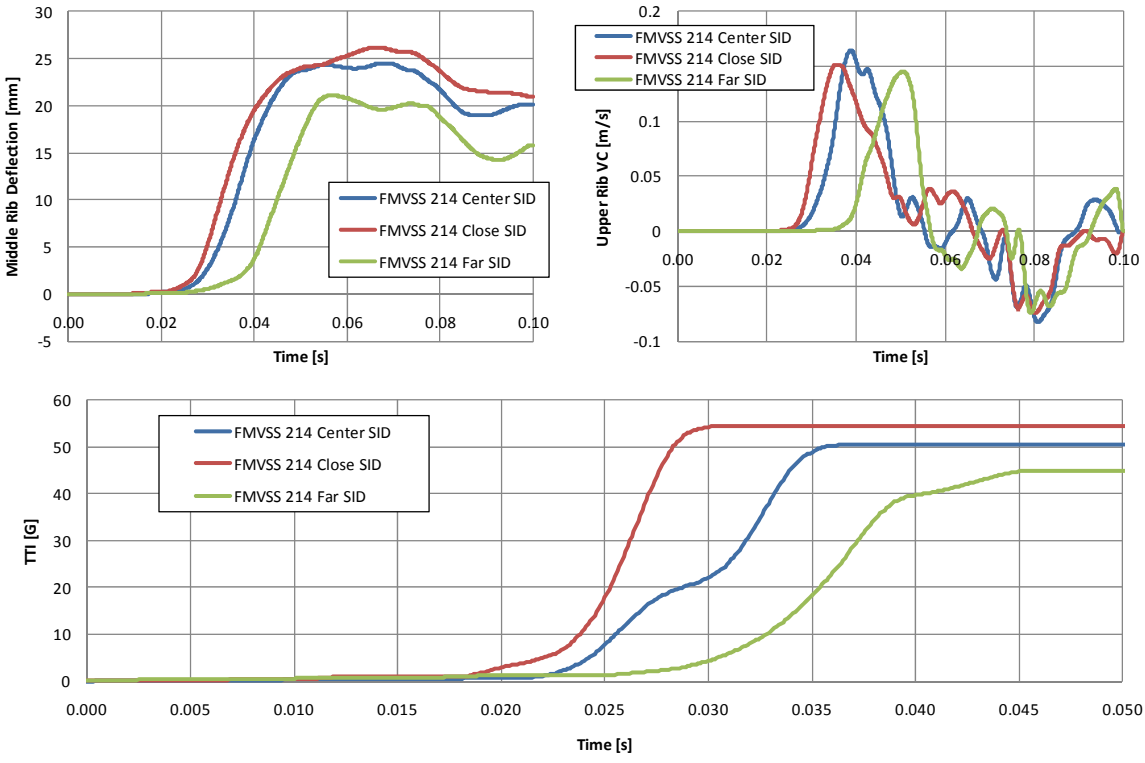

Figure C.6: Occupant Response – SID at 3 Lateral Positions – FMVSS 214 Barrier Speed

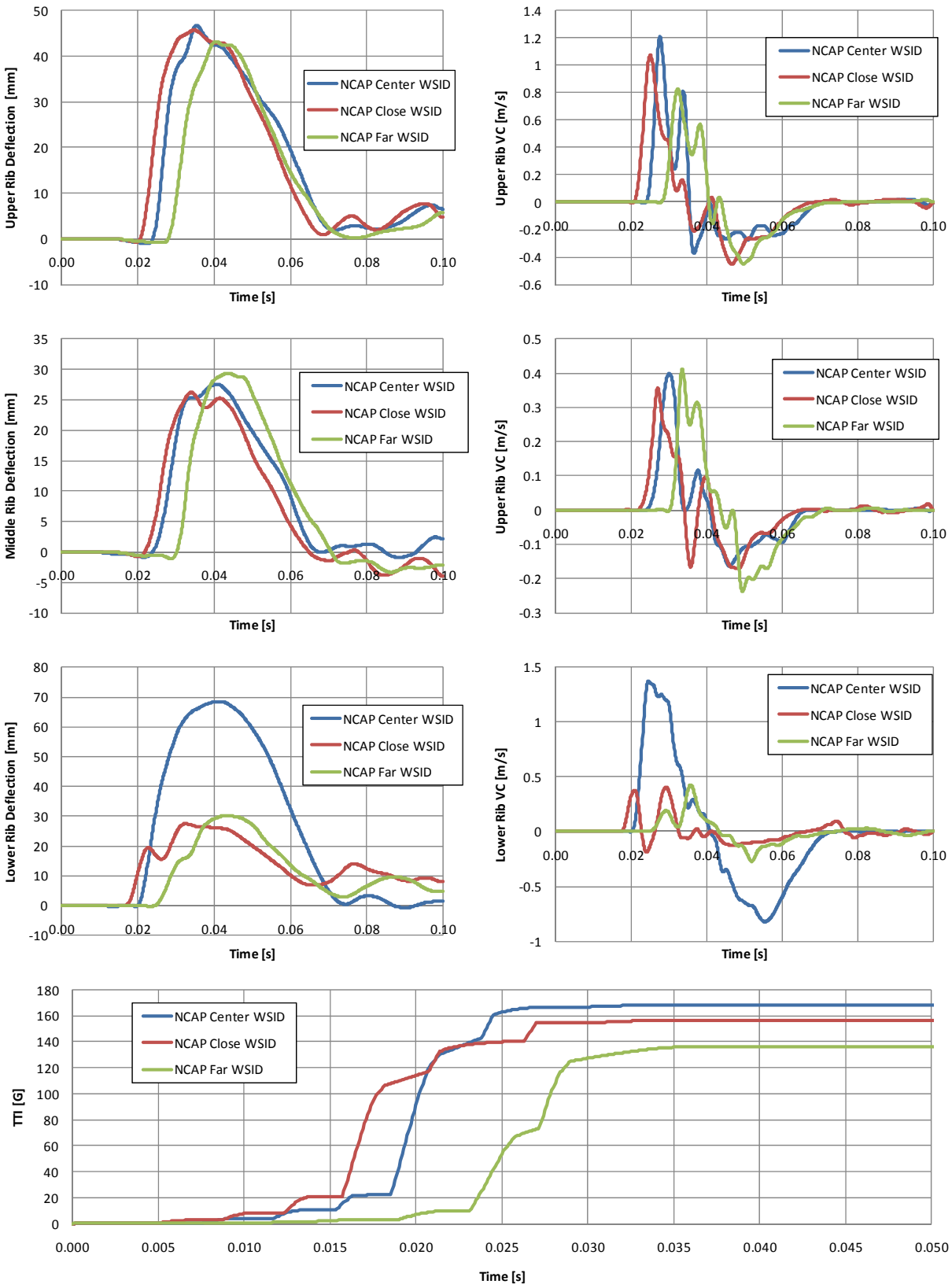

Figure C.7: Occupant Response – WSID at 3 Lateral Positions – NCAP Barrier Speed

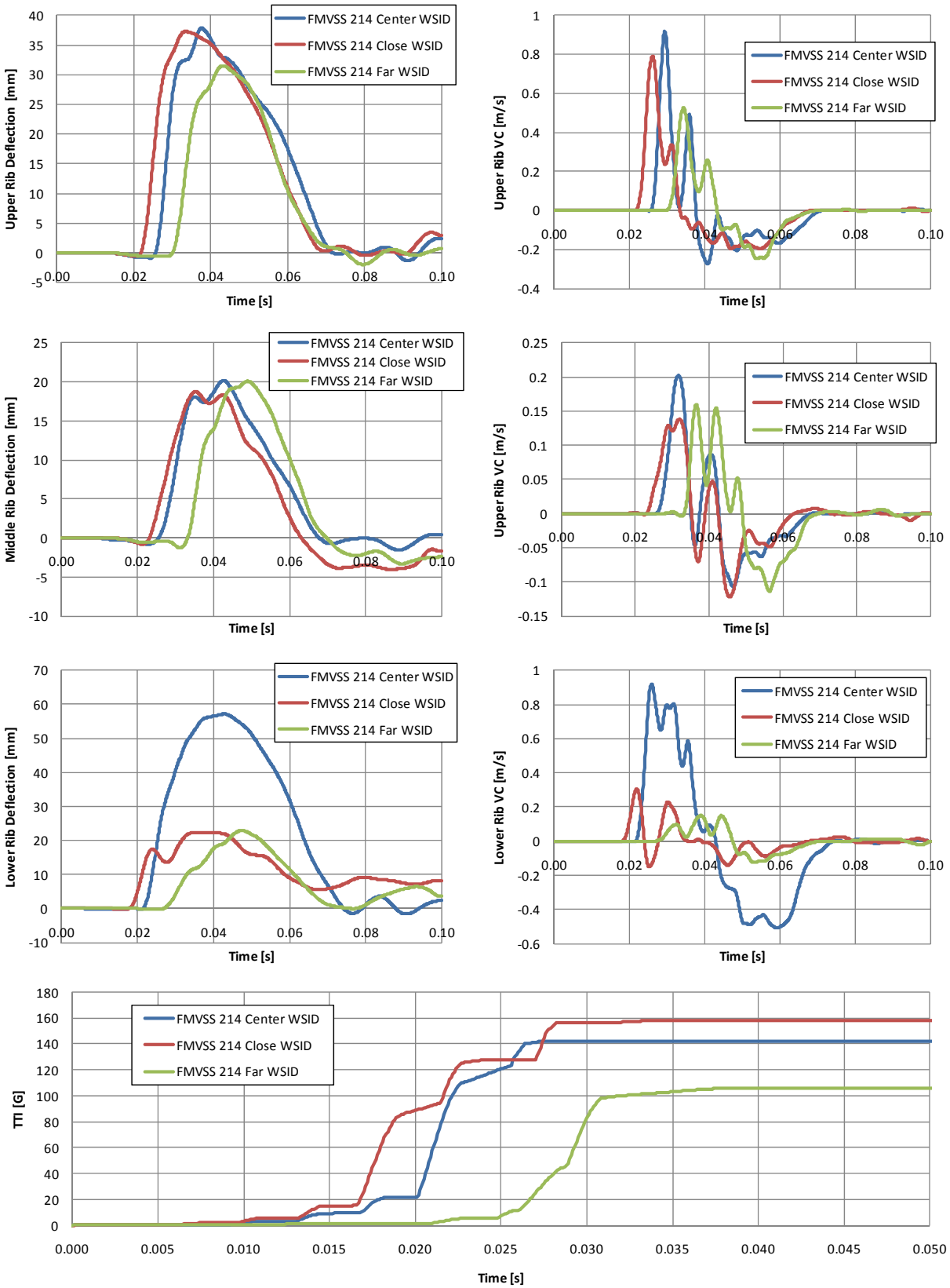

Figure C.8: Occupant Response – WSID at 3 Lateral Positions – FMVSS 214 Barrier Speed

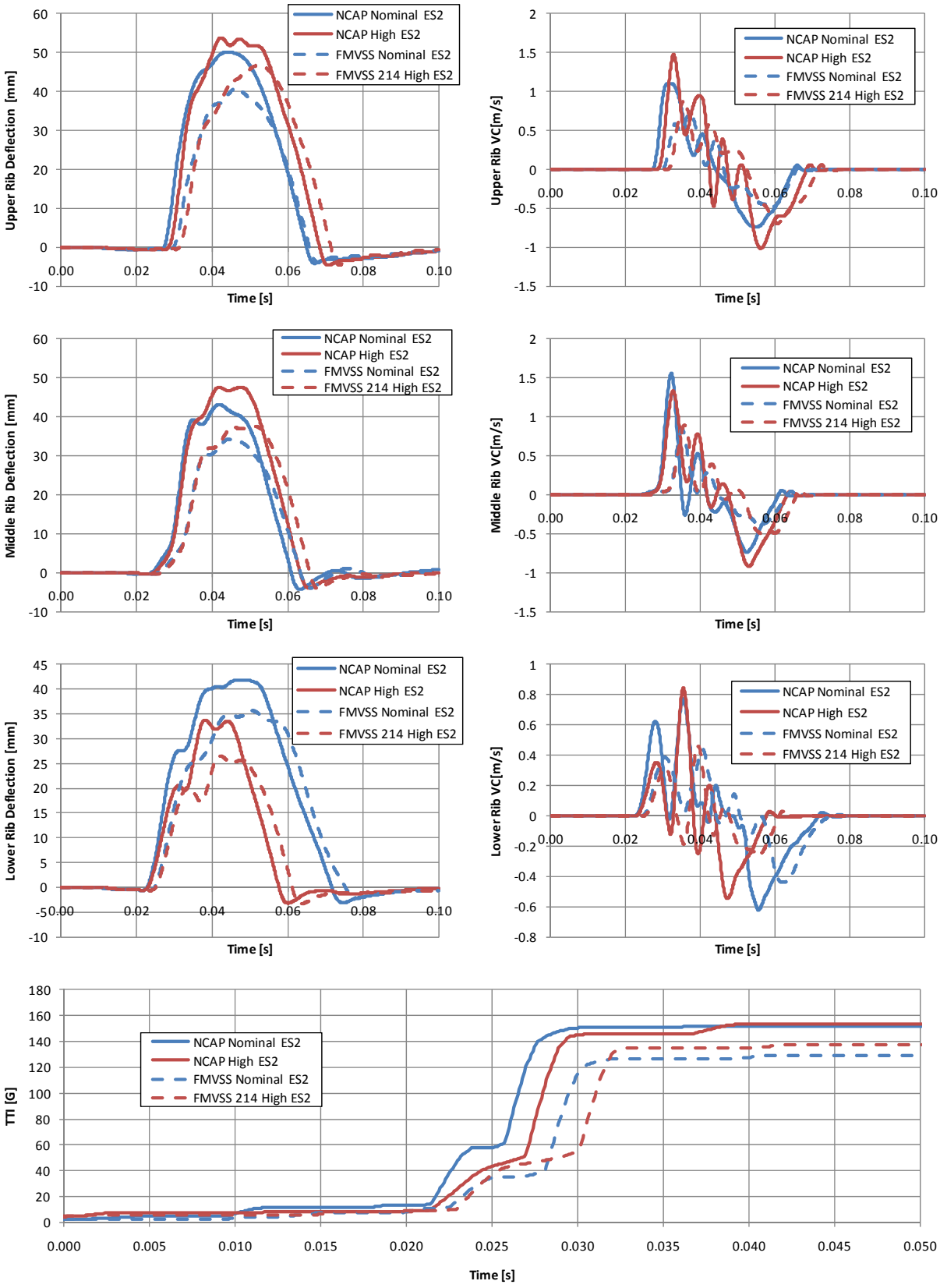

Figure C.9: Occupant Response – ES-2re at 2 Vertical Positions – Both Barrier Speeds

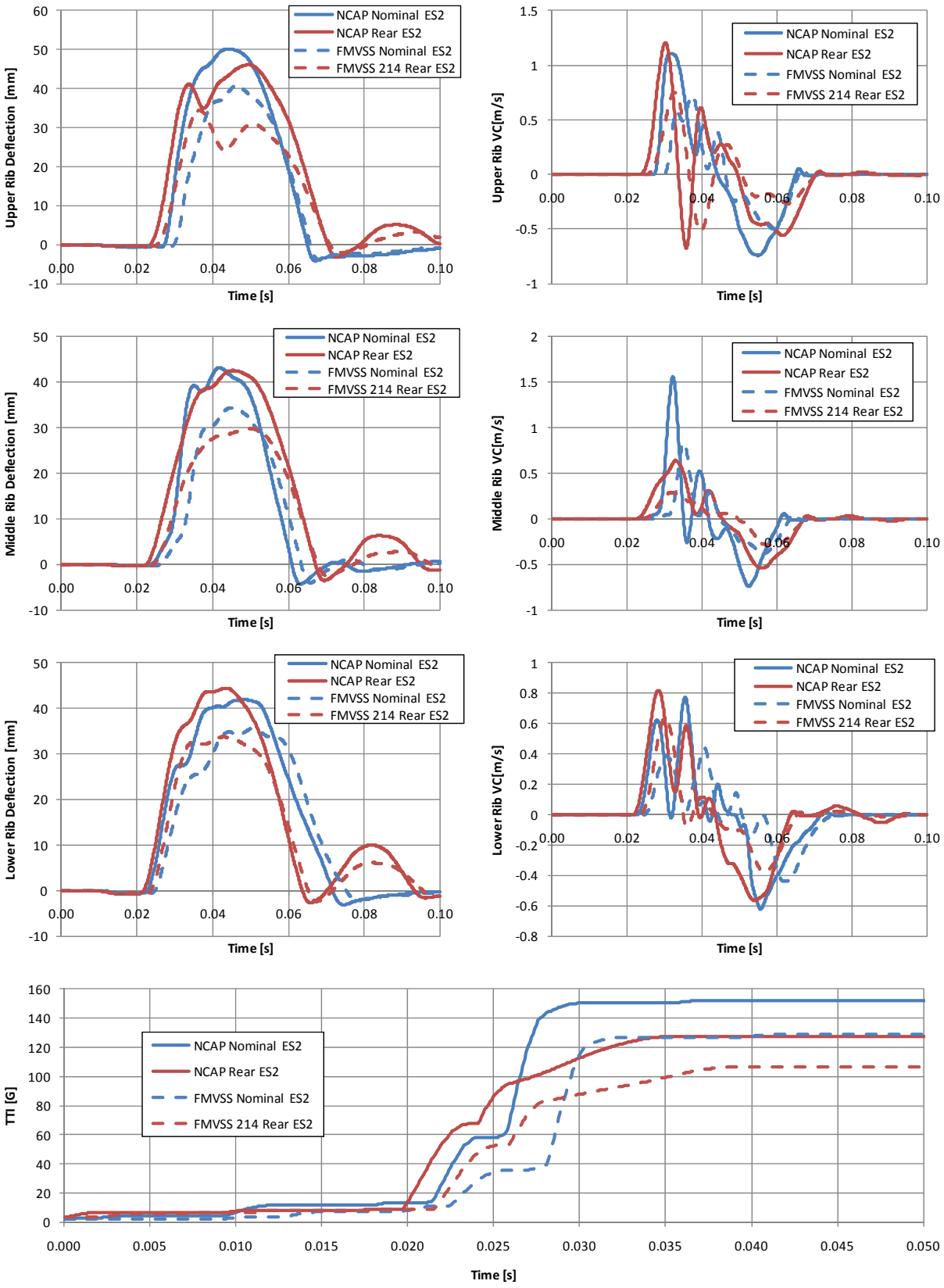

Figure C.10: Occupant Response – ES-2re at 2 Longitudinal Positions – Both Barrier Speeds

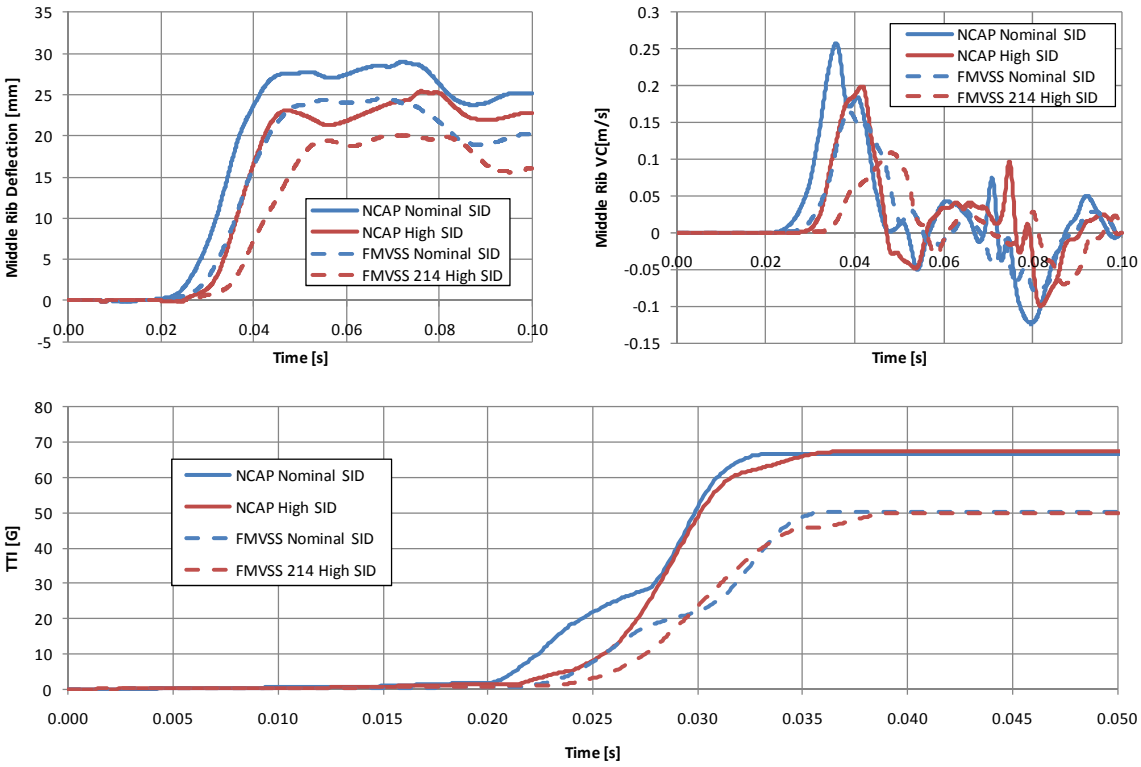

Figure C.11: Occupant Response – SID at 2 Vertical Positions – Both Barrier Speeds

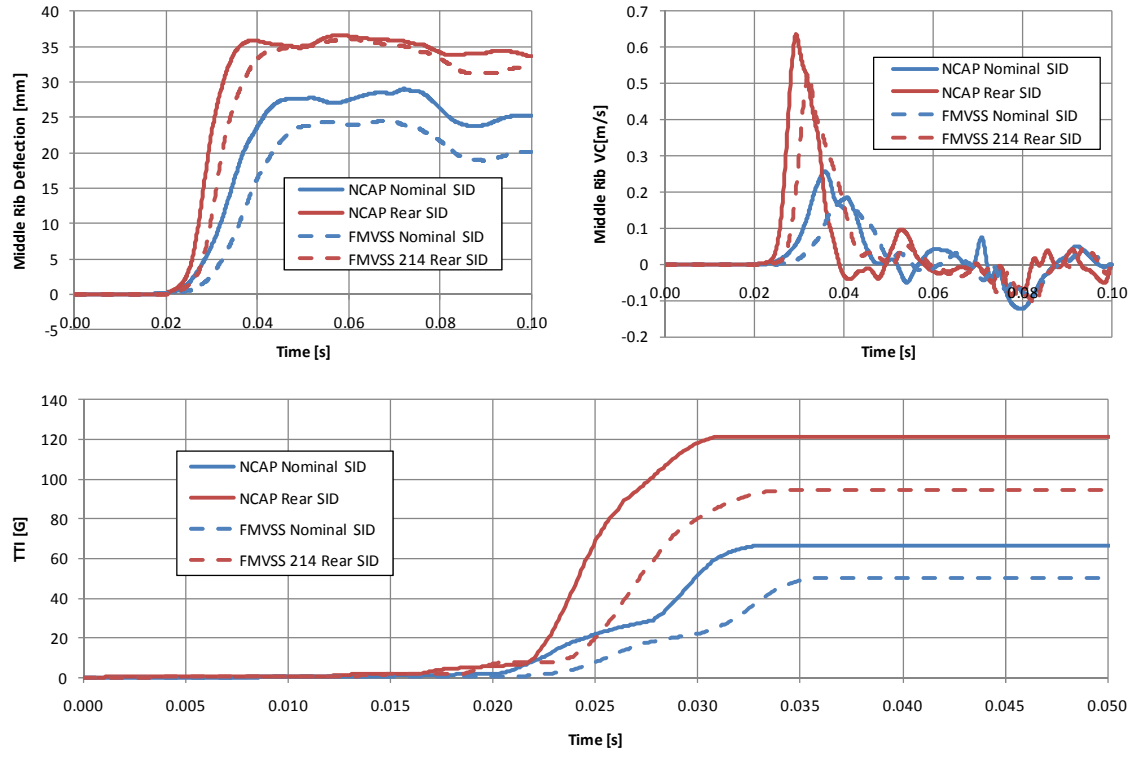

Figure C.12: Occupant Response – SID at 2 Longitudinal Positions – Both Barrier Speeds

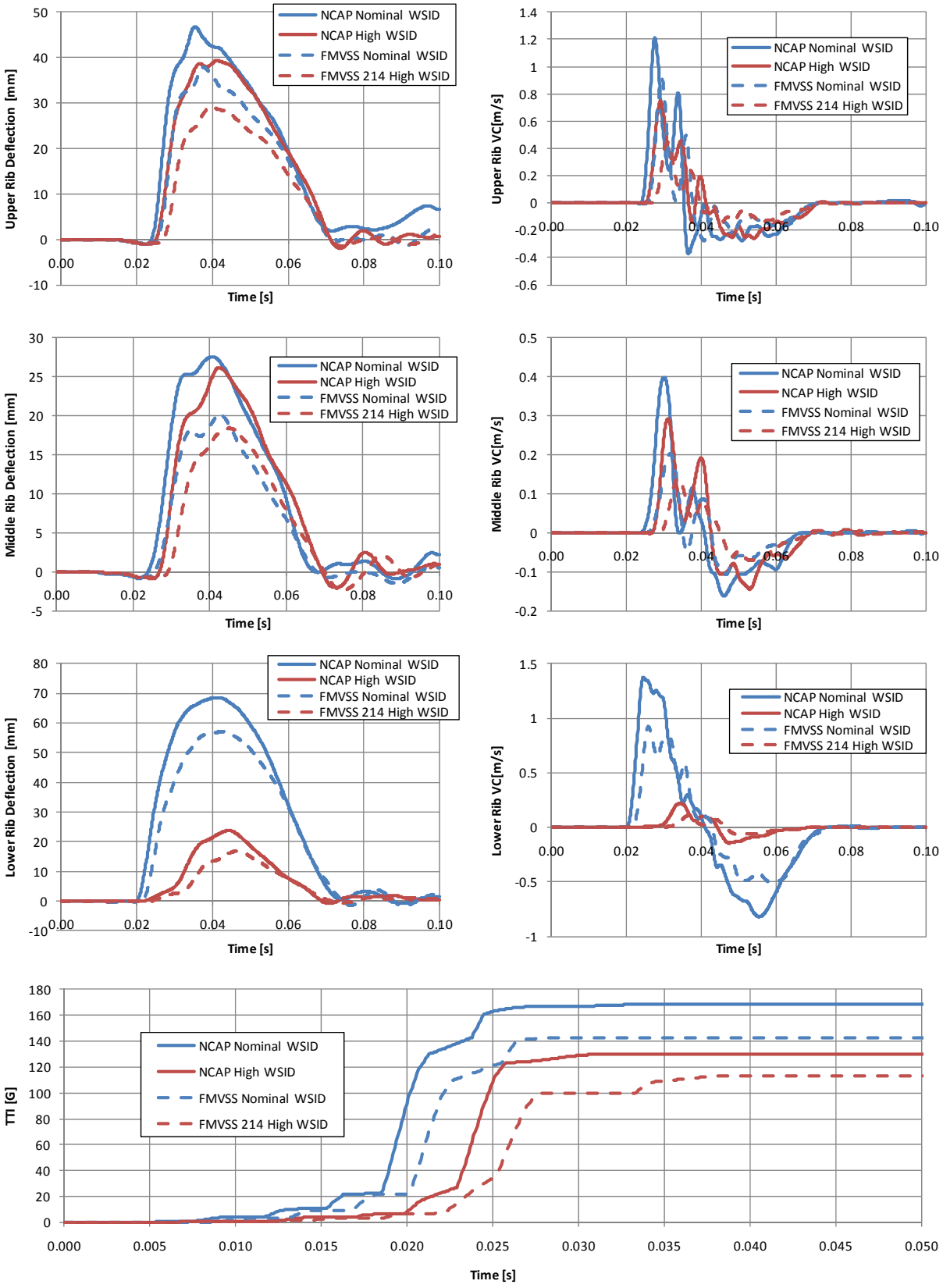

Figure C.13: Occupant Response – WSID at 2 Vertical Positions – Both Barrier Speeds

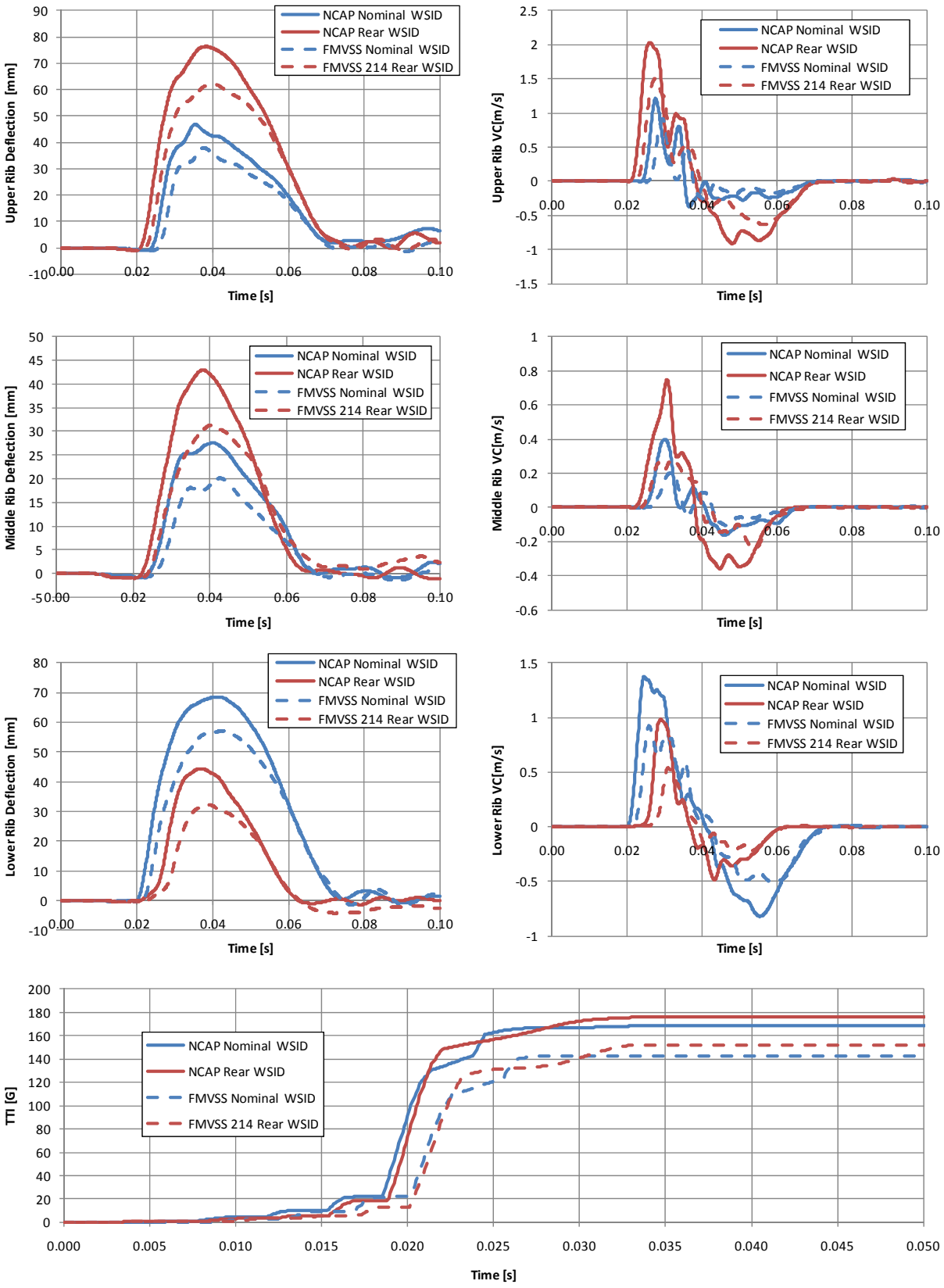

Figure C.14: Occupant Response – WSID at 2 Longitudinal Positions – Both Barrier Speeds

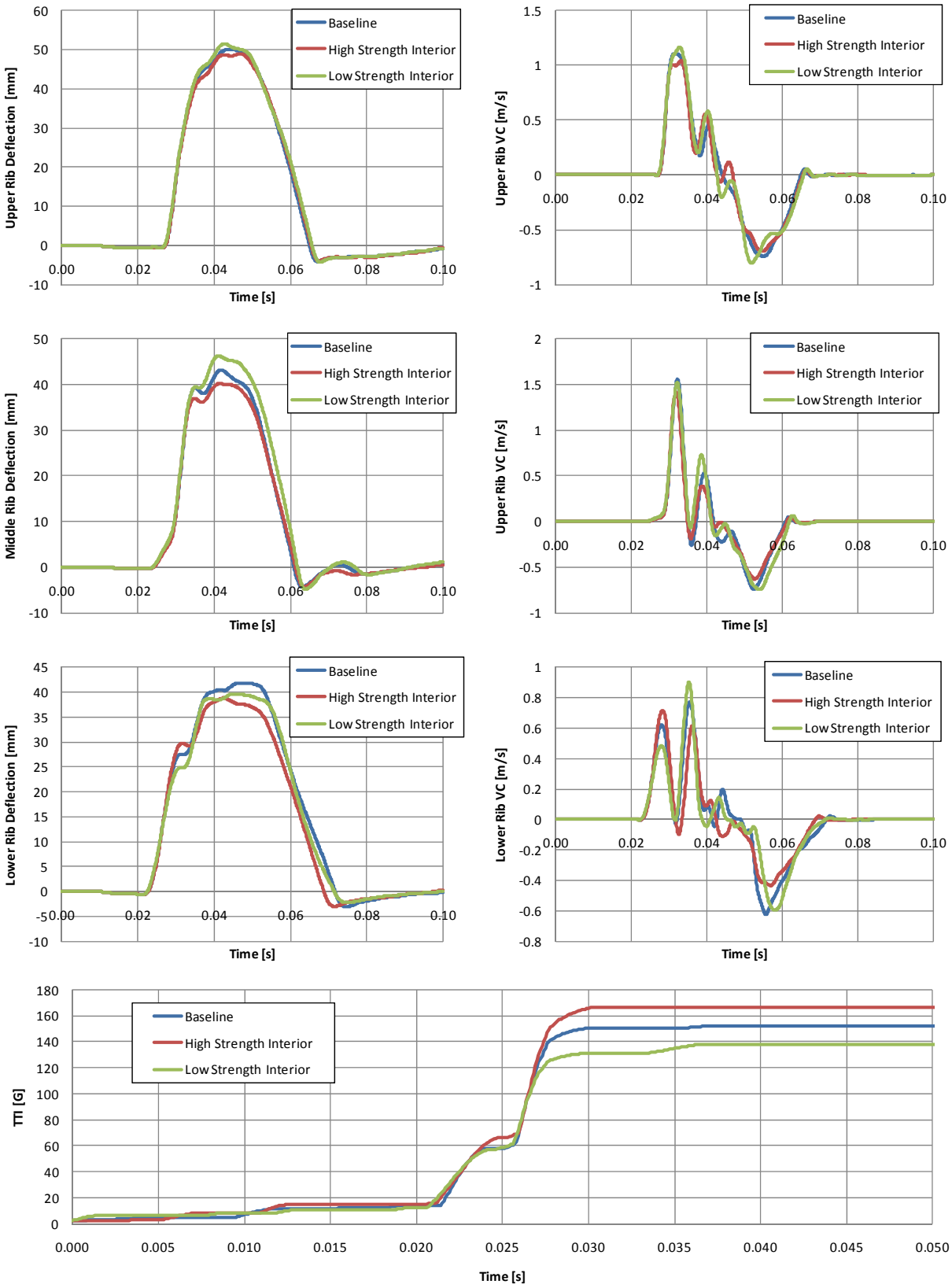

Figure C.15: Occupant Response – Effect of Interior Panel Strength

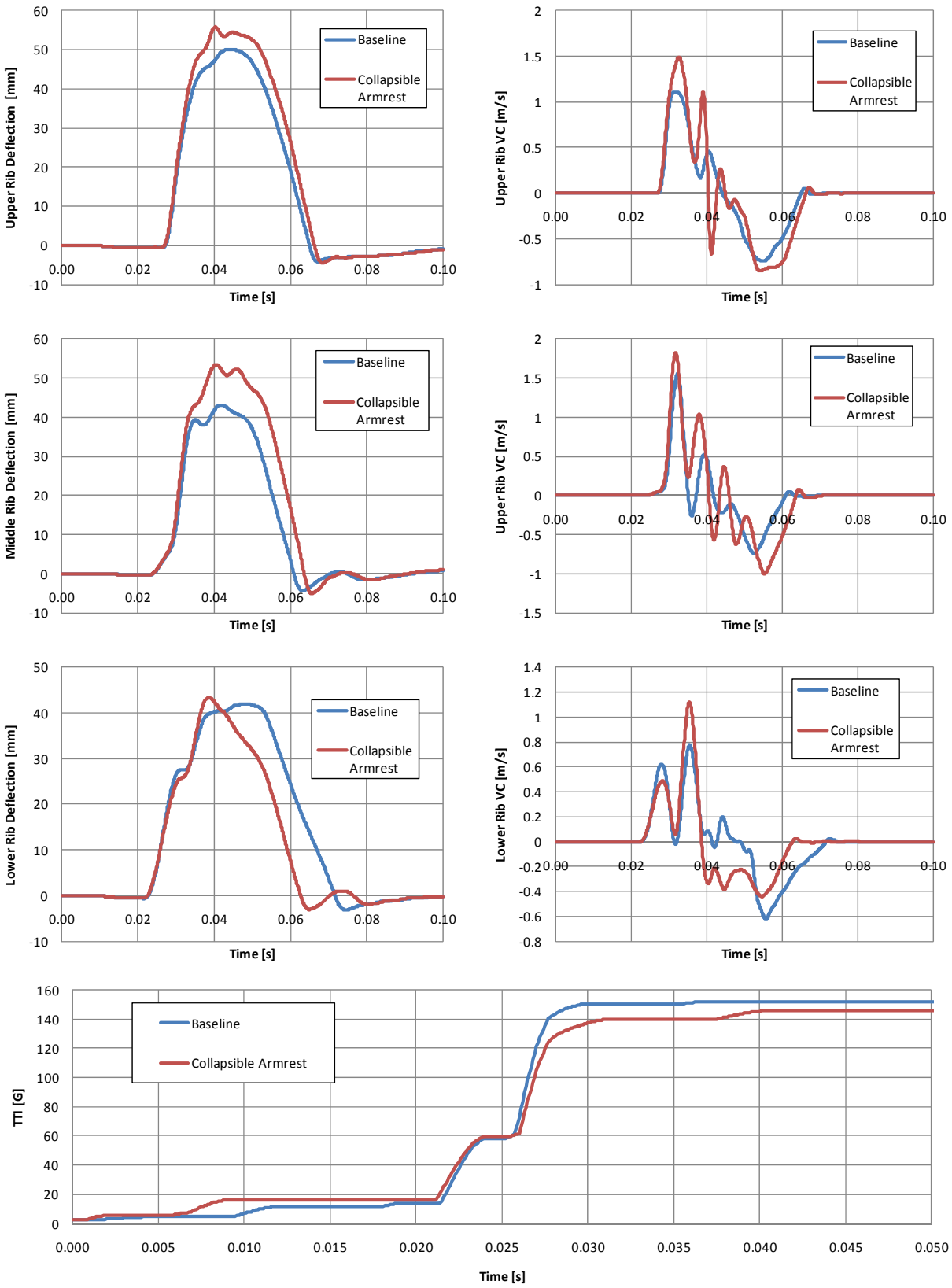

Figure C.16: Occupant Response – Effect of Collapsible Armrest

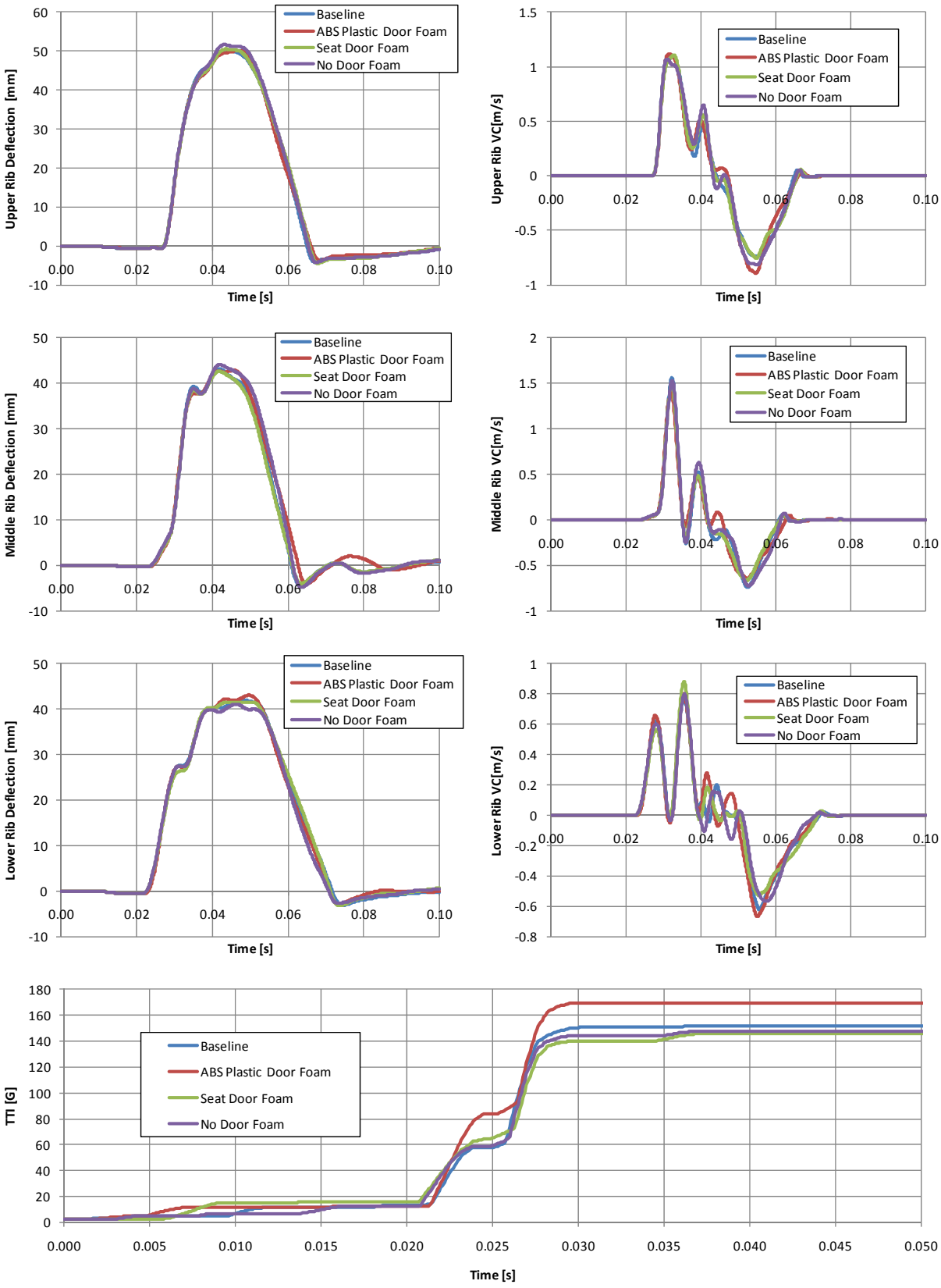

Figure C.17: Occupant Response – Effect of Door Foam Material

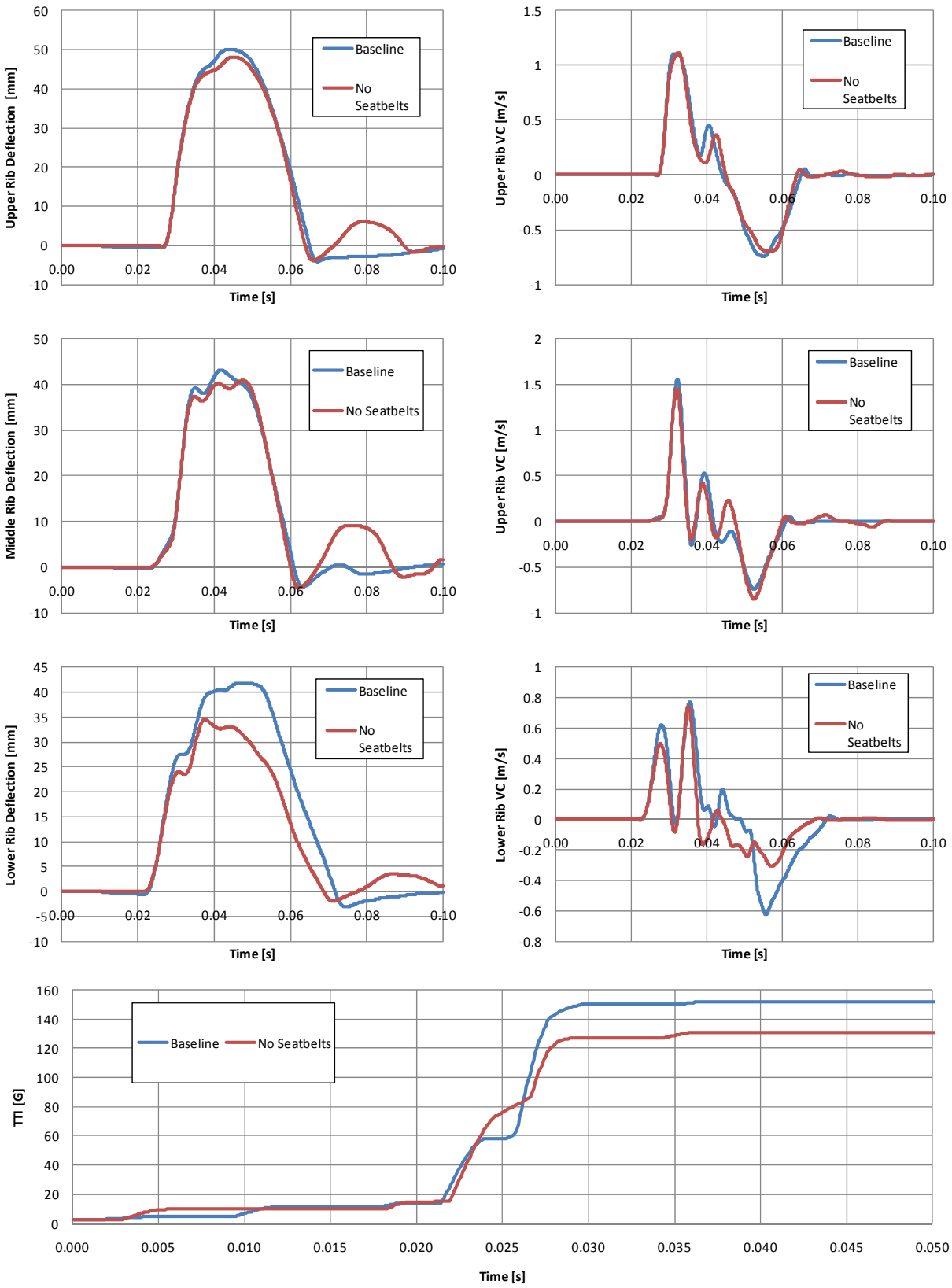

Figure C.18: Occupant Response – Effect of Seatbelts